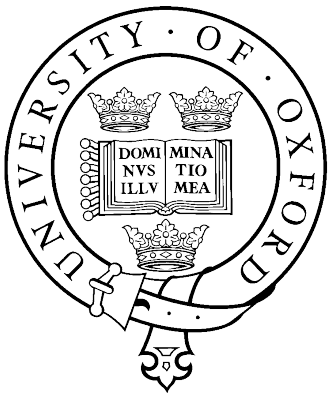
Investigating the pathogenesis of congenital insensitivity to pain using gene-editing in an *in vitro* model



Lucy A McDermott
St Cross College
University of Oxford

A thesis submitted for the degree of
Doctor of Philosophy
Michaelmas Term 2018

Abstract

The voltage gated sodium channel Nav1.7 is a key component of the mammalian nociceptive system. Homozygous loss of function mutations in SCN9A, the gene that encodes Nav1.7, cause congenital insensitivity to pain (CIP) in humans. Affected individuals are unable to perceive pain in response to any noxious stimulus, be it mechanical, chemical or thermal in form. Rare Mendelian disorders such as CIP can offer insight into the complexities of common, polygenic conditions such as chronic pain. As a result, the channel has attracted significant interest as a therapeutic and research target. However, a lack of primary material suitable for studying human Nav1.7 has hindered the characterisation of its function and cellular localisation. Here, we have developed an *in vitro* human model through the use of gene-editing tools suitable for the experimental interrogation of hNav1.7. Using CRISPR/Cas9, we genetically tag Nav1.7 and reveal the channel is robustly expressed at the soma cell surface, axons and enriched in the terminals of iPSC-nociceptors. Further, through the use of both novel gene-edited and CIP derived lines we demonstrate the channel has a key role in regulating neuronal excitability. Together, our findings provide mechanistic insight into the pathogenesis of congenital insensitivity to pain and contribute, more broadly, to our understanding of human nociceptive signalling.

Lucy A. McDermott

Michaelmas Term 2018

Publications arising from this work

McDermott, L.A., Weir, G.A., Themistocleous, A.C., Segerdahl, A.R., Blesneac, I., Baskozos, G, Millar, V, Clark A.J., Peck L.J., Ebner, D, Tracey, I, Serra, J, Bennett, D.L. (In press) Defining the functional role of NaV1.7 in human nociception. *Neuron*.

Baskozos, G., Dawes, J.M., Austin, J.S., Antunes-Martins, A., **McDermott, L.A**., Clark, A.J., Trendafilova, T., Lees, J.G., McMahon, S.B., Mogil, J.S., Orengo, C. and Bennett, D.L., 2018. Comprehensive analysis of long noncoding RNA expression in dorsal root ganglion reveals cell-type specificity and dysregulation after nerve injury. *PAIN*. (ahead of press).

Declaration statement

The work contained in this thesis has not previously been submitted for a degree or diploma at the University of Oxford or any other higher education institution. All the work described in this thesis is my own, unless otherwise stated clearly in the text.

Table of Contents

Chapter 1

Introduction 1

1.1 SCN9A, a spectrum of pain 2

1.1.1 Other congenital disorders of painlessness 4

1.2 The nociceptor - the receptor, conduit and modifier of pain. 7

1.2.1 Classification 7

1.2.2 Transduction 10

1.3 Conduction: voltage gated sodium channels 13

1.3.1 Structure and homology 13

1.3.2 Activation 15

1.3.3 Channel inactivation 15

1.3.4 Beta subunit association 16

1.3.5 Heterogeneity in function 17

1.4 Sodium channels of the DRG 18

1.4.1 Nav1.8/SCN10A 19

1.4.2 Nav1.9/SCN11A 20

1.4.3 Nav1.3/SCN3A 21

1.5 Nav1.7/SCN9A 22

1.5.1 Localisation and expression of the channel 22

1.5.2 Biophysical properties of Nav1.7 23

1.5.3 Post-translational modifications of the channel 24

1.5.4 Nav1.7 as a therapeutic drug target 29

1.6 Human cellular models in pain research 32

List of Figures

1.1 Overview of primary afferent signalling (page 11)

1.2 Voltage gated sodium channel alpha isoform structure (page 14)

1.3 Percentage amino acid homology of human VGSCs (page 17)

1.4 Overview of the CRISPR/Cas mechanism (page 40)

3.1 Pathogenic SCN9A variants identified in patients CIP1 and CIP2 (page 71)

3.2 Site directed mutagenesis outline (page 72)

3.3 Verification of mutated cDNA constructs (page 73)

3.4 Voltage clamp of HEK293T transfected with Δ SCN9A cDNA constructs (page 74)

3.5 Sanger sequencing of CIP iPSC line mutations (page 76)

3.6 Patient and Healthy control iPSC stained with pluripotency marker OCT4 (page 77)

3.7 Timeline of the iPSC.nociceptor differentiation protocol (page 79)

3.8 Differentiated cultures express canonical sensory neuronal markers (page 80)

3.9 Temporal increase in SCN9A mRNA expression (page 82)

3.10 Relative SCN9A mRNA expression is reduced in CIP1 iPSC.nociceptors (page 83)

3.11 Spectrum of Neuronal VGSCs expressed by iPSC.nociceptors. (page 83)

3.12 Temporal pattern of SCN3A mRNA expression in iPSC.nociceptors (page 84)

3.13 PCA analysis of iPSC.nociceptors (page 85)

3.14 Loss of functional Nav1.7 significantly decreases cellular excitability in iPSC.nociceptors (page 87)

4.1 Loci of sgRNA sites relative to c.2488 the mutation in exon 16 of SCN9A (page 103)

4.2 *In vitro* SCN9A sgRNA validation using a T7E1 Assay in HEK293T (page 104)

4.3 Chemical transfection of iPSC (page 106)

4.4 Schematic of sgRNA3 associated with Sp.Cas9 binding to target strand of SCN9A (page 108)

4.5 Representative screening gel of BciI digestion products (page 109)

4.6 Redesigned Asymmetric repair template (page 110)

4.7 Successful correction of c.2488C>T CIP mutation in CIP1.2 iPSC (page 111)

4.8 Optimised workflow for CRISPR/Cas9 gene editing in iPSCs (page 112)

4.9 CRISPR/Cas9 generated indels in exon 16 of SCN9A HC1 (page 113)

4.10 CRISPR edited lines differentiate similar to isogenic lines (page 114)

4.11 Genetic correction of 2488C>T variant increases SCN9A transcript expression relative to isogenic parent lines (page 115)

4.12 Relative SCN9A expression in CRISPR Nav1.7 KO and isogenic control (page 116)

4.13 Excitability of CRISPR Cas9 SCN9A edited lines (page 117)

4.14 Nav1.7 KO has an impaired response to slow, graded suprathreshold current injections (page 119)

4.15 Characterising expression of PENK mRNA (page 120)

4.16 Long term axonal outgrowth does not significantly differ between Nav1.7 KO and HC1 (page 122)

5.1 Selected genomic site for knock.in of HA tag sequence in HC1 iPSC. (page 137)

5.2 Assessing HA sgRNA efficiency in vitro using T7E1 (page 137)

5.3 Asymmetric Repair template incorporating HA tag sequence (page 138)

5.4 Screening for Ha tag insertion (page 139)

5.5 HA tag chromatogram (page 139)

5.6 Western blot of SCN9A.HA iPSC (page 140)

5.7 Nav1.7.HA localisation in iPSC.nociceptors (page 141)

5.8 Verification of HA antibody specificity using the isogenic control HC1 (page 142)

5.9 hNav1.7 localised to growth cones in vitro (page 143)

5.10 Nav1.7.HA iPSC.nociceptor co.cultures with rat Schwann cells (page 144)

5.11 Pattern of localisation in non.myelinating Rat co.cultures (page 145)

5.12 Nav1.7 is trafficked to the nodes of Ranvier in iPSC Nociceptors (page 146)

5.13 Nav1.7.HA Western blot conditions (page 148)

5.12 Co-immunoprecipitation of SCN2B (page 151)

List of Tables

1.1 Congenital disorders of painlessness (page 5)

2.1 List of antibodies used (page 54)

2.2 *Escherichia coli* strains and genotype (Page 55)

2.3 Commercial software (page 59)

3.1 Site directed mutagenesis primers (page 63)

3.2 PCR cycling conditions for SDM (page 63)

3.3 RT.PCR primer sets (page 67)

3.4 SCN9A mutations found in the CIP patients CIP1 and CIP2 (page 70)

3.5 Biophysical properties of the iPSC.nociceptor lines (page 88)

4.1 Exon 16 sgRNA sequences (page 94)

4.2 Cycling conditions for T7E1 PCR (page 97)

5.1 Oligonucleotide sequences of HA_sgRNAs (page 131)

Abbreviations

AA	Amino acid
AIS	Axon initial segment
AP	Action potential
ATP	Adenosine triphosphate
Bp	Base pair
CCI	Chronic constriction injury
CFA	Complete Freud's adjuvant
CIP	Congenital insensitivity to pain
cKO	Conditional knockout
CNS	Central nervous system
CRISPR	Clustered regularly interspaced short palindromic repeats
Dcas9	Catalytically dead Cas9
DIV	Days in vitro
DNA	Deoxyribonucleic acid
DRG	Dorsal root ganglia
EM	Primary erythromelalgia
ER	Endoplasmic reticulum
ESC	Embryonic stem cell
GDNF	Glial derived nerve factor
GE	Genome engineering
HA	Haemagglutinin
HDR	Homology directed repair
hDRG	Human DRG
HEK293(T)	Human embryonic kidney cells 293(T)

hNav1.7	Human Nav1.7
HR	Homologous recombination
HRP	Horse radish peroxidase
HTMR	High threshold mechanoreceptor
ICC	Immunocytochemistry
IP	Immunoprecipitation
iPSC	Induced pluripotent stem cell
IRES	Internal ribosome entry sequence
KO	Knockout
KSR	Knockout serum replacement medium
LTMR	Low threshold mechanoreceptors
mDRG	Mouse DRG
MEF	Mouse embryonic fibroblast
MMEJ	Microhomology end joining
mNav1.7	Murine Nav1.7
N2M	Neural maintenance medium
NGF	Nerve growth factor
NHEJ	Non-homology end joining
NMD	Nonsense mediated decay
OSMK	OCT4, SOX2, MYC and KLF4
PAM	Protoadjacent motif
PCD	Programmed cell death
PEPD	Paroxysmal pain disorder
PGE	Prostaglandin E
PKA	Protein kinase A
PKC	Protein Kinase C
PTM	Post translational modification
qPCR	Quantitative polymerase chain reaction
RMP	Resting membrane potential
RNA	Ribonucleic acid

RT	Room temperature
RT-PCR	Reverse transcriptase polymerase chain reaction
SMAD	Small mothers against decapentaplegic
SNI	Spared nerve injury
SSN	Site specific nuclease
ssODN	Single stranded oligonucleotide donor
TALENS	Transcription activator-like effector nuclease
TracrRNA	Trans-acting cRNA
TG	Trigeminal ganglia
TRP	Transient receptor potential
TRPM8	Transient receptor potential subfamily M member 8
TRPV1	Transient receptor potential vanilloid 1
TTX	Tetrodotoxin
TTX-R	Tetrodotoxin resistant
TTX-S	Tetrodotoxin sensitive
VGCC	Voltage gated calcium channel
VGSC	Voltage gated sodium channel
VSD	Voltage sensing domain
ZFN	Zinc finger nuclease

Chapter 1 *Introduction*

Pain is a critical evolutionary adaptation, serving to warn of impending or realised tissue damage. However, erroneous or prolonged pain in the absence of noxious stimuli constitutes a significant healthcare burden. One in five European adults are affected by chronic pain and the collateral effects on the workforce including lost productivity and absenteeism pose a further socioeconomic insult (Breivik et al., 2006). Current analgesics often lack efficacy and are associated with side effects such as addiction and physical dependency, exemplified by the US "opioid crisis". There is, therefore, a significant unmet clinical need, which requires the development of novel analgesics with improved safety profiles and therapeutic indices. Drug development should be strongly informed by physiology, yet there remains a relative paucity in our knowledge of human pain disorders and the pathogenic mechanisms underlying them.

Pain perception, as a sub-modality of sensory processing, involves a series of complex events originating from the periphery. A subset of peripheral primary afferent neurons, nociceptors, respond to noxious stimuli relaying this information to the CNS. The biological importance of this conduit is reflected by its complexity and the degree of regulation the body imparts on this process. A homeostatic imbalance in this relay mechanism can manifest in a reduction or increase in the sensation of pain. Known regulators of nociceptor excitability are the voltage gated sodium channels (VGSCs). These channels, to be discussed in greater detail later, are primarily responsible for action potential generation (Catterall, 2012). Recent advances in clinical genetics and

molecular biology have framed a central role for select members of the voltage gated sodium channel family in nociceptive transmission.

The VGSC Nav1.7, the focus of this thesis, has emerged as a compelling target for the treatment of pain. This follows the study of 3 consanguineous families in north west Pakistan in 2006 (Cox et al., 2006). Affected members of the families were completely insensitive to painful stimuli, whilst maintaining normal touch sensitivity. The pain-free phenotype segregated in an autosomal recessive fashion and the highly inbred population allowed for autozygosity mapping. Further bioinformatic analysis filtered the search to SCN9A, the gene encoding Nav1.7; Sanger sequencing revealed all affected individuals possessed homozygous non-sense mutations in the channel. The authors subsequently demonstrated in a heterologous Nav1.7 expression system that the familial mutations caused a complete loss of sodium ion conductance. The work was an elegant example of the power of forward genetics, however despite a decade passing since the discovery, we still understand little about the fundamental biology of human Nav1.7 in general and in relation to the pathophysiology of congenital insensitivity to pain. The aim of this thesis is therefore to develop an *in vitro* model to facilitate the study of human Nav1.7 in order to appreciably understand its role in human nociception. It is hoped by doing so that the results may improve the generation and/or refinement of therapeutics for the treatment of pain.

1.1 SCN9A, a spectrum of pain

Mendelian disorders, although rare, have significant potential to inform our understanding of complex polygenic conditions. Hereditary pain disorders are, in essence, a reductionist model *in natura* of a manifestly complex human sensation. Pathogenic mutations in SCN9A cause a striking spectrum of human pain disorders and

therefore the study of this ion channel should provide important mechanistic insights into human nociception.

So called 'gain of function' mutations in SCN9A cause several painful autosomal dominant disorders including primary erythromelalgia (EM) and paroxysmal extreme pain disorder (PEPD) (Bennett and Woods, 2014). Primary erythromelalgia is characterised by episodes of symmetrical burning like pain of the feet, lower legs, and occasionally hands, with an elevated skin temperature of affected areas and severely reddened extremities. The described symptoms are precipitated by warmth or mild exercise, and the disease is highly penetrant. To date, all mutations associated with the condition are non-synonymous missense substitutions causing a hyperpolarising shift in the voltage dependent activation threshold of the channel (Dib-Hajj et al., 2005).

Paroxysmal extreme pain disorder (PEPD), previously known as familial rectal pain, is associated with paroxysms of rectal, ocular and or submandibular pain with flushing (Fertleman et al., 2006). Unlike EM, PEPD is essentially a visceral pain disorder that appears to be unprovoked by environmental stimuli. The distinct clinical features reflect mechanistic differences between the two disorders. Although several PEPD mutations have been shown to cause a significant hyperpolarising shift in activation (common to both disorders), the majority of PEPD variants show marked deficits in channel fast inactivation leading to enhanced resurgent currents, a feature not found in EM (Theile et al., 2011). Consistent with this, many PEPD patients respond well to the antiepileptic carbamazepine, which has been shown to preferentially suppress persistent Na^+ currents (Choi et al., 2011).

At the opposing end of the spectrum, the loss of functional Nav1.7 expression causes congenital insensitivity to pain. These patients usually present with a history of multiple painless injuries including burns, bone fractures and severe orofacial injuries (resulting from self-mutilation). Charcot joints are frequently found, and patients do

not experience any visceral body pain. Surprisingly, despite expression of Nav1.7 in the sympathetic ganglion, no deficits in autonomic function have been noted, distinguishing CIP from other disorders of painlessness to be discussed later. Cardiac, respiratory function and thermal regulation are normal, as are mechanical, vibration and proprioception as confirmed by quantitative sensory testing. Interestingly, axonal reflex following cutaneous histamine application is preserved (Ramirez et al., 2014; Goldberg et al., 2007) and patients have deficit in thermal limen detection, i.e. the ability to distinguish between alternating thermal stimuli. The only other remarkable feature is anosmia, consistent with Nav1.7 expression in the olfactory epithelia (Weiss et al., 2011). It is perhaps precisely the dearth of salient clinical consequences (besides painlessness) that have made Nav1.7 such an attractive pharmaceutical target. This can be contrasted with many of the other congenital disorders of painlessness described, which are often associated with gross neurological defects. A table summarising known genes is shown below (Table 1.1) and a short discussion of a few of these genes is to follow.

1.1.1 Other congenital disorders of painlessness

The congenital disorders of painlessness described to date can be broadly segregated into those that cause structural deficits in nociceptor development or, alternatively, those that result in ion channel dysfunction.

Table 1.1 Congenital disorders of painlessness

Gene	Protein	Inheritance	Clinical presentation
NTRK1	TRKA	Autosomal recessive	No nociception and thermosensation, no sweating, learning difficulties (Indo, 2001)
NGF	NGFβ	Autosomal recessive	No nociception and thermosensation, no sweating, learning difficulties (Carvalho et al., 2011)
SCN9A	Nav1.7	Autosomal recessive	Anosmia, no nociception. Normal Mechanosensation, Loss of thermal limen detection (Cox et al., 2006)
SCN11A	Nav1.9	De novo dominant	Intestinal hypoperistalsis, hypotonia and mild weakness, hyperhidrosis, itching, altered temperature sensing (Leipold et al., 2013)
PRDM12	PRDM12	Autosomal recessive	No pain- and temperature-sensing neurons. Reduced sweating and tearing (Chen et al., 2015)
CLTCL1	CHC22	Autosomal recessive	No nociception or mechanosensation, learning difficulties (Nahorski et al., 2015)

(Table adapted from Nahorski et al., 2015)

The first gene to be associated with a congenital disorder of painlessness was NTRK, encoding the NGF sensitive receptor tyrosine kinase (TRKA) (Indo et al., 1996). NGF is required for the survival of sympathetic ganglion and nociceptive sensory neurons derived from the neural crest. Loss of the cognate receptor TRKA and therefore the concomitant loss of NGF signal transduction, results in cell death and axonal degeneration of small-diameter sensory neurons. The phenotype is recapitulated in mouse models, where *trka* deletion leads to the loss of small diameter neurons of the DRG, lack of small fibres in the dorsal roots and absence of Lissauer's tract (Indo, 2001) An effort to identify novel patients with a similar HSAN4 phenotype, but lacking mutations in NTRK1 or NGF led to the identification of a new gene candidate, PR/SET domain 12 (PRDM12) (Chen et al., 2015). PRDM12 is the first known epigenetic regulator of painlessness. The gene is a member of the PRDM family of histone methyltransferase factors; although, the protein lacks intrinsic methyl transferase activity, instead requiring cooperative binding to the factor G9a (Zannino and Sagerström, 2015). The protein structure consists of a PR domain (related to the SET methyl transferase domain), three zinc fingers and a C-terminal poly-alanine tract. Temporal and regional expression of the gene appears to be tightly controlled and in mice it is predominantly

expressed in neuronal sub-populations of the dorsal root ganglia during development. The gene is highly conserved amongst vertebrates (Nagy et al., 2015). The pathogenic mutations identified in patients are broadly dispersed in the protein structure, but in all cases thought to affect the downstream signalling of the protein. The precise mechanism by which loss of appropriate PRDM12 function causes painlessness is still to be resolved, however studies using *Xenopus laevis* provide some indication. In *Xenopus* the gene is highly expressed in the lateral pre-placodal ectoderm and over expression causes an increase in a number of sensory neuron markers including Isl1/2 and Brn3a. Morpholino knockdown of the *prdm12* transcript meanwhile causes a loss of presumptive trigeminal placode markers and expansion of the neural crest region (Matsukawa et al., 2015). This suggests the gene is critical for nociceptor development and appropriate differentiation and that loss of functional expression in the DRG during early development is sufficient to grossly affect normal nociceptive function, perhaps via programmed cell death of undifferentiated neural crest precursors.

SCN11A, the gene encoding Nav1.9, was the second member of the VGSC family to be associated with insensitivity to pain. In the original report, two isolated non-consanguineous cases were identified with a heterozygous L811P mutation in exon 15 of the channel causing a painless phenotype (Leipold et al., 2013). Paradoxically, the described mutation is associated with gain of function properties of the channel which leads to hypo-excitability at a cellular level. The mutation causes a significant leftward shift in channel activation and deactivation kinetics as well as a slowing of channel inactivation. Two such theories have been suggested to account for the loss of pain perception in affected individuals. The first suggests conduction block is mediated by excess sodium ion influx at rest, progressively inactivating the main constituent channels of the action potential including Nav1.7, Nav1.8 and emphasised a role for voltage gated calcium channels. A later study has suggested that in fact the primary

cause is due to the significantly depolarised resting membrane potential (Huang et al., 2017). Small DRG neurons expressing the mutation that had a resting membrane potential (RMP) of between a -20mV and -35mV range, were unable to fire action potentials in response to external stimuli at their native resting potentials but fired spontaneously when held at −60 mV. Thus the effect of the 'activating' mutations of Nav1.9 is thought to adopt a U shaped pattern of influence; mildly activating mutations are sufficient to cause neuronal hyperexcitability and pain, however, at a hitherto unknown critical threshold, mutations that cause 'extreme' activation cause, conversely, a hypoexcitable phenotype due to massive depolarisation of the RMP, which results in a depolarizing block due to inactivation of VGSCs. Other genes associated with painlessness have been identified including WNKI and SPLTC2 (Lafreniere et al., 2004; Rotthier et al., 2010), however these are degenerative disorders associated with a progressive loss of nociceptor function and are more often associated with marked deficits in other sensory modalities.

1.2 The nociceptor - the receptor, conduit and modifier of pain.

1.2.1 Classification

The described Mendelian disorders of painlessness all share a common dysfunctional unit: the nociceptor. The name nociceptor derives from the Latin *nocere* 'to harm' and was first used by Sherrington in 1906 (Sherrington, 1906). This population of primary afferents is responsible for the transduction, transmission and propagation of noxious stimuli which gives rise to the sensation of pain.

The field has devoted considerable effort in assembling a 'taxonomy' of nociceptors. The detailed classification of these neurons is not simply academic, it has important functional implications for mapping nociceptive transmission of multiple noxious

modalities. The classification of these primary afferents continues to be serially revised, a function of increased transcriptional and proteomic data. It is also undoubtedly complicated further by species differences (Price and Flores, 2007; Rostock, Schrenk-Siemens, Pohle and Siemens, 2017). However, historically a useful heuristic for classification has been a division based on somal size and condition velocity. Using these parameters, nociceptors may be divided into two subsets: Aδ neurons and C-fibres. Aδ nociceptors are thinly myelinated, fast medium conducting neurons (3–30 m/s), whilst C-fibres are slow conducting (0.5–2.0 m/s) and have thin, unmyelinated processes, the latter are thought to thought to constitute the majority of human nociceptors. Both assume typical primary afferent morphology as pseudo-unipolar neurons with bifurcated afferent processes projecting to the periphery and a central terminal innervating the spinal cord or trigeminal subnucleus caudalis. The cell bodies are located either in the dorsal root ganglia or trigeminal ganglia depending on the respective peripheral target.

Aδ Nociceptors

Aδ neurons mediate acute localised "first wave" or fast pain, often associated with a pricking like quality. This group of neurons can be further divided into type I; high threshold mechanoreceptors and type II Aδs. High threshold mechanoreceptors (HTMRs) respond to both mechanical and chemical stimuli of moderate and noxious intensity, these fibres respond to temperatures above those typically provided in a noxious experimental heat ramp >50 ℃. Type II Aδ nociceptors have a lower heat threshold than HTMR, but a very high mechanical threshold, these fibres are therefore associated with immediate pain following application of a noxious thermal stimuli.

C-fibre nociceptors

C-fibre nociceptors may have evolved as a protective mechanism during the convalescence period. The lingering 'second wave' of dull pain mediated by these unmyelinated neurons should elicit a protective response by the organism, designed to shield the affected body part from further insult. Unfortunately, this persistent pain can prove maladaptive if it continues despite functional recovery, as illustrated by acquired pain disorders. The majority of C-fibres are polymodal afferents, capable of responding to thermal, mechanical and chemical stimuli, and the remainder are considered mechano-insensitive fibres (Sugiura, Lee and Perl, 1986). A notable group are the 'silent' nociceptors - a misleading descriptor given most C-fibres exhibit little to no basal activity without stimulation. However, this term was first used to describe a group of afferents which did not elicit a response to physiologically relevant stimuli, yet upon electrical stimulation of the receptive fields, the neurons were shown to fire action potentials (Schmelz et al., 1994; Schmidt et al., 1995). This group are activated following tissue injury via inflammatory mediators and thus bare significant clinical relevance (Prato et al., 2017).

In addition to functional and anatomical classification, C-fibre nociceptors can be further distinguished by the presence or absence of certain neuropeptides (e.g. CGRP and substance P). Both peptidergic and non-peptidergic nociceptors derive from the same $TrkA^{+}$ and $Runx1^{+}$ neural progenitor population, however, a loss of Runx1 expression in prospective peptidergic cells at E12.5 segregates the group. Non-peptidergic cells retain Runx1, but subsequently lose Trka expression and NGF dependency, and become sensitive to glial cell line-derived neurotrophic factor (GDNF) via Runx1 induced RET expression (Chen et al., 2006). The peptidergic neurons predominantly express the

neuropeptides CGRP and Substance P, whilst the non-peptidergic group are often defined in the literature by their immunoreactivity to the glycoprotein isolectin B4 (iB4) (Silverman and Kruger, 1990).

The brief discussion of classification here belies the true complexities of nociceptor classification, with iterations continually revised following characterisation of transcriptional signatures. The seminal paper by Usoskin et al. used unbiased single cell RNA-seq to define eleven new classes of sensory neurons, comprising four types of low threshold mechanoreceptors (LTMRs), two types of proprioceptors and five types of nociceptors (Usoskin et al., 2015), significantly expanding the canonically described groups. Recent sequencing (Zeisel et al., 2018) has also predicted sub-clusters within those originally identified by Uroskin, emphasising further the complexities of establishing nociceptor divisors.

1.2.2 Transduction

The terminal structures of the nociceptors form the receptive interface of the nociceptive unit. The transduction of external noxious stimuli within this specialised domain causes a spatially restricted electrical-potential known as the generator or 'receptor' potential; this is a required intermediary before AP generation and propagation of the encoded stimuli (Fig. 1.1). Terminals are populated by highly specialised proteins for stimuli transduction and research has revealed a remarkable diversity in channel expression. In the last decade, a large range of ligand gated ion channels and G-protein coupled receptors expressed in nociceptors have been identified, which respond to a variety of chemical algogens including ATP (P2RX3), low pH (ASICs) and bradykinin (BK1 and 2) (Dubin and Patapoutian, 2010).

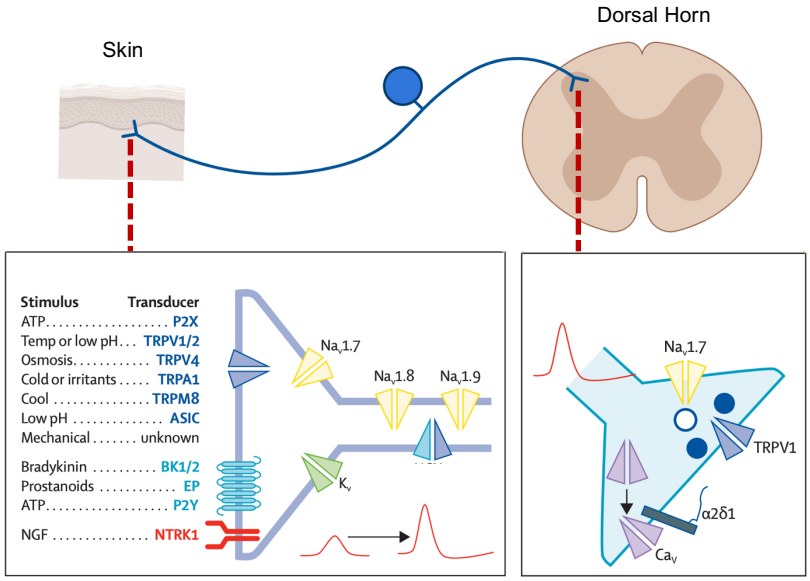


Figure 1-1 Overview of primary afferent signalling

Nociceptors provide connectivity between peripheral targets and the dorsal horn of the spinal cord. A schematic view of a primary afferent with a peripheral terminal innervating the skin and central terminal in the dorsal horn of the spinal cord. A selection of notable stimuli transducers is pictured in a magnified view of the peripheral terminal including several members of the TRP family (TRPV1, TRPA1, TRPM8), and GPCRs responsible for the transduction of inflammatory compounds (BK1/2, EP, P2Y). Opening of these channels causes an increase in cationic permeability, leading to local depolarisation of the terminal membrane (generator potential). Members of the voltage gated sodium channel family (Nav1.7, 1.8, 1.9) can amplify these graded electronic signals and initiate action potential firing if the threshold is reached, permitting faithful conduction of the stimuli to the central terminals. Neurotransmitter release in the CNS requires invasion of the AP into the central terminal. This activates voltage gated calcium channels, which in turn, mediate Ca^{2+} influx, facilitating neurotransmitter release and higher order transmission to spinal neurons. Also pictured are K+ channels a variety of which are expressed in nociceptors: (K_v), 2-pore K1 channels (K2P), Ca^{21}-activated K1 channels (K_{Ca}), Na1-activated K1 channels (K_{Na}). These channels dampen the excitability of nociceptors by regulating several properties of the neuron including resting membrane potential; action potential threshold, shape and firing frequency.
Figure adapted from Bennett and Woods, 2014

One of the most notable families includes the transient like potential receptor (TRP) channels. The founding member was first identified in *drosophila melanogaster* photoreceptors and the protein superfamily now encompasses 28 channels, which have been subdivided into 6 groups: TRPC (canonical), TRPV (vanilloid), TRPM (melastatin), TRPP (polycystin), TRPML (mucolipin), and TRPA (ankyrin) channels. The channels are multi-pass membrane proteins comprising 6 transmembrane segments, permeable to

mono and divalent cations. Although they share a topology structurally similar to other ion channels, they are unusual for their diverse cation selectivity and means of activation. TRP channels are widely expressed in the body with the majority of cell types expressing multiple family members. Select TRP channels however, show a more restricted pattern of expression. Important family members expressed in sensory neurons include TRPV1 and TRPM8, responsible, respectively, for the transduction of noxious heat, and non-noxious cold.

TRPV1 is a noxious heat–activated channel with a steep temperature coefficient (Q10 > 20) and a thermal activation threshold of ~43°C. The channel is strongly implicated in inflammatory thermal hyperalgesia, demonstrated by studies using *Trpv*1 null mice which fail to exhibit hypersensitivity to thermal stimuli following acute hind-paw injection of pro-inflammatory agents such as CFA. Interestingly, despite clear noxious heat activation of the channel, *Trpv*1 null mice still exhibit response to *acute* noxious thermal stimuli (Caterina, 2000). A recent paper has suggested a TRP channel triad: TRPV1, TRPM3 and TRPA1, are together, responsible for mediating acute thermal pain (Vandewauw et al., 2018). The authors demonstrated that triple knockout mice lack an acute withdrawal response to noxious heat, while showing normal nociceptive responses to cold or mechanical stimuli and intact preference for moderate heat conditions. Thus at least in mice, it appears a strong functional redundancy has evolved in order to preserve avoidance of noxious heat. Besides thermal stimuli, TRPV1 is also a target of a number of chemical compounds, it is activated classically by capsaicin, the active compound in chili peppers and latterly it has been shown to interact with a number of inflammatory stimuli including bradykinin, ATP as well as low pH (Vriens et al., 2009).

TRPM8 operates on opposing end of the thermo-spectrum; the channel was the first cold transducer to be identified. TRPM8 is directly activated by temperatures ranging from innocuous cool (26–15°C) to noxious cold (<15°C), (<28°C, Q10 > 20), and is responsive to chemical ligands such as menthol and ilicin. A role for the channel in the transduction of noxious cold is controversial and the literature is generally divided. In several studies cold hypersensitivity associated with inflammatory and neuropathic injury is diminished with loss of functional TRPM8 expression (Knowlton, et al., 2010; Colburn et al., 2007). Conversely, others have shown *Trpm8* null mice show no deficits in nociceptive response in response to noxious cold plate test (Bautista et al., 2007). Less controversial is a role for the channel in temperature discrimination, where a number of studies have shown a requirement for the channel (Dhaka et al., 2007). Both TRP channels covered here illustrate well the potential redundancy in modality transduction and by virtue, reflect the strong evolutionary pressure to preserve nociceptive signalling.

1.3 Conduction: voltage gated sodium channels

The generator potential is a locally dissipated, transient depolarisation of the membrane, long range propagation of the stimuli therefore requires action potential generation; this is orchestrated by the voltage gated sodium channel family. Although this thesis focuses predominantly on the role of only one of these channels, it is worthwhile to consider the general structure and function of the VGSC family as a whole, before narrowing to the isoforms relevant to nociceptive transmission.

1.3.1 Structure and homology

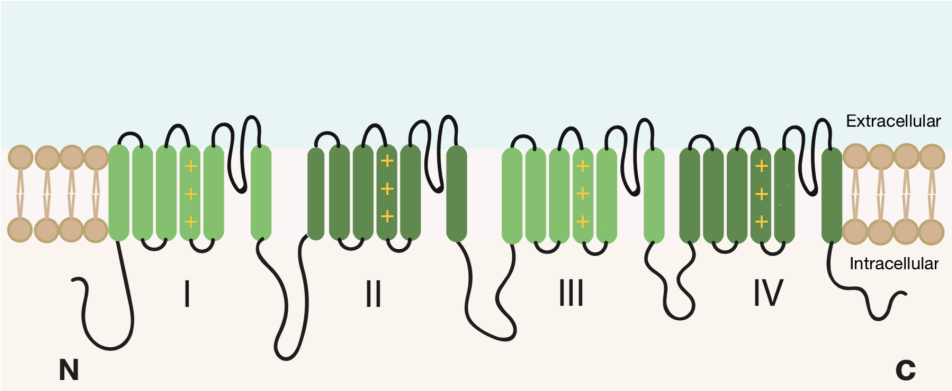


Figure 1-2 Voltage gated sodium channel alpha isoform structure

A schematic, linear view of VGSC membrane topology, the alpha subunit consists of four homologous transmembrane domains (indicated by roman numerals). Each domain contains 6 transmembrane alpha-helices, (S1-S6). S1-S4 function as the voltage sensing module, S4 contains repeated motifs of a positively charged amino acid residues (typically arginine) followed by two hydrophobic residues which are thought to act as the gating charges. S5-S6 form the pore domain with the intervening P-loop acting as the sodium ion selectivity filter. The N-terminus and C-terminus of the channel are labelled N and C, respectively.

The primary physiological role of voltage gated sodium channels is the initiation and conduction of action potentials. The family (Nav1.1-9) share a common architecture consisting of a central ion-conducting pore and four peripheral voltage sensing domains (VSDs), each with 6 transmembrane alpha helices (Fig. 1.2). Segments 1-4 of the VSD function as the voltage sensing module, and S5-S6 constitute the pore domain with an intervening P-loop acting as the ion selectivity filter (SF) (Catterall, 2000).

Voltage gated sodium channels exhibit remarkable selectivity and conductance for sodium ions; a single channel is capable of conducting 10^7 Na^+ per second and exhibits a ten-fold selectivity over K^+ ions, and greater than fifty-fold for Ca^{2+} (Favre et al., 1996). The P-loop between S5 & S6 has been identified as the selectivity filter, enabling the channel to effectively discriminate between ions with the same net charge (K^+) and similar ionic radius (Ca^{2+}). The critical residues thought to confer ion selectivity have been identified via mutagenesis studies, they comprise aspartate (DI S5–S6 loop), glutamate (DII S5–S6 loop), lysine (DIII S5–S6 loop), and alanine (DIV S5–S6 loop),

collectively known as the DEKA motif. Of the four, the interaction of Na^+ with the carboxyl group of glutamate DII and the positively charged lysine may be the most critical for maintaining appropriate ionic selectivity (Sun et al., 1997). The permeability and conductance of the channels is dependent on a voltage driven change in protein conformation and the channel can occupy three conformational states: activated, inactivated and deactivated, depending on the gate open (either the activation or inactivation gate).

1.3.2 Activation

In the 1980s, Catterall proposed a sliding helix model of activation (Catterall, 1986). The model assumes the four highly charged arginines in S4 serve as the voltage sensor. At rest, the residues are stabilised by interactions with negatively charged residues on opposing helices. Following depolarisation of the membrane they are thought to rotate such that they exchange these ion-pairs and push outwards, opening the pore and activating the channel. This theory is generally supported and consistent with experimental evidence including the site directed neutralisation of the charged residues, which has been shown to shift voltage dependence of activation and reduces its steepness (DeCaen et al., 2008). It is also complemented by recent disulphide-locking studies showing S4 gating charges exchange ion-pair partners during outward motion of the S4 segment (DeCaen et al., 2011; Yarov-Yarovoy et al., 2012).

1.3.3 Channel inactivation

Mammalian VGSCs can either undergo fast or slow inactivation. Fast inactivation (FI) occurs within milliseconds, despite on-going depolarisation. An early model for this form suggested that a hydrophobic linker (IFM) between VSD III and VI swings into

place to physically block the pore opening. Competitive blockade of the IFM motif within this loop was sufficient to block open the channel in a voltage and frequency-dependent manner (Caterall, 1988). In contrast, slow inactivation occurs in the order of hundreds of ms, it is thought that a significant conformational change in the channel including pore collapse may occur, however the exact mechanism is currently poorly understood (Goldin, 2003). Recent advances including the first solved structure of a human VGSC (Pan et al., 2018) may serve to clarify this.

1.3.4 Beta subunit association

VGSCs function as multiprotein complexes in which the pore forming alpha subunit is associated with one or more auxiliary beta subunits. The β subunits (encoded by the genes SCN1-4B) are small, type I transmembrane glycoproteins with an N-terminal immunoglobulin (Ig) loop (Kruger and Isom, 2016). SCN2B and SCN4B are covalently linked to alpha unit via a disulphide bond, whilst SCN1B and SCN3B maintain a non-covalent interaction. There is extensive literature to suggest that these proteins significantly modulate α-subunit function and this appears to be cell type and localisation dependent (Isom et al., 1992; 1995; Meadows et al., 2002; Aman et al., 2009). The modulation of cellular excitability by the beta subunits is a product of several mechanisms, principally affecting either VGSC α-subunit localisation/trafficking or by influencing directly the channel kinetics. For example, SCN2B is thought to increase sodium currents by associating with the nascent pore-forming α-subunit in the endoplasmic reticulum (ER), facilitating membrane insertion following trafficking to the cell surface. Consistent with this role, a significant reduction in the level of plasma membrane saxitoxin binding is found *scn2b-/-* hippocampal neurons (Chen et al., 2002). A similar effect was noted in small diameter neurons of the DRG, but not in neurons

isolated from the dentate gyrus (Lopez-Santiago et al., 2006), emphasising the context dependent roles of the β subunits.

In addition to effects on α-subunit subcellular localisation, the β subunits have an important role in regulating channel kinetics. SCN4B is thought to influence resurgent sodium currents in Purkinje neurons by physically blocking the Nav1.6 inactivation gate from closing via its cytoplasmic tail, thereby allowing for more rapid channel recovery and supporting burst firing (Bant and Raman, 2010).

In vitro the β subunits are important accessory proteins for VGSC heterologous expression studies. Although alpha subunits can be expressed in these systems in absence of auxiliary β units, they are, in many instances, required for the production of physiologically relevant recordings. However, in keeping with theme *in vivo*, the respective effects of beta subunit expression vary according to cell type (e.g. Xenopus oocytes, vs HEK293 (Sangameswaran et al., 1996)), hence many conflicting accounts of their effect.

	hNav1.1	hNav1.2	hNav1.3	hNav1.4	hNav1.5	hNav1.6	hNav1.7	hNav1.8	hNav1.9
hNav1.1	100	87.9	84.74	71.17	64.95	77.62	77.5	58.55	52.65
hNav1.2	87.9	100	87.67	71.94	65.78	77.17	78.8	59.06	53.67
hNav1.3	84.74	87.67	100	70.74	66.04	76.1	77.22	58.92	53.29
hNav1.4	71.17	71.94	70.74	100	67.37	70.35	70.18	61.02	52.97
hNav1.5	64.95	65.78	66.04	67.37	100	65.33	63.66	64.73	55.5
hNav1.6	77.62	77.17	76.1	70.35	65.33	100	72.41	59.18	53.03
hNav1.7	77.5	78.8	77.22	70.18	63.66	72.41	100	58.24	53.5
hNav1.8	58.55	59.06	58.92	61.02	64.73	59.18	58.24	100	54.61
hNav1.9	52.65	53.67	53.29	52.97	55.5	53.03	53.5	54.61	100

Figure 1-3 Percentage amino acid homology of human VGSCs

Percentage amino acid identity homology matrix for human VGSCs. Highlighted cells contain percentage homology compared to hNav1.7. Human protein sequences were aligned using CLUSTAL Omega, and in all instances the Uniprot reference transcript was used.

1.3.5 Heterogeneity in function

Despite assuming near identical form, from a functional view, VGSCs adopt quite distinct physiological roles, which is remarkable given the degree of amino acid

homology they share (Fig.1.3). Classic studies assigned a relatively simplistic role for the VGSC in AP generation, remarking narrowly on their contribution to the upstroke of the action potential. Whilst VGSCs in the CNS in many cases fulfil this role as fast activating, rapidly inactivating conductors of current (e.g. Nav1.3), VGSC activity in the PNS appears markedly more nuanced and complex. Studies using tetrodotoxin (TTX) provided early evidence for VGSC heterogeneity. The toxin was shown to be a highly selective blocker of CNS and skeletal muscle sodium currents (IC50 ~ 5-20 nM; (Ritchie and Rogart, 1977)), whilst being a comparatively weak blocker of cardiac muscle sodium currents (IC50 ~ 1-2 μM; (Baer, Best and Reuter, 1976)). Sensitivity to TTX is now used to broadly group the VGSC α-isoforms. Nav1.1-1.4, Nav1.6 and 1.7 are TTX-S (TTX-sensitive) channels, inhibited by nanomolar concentrations of the toxin, whilst the TTX-R (TTX-resistant) channels (Nav1.5, 1.8, and 1.9) require millimolar TTX to be blocked.

1.4 Voltage gated sodium channels of the DRG

The range of VGSCs expressed in the DRG manifest a complex sodium current, components of which are pharmacologically distinguishable, differ in kinetics and in voltage dependence. Historically, two VGSC profiles have been assigned to small and large diameter neurons of the dorsal root ganglia. Small-medium diameter neurons isolated from rodents express a combination of fast TTX-sensitive (Nav1.1, Nav1.2, Nav1.6, Nav1.7) and slow TTX-resistant channels (Nav1.8, Nav1.9), whilst larger neurons (>35μm) predominantly express a TTX-S sodium current. There is, however, evidence to suggest that this binary may not be absolute and recent studies in conjunction with advances in transcriptional profiling have conflicted with this theory, finding for instance convincing expression of Nav1.8 in subset of larger diameter

neurons (Ramachandra et al., 2013). Work in primary human DRGs has complicated this further and suggests the pattern of sensory sodium channel expression may be quite distinct from murine. Cheng et al suggest that among human DRG neurons, there is not a comparable relationship between cell body size and VGSC expression, as has been documented in rodent (Chang et al., 2018).

Another layer of complexity is the dynamic expression of these channels. Plasticity is a hallmark of VGSC expression and this is especially true within the DRG and a particular feature of pathological states - significant changes are known to occur in the profile of VGSCs expressed within nociceptors following injury and disease (Devor, 2006; Abdulla and Smith, 2002). I will now discuss several of the channels implicated in pathological pain states before narrowing focus to Nav1.7.

1.4.1 Nav1.8/SCN10A

Nav1.8 produces a slowly inactivating TTX-R current, which contributes to the majority of the action potential upstroke in small DRG cells. Consistent with this role, DRG neurons derived from Nav1.8 null mice have significant deficits in action potential electrogenesis compared to DRG neurons derived from wild type, with the majority of cells exhibiting graded responses to current injections (Renganathan et al., 2001). The rapid repriming kinetics of Nav1.8 also support a significant role for the channel in repetitive firing under conditions of sustained stimulation. Studies using Nav1.8 null mice have suggested a role for the channel in inflammatory pain; null mice demonstrate an impaired pain response in several experimental inflammatory pain models (Akopian et al., 1999; Laird et al., 2002). Supporting this, the channel is thought to be a downstream target of multiple inflammatory mediators including TNF-α (Gudes et al., 2015), CXCR4 (Yang et al., 2015) and Prostaglandin E2 (PGE-2) (Liu et al., 2010).

The role of Nav1.8 in neuropathic pain is less clear with several groups producing conflicting findings. Studies have shown a down regulation in Nav1.8 transcript, protein, and associated currents, following nerve transection (Cummins and Waxman, 1997) (Dib-Hajj et al., 1996). However, an increase in immunolabelling has been observed in spared small fibre neurons and neuronal cell bodies (Gold et al., 2003), which may serve to explain the efficacy of anti-sense Nav1.8 siRNA in these models (Lai et al., 2002).

A role for the channel in human pain pathologies has recently been emphasised with the discovery of Nav1.8 variants associated with painful small-fibre neuropathy (Faber et al., 2012). Functional analysis of the mutations performed *in vitro* showed an increase in DRG hyperexcitability including a lower threshold and higher firing frequency; this profile may underlie the allodynia and hyperalgesia experienced by the patients.

1.4.2 Nav1.9/SCN11A

Nav1.9 is another TTX-R channel enriched in the small diameter neurons of the DRG. Expression often overlaps with that of Nav1.8, however the two are distinct and non-redundant in their biophysical properties. Nav1.9 produces a larger, remarkably persistent current owing to extremely slow activation and inactivation kinetics (Dib-Hajj et al., 2015). These properties suggest the channel does not contribute to the action potential upstroke, but instead that it is likely to play a role in RMP and initiation thresholds and therefore may be an important channel in regulating the excitability of nociceptors. The channel is upregulated in inflammatory PGE-2 mediated pain models. PGE-2 interacts with Nav1.9 via G-protein-coupled mechanism leading to a reduction in threshold and an increase in spontaneous firing (Hockley et al., 2014).

The evidence for a role Nav1.9 in neuropathic pain models is weaker than that of inflammatory conditions. Again similar to Nav1.8, conflicting studies exist on expression of the channel following injury (Dib-Hajj, Tyrrell, Black and Waxman, 1998) (Abdulla and Smith, 2002). Nav1.9$^{-/-}$ mice do not appear to have significant deficits in neuropathic pain, demonstrating behavioural responses similar to controls in spared nerve injury and partial sciatic nerve (Seltzer) injury models (Amaya, 2006; Luiz et al., 2015). Historically, studying Nav1.9 isolated current has been challenging due to less than optimum expression in heterologous expression systems and rapid current run down (Goral, et al., 2015). Recent improvements in *in vitro* expression and genetic techniques are leading to a greater appreciation of the channels role in human pain conditions (Zhou et al., 2017).

1.4.3 Nav1.3/SCN3A

SCN3A, the gene encoding the TTX-S channel Nav1.3, is highly expressed during rodent embryonic and early postnatal development. Expression is subsequently down regulated in adult DRG, except in instances of axotomy where the channel is strongly upregulated in a number of pain models (Eriksson et al., 2005; Hains et al., 2003; Moyer et al., 2012). The channel generates a fast activating and inactivating current, with rapid repriming kinetics. It has been suggested that this positions the channel as a key contributor to ectopic spontaneous firing post injury. Consistent with this, intrathecal delivery of SCN3A antisense oligodeoxynucleotides (ODNs) was sufficient to significantly reduce mechanical allodynia and thermal hyperalgesia following spinal cord injury in rats (Hains et al., 2003). A gene therapy mediated knockdown of Nav1.3 following SNI also showed some efficacy in reducing increasing mechanical thresholds in rats (Samad et al., 2013). In contrast to these findings, neuropathic pain has been shown to develop normally in Nav1.3 null mice. Lindia et al. also demonstrated that

Nav1.3 knockdown to 50% of the control levels had no effect on pain in the SNI model (Lindia et al., 2005). The relevance of the channel to human pain disorders is less certain with no known hereditary pain disorders associated with Nav1.3 dysfunction. Only a few studies exist to associate the channel with painful conditions in humans, one showing an accumulation of the channel in human neuromas (Black et al., 2008). Moreover, therapeutic targeting of the channel may not be suitable therapeutic goal as Nav1.3 is highly expressed in the CNS, complicating selective block in the periphery.

1.5 Nav1.7/SCN9A

1.5.1 Localisation and expression of the channel

Nav1.7 was first cloned from a human medullary neuroendocrine cell line in 1995, and adopted the original name of PN1 (Toledo-Aral et al., 1997). The channel has a relatively restricted pattern of expression in comparison to other TTX-S α-isoforms. In the CNS, Nav1.7 is limited to a small population of neurons including those of the amygdala, a subset hypothalamic neurons and the olfactory epithelium (Kanellopoulos et al., 2018) (Weiss et al., 2011). The channel is found at significantly higher levels within the peripheral nervous system and is remarkably enriched in the dorsal root ganglia and in trigeminal neurons. Importantly, Nav1.7 has been found in the majority of nociceptors; in rat, virtually all small diameter neurons of the DRG are positive for Nav1.7 mRNA expression and a significant, ~70% $NF200^+$ (a marker of large diameter neurons in rodent) neurons also express the transcript (Fukuoka et al., 2008). A similar level of expression is noted in mice. Characterisation of human Nav1.7 within the DRG has been hampered by the perennial difficulty in obtaining primary tissue and the availability of specific commercial antibodies. One study examining only the $TrkA^+$ population of C-

fibres found 57.0% expressed Nav1.7 transcript by in situ hybridisation, a similar but slightly increased percentage than in mice (53.8%) (Rostock et al., 2018).

The channel is distributed extensively within unmyelinated rodent DRG neurons, expression spans from the central, through to the peripheral terminals (Black et al., 2012). As with many VGSCs, subcellular membranous immunolabelling has also been observed, this is consistent with a large intracellular pool of nascent α-subunits which require further posttranslational modification before trafficking to the outer membrane (Schmidt et al., 1985).

In myelinated neurons, Nav1.7 has been shown to localise to the nodes of Ranvier in a subset of thinly myelinated A-δ fibres in mice, as well as in human dental pulp (Luo et al., 2008). The subcellular dispersion in neuronal subtypes is quite unusual, with many of the VGSC showing stereotyped subcellular localisation in the PNS, for instance Nav1.6 is classically associated with the nodes, whilst Nav1.2 is often found localised to the axon initial segment in adult neurons (Kaplan et al., 2001). It is highly likely that Nav1.7 is contributing different roles in the shaping of action potential depending on the pattern of intracellular expression.

1.5.2 Biophysical properties of Nav1.7

The biophysical properties of the channel are thought to be quite distinct from other TTX-S α-isoforms. Nav1.7 produces a rapidly activated and inactivated current (Sangameswaran et al., 1997), however, in contrast to other TTX-S channels, Nav1.7 recovers slowly from fast inactivation (Herzog et al., 2003). This theoretically suggests that Nav1.7 is unlikely to contribute to high frequency firing within the DRG, however the channel has slow closed-state inactivation kinetics (Cummins et al., 1998), which allows Nav1.7 to produce a substantial ramp current in response to small, slow

depolarisations. Cummins et al. demonstrated this in a heterologous expression system, contrasting the response with Nav1.4, a channel capable of firing at high frequency. Nav1.4 channels transfected into HEK293 do not activate in response to slow ramp stimuli (0.23mV/ms) depolarisation. In contrast, the same stimulus applied to cells transfected with Nav1.7, generates distinct inward currents, evoked close to the resting potential. Together, the functional properties suggest Nav1.7 may act as a sub-threshold amplifier and is thus acting to boost subthreshold stimuli, increasing the probability of action potential firing. This has physiological significance *in vivo* if one considers it in context of probable terminal expression of the channel. If localised to this domain in humans, it is suitably positioned to amplify generator potentials.

1.5.3 Post-translational modifications of the channel

The α-isoforms of the voltage gated sodium channel family are heavily glycosylated proteins; carbohydrate moieties can account for up to 30% of the molecular mass of these channels (Catterall, 2012; Moremen et al., 2012). This PTM appears to have a regulatory role, affecting membrane localisation and structural folding with an influence on gating characteristics. Interestingly, it appears also to be developmentally regulated with changes in weight influencing channel kinetics (Laedermann, Abriel and Decosterd, 2015). The influence of glycosylation on native Nav1.7 has not been well documented to date, however Laedermann et al. (2013) examined glycosylation patterns of Nav1.7 cotransfected with β1/3 in HEK293; they found multiple glycosylated states including a core-glycosylated form with a molecular weight of ~250 kDa and a fully-glycosylated form with a molecular weight of ~280 kDa. They also suggested an alternative intermediate form exists resulting from β1 expression. The contribution of these forms to the overall Nav1.7 current or indeed if they are reflected *in vivo,* remains

to be examined. Other post-translational modifications known to affect Nav1.7 function include protein phosphorylation and SUMOylation.

Dynamic phosphorylation of Nav1.7 is thought to significantly affect channel function downstream of inflammatory mediators. PKA and PKC have both been shown to reduce Nav1.7 currents in transfected *X. laevis* oocytes (Vijayaragavan et al., 2004), however in HEK293 PKC activation significantly enhanced hNav1.7-mediated resurgent currents, an effect that could be prevented by the PKC antagonists Bisindolylmaleimide I (Bis I) or Chelerythrin (Tan et al., 2014). In an *in vivo* model, activated ERK1/2 (phosphorylated ERK1/2, pERK1/2), shifts activation and steady-state fast inactivation of Nav1.7 channels in a hyperpolarizing direction (Stamboulian et al., 2010). The conflicting effects of protein phosphorylation generally emphasise the importance of cellular background to Nav1.7 function.

The phosphoprotein CRMP2 is known to regulate Nav1.7 activity and is one of only a few interacting proteins identified to date (Dustrude et al., 2013; 2016; Moutal et al., 2017). CRMP2 was first identified in chick DRG where it was shown to be required for axonal determination and outgrowth during development (Goshima et al., 1995). The protein is downstream of a number of signalling pathways and is controlled by a series of reversible PTMs, including SUMOylation (Geiss-Friedlander and Melchior, 2007). Loss of SUMO moieties (small ubiquitin like modifiers) on Lysine 374 of CRMP2 lead to a decrease in Nav1.7 membranous expression through a reduction in CRMP2 binding (Dustrude et al., 2013). This occurs concomitantly with an increase in Nav1.7 internalisation in a clathrin-dependent manner via the E3 ubiquitin ligase Nedd4-2. Interestingly, the antiepileptic lacosamide is known to inhibit CRMP2 and thus may have a dual effect on VGSC activity, decreasing surface expression of Nav1.7 as well directly affecting channel gating (Wilson and Khanna, 2015; Hensley et al., 2011).

1.5.3.1 The role of Nav1.7 in determining acute pain related behaviour in animal models

The striking deficit of acute pain in CIP is well established and used as a clinical determinant. However, the recapitulation of this in rodent models is inconsistent and appears to vary depending on the experimental model of Nav1.7 loss used. In a conditional knockout, where $Nav1.7^{fl/fl}$ mice were crossed with a $Nav1.8^{cre}$ line preferentially ablating Nav1.7 in nociceptive neurons, Nav.1.7cKO mice did not differ in their response to noxious temperatures using a hotplate assay (Nassar et al., 2004). However, they showed a slight reduction in sensitivity to *acute* thermal stimuli applied with Hargreaves apparatus. The mice also demonstrated profound analgesia to noxious mechanical pressure as assessed by the Randall-Selitto test.

Global knockout of Nav1.7 in mice was shown to cause early post-natal mortality with the pups failing to thrive, presumably due to anosmia (hence the early use of conditional models) (Weiss et al., 2011). Improvements in animal husbandry have latterly permitted the use of global Nav1.7 null mice. In contrast to the conditional knockout described earlier, these mice show gross deficits in response to hotplate sensitivity, reaching the predetermined maximum latency time, without exhibiting any pain behaviour (Gingras et al., 2014). Null mice also failed to exhibit mechanical hypersensitivity to a tail-clip stimulus, this was despite normal responses to non-noxious stimuli with von Frey hairs, suggesting that rather than a loss of mechanical sensation underlying this phenotype, the deficit is limited, as in humans, to noxious mechanosensation.

Further to this, a recent paper has shown a dramatic loss of pain sensitivity upon adult-onset deletion of Nav1.7 in mice (Shields et al., 2018). The authors generated a tamoxifen-inducible KO mouse enabling genetic deletion of Nav1.7 from adult mice. Strikingly, these mice acquired a gradual increase in pain insensitivity over the

course of several weeks following tamoxifen administration, concomitant with the intracellular decay of Nav1.7 protein. At 6-8 weeks after tamoxifen injection, the mice showed greatly prolonged response latencies to noxious heat in the hot plate, tail immersion, and Hargreaves tests, often reaching the maximum cut-off required to prevent tissue damage.

1.5.3.2 Nav1.7 and inflammatory pain

The sensitisation and activation of peripheral nociceptors by inflammatory mediators makes an important contribution to inflammatory pain. The extra-cellular milieu in the inflamed state, often referred to as the inflammatory soup, significantly increases nociceptor excitability via interactions with a number of neuronal ion channels and signalling pathways. In the DRG peripheral tissue inflammation causes a significant increase in TTX-S currents and this is partly a result of *de novo* sodium channel synthesis. Nav1.7 transcripts and protein are upregulated in number of inflammatory pain models (Strickland et al., 2008; Black et al., 2004) an increase comparatively greater than Nav1.3, another TTX-S also shown to be upregulated (Gould et al., 2004). Knockout models have also shown a direct role for Nav1.7 in inflammatory pain. Nassar et al. demonstrated using the conditional knockout described earlier (Nav1.7cKO) that Nav1.7 is required for the inflammatory pain response evoked by a wide range of stimuli. Inflammation induced by the injection of complete Freund's adjuvant (CFA) caused substantial thermal and mechanical hyperalgesia in litter mate controls, whereas the Nav1.7cKO mice were essentially unaffected at all timepoints evaluated by the authors. *In vitro* application of the inflammatory mediator NGF has been shown to upregulate Nav1.7 expression in DRG neurons and PC12 cells (Toledo-Aral et al., 1997) however, the mechanistic details underlying this are unclear and the downstream effects of other

inflammatory mediators on Nav1.7 expression and localisation remain to be investigated.

1.5.3.3 Nav1.7 and neuropathic pain

Neuropathic pain is defined as pain that arises as a consequence of a lesion or disease of the somatosensory nervous system. The pain is typically persistent and prolonged, even in the absence of the lesion *ab initio* and is usually refractory to treatment. It is a result of maladaptive plasticity within the somatosensory system that may be both nociceptive and CNS mediated, which reasons why it is especially challenging to treat. Nav1.7's role in neuropathic pain is less clear than that of inflammatory pain, but this may be due to the heterogeneity of the pain models used. One of the main components of neuropathic pain is pain in the absence of an identifiable stimulus. This ongoing or spontaneous pain is thought to arise as a result of ectopic action potential generation in sensory neurons. VGSCs are probable key contributors to this process. Nassar et al. suggested Nav1.7 in nociceptors was not required for neuropathic pain by demonstrating the Nav1.7cKO mice still developed mechanical allodynia following ligation of the L5 spinal nerve. The extent and time course of development was identical in both the Nav1.7 conditional knockout and littermate controls. Interestingly, the same group later showed that deletion of the channel in both sensory and autonomic neurons is sufficient to stop the development of neuropathic pain in a number of experimental neuropathic pain models, including spinal nerve transection and the same constriction model used in the initial study (Minett et al., 2012). They suggested that Nav1.7 is required for the sympathetic sprouting that develops in parallel with nerve-transection pain, demonstrating the importance of sympathetic neurons in mediating neuropathic pain states. Although the authors demonstrated a role for Nav1.7 in surgical models of

neuropathic pain, they were unable to show a role in cancer induced bone or oxaliplatin induced pain - suggesting both models are mechanistically independent of lesion models usually used in the field. These findings are in contrast to recent studies investigating Nav1.7 in chemotherapy-induced peripheral neuropathy. (Xiao et al., 2016; Li et al., 2018). Li et al. showed that acute and chronic treatment of the chemotherapeutic drug Paclitaxel in rats significantly upregulated Nav1.7 transcripts and protein expression in sensory neurons. The authors used a selective Nav1.7 inhibitor showing that it prevents the development of and alleviates established mechanical behavioural hypersensitivity following paclitaxel treatment. The reasons underlying this discrepancy are unclear, it could be due to the species difference - perhaps other sodium channels implicated such as Nav1.3 or Nav1.6 play a greater role in mouse vs rat.

1.5.4 Nav1.7 as a therapeutic drug target

The channel has naturally attracted significant interest as an analgesic target as a result of the striking phenotype of congenital insensitivity to pain, complemented by the described evidence from CIP animal models. Astra Zeneca, Pfizer and Genentech are but a few of the pharmaceutical companies running active Nav1.7 drug development programmes (Storer et al., 2017; Kemp, 2010). The challenge, as described earlier, is the degree of shared sequence homology between the VGSC family members. Indeed, critical protein domains of the channel show even greater sequence similarity and where a divergence is found, it is often with substitutions of structurally similar residues. The Na_v modulators developed to date can be broadly segregated into either pore blockers or 'gate modifiers'. Analgesics in clinical use, including prototypical local anaesthetics, target the channel pore; this region is highly conserved among VGSC family members, reflecting the common lack of compound specificity for this class.

Other sodium channel blockers in use include the anti-epileptics carbamazepine and lacosamide, which have shown some efficacy in relieving certain neuropathic pain states including paroxysms in trigeminal neuralgia (Finnerup et al., 2010). However, the indiscriminate targeting of VGSC in the heart and or CNS greatly restricts the therapeutic index of this class and restricts patient population. Therefore, in the pursuit of improved efficacy, compound selectivity for Nav1.7 is a highly desirable aim. A group of small molecules recently identified have shown significant selectivity for hNav1.7 *in vitro*. The aryl-sulfonamide group function as gate modifiers and target a site distinct from the pore (Focken et al., 2016). Two such examples include PF-04856264 and CNV1014802 generated by Pfizer, both show low nanomolar selectivity for Nav1.7 (McCormack et al., 2013). Ahuja et al. (2015) revealed the structural basis of channel inhibition by using the bacterial VGSC Nab structure substituted with portions of Nav1.7 VSD4. The group demonstrated compound binding traps VSD4 in an activated conformation and thereby stabilises a nonconductive state of the channel. This mechanism has been referred to as 'voltage trapping'. Importantly, these small molecules are thought to target domains of the protein which have greater AA diversity, the extra-cellular domain of VSD IV for instance has attracted interest for this reason. *In vivo* studies performed in mice have supported the therapeutic potential of this class, orally available derivatives have shown good efficacy in neuropathic pain models, significantly reducing formalin-induced nociceptive behaviour (Pero et al., 2017).

Other therapeutic approaches include antibody mediated targeting of the channel. A monoclonal antibody (SVmab) was developed by Lee et al. (2014) and raised with an epitope against the voltage paddle domain (S3-S4 loops) of hNav1.7. This region is already targeted by a variety of toxins including protoxin II, however they have significantly lower selectivity than the antibody, which may be a function of the lipid

partitioning required for protoxin II's action (Henriques et al., 2016). The authors demonstrated a significant reduction in pain responses to formalin injections to the paw in mice whether the antibody was delivered intrathecally into the spinal cord, or systemically under the skin. Motor function was preserved, and the antibody was also able to reduce mechanical allodynia following CCI with no apparent increase in tolerance following multiple injections of SVmab. However, there has been difficulty in replicating these findings. Liu et al. (2016) attempted to replicate the antibody based on the sequence published. Unexpectedly, they found that SVmab did not bind the peptide immunogen, purified Nav1.7 DII voltage sensor domain, or Nav1.7 in live HEK293, U-2 OS or CHO-K1 cells. Consistent with this, the application rSVmab had no significant effect on Nav1.7 current. In an attempt to explain this discrepancy and as a rebuttal to Liu et al., the original group contrasted the efficacy of hybridoma-derived and recombinant SVmab antibodies (Bang et al., 2018). They too found that rSVmab was unable to substantially effect Nav1.7 currents, whereas SVmab replicated their original findings. They therefore proposed the discrepancy may be a function of the production process; it is thought that patterns of antibody glycosylation may differ between hybridoma and HEK293 systems, and this may, as a consequence, impede binding.

This study has important implications for Nav1.7 antibody production; the channel itself is known to be heavily glycosylated (see earlier), it is quite possible that the *in vivo* pattern of glycosylation does not match that found in heterologous expression systems. In addition to antibody glycosylation, post translational modification of Nav1.7 itself could sterically hinder epitope access. Therefore, a model in which hNav1.7 is expressed endogenously, such as that described in this thesis, could have value for screening purposes.

1.6 Human cellular models in pain research

In lieu of primary material, the field has historically depended on immortalised cell lines as *in vitro* tools, often with little characterisation of the cells themselves. Commonly used lines in pain research are the human neuroblastoma-derived cell line SH-SY5Y, and two dorsal root ganglion hybridoma cell lines, F-11 and ND7/23. Upon differentiation the cells acquire select morphological characteristics of PNS neurons including axon arborisation and rounded cell bodies, however, their transcriptional profiles diverge starkly from their primary counterpart (Kovalevich and Langford, 2013).

In ion channel research the most frequently used cell line is HEK293, derived from human embryonic kidney cells transformed with Adenovirus 5 sheared DNA (Graham et al., 1977). The cells are robust and easy to transfect with standard reagents, it is partly for this reason that they have become the *de facto* host for heterologously expressed ion channels. Single channel studies and whole cell recordings using this system are an essential element for characterising the biophysical properties of channels and the effects of associated mutations - particularly, as in this thesis, for the parsing of compound mutations. However, cellular background is important determinant of channel behaviour. Although considered to have a neutral background, there is some evidence to suggest HEK293 express voltage gated sodium channels endogenously, and Nav1.7 has in particular been characterised in these cells (He and Soderlund, 2010). Whether these endogenous channels have an appreciable effect on the recordings is debatable and owing to the age and dissemination of the line, these findings are perhaps unlikely to be relevant to all 'strains' of HEK293. More of a concern are the presence or absence of cellular cofactors and interactors of Nav1.7. Ion channels undergo extensive post translational modifications, with the majority thought to alter gating dynamics or channel recruitment. HEK293 are unlikely to express many of the endogenous interactors, indeed functional expression of the channel requires co-transfection of

VGSC beta subunits. The adoption and characterisation of a neuronal model capable of recapitulating endogenous expression of Nav1.7 and with a cellular milieu similar to primary counterpart is therefore highly desirable.

1.6.1 Developing alternative *in vitro* models, iPSC technology

Relevant *in vitro* models are an important complement to *in vivo* research. Unfortunately, as discussed in the section prior, the cell lines currently in use are unsatisfactory intermediates for the study of sensory biology and especially disorders afflicting this system. Further adding to the problem is scarcity of human primary tissue and, unlike rodent, culture conditions for primary human dorsal root ganglia have not yet been optimised. A significant advance for the field has therefore been the development of induced pluripotent technology in tandem with robust cellular differentiation protocols. Induced pluripotent stem cells are somatically derived pluripotent cells that are broadly indistinguishable from embryonic stem cells. The seminal paper by Yamanka et al. showed that the ectopic induction of just four transcription factors (TFs) is sufficient to reprogram a somatic cell to an induced pluripotent state (Takahashi and Yamanaka, 2006) - a theoretical tipping of Waddington's eponymous model of cellular fate. The four transcription factors: Oct3/4, Sox2, c-Myc, and Klf4, (herein referred to as OSMK) were identified through enrichment analysis of early murine embryonic tissue and embryonic stem cells. An EST database was used to acquire a list of transcription factors highly expressed in the pluripotent tissue. The group then performed a systematic screen of the 24 candidate TFs using a $Fbx15^{neo/neo}$ mouse. Fbx15 is selectively expressed in ESCs, but not in somatic cells, enabling G418 selection of cells possessing pluripotent traits. Integration of single TFs failed to produce G418 resistant colonies, whereas when multiple candidates were introduced a number of resistant colonies could be isolated. The group then

systematically eliminated individual factors until the four transcription factors OSMK were shown to be essential and sufficient for reprogramming somatic cells.

Refinements to the reprogramming process have now simplified the derivation and significantly increased the efficiency of generating iPSC (Hu, 2014). Complementing this has been the development of cellular differentiation protocols including many for neuronal lineages (Sances et al., 2016) (Shi, Kirwan and Livesey, 2012) (Ohlemacher et al., 2016). The capacity to generate a physiologically relevant cell type is naturally of interest to disease modelling. Critically the source of the cells can be patient derived, and thus their genetic background of disease is retained. For this reason, the neurodegenerative field have been quick to adopt the technology and a number of important insights into disease biology have already been gained which may not have been possible using conventional mouse models (Ryan et al., 2013) (Schwab and Ebert, 2015). In contrast, however, the pain field has been notably slower to engage. The rate limiting factor has been the slow development of appropriate differentiation protocols. Fortunately in 2012, Chambers et al. published a method for generating iPSC derived nociceptors using a small molecule based approach and dual SMAD inhibition. In doing so, the group brought to fore the prospect of modelling hereditary pain disorders, particularly those of congenital onset.

1.6.1.1 Considerations for use

Although iPSCs have many clear advantages, as with any model there are a number of experimental caveats associated with their use. Differentiated progeny of iPSCs appear in general to lack cellular maturity, most likely a by-product of the significant epigenetic erasure during the reprogramming process (Belinsky et al., 2014). Reassuringly, differentiated cells do appear to adopt more mature profiles with increasing time *in vitro*, however they are still likely representative of neonatal cell

types, developing the capacity to age neurons *in vitro* is therefore an important and active area of research. Perhaps the chief consideration for the purpose of disease modelling is evidence of significant interline variability. A number of factors underlie this heterogeneity which can be crudely grouped into technical, genetic and epigenetic factors, although it should be said these are not mutually exclusive. The contribution of epigenetic factors to iPSC variation has been well documented (Kim et al., 2010). iPSCs have been shown to retain residual DNA methylation signatures characteristic of their tissue origin, a phenomenon known as somatic memory. The persistent expression of somatic genes resulting from incomplete promoter DNA methylation can significantly affect differentiation capacity and bias lineage proclivity.

A number of recent studies have sought to account for the influence of genetic factors by profiling hundreds of iPSC lines (Kilpinen et al., 2017; Carcamo-Orive et al., 2017). Kilpinen et al. profiled 711 iPSC lines, finding that donor effects (differences between individuals) accounted for 5–46% of the variation in iPS cell phenotypes such as pluripotency, mRNA abundance and morphology. They found eQTLs (expression quantitative trait loci) contribute significantly to cross-individual variation. These studies are important for the analysis of complex gene traits, but also emphasise the challenge in extracting reproducible cellular phenotypes which may be buried in transcriptional noise, a result of inter-individual copy number variations in eQTLs. Together, these findings stress the importance of the use of multiple clones to investigate disease variants. However, this is not always practical for rare hereditary disorders such as CIP where the patient population is evidently limited.

A powerful technical approach to minimise the impact of cellular heterogeneity in phenotyping has recently emerged with the advent of site-specific nucleases such as CRISPR/Cas9. These genome editing technologies permit the *de novo* introduction or

correction of pathogenic variants and can thus be used to establish comparator 'isogenic lines'.

1.7 Genome engineering

The utility of a model system is dependent on its tractability. Genome engineering (GE) permits the delineation of genotype and phenotype and is a fundamental tool of modern research. The isolation of mutations may be the cornerstone of genetic analysis, but it is the subsequent manipulation that is required for meaningful interpretation. The GE field has developed rapidly in the past decade with three major waves of advances; the succession of each bringing an increase in precision and ease of targeting. The advent of the field began in the early 1980's. It was work performed in the model yeast *Saccharomyces cerevisiae* that established a paradigm for mammalian genome engineering. Rothstein et al. demonstrated exogenous DNA could be successfully integrated into yeast chromosomes by a process of homologous recombination (Orr-Weaver et al., 1981) and importantly this phenomenon was later replicated in mammalian cells (Thomas et al., 1986).

Targeting by unassisted homologous recombination requires the construction of long range homology repair (HR) templates, constructed as either substrates for gene replacement or gene insertion. The efficiency of such attempts is highly dependent on nucleotide homology and length of the HR arms. The first instance of targeting in embryonic stem cells described the disruption of the *Hprt* gene with a neomycin cassette (Thomas and Capecchi, 1987). The work was an elegant proof of principle, complemented by the judicious selection of the X-linked gene *Hprt* as the target.

Hprt $^{-}$ cells are selected by growth in the presence of the base analogue, 6 thioguanine (6-TG), which kills *Hprt* $^{+}$ cells, and since the gene is x-linked only one mutant copy was needed to yield the recessive *Hprt* $^{-}$ phenotype in male embryonic stem cells. The group were able to successfully target the loci with a vector containing 9.2kb of sequence homologous to the region. Until relatively recently, homologous recombination was the most commonly used method of genomic manipulation *in vitro*, particularly for the generation of knockout mouse models. However, the frequency of successful recombination events is typically very low, especially in iPSC, therefore significant effort has been invested in the development of new gene targeting techniques.

1.7.1 The advent of site specific nucleases

The development of site specific nucleases (SSN) followed the early observation that double stranded breaks in DNA significantly increased the rates of HDR by a two-to-three-fold magnitude (Szostak et al., 1983). Restriction endonuclease sites are typically too numerous to offer loci selectivity therefore attention turned to rare homing endonucleases in order to produce break sites near preferred loci. An early SSN strategy used the rare cutting meganuclease I-SceI, derived from *Saccharomyces cerevisiae* (Choulika et al., 1995). The nuclease has no known endogenous cutting sites within the mammalian genome, activity therefore requires the *de novo* introduction of the cognate 18bp recognition site into the desired genomic loci. The first use of I-SceI in mouse ESCs demonstrated a 50 fold increase in targeting at a selectable locus (Cohen-Tannoudji et al., 1998). Although effective, the approach permits only a two step (or greater) process of gene targeting at a defined locus, limited by the *a priori* introduction of the I-SceI cutting site.

Chimeric programmable nucleases soon followed, simplifying the process and allowing endogenous loci to be targeted in a single step. Engineered nucleases are composed of the sequence specific DNA-binding domains fused to a non-specific DNA cleavase. A customisable DNA binding domain is central to their use and hence they are often referred to as 'designer nucleases'.

1.7.2 Zinc finger nucleases (ZFNs)

Zinc finger nucleases were one of the first engineered site specific nucleases to be developed (Durai, 2005), they are artificial bipartite proteins consisting of fokI endonuclease linked to Cys_2His_2 zinc-finger DNA binding domain. The zinc finger motifs are arranged in a multi-array structure consisting of 3-6 fingers - it is these motifs that confer nucleotide specificity. Each zinc finger contains the motif $X_2–C–X_{2-4}–C–X_{12}–H_{35}–H$ which, when chelated with a zinc ion, forms a ββα fold capable of making specific contacts with approximately three bases in the major groove of double-stranded DNA. However, in order for DNA cutting to occur, the fokI domain must first dimerise, ZFNs are therefore constructed as pairs enabling the specific targeting of long (18-36bp) and potentially unique recognition sites. The construction of ZFNs is technically challenging. Early efforts used a modular approach, joining individual pre-characterised finger units. This approach was context independent and suffered from high failure rates (Kim et al. 2009; Ramirez et al. 2008). Later improvements sought to account for the known context dependent behaviour of individual fingers – a 'context sensitive' approach (Sander et al., 2011). Iterations of this method largely comprise of sequential screening of combinatory pairs using phage display or bacterial two hybrid models. This approach significantly increases targeting efficacy however it is fairly laborious one, leading many to turn to commercially validated ZFNs at significant expense.

1.7.3 Transcription activator-like effector nucleases (TALENS)

Researchers frustrated with the technical challenges associated with ZFN assembly were soon presented with an alternative option: transcription activator-like effector nuclease (TALENS) (Sanjana et al., 2012). TALENS share a similar bipartite structure to ZFNs comprising of a fokI endonuclease and DNA specific binding domain. The latter structure is formed from modular tandem repeat arrays 34 amino acids in length. The AA sequence is largely invariant between each monomer, save for two critical residues known as the repeat variable di-residue (RVD). It is the RVDs that impart nucleotide specific binding to the TALE domain; each RVD recognises one nucleotide with some degeneracy and no apparent context dependence thereby offering a simple cipher amenable to experimental use (Moscou and Bogdanove 2009). The requirement, as with ZFNs, for dimerisation prior to nuclease activity means that off-target cutting is generally low. TALENS has been used successfully in iPSC cells, and exhibit lower toxicity than ZFNs (Hockemeyer et al., 2011) (Ye et al., 2014) (Chen et al., 2014). However, there are site selection restrictions owing to the T- base requirement in -1 position.

1.7.4 Clustered regularly interspaced short palindromic repeats–CRISPR-associated proteins (CRISPR-Cas)

The arrival of CRISPR-Cas9 has revolutionised the genome engineering field and, seemingly, usurped the use of older site specific nucleases. The simplicity and flexibility of the system has served as a potent democratizer of the technology, with the broad scientific community adopting the system to great effect. The CRISPR Cas system is an adaptive immune mechanism common to many bacterial and Archaea phyla (Marraffini et al., 2010) and is designed to prevent the invasion of foreign DNA elements such as viruses and plasmids (Fig. 1.4). The system is remarkably diverse, reflecting a rapid

evolution resulting from dynamic selection pressures and in particular, the competitive

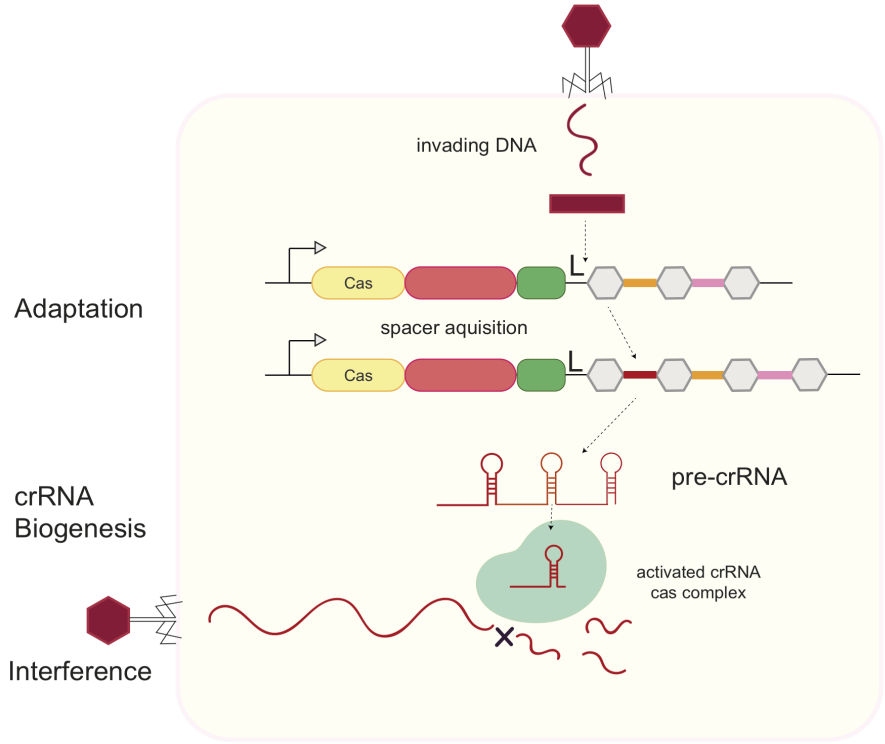


Figure 1-4 Overview of the CRISPR/Cas mechanism

During the first phase of the system foreign nucleic acids are recognised by Cas proteins, and short fragments (30–50 base pairs) of invading DNA, termed protospacers, are acquired. Protospacer selection is non-random and depends on the presence of a flanking 2–5 bp nucleotide protospacer adjacent motif (PAM), the sequence of which is species and system specific. Spacer acquisition is complex, and details have only recently been revealed. The proteins Cas1 and Cas2 appear to be essential for spacer acquisition in the majority of CRISPR-Cas systems. The two proteins form a stable complex (Cas1-Cas2) and act as an integrase in which Cas1 serves a catalytic role, essential for spacer acquisition and Cas2 has a predominantly structural function (Nuñez et al., 2014). Spacers are integrated between the leader end (indicated by L) and the first repeat of the CRISPR array, maintaining a chronological record of previous infections. The crRNA biogenesis or 'expression stage' involves transcription of the CRISPR locus, often as a single transcript. Maturation of the pre-crRNA therefore requires nucleolytic processing, for type I systems this is performed by Cas6 endoribonuclease of the cascade complex. In the type II system, pre-crRNA processing relies on trans-acting crRNA (tracrRNA) which is complementary to the repeat sequence. The tracrRNA binds to the pre-crRNA in the presence of Cas9 (which is thought to stabilise the tracrRNA:crRNA duplex) endogenous RNAse III then cleaves the pre-crRNA at the repeat, this is then followed by trimming of the 5' end to remove flanking repeat sequences and a portion of the spacer (Amitai and Sorek, 2016). The processed, mature crRNAs guide Cas proteins to complementary targets, for type II interference (predominantly used in GE), Cas9 in complex with tracrRNA and crRNA scans the target DNA for the cognate PAM sequence before probing for sequences complementary to the crRNA (Jiang et al., 2016). Recognition induces a structural change and R-Loop formation which triggers to the cleavage of the target and non-target strand, mediated respectively by the Cas9 HNH and RuVC endonuclease domains.

coevolution of virus encoded anti-CRISPR proteins (Hynes et al., 2018). The lack of universal *Cas* genes and the heterogeneity of the system means it cannot be classified using a single phylogenetic tree and therefore has been divided into two main classes, each with a number of subtypes. The classes differ in their effector modules; RNA guided target cleavage in class I (subtypes I, III, and VI) requires elaborate multiprotein complexes whereas type II (subtypes II-A, II-B, II-C) utilise simple, single-protein effectors. (Makarova et al., 2011). Though class I is far more common in bacteria, comprising approximately 90% of CRISPR-Cas systems, it is type II that is predominantly used for genome engineering, as such, this class will be discussed in greater detail.

1.7.4.1 Adapting to suit, development and adaptation of CRISPR-Cas9 to a mammalian system

The functional characterisation of native type II systems was fundamental to the repurposing of CRISPR-Cas. The most commonly used class II Cas protein, Cas9, was first discovered by bioinformatic analysis in 2002 and identified as a large multifunctional protein with two putative nuclease domains, HNH and RUVC (Jansen, et al., 2002). Eight years later, Garneau et al. (2010) demonstrated in *Streptococcus thermophilus* that Cas9 mediates target phage DNA cleavage *in vivo.* The next critical component of the system to be discovered was tracrRNA. The maturation of cRNA, an integral event in CRISPR activation, had previously been shown to be catalysed by a selection of endoribonucleases (Bhaya, Davison and Barrangou, 2011), however homologues of these proteins were missing in many subtypes. Deltcheva and colleagues identified tracrRNA, a small 24 nucleotide trans-activating crRNA (tracrRNA), complementary to the repeat region of the precursor cRNA (Deltcheva et al., 2011). They showed in *S.pyogenes* that this tracrRNA is sufficient to

direct the maturation of cRNAs by complexing with endogenous RNAse III and Cas9, ultimately conferring sequence specific immunity against invading genomes.

Following these mechanistic insights, work rapidly began to co-opt the system for gene editing. In 2013, the seminal paper by Cong et al. described the first instance of genome engineering using the *S.pyogenes* Cas9 in eukaryotes (Cong et al., 2013). Use in human and other mammalian cells has required codon optimisation and the addition of a nuclear localisation sequence to the Cas9 protein. The assembled functional Cas9 complex has been further streamlined via the fusion of crRNA-tracrRNA, yielding a chimeric, single-guide RNA (sgRNA) such that the experimenter need only modify a short 20 nucleotide sequence appropriate to the target for efficient cleavage.

1.7.4.2 Gene editing, manipulating the repair

The most active repair pathway in eukaryotes is non homology end joining (NHEJ), the pathway operates throughout the cell cycle and predominantly results in the insertion or deletion of a few nucleotides (indels) (Chang et al., 2017). The second pathway, homology directed repair (HDR), is by contrast, restricted to only S & G2 phase; operating concurrently, and competitively, with NHEJ (Jasin and Rothstein, 2013). In order for HDR to occur, double stranded breaks need to undergo endo and exonucleic processing, exposing a 3' hydroxyl overhang. This end resection blocks canonical NHEJ, but also permits repair via alternative-NHEJ, meaning therefore, there is a second tier of competition for error free repair. The resectioned ends allow strand evasion mediated by the recombinase RAD51. In the normal physiological process the sister chromatid functions as the repair template in S Phase, mediating perfect repair. For genome engineering purposes the repair template is provided in trans, either as a dsDNA or as is the case in this work, a single stranded oligonucleotide donor (ssODN). Quite in contrast to gene targeting templates historically used, the length of homology

required for small edits is short, homology of >60bp seems to be sufficient for HDR (Kim et al., 2014). Interestingly, the non-canonical pathway operating concurrently during G2 phase can also be manipulated for precise editing and repair. The CrisPITCH method uses the MMEJ (microhomology mediated end joining) pathway to produce precise repairs and target knock in (Sakuma et al., 2016). The vector template contains very short microhomology regions (15-20bp) flanking the desired repair element, and two artificial sgRNA sites either side which are linearised in addition to cutting of the gene target upon Cas9 expression. The authors' strategy proves fairly efficient in HeLa cells but has yet to be shown in iPSC. Finally, although rather vexatious in the pursuit of homology directed repair, NHEJ can be purposefully employed for the rapid generation functional knockouts. The indels associated with this repair mechanism can be suitably targeted to critical protein domains in order to disrupt function, as is to be shown.

1.7.5 Challenges of genome engineering

One of the major challenges in the GE field is extrapolation of editing efficiency between cell types, whilst many papers will purport increased efficiency, the audience to which this offers any real experimental value is often to those only working on the same cell type. Often the exemplary cells lines used have idiosyncratic repair pathway defects or alterations in DNA repair mechanisms compounding the issue (Boyer et al., 1995). In addition to cell type efficiency, it is difficult and often not appropriate to draw comparisons between differing target loci as Cas9 has been shown to be highly sensitive to cellular chromatin dynamics. Heterochromatin structures have been shown to block Cas9 activity and a strong correlation exists between successful gene editing and chromatin accessibility. Interestingly, chromatin structure may not completely inhibit Cas9 targeting per se but have a greater influence on the nuclease activity. D.Cas9 (catalytically dead Cas9) can successfully localise to sites within closed chromatin, albeit

at lower efficiency (Polstein et al., 2015), however successful gene edits of heterochromatin are significantly reduced. Nucleosome occupancy is also detrimental to nuclease activity, perhaps unsurprising given the evolutionary origins of the system - it is unlikely to be optimised to explore and modify large chromatin-bound eukaryotic genomes. The addition of chromatin remodelling enzymes *in vitro* can restore Cas9 access to nucleosomal DNA, however given the importance of chromatin states to the pluripotency of iPSC, a blanket application of such remodelling agents may be ill-advised.

Common to all gene editing tools is the potential for off-target activity, although the targeting of Cas9 to DNA loci is thought to be tightly controlled by the specific 20 nucleotide sgRNA and the requirement for the PAM motif, a number of papers have shown off-target cleavage activity (Lin et al., 2014) (Cho et al., 2014) (Pattanayak et al., 2013). There appears to be a degree of tolerance (3-5bp) for mismatches in the PAM-distal part of the sgRNA sequence. Interestingly, analysis by ChIP-sequencing suggests that Cas9 DNA *binding* is far more promiscuous than DNA cleavage (Wu et al., 2014), suggesting that DNA binding per se is not sufficient to direct DSB and a multi-step process including conformational change within the activated structure is required. This finding complicated original *in silico* predictions of sgRNA off-target sites. However, the field is rapidly refining predictive tools incorporating training data from experimental sources (Wilson, O'Brien and Bauer, 2018). Other efforts to mitigate off-target activity include protein engineering of Cas9 to enhance specificity, notable examples include SpCas9-HF1 (Kleinstiever et al.,2016), eSpCas9 (Slaymaker et al., 2016) and HypaCas9 (Chen et al., 2017). Continued developments in both sgRNA selection and greater knowledge from structural studies are likely to further reduce the risk of off-target activity, an important goal for future therapeutic use.

A challenge to the gene editing of iPSCs is the fragility of this cell type - it has, and continues to be, a major limiting step for iPSC genome engineering. Cellular detachment and single cell dissociation cause considerable cell death, such that the cloning efficiency of dissociated iPSC cells is <1%, thus clonal isolation is difficult, if not impossible (Watanabe et al., 2007). Yet, this is absolutely required for derivation of edited lines therefore one of the most significant advances in the gene editing field, (specific to stem cells) have been improvements in clonal survival. The discovery that Y-27632, a selective inhibitor of p160-Rho-associated coiled-coil kinase (ROCK), could significantly improve survival following single cell dissociation has been a critical advance.

Genome engineering remains intrinsically challenging in this cell type due to a variety of other factors including low transfection rates and poor tolerance to culturing stress causing a loss of "stemness". That said, the prospect of an essentially unlimited resource with which to model pathogenic variants makes gene editing in iPSC extremely worthwhile to pursue. The creation of isogenic lines significantly increases the robustness of the data gathered from iPSC models and for monogenic pain disorders can essentially solve the issue of patient recruitment.

Main aims of the thesis:

- To optimise and generate iPSC CRISPR-Cas9 gene editing workflow
- To generate gene edited isogenic iPSC lines for functional interrogation of human Nav1.7
- To characterise the neuronal localisation of hNav1.7 *in vitro*

Chapter 2 General methods

2.1 General Cell Culture

All tissue culture techniques were performed under a sterile class II biosafety cabinet. Cells were maintained in an atmosphere of 5% (v/v) carbon dioxide at 37°C in humidified incubators.

2.1.1 HEK293T Culture

Human Embryonic Kidney 293T (HEK293T) sourced from ATCC (CRL-11268) were cultured in DMEM + Glutamax (ThermoFisher), supplemented with 10% FBS (Gibco) and maintained in T-75 TC treated flasks (Greiner). Cells were passaged at 85% confluency and routinely split at 1:20 ratio using Versene EDTA (Gibco). Cultures greater than P.30 were discarded and fresh stocks were thawed.

Cryopreservation of HEK293T

Adherent cells were lifted using Versene EDTA (Gibco), spun at 500 x g in Mg^{2+}/Ca^{2+} free PBS for 5 minutes and resuspended in chilled freeze medium consisting of 10% DMSO, 20% FBS and 70% DMEM. Cryotubes were transferred to Mr Frosty (Nalgene) for slow cooling before being transferred 12 hours later to a liquid nitrogen tank for long term storage.

2.2 iPSC culture

2.2.1 Derivation of iPSC

Healthy control iPSCs were derived from fibroblasts as described in (Clark et al. 2017). AD2 (termed HC1 throughout the study) from 51-year-old male, was reprogrammed by non-integrating Sendai viral vectors using the CytoTune™-iPS Reprogramming Kit (ThermoFisher). NHDF (termed HC2 throughout the study) from 44-year-old female,

was reprogrammed with retroviral vectors (Addgene: 17220: pMXs-hc-MYC, 17219: pMXs-hKLF4, 17218: pMXs-hSOX2, 17217: pMXs-hOCT3/4, 13354: pMXs-Nanog). AH017-7 (termed HC3 throughout the study) from 67-year-old female, was reprogrammed using the tetracistronic Sendai virus vector 40 SeVdp(KOSM)302L.

CIP iPSC patient lines were obtained through the IMI/EU sponsored StemBANCC consortium via the Human Biomaterials Resource Centre, University of Birmingham, UK (http://www.birmingham.ac.uk/facilities/hbrc). Fibroblasts from CIP 1 (31-year-old male) and CIP 2 (34-year-old male) were reprogrammed using the CytoTune™-iPSC Reprogramming Kit (ThermoFisher) to generate two clones from CIP 1 (CIP1.1, and CIP1.2) and one from CIP 2 (CIP2). All iPSC lines were subject to quality control checks. This included CytoSNP analysis (Illumina CytoSNP-12-v2.0 array) and pluripotency characterisation. All cells were karyotypically normal and negative for mycoplasma.

2.2.2 Culture of iPSCs under feeder-free conditions

2.2.2.1 iPSC basement membrane preparation

iPSC grown in feeder-free conditions require the use of a specialist basement matrix membrane in order to maintain viability and pluripotency. Matrigel matrix (Corning) was used as a coating solution for all growth vessels. Plates were prepared as follows: an aliquot of Matrigel was slowly thawed and added to chilled KnockOut DMEM (ThermoFisher), 1 ml of the prepared solution was used to coat a growth area of 9.5 cm^2 (scaled as appropriate), coated dishes were placed at 37°C for a minimum of 40 minutes before use.

2.2.2.2 iPSC maintenance and routine passaging

iPSCs were fed once daily with warmed mTeSR (StemCell Technologies) medium. Cells were passaged twice per week before they reached 100% confluency at a 1:3 ratio. Routine passaging was achieved using Versene EDTA; cells were washed twice with

Mg^{2+}/Ca^{2+} free PBS, and room temperature Versene EDTA was added to the wells, plates incubated at 37°C for a minimum of 5 minutes and a maximum of 10. The Versene was gently aspirated and mTeSR was used to flush the cells from the plate taking care not to dissociate cell clumps. The cell suspension was gently dispensed into Matrigel coated dishes using a 5 ml stripette.

2.2.2.3 Single cell passaging

For single cell isolation, required either for clonal or counting purposes, passaging was performed using Accutase (Gibco) or TryplE (Gibco). iPSCs were washed twice with Mg^{2+}/Ca^{2+} free PBS and the prewarmed reagent was added to the wells. Plates were incubated for 5 minutes and the dissociated cells were added to a falcon containing ~8ml of PBS then spun at 400 x g for 5 minutes. The cell pellet was resuspended in in the required volume of mTeSR, supplemented with the Rho Kinase inhibitor Y-27632, 10 μM (Tocris). iPSCs were dispensed into Matrigel coated dishes.

2.2.2.4 Cryopreservation of iPSC

Cells were lifted using Accutase, spun at 400 x g for 5 minutes and resuspended in chilled mTeSR. 2X freeze media containing [20% DMSO, 60% ESC qualified FBS, 20% Knock Out DMEM (all Invitrogen)] was added dropwise at a 1:1 ratio. Cryotubes were immediately transferred to a Mr Frosty and placed at 80°C. Twelve hours later, cells were transferred to a liquid nitrogen tank for long term storage.

2.3 Nucleic acid techniques

2.3.1 PCR

PCR Primer design

In general, primers were designed using the tool available in the Benchling application suite (http://benchling.com). Optimal design parameters included a melting temperature of 60°C with 50% GC content and length between 19-24 bp. Where possible, a GC clamp was included at the 3' of the oligonucleotide. Unless otherwise stated, all primers were purchased de-salted from IDT Technologies and resuspended in ddH_2O prior to use.

2.3.1.1 General PCR

PCR reactions were generally assembled in a 20μl reaction size, using Phusion DNA polymerase (ThermoFisher/New England Biolabs) and run using the following cycling conditions: 98°C for 3 min, 35 x [98°C 30 sec, X°C 30 sec, 72°C 1 min], 72°C 5 min, where X is the optimum Tm for the primer pair.

2.3.1.2 Touchdown PCR

'Touchdown PCR' was used for challenging amplicons - generally all Nav1.7 genomic sequences. For the first ten cycles a higher annealing temperature than the predicted optimum Tm for primer pairs was used (Tm+10°C). At every cycle the annealing temperature was decreased by 1 °C until Tm -1 °C was reached. At that point, 25 further cycles at the predicted optimum Tm were used.

2.3.1.3 PCR product purification:

PCR products were purified with one of two methods, either DNA precipitation (see Ethanol Precipitation of DNA) or with Genejet PCR Purification Kit (ThermoFisher). In brief, a 1:1 volume of Binding Buffer was added to the PCR product, pH was adjusted where required with 3 M sodium acetate and the solution was passed through a

purification column. The supernatant was discarded, and the column was washed twice with an ethanol-based wash buffer. Products were eluted with 20µl ddH_2O.

2.3.2 DNA techniques

2.3.2.1 DNA extraction

Genomic DNA was isolated from pelleted cells using PureLink Genomic DNA Mini Kit (Invitrogen) according to the manufacturer's instructions. DNA was eluted in 50µl of ddH_2O.

2.3.2.2 Ethanol precipitation of DNA

Where required, DNA was concentrated following extraction using ethanol precipitation. 0.1 volumes of 2M sodium acetate and 2.5 volumes of 100% ethanol were added to DNA. The solution was briefly vortexed then incubated -20°C for at least 20 minutes prior to centrifugation at 16,000 x g for 15 minutes. The supernatant was removed, and the pellet was washed once in 70% ethanol, before being spun again at 16,000 x g for 1 minute. The supernatant was discarded, and the pellet was dried under vacuum before being resuspended in ddH_2O.

2.3.2.3 DNA gel electrophoresis

DNA fragments were separated on horizontal agarose gels by electrophoresis.

The concentration of agarose varied depending on the size of DNA fragments to be resolved, typically 2% w/v for fragments <500bp, 1.5% <2000bp, 0.8%<10,000bp. Agarose (Sigma Aldrich) was added to TAE buffer (1 x TAE 40 mM Tris-acetate and 1 mM EDTA at pH 8.3.), the solution was boiled and ethidium bromide (Sigma) 0.5 µg/ml was added immediately prior to use. Once set, agarose gels were run in a Bio-Rad Gel

Electrophoresis tank with TAE running buffer at constant voltage. The following DNA standards were used to infer DNA fragment length; 100bp DNA ladder (NEB), QuickLoad 1kb ladder (NEB), Promega 1kb ladder. Gels were visualised using a UV transilluminator.

2.3.3 Quantification of nucleic acid concentration and quality

DNA and RNA were quantified using Nanodrop x100. Absorbance was read at 260nm with a co-extinction coefficient of 50 ng-cm/µl for dsDNA and 40 ng-cm/µl; RNA.

Nucleotide quality was inferred from 260/280 and 260/230 ratios, where 'pure' DNA/RNA was considered to be: ~ 1.8 DNA, ~2.1 RNA.

2.3.4 Sanger sequencing

In preparation for sequencing plasmids were diluted to 100ng/µl and PCR products; 5ng/µl in ddH_2O. Sequencing primers were diluted to 3.2 pmol/µl. All Sanger sequencing reactions were performed by Source Bioscience Ltd, Nottingham, UK.

The resulting chromatograms were read with either 4Peaks or Snapgene Viewer software.

2.3.5 RNA techniques

2.3.5.1 RNA extraction

Cells were rinsed with PBS and lysed *in situ* using 500 µl of Trizol (ThermoFischer). Samples were either stored at -80°C or processed immediately for RNA extraction. RNA was extracted using a hybrid method comprising a phenol-chloroform extraction with silica column purification. In brief, chloroform (Sigma-Aldrich) was added in a 1:5 ratio. Samples were vigorously shaken and incubated at room temperature for 2 min prior to centrifugation at 12,000 x g for 15 min at 4°C. The aqueous phase was transferred to 1:1

ratio of 100% ethanol, briefly vortexed then applied to a ROCHE High pure Silica column. The column was spun at 14,000 x g for 1 minute and the elute was discarded. An on-column Genomic DNA digestion step was performed using the supplied DNase for 15 minutes at room temperature. The column was washed once with buffer WB1, and twice with buffer WB2. Before the final elution, the column was spun 'dry' for 3 minutes at max speed to eliminate residual ethanol. RNA was eluted in either 35 µl of tris-EDTA buffer or ddH_2O.

2.3.5.2 cDNA synthesis

RNA was reverse transcribed using Roche Evoscript Universal cDNA Master mix. Samples were incubated with Evoscript Buffer on ice for 25 minutes to allow the propriety mix of random and oligo(dT)18 primers to anneal to the RNA. 2 µl of reverse transcriptase enzyme mix was added and the samples were incubated in VWR Doppel PCR machine using the following programme; 42°C for 15 min, 85°C for 5 min, 65°C for 15 min. cDNA samples were stored at -20°C until further use.

2.3.6 qPCR

2.3.6.1 qPCR primer design

All qPCR primers were designed using NCBI Primer-BLAST (https://www.ncbi.nlm.nih.gov/tools/primer-blast/). For multi-exon genes, intron spanning primers were used. Primer efficiency and specificity were validated, only those demonstrating 90-110% efficiency and a single band product were used for experiments. Primer efficiency was calculated using:

$$Efficiency = (10^{-1/slope} - 1) \times 100$$

2.3.6.2 qPCR running conditions and analysis

Relative quantification of mRNA transcript expression was performed using SYBR Green Chemistry. In brief, 10 µl reactions comprising 5 ng cDNA, 0.5 µM Primer mix, and 2 X SYBR Green Master Mix (Roche) were amplified on Light cycler 480 II system (Roche) in 384 well plates sealed with adhesive film (ThermoFisher).

Samples were run on a 45 cycle protocol: 95°C initial denaturation, 45 cycles of 95°C 5 sec (denaturation), 60°C 10 sec (annealing), 72°C 10 sec (acquisition).

Relative mRNA abundance was quantified using the ΔΔCT method (Livak and Schmittgen 2008). Unless otherwise stated the housekeeping gene YWHAZ was used to normalise the data, the gene was selected as it appeared the most stable of a selection of housekeeping genes tested.

2.4 Immunocytochemistry

2.4.1 Glass coverslip preparation

To increase neuronal adherence, all coverslips intended for neuronal cultures were treated before use. #1.5 German Borosilicate glass coverslips (VWR) were cleaned and acid etched with 3:1 Hydrochloric and Nitric acid solution for a minimum of 2 hours with occasional agitation. Coverslips were washed extensively with ddH_2O then stored in 100% ethanol prior to use.

2.4.2 Cell fixation and immunocytological staining

Cells were fixed *in situ* on glass coverslips using 4% paraformaldehyde (PFA), (Invitrogen). Cells were, in general, washed once with Mg^{2+}/Ca^{2+} PBS as the inclusion of ions appeared to better stabilise the cultures. Room temperature PFA was gently dripped onto the cells and coverslips were incubated for 10-15 minutes at room

temperature. Cells were washed twice with PBS then blocked for 30 minutes with Blocking solution containing 0.1% Triton-X 100, 5% Normal Goat/ Donkey Serum (both, Sigma). Primary antibodies (Table 2.1) were diluted in blocking solution and applied overnight at 4°C or 1 hour if performed at room temperature. Unadsorbed primary antibody was removed with two PBS washes and the relevant species-specific secondary antibody was applied (again diluted in blocking solution). Coverslips were incubated in the dark at room temperature for 2 hours, washed 3 times in PBS before mounting in Vectorshield with or without DAPI (Vector Biolabs). Coverslips were sealed with nail polish and stored at 4°C if not immediately imaged.

2.4.3 Image acquisition

Unless stated otherwise, confocal microscopy was performed using a Leica LSM-700 system with Zen 2012 software. Image processing was performed using FIJI.

Table 2.1 List of antibodies used

Antibody	Source	Identifier	Usage concentration
Rabbit anti-Brn3a	Millipore	Cat# AB5945, RRID:AB_92154	1:400
Mouse anti-Isl1/2	DSHB	Cat#39.4D5, RRID:AB_2314683	1:200
Rabbit anti-Oct4	Cell Signalling Technology	Cat# 2890, RRID:AB_2167725	1:100
Rabbit anti-Nanog	Cell Signalling Technology	Cat#4903 RRID:AB_10559205	1:100
Chicken anti-NF200	Abcam	Cat# ab4680, RRID:AB_304560	1:10,000
Rabbit anti-SCN2B	Cell Signalling Technology	Cat#14686	1:1000
Mouse anti-NF200	Abcam	Cat#ab3966, RRID:AB_2282509	1:1000
Rabbit anti-HA	Cell Signalling Technology	Cat# 3724, RRID:AB_1549585	1:750 (ICC), 1;1000 (WB)
Mouse anti-HA	Sigma-Aldrich	Cat# A2095, RRID:AB_257974	1:400
Mouse anti-βActin	Sigma-Aldrich	Cat# A5316, RRID:AB_476743	1:20,000
Rat anti-MBP	Abcam	Cat# ab7349, RRID:AB_305869	1:400
Mouse anti-S100	Abcam	Cat# ab14849 RRID:AB_301508	1:400

Phalloidin-Tetramethylrhodamine B isothiocyanate (TRITC)	Sigma-Aldrich	Cat: P1951, RRID: AB_231514	1:100
Amersham ECL Mouse IgG, HRP-linked whole antibody (from sheep)	GE Healthcare Life Sciences	Cat# NA931V, RRID: AB_772210	1:10,000
Amersham ECL rabbit IgG, HRP-linked whole antibody (from donkey)	GE Healthcare Life Sciences	Cat# NA934V, RRID: AB_772206	1:10,000
Donkey anti-rabbit IgG Alexa 488	Thermo Fisher Scientific	Cat# A-21206, RRID:AB_2535792	1:1000
Donkey anti-rabbit IgG Cy3	Jackson Immuno Research Labs	Cat# 711-166-152, RRID:AB_2313568	1:500
Donkey anti-mouse IgG Alexa 488	Thermo Fisher Scientific	Cat# A-21202, RRID: AB_141607	1:1000
Goat anti-chicken Alexa 488	Thermo Fisher Scientific	Cat# A-11039, RRID: AB_2534096	1:1000
Donkey anti-rabbit IgG Alexa 546	Thermo Fisher Scientific	Cat# A10040, RRID: AB_2534016	1:1000
Goat anti-rabbit IgG Alexa 488	Thermo Fisher Scientific	Cat# A-11008, RRID:AB_143165	1:1000

2.5 Bacterial techniques

2.5.1 *Escherichia coli* strains

The *Escherichia coli* strains used for plasmid propagation can be seen in Table 2.2

Table 2.2 *Escherichia coli* strains and genotype

NEB Stable (NEB)
F' *proA+B+ lacI*^{q} *Δ(lacZ)M15 zzf::Tn10* (Tet^{R}) *Δ(ara-leu) 7697 araD139 fhuA ΔlacX74 galK16 galE15 e14- Φ80dlacZΔM15 recA1 relA1 endA1 nupG rpsL* (Str^{R}) *rph spoT1 Δ(mrr-hsdRMS-mcrBC)*
DH10Beta (NEB)
Δ(ara-leu) 7697 araD139 fhuA ΔlacX74 galK16 galE15 e14- ϕ80dlacZΔM15 recA1 relA1 endA1 nupG rpsL (Str^{R}) *rph spoT1 Δ(mrr-hsdRMS-mcrBC)*
DH5alpha (NEB)
fhuA2 Δ(argF-lacZ)U169 phoA glnV44 Φ80 Δ(lacZ)M15 gyrA96 recA1 relA1 endA1 thi-1 hsdR17
XL-gold (Stratagene)
endA1 glnV44 recA1 thi-1 gyrA96 relA1 lac Hte Δ(mcrA)183 Δ(mcrCB-hsdSMR-mrr)173 tet^{R} *F'[proAB lacI*^{q}*ZΔM15 Tn10(Tet*^{R} *Amy Cm*^{R}*)]*

2.5.2 Bacterial growth media

Solid media

Luria Broth (LB) agar plates were prepared by adding 32.5 g of LB-Agarose (Lennox variety, Invitrogen) to one litre of distilled water. The solution was

autoclaved and allowed to cool to approximately 55C before the required selective antibiotic was added. The media was poured into sterile Petri Dishes (ThermoFisher) and allowed to cool next to an open flame. Plates were Para-filmed and stored at 4°C for a maximum of 4 weeks until required.

Liquid media

LB Broth was prepared using 20 g of LB Broth Powder (Lennox variety) (Invitrogen) dissolved in one litre of distilled water. The solution was autoclaved and stored at room temperature. Selective antibiotics were added immediately before use. Super Optimal broth with Catabolite repression (S.O.C) media was used for outgrowth steps prior to antibiotic selection (Invitrogen).

Media additives

Antibiotics for plasmid selection were used at the following concentrations: Ampicillin (Sigma), 100µg /ml, Kanamycin (Sigma), 30µg /ml. Stocks were prepared at 1000x concentration and stored at -20°C.

2.5.3 Transformation of plasmids,

Escherichia coli were transformed using the heat shock method as follows: cells were thawed on ice, 1µl of plasmid DNA was added without repeat pipetting. Suspensions were gently tapped 5 times, left on ice for 15 minutes, then heat shocked at 42°C. for 45 seconds. Cells were subsequently transferred to S.O.C media for outgrowth and incubated at 37°C, 250RPM for 1 hour prior to plating on selective LB-Agar plates

2.5.4 Digestion of DNA using restriction enzymes

In general, restriction digests of plasmid, or PCR products were performed in a 50 µl reaction mix consisting of 1 µl of restriction endonuclease (all NEB), 5X Cutsmart Buffer,

1 µl of enzyme, 1 µg DNA. Reactions were incubated at the optimum temperature for the enzyme.

2.5.5 Ligation of insert and vector DNA

Ligation of DNA fragments for plasmid assembly were performed with a 3:1 insert to vector molar mass ratio. Reactions were assembled in a 10µl volume with the following: 1µl 10x Ligase Buffer, 1µl T4 Ligase (NEB), DNA, ddH_2O and incubated overnight at 16°C. Cells were transformed with 1µl of the ligation reaction

2.5.6 Colony PCR

For rapid screening of bacterial transformants, colony PCR was occasionally used as an intermediary selection step before further analysis. An individual colony was gently touched with a sterile 10µl pipette tip and the tip was swirled 8 times into a standard PCR Mix.

2.5.7 Miniprep of plasmid DNA

Plasmid DNA was isolated from 6 ml overnight cultures using Qiagen Miniprep kit, briefly, pelleted cells were resuspended in P1 buffer, lysed using P2 lysis buffer for 2 minutes with constant inversion and neutralised with buffer N3. The solution was then spun for 15 min at 15,000 x g to pellet the flocculant. The supernatant was passed through a silica matrix column washed with WB1 then WB2 and finally eluted with 30µl pre-warmed ddH_2O.

2.5.8 Midiprep of plasmid DNA

Midipreps were used for larger preparations of Plasmid DNA where greater than >1mg was required. A single transformant colony was used to inoculate a 5ml

'starter culture' and grown for 8 hours at 37°C, 500µl was then dispensed into 200ml of selective LB broth, incubated for 16 hours overnight. DNA was isolated using Zymo Fast Midiprep kit (Zymo), according to manufacturer's instructions. Plasmids were eluted with warmed 100µl ddH_2O.

2.5.9 Plasmid storage

Stable vectors were stored as glycerol stocks consisting of 750µl overnight culture and 250µl of glycerol (Sigma). The solution was vortexed to mix and stored at -80°C indefinitely. Unstable plasmids, including all cDNA Nav1.7 constructs, were stored as plasmid preparations at -20°C and retransformed as required.

2.6 Protein techniques

2.6.1 Protein solubilisation

Radioimmunoprecipitation assay buffer (RIPA buffer) was routinely used to solubilise cellular proteins for immunoblotting applications using the following commercial preparation (Sigma, Aldrich) comprising 25 mM Tris, pH 7.4, 137. mM NaCl, 50 µM EDTA, 1 %. Triton X100, 0.5% sodium deoxycholate, 0.1% SDS (Sigma). In all instances, protease inhibitors (Roche complete mini protease cocktail; Naf 50mM, PMSF 0.5mM (both Sigma) were added immediately prior to use.

2.6.2 BCA assay

Total protein concentration was determined using BCA (BiCinchoninic Acid) assay kit (Pierce, thermofisher). 200µl of the premixed cupric sulfate, bicinchoninic acid reagent was added to protein samples run in duplicate. After incubation for 1 h at 37 °C absorbance of the coloured complexes was assayed at 562 nm using a colour-metric

plate reader (iMark™ Microplate Absorbance Reader, Biorad). Protein concentrations were determined based on the standard curve of known concentrations (20-400 μg/mL) of the reference protein, bovine serum albumin (BSA).

2.6.3 Band densitometry

Band intensities were quantified using FIJI, image J. In brief, the area under the peak for each band was recorded and a ratio was generated by dividing the sample value by the reference value.

2.7 Software and applications

Table 2.3 Commercial software used

Name, version	Source	Use
IN Cell Developer Toolbox analysis software build 1.9.2	G.E.	Image analysis
Prism 6.0	GraphPad software	Graphs, statistical tests
FIJI/image J	NIH	Image analysis
Benchling (web application)	https://benchling.com	General molecular biology applications
ZEN Black 10.0	ZEISS Microscopy	Image analysis
4PEAK	Nucleobytes	Chromatogram viewer

Chapter 3

Investigating the impact of Nav1.7 CIP variants on channel properties and cellular excitability

3.1 Introduction

Congenital insensitivity to pain is a rare heredity disorder with a global prevalence estimated to be less than one in a million individuals. The disorder typically presents in childhood with recurrent incidents of self-mutilation and a history of painless bone fractures. CIP is caused by bi-allelic pathogenic mutations SCN9A, the gene encoding the voltage gated sodium channel Nav1.7. To date, all mutations associated with the disorder cause a loss of prototypical channel function. Many pathogenic variants are situated in DII, a central transmembrane domain of the channel and thus abolish voltage gated conduction of sodium ions. The scarcity of the disorder has, in part, frustrated mechanistic studies of the underlying pathophysiology. Significant questions remain as to the locus of action, and the discrepancies observed between animal models of the disorder - where although loss of mNav1.7 function recapitulates insensitivity to acute noxious thermal and mechanical stimuli, neuropathic pain appears to be at least partly preserved (Gingras et al., 2014).

A number of mechanisms, which are not mutually exclusive, have been proposed for this phenotype. The channel kinetics could position Nav1.7 as a threshold channel (Cummins, Howe and Waxman, 1998), amplifying sub-threshold depolarisations in nociceptor terminals, by virtue, conferring a critical role for Nav1.7 in action potential electrogenesis. Nav1.7 may also be necessary for action potential propagation along

axons and neurotransmitter release at central terminals, in an analogous fashion to the olfactory system where it has been suggested to regulate synaptic signalling (Weiss et al., 2011). Finally, Nav1.7 may intersect with other signalling systems, such as endogenous opioids, which are up-regulated in the absence of Nav1.7 in mice and thought to feedback onto DRG neurons/terminals to suppress excitability (Minett et al., 2015).

The contribution of the channel to human nociceptor conduction has recently been challenged. Zhang et al. (2017) concluded that there may be a relative dearth of Nav1.7 in human DRG neurons, and although Nav1.7 makes a significant contribution to the TTX-sensitive sodium current in rodent, the authors suggest this may not similarly be the case in humans. This conclusion was largely based on the use of protoxin II as a specific Nav1.7 blocker (Sokolov et al., 2008). Application of this peptide to human DRG *in vitro* failed to significantly impact TTX-S currents. However, within the same study they also describe PF-05089771, another putatively selective Nav1.7 inhibitor (Alexandrou et al., 2016), fully inhibiting TTX-s currents.

The striking loss of pain sensation in CIP patients, in absence of other clinically remarkable features (aside for anosmia) clearly position the channel as a highly attractive therapeutic target. There is a strong impetus for the development of novel analgesics, with a significant unmet clinical demand for treatment of common acquired pain disorders. A greater understanding of the contribution of Nav1.7 to the human nociceptive system should facilitate this effort and help to resolve conflicting data.

Recent advances in induced pluripotent stem cell technology have permitted *in vitro* modelling of a number of neurological disorders via the differentiation of somatic cells derived from affected patients. We describe here the generation of functional iPSC-derived nociceptors from two CIP patients both harboring compound heterozygous mutations in Nav1.7 and begin to investigate the impact loss of Nav1.7 function has on

the intrinsic excitability of the neurons. We first characterised the effect of the pathogenic variants on the channel biophysics in a heterologous expression system.

Chapter aims:

- Generate and characterise iPSC-nociceptors derived from CIP patients
- Investigate the spectrum of VGSC expression in iPSC-nociceptors
- Perform site directed mutagenesis of Nav1.7 cDNA constructs to isolate CIP patient mutations and characterise the impact of the variants on Nav1.7 biophysical properties.

3.2 Chapter Methods

3.2.1 Site directed mutagenesis of Nav1.7 cDNA constructs.

The mutations isolated from the patient CIP1: R830X and FS1773 and CIP2: R896W, were introduced into the bicistronic Nav1.7 cDNA vector p.cD-SCN9A-IRES-DSRED (gift, James Cox, published in (Cox et al., 2006)) using site directed mutagenesis. Complementary forward and reverse primers 30bp in length were used with the nucleotide substitution situated centrally within the string (underlined/ demarcated). The following primer sets were used:

Table 3.1 Site directed mutagenesis primers

Mutation	Forward 5'-3'	Reverse 5'-3'
R830X (CIP1)	CAGACTGCTC**T**GAGTCTTCAAG	CTTGAAGACTCAGAGCAGTCTG
FS1773 (CIP1)	GATGTTCTATGG|GTTTGGGAGAAG	CTTCTCCCAAACCCATAGAACATC
R896W (CIP2)	TACGCTCCCA**T**GGTGGCACAT	ATGTGCCACCATGGGAGCGTA

The PCR reaction was performed in a 50µl volume (10X buffer, 1µg plasmid template, 150ng forward and reverse primers, 8µl DMSO, *Pfu* polymerase 2.5 U) and the run conditions were as follows:

Table 3.2 PCR cycling conditions for SDM

Step	Temperature/ Time	No. of cycles
Initial denature	95°C, 3 min	1
Denaturation	95°C, 60 sec	25
hybridisation	55 °C, 60 sec	
Elongation	68 °C, 26 min	
Final Elongation	68 °C, 20 min	1

Reaction parameters were optimised and extension time was significantly extended to allow for proper amplification of the large, 13 kb template. DMSO was also added above recommended reaction concentrations to relax the strong secondary structure present in the plasmid (noted during optimisation of the protocol). DpnI was added to the reaction product and incubated for a minimum of 6 hours at 37℃. Prior to transformation the PCR product was concentrated by ethanol precipitation (Methods 2.3.2.2) and reduced to a 10µl volume. The entire reaction was then used to transform XL-Gold cells (Method 2.5.3). Cells were plated on ampicillin LB Agar plates and incubated at 37℃ overnight. Individual colonies were picked and used to inoculate liquid cultures for plasmid isolation. To ensure that no unintentional mutations were introduced as a result of polymerase error the plasmid was sequenced in its entirety. Following successful verification of vectors, a larger scale preparation of DNA was performed as in (Method 2.5.8), save liquid cultures were grown at a lower temperature (32℃) than normal, since Nav1.7 containing plasmids are prone to spontaneous recombination and appear to be cytotoxic when incubated at higher temperatures. In view of this, Sanger sequencing was repeated following the final plasmid preparation.

3.2.2 Transfection of cDNA constructs in HEK293T

Human embryonic kidney HEK-293T cells ($3x10^6$) were transfected using the jetPEI transfection reagent (Polyplus-transfection Inc.) with either the wild-type or mutant NaV1.7 channel combined with β1 and β2 subunits (plasmid: pcDNA-SCN1B-IRES-SCN2B-IRES-eGFP) at a 40:1 ratio. The transfection was performed using a 'reverse' protocol; DNA:PEI (3:1) complexes were added to cells immediately after passaging whilst they were in suspension. Recordings were made 72-96 hours after transfection.

3.2.3 HEK-293T voltage clamp.

Whole-cell voltage clamp experiments were performed on HEK293T cells showing both red and green fluorescence in the expectation that such cells were expressing Nav1.7, in combination with β1 and β2 subunits. All the recordings were conducted at room temperature using an Axopatch 200B Amplifier, the Digidata 1550B Low Noise Data Acquisition System and the pClamp10.6 software (Molecular Devices). Data were filtered at 5kHz and digitized at 20kHz. Capacity transients were cancelled, and series resistance compensated at 70-90% in all experiments. The extracellular solutions contained (in mM): 140 NaCl, 3 KCl, 1 $CaCl_2$, 1 $MgCl_2$, 10 HEPES, pH 7.3 with NaOH (adjusted to 320 mOsm/L with glucose). Patch pipettes were filled with an internal solution containing (in mM) 140 CsF, 10 NaCl, 1 EGTA, 10 HEPES, pH 7.3 with CsOH (adjusted to 310 mOsm/L with glucose) and had a typical resistance of 2-3MΩ.

3.2.4 Neuronal differentiation of iPSCs

iPSCs were differentiated following a previously published protocol (Chambers et al. 2012) with modifications. In brief, iPSCs were passaged using Versene EDTA (ThermoFisher) and plated at high density. Neural induction commenced with the addition of SMAD inhibitors SB431542 (Sigma, 10 μM) and LDN-193189 (Sigma, 100 nM) to KSR base medium (Knockout-DMEM, 15% knockout-serum replacement, 1% Glutamax, 1% nonessential amino acids, 100 μM β-mercaptoethanol, (ThermoFisher)). Three additional small molecules were introduced on day 3: CHIR99021 (Sigma, 3 μM), SU5402 (R&D Systems, 10 μM) and DAPT (Sigma, 10 μM). The dual SMAD inhibitors were withdrawn on day 5. The base medium was gradually transitioned to N2/B27 medium (Neurobasal medium, 2% B27 supplement, 1% N2 supplement, 1% Glutamax, (ThermoFisher)) in 25% increments. Cells were re-plated onto treated (General methods) glass coverslips at day 12 of the differentiation in N2/B27 medium supplemented with

four recombinant growth factors at 25ng/ml (BDNF; ThermoFisher, NT3, NGF, GDNF; Peprotech). CHIR90221 was included for 4 further days. Laminin (Cultrex Mouse Laminin I, R&D systems, 500ng/ml) was included in long-term maintenance medium from 25 days onwards. Medium changes were performed 2-3 times weekly. Where required, cultures were treated with the anti-mitotic agent AraC (1µm, Sigma) for <4 days to eliminate non-neuronal cells.

3.2.5 End point RT-PCR

End-point reverse transcriptase PCR (RT-PCR) was used to analyse VGSC transcripts expressed in iPSC-nociceptors. Primers were designed to span intron boundaries to exclude genomic DNA amplification. For each reaction 5 ng of cDNA (synthesised as in Method 2.3.5.2) was used with Phusion polymerase using standard PCR conditions, amplification was limited to 30 cycles. End products were loaded on a 2% agarose/ethidium bromide gel, run and visualised as described in Method 2.3.2.3. The following primers were used:

Table 3.3 RT-PCR primer sets

Oligonucleotides 5'-3'	Gene
TGTCTCGGCATTGAGAACATT	SCN1A F
ATTGGTGGGAGGCCATTGTAT	SCN1A R
TCTAAGCGTGTTTGCGCTAAT	SCN2A F
ACCATTCCCATCCAATGAATTGT	SCN2A R
AGAGGAGGTCCATGCCAAAC	SCN3A F
GCTTCACAGAGTTGCAGTGAC	SCN3A R
GCCAGAGGCTACAACTGAGG	SCN8A F
CGCCCGTAGGAGGCTAATTG	SCN8A R
GGCATAGGCGAGCACATGAA	SCN9A F
AACAAGGAGCCACGAATGCT	SCN9A R

ATCCGTTCTACAGCACACACC	SCN10A F
GCACTAAACCGGGAAATGGT	SCN10A R
CCTTCAGAGTGCTCAGGGTC	SCN11A F
CTCCGACAGAGTTGCCGATT	SCN11A R

3.2.6 qPCR of mRNA transcripts

qPCR reactions were performed as in Method 2.3.6 with the following primer sets:

Oligonucleotide 5'-3'	Gene
GGCATAGGCGAGCACATGAA	SCN9A F
AACAAGGAGCCACGAATGCT	SCN9A R
CCTGCATGAAGTCTGTAACTGAG	YWHAZ F
GACCTACGGGCTCCTACAACA	YWHAZ R

3.2.7 RNA-seq and PCA analysis

RNA from 4 HC lines (HC1, HC1.2, HC2, HC3) was extracted from 60DIV iPSC-nociceptors using the protocol described in general methods. Samples were submitted for RNA sequencing at the Oxford Genomics Centre. Sequencing was performed using the Illumina HiSeq4000 with paired end 75 bp reads. Principal component analysis (PCA) was performed by Dr Georgios Baskozos as follows. Publicly available RNA-seq data was mapped in GRC.h.38 Human Genome using the STAR aligner (Dobin et al. 2013) with the ENCODE standard options. Read counts were calculated at the gene level using HTSeq (Anders et al. 2015) and the ENSEMBL gene set annotation GRC.h.38.88. Raw counts were normalised using the effective library size and transformed using the variance stabilising transformation (VST) in R using DESeq^2 (Love et al. 2014). Principal component analysis (PCA) plots were generated from 100 randomly selected samples per GTEx human tissue, the human iPSC and iPSC-nociceptor, the single-cell Human iPSC and iPSC-nociceptor and the human DRG RNA-seq data. The top 500 ENSEMBL genes ranked by the standard deviation of their VST counts were selected for PCA. Data was

centred and scaled before PCA and samples are projected to standardised components. Ellipses represent the 95% confidence interval of a tissue's gene expression distribution. Distances between samples in the plot are proportional to Mahalanobis distance, i.e standard deviations from a distribution's mean. Data for comparison were obtained from the following sources: Human DRG L2 RNA-seq data are from 6 consent donors previously published (Ray et al. 2018) and is available at phs001158.v1.p1. Single cell RNA-seq human iPSC and iPSC-nociceptor data are previously published (Schwartzentruber et al. 2018) and is available at ERP020576. Human tissue raw counts (including whole blood, skin, fibroblasts) were downloaded from GTEx V7 Human tissues.

3.2.8 Patch clamp

iPSC nociceptors were assessed for their biophysical properties 50-70 DIV, where 0 is replating and transition to maintenance media. Whole-cell patch clamp recordings using an Axopatch 200B amplifier and Digidata 1550 acquisition system (Molecular Devices) were performed at room temperature (22°C). Data were low-pass filtered at 2 kHz and sampled at 10 kHz. Series resistance was compensated 60-80% to reduce voltage errors. All data were analysed by Clampfit 10 software (Molecular Devices). Current clamp. Filament borosilicate glass capillaries (1.5 mm OD, 0.84 mm ID; World Precision Instruments) were pulled to form patch pipettes of 3–5 MΩ tip resistance and filled with internal solution containing (mM): 130 KCl, 1 $MgCl_2$, 5 MgATP, 10 HEPES, and 0.5 EGTA; pH was adjusted to 7.3 with KOH and osmolarity set to 305 mOsm. Extracellular solution was perfused at a continuous rate of 1ml/min and contained (mM): 140 NaCl, 3 KCl, 2 $MgCl_2$, 2 $CaCl_2$, 10 HEPES and 10 glucose; pH was adjusted to 7.3 with NaOH and osmolarity was set to 315 mOsm. Resting membrane potential was assessed in bridge mode, while firing properties were assessed in current clamp mode. Input

resistance (RInput) was derived from the membrane potential deflection caused by a 20 pA hyperpolarising current pulse at -60 mV. Cells were depolarised from a holding potential of -60 mV by current steps (50 ms) of increasing magnitude (Δ10 pA) until an action potential was generated, to determine rheobase. Repetitive firing was evoked by prolonged (500ms) depolarising steps of increasing increments (Δ25 pA). The ability of neurons to fire at high frequency was assessed by seventeen current stimuli of 1.5x rheobase (50ms) given at 20Hz.

Data Acknowledgements:

Dr Iulia Blesneac performed voltage clamp of HEK293T. Patch clamp of iPSC-nociceptors was performed by Dr. Gregory Weir using iPSC-nociceptors I generated and maintained.

3.3 Results

3.3.1 Pathogenic SCN9A variants identified in CIP1 and CIP2

The patient CIP1 and in the late stages of this work, patient CIP2, were recruited into Painful Channelopathies Study, NRES reference: 12/LO/0017. Phenotyping of the patients was performed by Prof Bennett and Dr Thermistocleous (see Appendix), both patients had an established CIP diagnosis and a typical history of painless injuries (burns, wounds, bone fractures) from early childhood.

Whole genome sequencing of proband (CIP1) revealed compound heterozygote mutations in exons 16 and 27 of SCN9A. The paternal allele showed a cytosine to thymine substitution c.2488C>T, producing a premature stop codon R830X. A novel mutation was identified in exon 27 of the maternal allele (c.5318delA), leading to frame shift mutation FS1773. CIP2 also harboured compound heterozygous SCN9A mutations, including an intronic variant c.377+5C>T and as cytosine to thymine substitution c.2686C>T in exon 16 R896W (Figure 3.1). A summary of the mutations and predicted effect on the Nav1.7 protein structure can be found in Table 3.4

Table 3.4 SCN9A mutations found in the CIP patients CIP1 and CIP2

Identifier	Compound Heterozygote	Mutation	Description	iPSC clones
CIP1	Y	c.2488C>T; p.R830X	Introduces premature stop codon in exon 16	CIP1, CIP1.2
		c.5318delA; p.FS1773	Deletion, leads to a frameshift in the c-terminal of the channel affecting exon 27	
CIP2	Y	c.377+5C>T	Intronic variant predicted to alter splicing	CIP2
		c.2686C>T; p.(R896W)	Substitution of a highly conserved residue in exon 16	

A

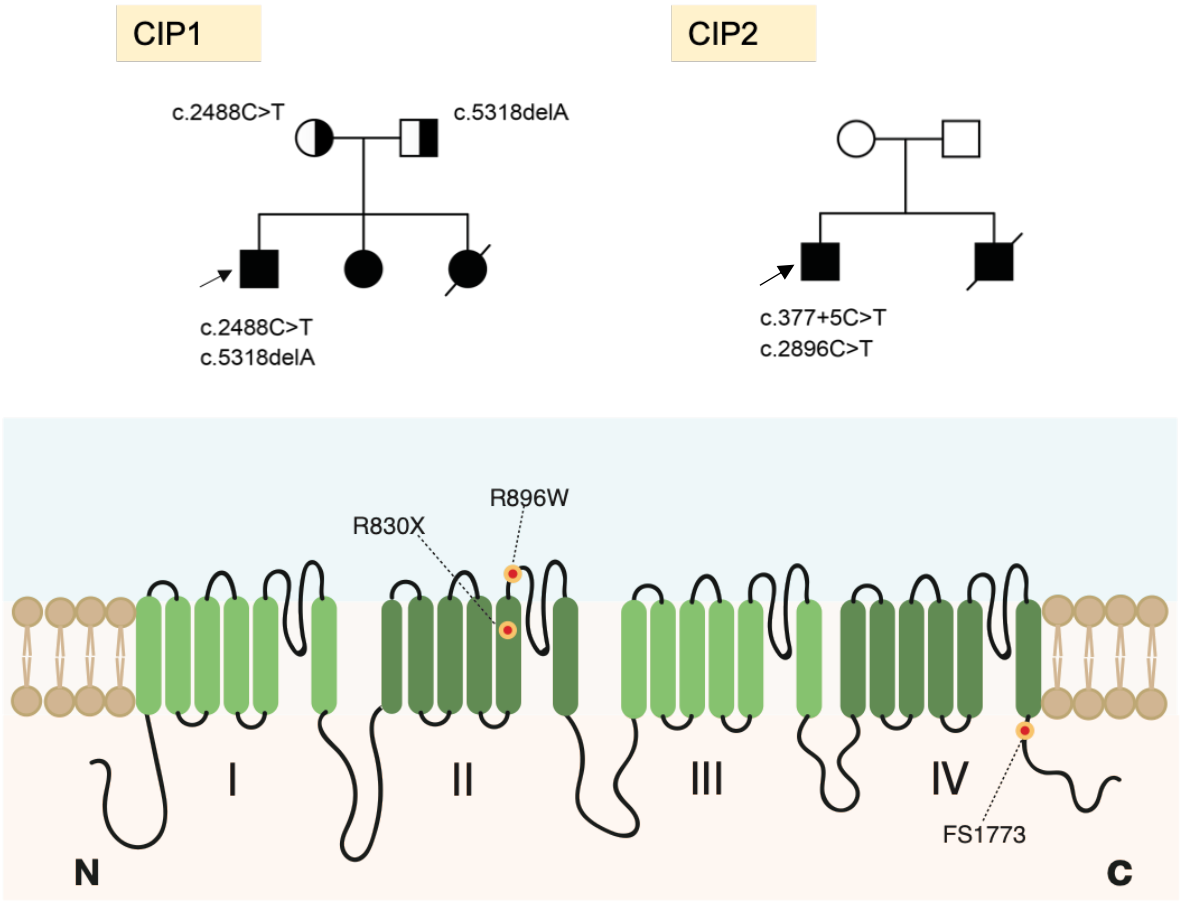


Figure 3-1 Pathogenic SCN9A variants identified in patients CIP1 and CIP2.

Family pedigree for CIP1 (left) and CIP2 (right); arrow indicates proband. Genotyping of CIP2 parents was not performed. (B) Schematic of Nav1.7 membrane topology. Nav1.7 shares canonical VGSC form with 4 protein domains (numbered) consisting of 6 transmembrane alpha helices (cylinders). CIP mutations are represented with red dots. Both R830X and R896W affect residues in domain II. R830X produces a premature stop codon in S5, R896W is missense substitution occurring at a conserved position within in the extracellular loop between the S5 and S6 transmembrane segments of the domain, whilst FS1773 is located in the C-terminal tail of the channel. N and C indicate the N-terminus and C-terminus of the peptide chain respectively.

3.3.2 Functional analysis of exonic CIP1 and CIP2 variants in HEK293T

The co-expression of multiple VGSCs in neuronal cells often with overlapping currents, hinders the biophysical characterisation of individual channels. Prior to investigating Nav1.7 in an endogenous model of expression, we first used a heterologous HEK293T expression system to dissect the individual impact of each of the compound mutations harboured by the CIP patient CIP1 and the exonic variant of patient CIP2.

To determine the effect of each variant on channel function, the mutations were independently introduced into a SCN9A cDNA construct encoding the NM_20977.3 transcript - this corresponds to the full length adult Nav1.7 isoform (see Appendix). Nucleotide substitutions were performed using site directed mutagenesis of the bi-cistronic vector p.cD-SCN9A-IRES-DSRED (Fig. 3.2). Verified sequences of the successfully mutated plasmids can be seen in (Fig. 3.3).

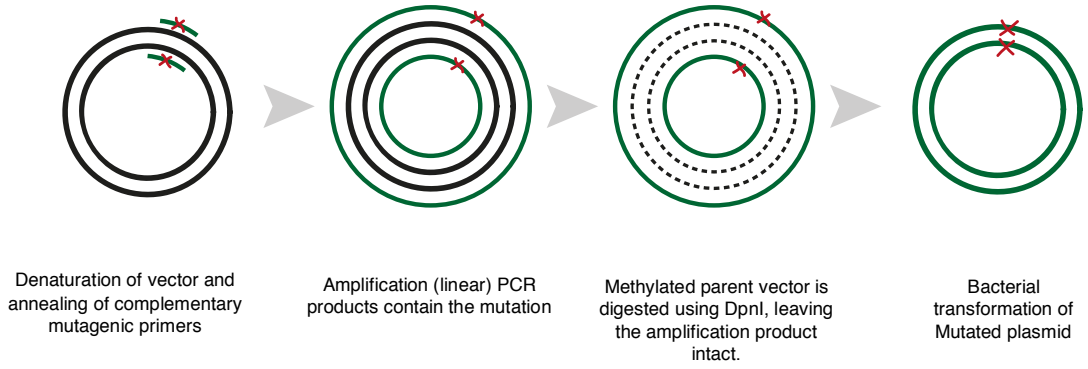


Figure 3-2 Site directed mutagenesis outline

The whole plasmid is amplified using complementary primers containing the desired mutation. The reaction proceeds in a linear rather than exponential fashion. Following amplification, the methylated parent template is digested using the methylation sensitive endonuclease DpnI, sparing the mutant product. Bacterial transformation of the reaction leads to recovery of mutant clones.

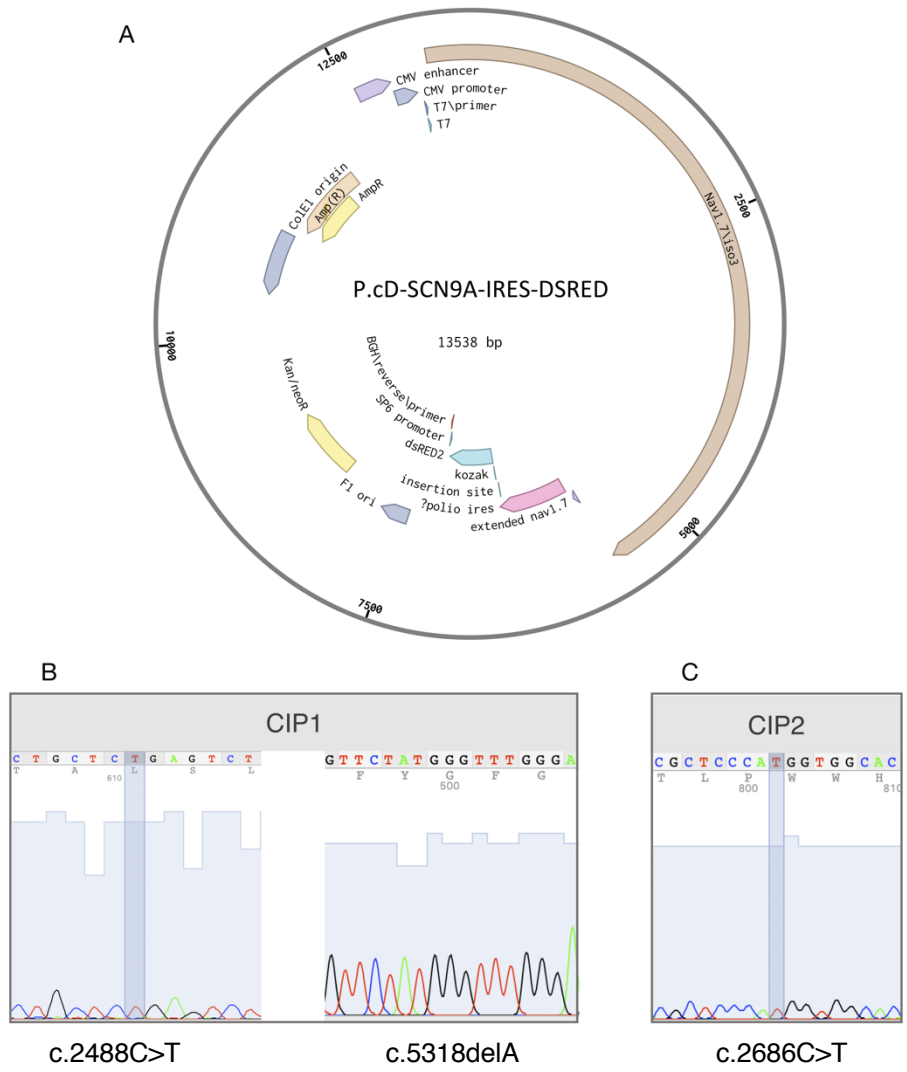


Figure 3-3 Verification of mutated cDNA constructs

(A) Plasmid map of Nav1.7 cDNA vector P.cD-SCN9a-IRES-DSRed. Nav1.7 expression is driven by the ubiquitous CMV promoter. A polio derived IRES sequence is located 3' to Nav1.7 forming a bi-cistronic ORF allowing the independent translation of the red fluorophore DsRed. (B, C) for each mutation the verified sequence is shown.

Each construct was transfected into HEK293T cells together with the plasmid p.SCN1B-SCN2B-IRES-GFP expressing the β1 and β2 sodium channel subunits. Surprisingly, we were unable to observe expression of the red fluorophore using conventional forward transfection. This was despite robust expression of GFP from the co-transfected ß subunit vector and (data not shown) currents from DsRed negative cells. This required

a modification of the transfection method and a reverse protocol was adopted. We were subsequently able to isolate cells expressing both GFP and DsRed, although still noted that red fluorescence was poor and lagged 72 hours behind GFP expression (Fig.3.4, A) Sodium currents were examined using whole cell patch clamp recording of $GFP^+/DsRed^+$ cells. A voltage step to -10mv was applied to the cell from the holding potential -100mV to elicit channel current. Representative whole-cell voltage clamp currents from transfected cells are shown in (Fig.3.4, B & C).

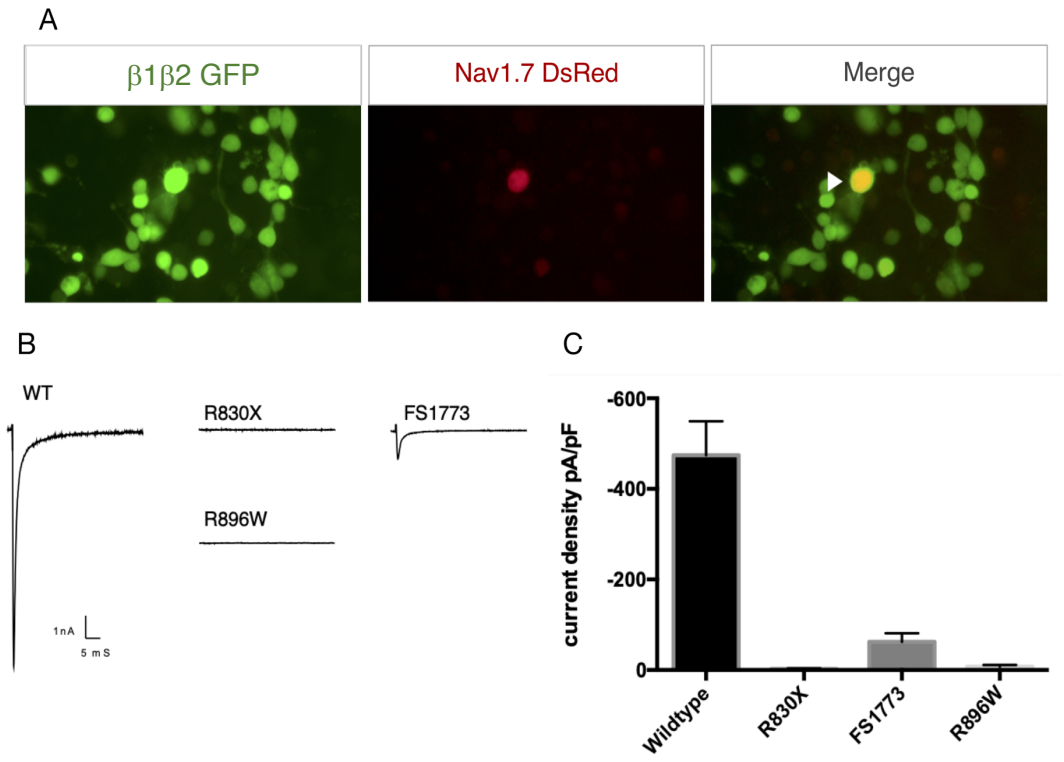


Figure 3-4 Voltage clamp of HEK293T transfected with Δ SCN9A cDNA constructs

(A) GFP and DsRed fluorescence of HEK293 cells transiently co-transfected with plasmids P.cD-SCN9a-IRES-DSRed and p.SCN1B-SCN2B-IRES-GFP. Note the disparity between number of GFP^+ and $DsRed^+$ cells. (B) Representative currents elicited by a test potential at -10mV from a holding potential of -100 mV for the WT, R830X, R896W, or FS1773 channels. (C) Summarised data for whole-cell current density elicited by a test potential at -10 mV from a holding potential of -100 mV for the WT (-474.2 ± 75 pA/pF, n = 17), R896W (-7.6 ± 3.8 pA/pF, n=9), R830X (-2.8. ± 0.9 pA/pF, n=8) and FS1773 (-62.2 ± 18.8, n=8). Data are presented as mean ± SEM. For all, $P \leq 0.0001$ compared with WT. Statistical test performed using one-way ANOVA combined with Dunnett's post hoc analysis for multiple comparisons.

Each mutation drastically reduced Nav1.7 current. The mutations R830X and R896W abolished sodium conductance to negligible levels. The C-terminal mutation FS1773 also significantly decreased ($P<0.0001$) Nav1.7 associated current, however a small, likely physiologically irrelevant fraction of current was produced - approximately 8-fold lower than the control construct. The result suggests at least in a heterologous system, a fraction of the truncated protein can transit to the cell surface. This finding is consistent with other C-terminal CIP associated mutations (Emery et al., 2015).

3.3.3 Studying Nav1.7 in a system of endogenous expression

Following the biophysical characterisation of the CIP mutations we next sought to examine their impact in an endogenous model of expression using iPSC technology. The utility of an iPSC-based model fundamentally depends on the capacity to differentiate a relevant cell type. The heterogeneity of the DRG and model specificity are important considerations for the purposes of *in vitro* modelling. The desired cell type suitable for downstream analysis within this work is the nociceptor, and importantly, Nav1.7 expression is thought to be the highest in this class of afferent. The majority of sensory neuron differentiation protocols described to date have sought to generate nociceptors and have done so via experimental recapitulation of the key developmental signalling pathways. We describe here the differentiation of healthy and patient derived iPSC using the previously published (Chambers et al., 2012) protocol, with minor modifications.

Reprogramming of donor fibroblasts to iPSCs was performed as described in General Methods, by the StemBancc Consortium. In total, three control lines (HC1-3) and three patient lines (CIP1.1, CIP1.2, CIP2), were used for the study. The described CIP

mutations were verified in the iPSC using Sanger sequencing (Fig.3.5). Prior to use in the differentiation, each line was subject to cytoSNP analysis to confirm absence of chromosomal aberrations that can accumulate during the reprogramming process and during subsequent cellular passaging. All lines showed normal karyotype. All clones exhibited a compact morphology and high nuclear to cytoplasmic ratio characteristic of pluripotent cells. The canonical pluripotency marker Oct4 was selected for ICC to confirm pluripotency and cultures were highly enriched (Fig.3.6). If patches of differentiation appeared during the course of expansion, they were manually removed prior to passaging.

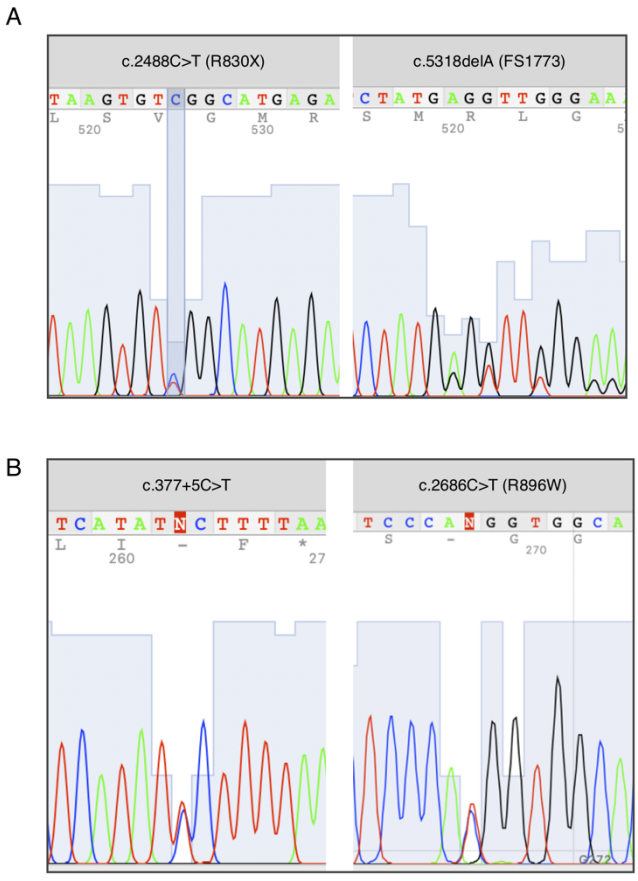


Figure 3-5 Sanger sequencing of CIP iPSC line mutations

Genomic DNA was extracted from the iPSC lines CIP1.1, CIP1.2 and CIP2 and each pathogenic SCN9A variant was verified by Sanger sequencing. Chromatograms from CIP1.1 (A) and CIP2 (B).

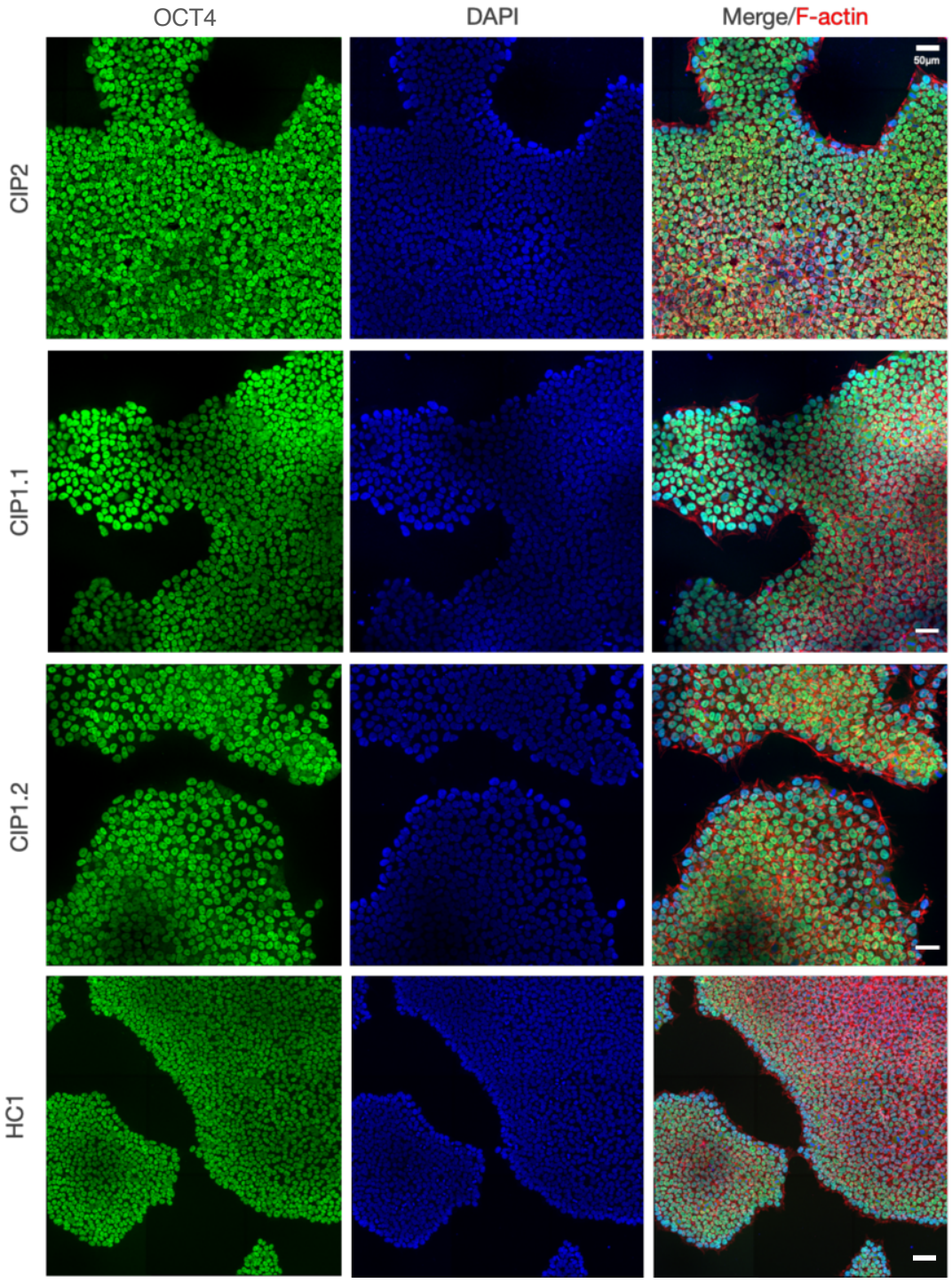


Figure 3-6 Patient and healthy control iPSC stained with pluripotency marker OCT4

Patient-derived and healthy control lines were highly enriched for the pluripotency marker OCT4. Representative images of co-immunostained cultures. Separated channels showing OCT4 (green), DAPI (blue) and merged images with the actin marker F-actin (red). Scale bar: all 50 µm

Thawed iPSCs were passaged twice before commencing the differentiation as efficiency was notably lower in lines differentiated immediately post-thaw. Prior to the addition of small molecules, iPSC were seeded in mouse embryonic fibroblast conditioned medium (MEF-CM) supplemented with FGF2 to synchronise the population in the 'primed' state in order to increase intrinsic cellular propensity for differentiation (Takahashi et al., 2018). One to two days following addition of MEF-CM, the program of differentiation was initiated per the protocol outlined in (Fig. 3.7, A). Cellular morphology flattened and proliferation rapidly increased until approximately day 4. Pronounced clustering and rounding of cells appeared in patches from day 8 onwards, these areas correlated with the highest rates of neurogenesis and were an early indicator of a successful differentiation. Early neurites became visible between cells at approximately day 10 (Fig. 3.7, D). On day 12, cells were passaged and seeded on Matrigel coated coverslips; after settling, neurons rapidly extended neurites. Following re-plating, small molecule treatment ceased, and cultures were maintained thereafter using long term maintenance medium (N2M) supplemented with recombinant growth factors. No overt morphological differences between healthy and CIP lines were observed. Following long-term culture, the cells autonomously clustered into ganglion like structures with extensive neurite outgrowth and round, phase-bright somas (Fig. 3.7, E).

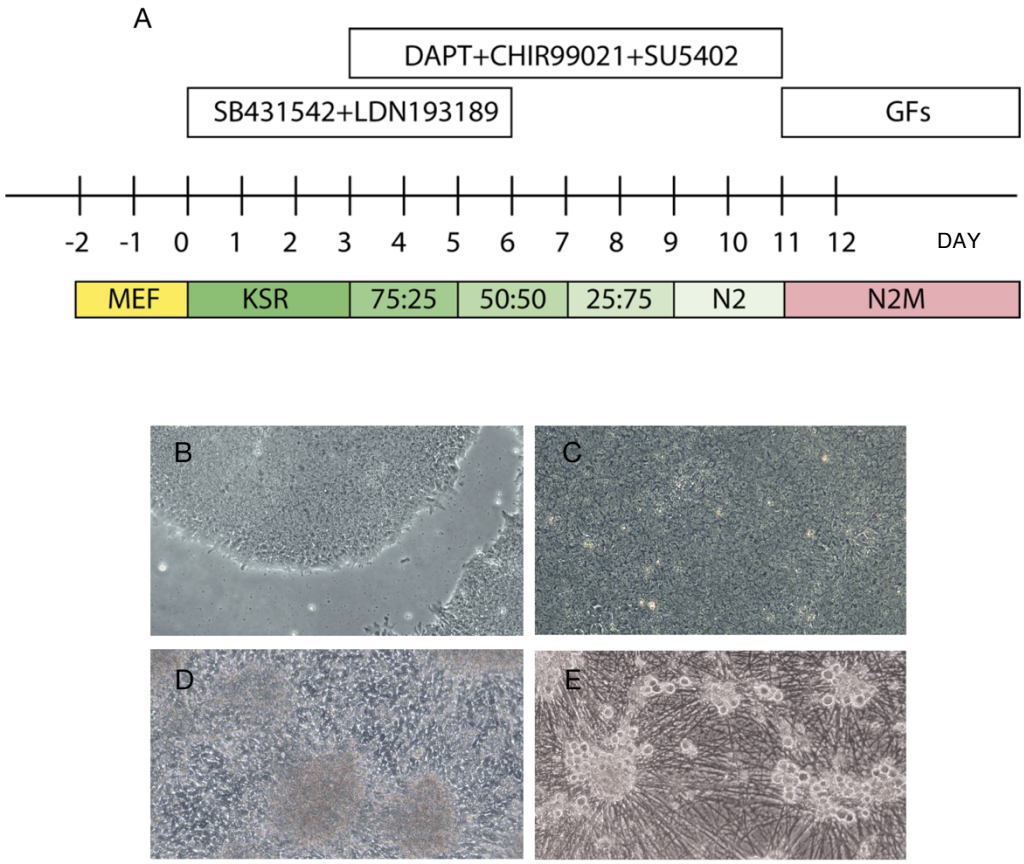


Figure 3-7 Timeline of the iPSC-nociceptor differentiation protocol.

Neural induction commences with the addition of the compounds SB43152 and LDN193189 which block BMP and Activin/Nodal/TGFβ branches of the SMAD signalling pathway, their combined action directs the cells to a neural ectoderm fate - blocking endodermal and mesodermal differentiation. Dual SMAD inhibition is followed on day 3 by inhibition of GSK-3, γ-secretase, and vascular endothelial growth factor receptor (VEGF)/ fibroblast growth factor receptor (FGF) signalling using three additional small molecules: CHIR99021, DAPT, SU5402. This combined blockade directs fate specification towards a sensory phenotype. Following release of small molecule treatment and the end of differentiation protocol, neurons are maintained in Neurobasal medium (N2M) supplemented with the human growth factors (GFs): NT3, BDNF, NGF and GDNF, for a minimum of 50 days before functional analysis begins. During the differentiation process, pronounced morphological changes are observed with increasing neuralisation, (B) day 0, (C) day 5, (D) day 11, (E) day 55.

3.3.4 Differentiated cells express canonical sensory neuron markers.

The described protocol directs cells through a quasi-neural crest state to generate sensory neurons. The cultures are treated with the nucleoside analogue AraC immediately following plating to remove non-neuronal cells, however the neural crest lineage can also give rise to a number of neuronal subtypes besides the sensory lineage desired here (e.g. enteric and sympathetic neurons (Baroffio et al., 1988)). Therefore to confirm the neurons were of sensory neuron identity, I stained for the pan-sensory neuron markers BRN3A and ISL1/2 (Fig.3.8 A & B), Healthy and CIP cultures were highly and equally enriched for both markers and co-staining with DAPI revealed very

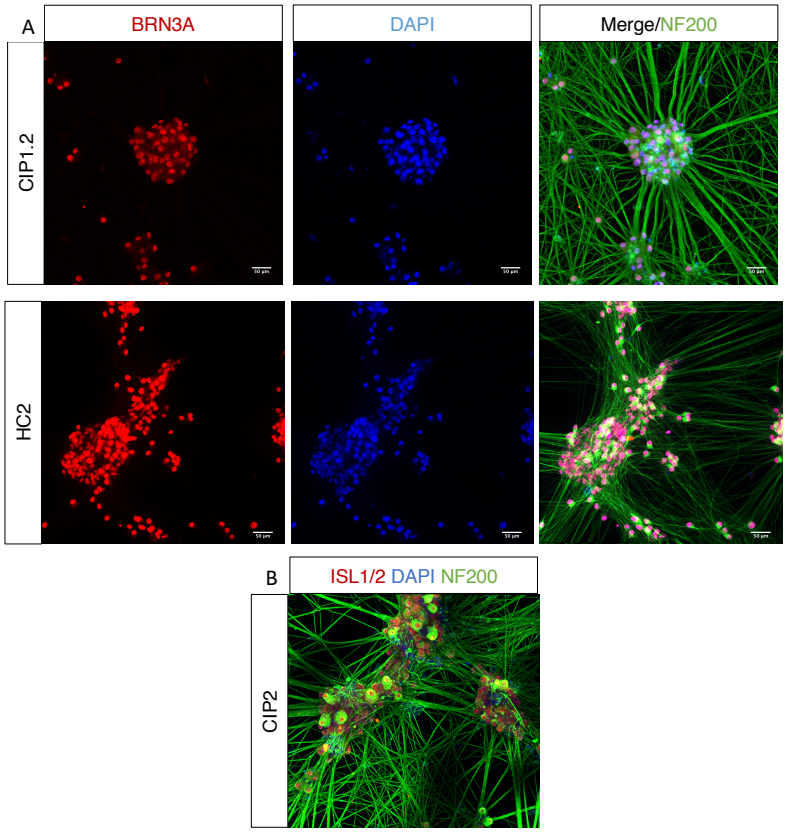


Figure 3-8 Differentiated cultures express canonical sensory markers

Representative ICC images from CIP1.2 (35DIV) and HC2 (30DIV) demonstrating the described protocol of differentiation produces highly pure sensory neuron cultures as shown by the high percentage of BRN3A$^+$ cells. (B) Representative image of Isl1/2 staining in CIP2 (50DIV), Similar to Brn3a, cultures appeared uniformly positive for the sensory neuron marker. Scale bar 50 µm.

few non-neuronal cells were present in cultures following AraC treatment, suggesting the protocol was capable of efficiently generating pure populations of sensory neurons. The cultures were also uniformly positive for the neurofilament heavy chain NF200. In rodents this has historically been used to mark intermediate to large diameter DRG neurons (Lawson and Waddell, 1991), however an increasing number of papers have recognised the majority of human DRG neurons express NF200 (Chang et al., 2018) suggesting this filament should not be used as a class discriminator in human sensory neurons.

3.3.5 SCN9A mRNA expression significantly increases with time *in vitro*

As neural cells differentiate and mature, the expression of voltage gated potassium and sodium channels shift the resting membrane potential towards a more hyperpolarised value, for human dorsal root ganglia the RMP is around -62 mV (Baumann et al., 1996; Davidson et al., 2014). At the end of the differentiation protocol, immediately following release of small molecule treatment, the neurons are electrophysiologically immature with a depolarised resting membrane potential and are unable to sustain firing - consistent with a low level of expression of voltage gated channels. Chambers et al demonstrated gene expression profiles of cells generated by the protocol plateau approximately 50 DIV (where 0 is replating) and consider the differentiated neurons to be 'mature' at this time point.

To characterise the temporal change in SCN9A mRNA expression and confirm ~50DIV to be an appropriate timepoint for functional analysis, I analysed the levels of the SCN9A transcript in healthy controls using qPCR (Fig. 3.9). There was a 19-fold increase in SCN9A mRNA levels at an intermediate timepoint of 20DIV ($p<0.05$) and this increased further to 32-fold difference following 50 days in culture ($p<0.001$), consistent with *in vitro* maturation of the cells. This timepoint also coincided with a change in

action potential morphology wherein an inflection was observed in the falling phase of the action potential. This is characteristic of primary rodent and human nociceptive DRG neurons (Blair and Bean, 2003; Davidson et al., 2014) and is attributed to high voltage activated calcium currents (type N and Q Ca^{2+} channels. The level of SCN9A

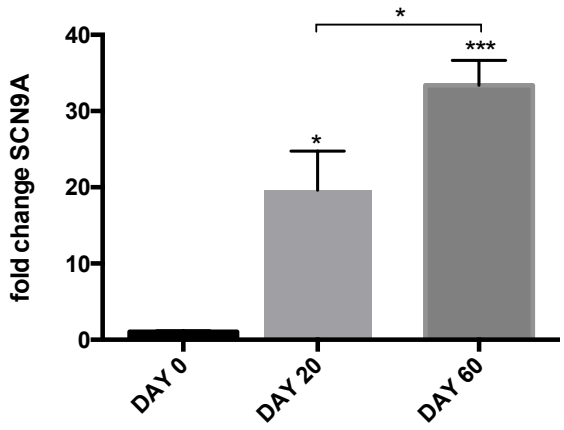


Figure 3-9 Temporal increase in SCN9A mRNA expression

SCN9A significantly increases with time in culture following differentiation as assessed by qPCR. Ordinary one-way ANOVA with Tukey's multiple comparisons test was used for statistical analysis. (95 % confidence interval, * = < 0.05, ** = < 0.01, *** = < 0.001.) Data are presented as the mean ± SE of three independent differentiations (n=3) from the HC1 line. Data are normalized to the housekeeping gene YWHAZ.

mRNA in CIP1 (the only line with a mutation thought to cause non-sense mediated decay) compared to HC lines was consistent with the loss of expression from a single allele, showing a significant downregulation of Nav1.7 transcript ($p<0.05$) (Fig. 3.10).

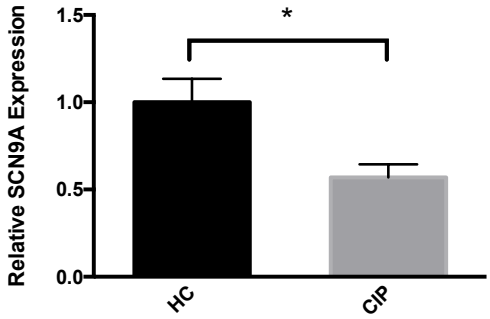


Figure 3-10 Relative SCN9A mRNA expression is reduced in CIP1 iPSC-nociceptors
SCN9A is significantly (P=0.0126) reduced in CIP1 compared to healthy control, qPCR was performed using RNA pooled from CIP1.1 and CIP1.2 (CIP) and RNA from the lines HC1, HC2, HC3 were pooled for the healthy control group (HC) in an equal ratio. SCN9A was reduced by an average of 43% in CIP compared to wild-type, which is consistent with nonsense mediated decay of the p.R830X SCN9A allele. Data are presented as the mean ± SE of four independent differentiations (n=4). Significance was determined using an unpaired two-tailed Student's T-Test, 95 % confidence interval, * = < 0.05). Data are normalised to the housekeeping gene YWHAZ.

3.3.6 Neuronal VGSCs expressed by iPSC-nociceptors

Sodium channels do not exist in isolation in DRG and the spectrum of channel co-expression can influence the interpretation of subsequent electrophysiological recordings in these cells. I therefore evaluated the expression of other VGSCs known to be present in primary DRG by RT-PCR. The iPSC-nociceptors were positive for a number of neuronally expressed VGSC (Fig. 3.11). Notably the cells did not appear to

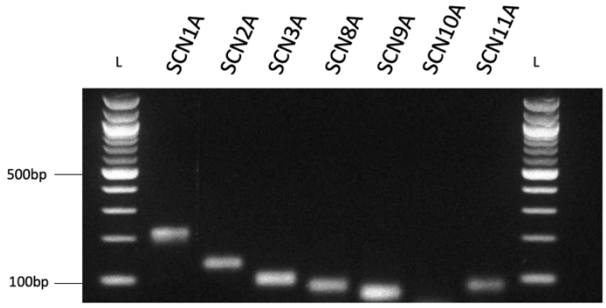


Figure 3-11 Spectrum of Neuronal VGSCs expressed by iPSC-nociceptors.

Representative agarose gel electrophoresis of reverse transcription-polymerase chain reaction (RT-PCR) for the detection of neuronally expressed voltage gated sodium channel in iPSC-nociceptors, 30 cycles of amplification with ~5ng input, from 52 DIV cultures. L; 100 bp ladder. No amplification product for SCN10A, the gene encoding Nav1.8, were observed. All primers were validated prior to use.

express TTX-R channel Nav1.8 transcript SCN10A. SCN3A, encoding Nav1.3, was also present. This channel is associated, at least in mice, with embryonic expression (Beckh et al., 1989) and known to be broadly expressed both in the CNS and PNS, before being downregulated postnatally. Having earlier demonstrated Nav1.7 expression increases with time *in vitro*, I evaluated whether, as in rodent, Nav1.3 is downregulated with increasing age. In contrast to SCN9A, there was no obvious temporal pattern for SCN3A

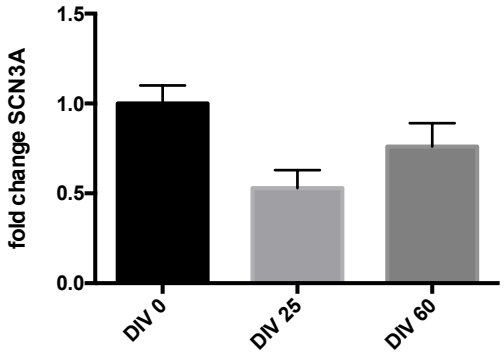


Figure 3.12 Temporal pattern of SCN3A mRNA expression in iPSC-nociceptors
Fold change in relative SCN3A mRNA expression, the gene encoding Nav1.3. In contrast to SCN9A, no clear temporal pattern was observed, a slight reduction in expression was found at the intermediate timepoint ($P<0.05$), however the ANOVA did not reach significance. Ordinary one-way ANOVA with Tukey's multiple comparisons test was used for statistical analysis. Data are presented as the mean ± SE of three independent experiments (n=3) from the HC1 line. Data are normalized to the housekeeping gene YWHAZ.

expression (Fig. 3.12). There was some evidence for a slight decrease in SCN3A transcripts, but this did not reach significance, suggesting SCN3A had broadly stabilised between this time. This is consistent with a plateau in global gene expression changes seen previously in iPSC-nociceptors at this time point (Young et al., 2014). This suggests that although there are clear changes in maturity for the iPSC-nociceptors, including for example a change in AP waveform, they are likely still representative of an embryonic or early postnatal neuron. Other changes notable during extended culture included a significant increase in soma size with cells identified >50μM in diameter at 100+ DIV (see appendix), this is within the range expected of post-natal human DRG (Davidson et al., 2014; Zhang et al., 2017).

3.3.7 Confirming molecular identity using RNA-seq of healthy control lines

Although several studies have previously characterised the gene expression profiles of neurons generated from the Chambers protocol (Young et al., 2014; Schwartzentruber et al., 2018). A degree of inter-lab variation is to be expected, therefore to further confirm the molecular profile of our iPSC-nociceptors we performed RNA-sequencing using the 3 control lines used for functional analysis (HC1, HC2, HC3) and an additional cell clone from HC1 (HC1.2). Principal component analysis demonstrated good clustering of iPSC-nociceptors with previously published studies (Schwartzentruber et al., 2018) and importantly, with primary hDRG tissue (Ray et al., 2018) (Fig. 3.13) further supporting the physiological relevance of the neurons and their use as a model for characterising loss of Nav1.7 function.

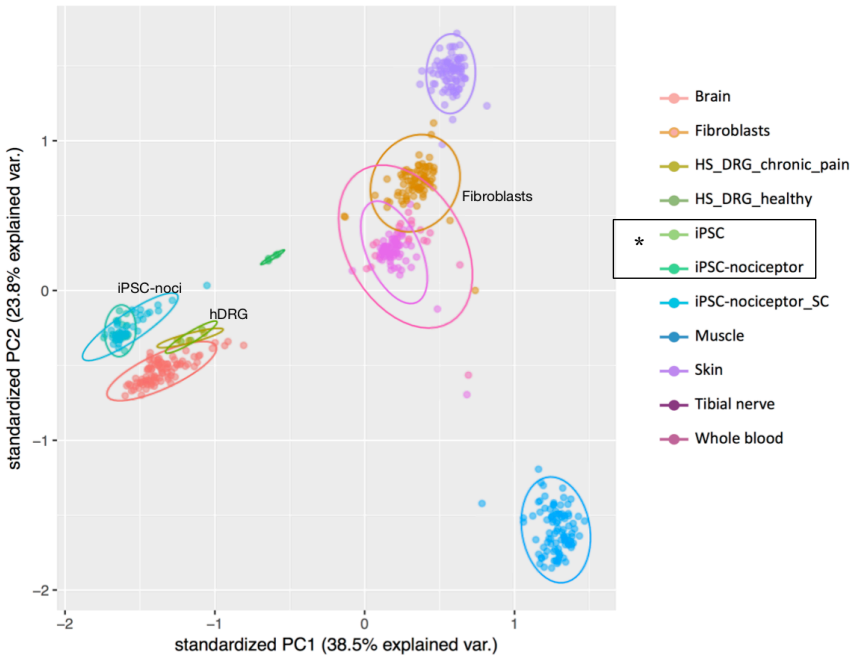


Figure 3-13 PCA analysis of iPSC-nociceptors

iPSC nociceptors derived in this study (iPSC-nociceptors) and previously published single-cell data (iPSC-nociceptor_SC), iPSC, human DRG from healthy patients (HS_DRG_healthy) and chronic pain patients (HS_DRG_chronic_pain) and other GTEx human tissues projected onto the two first standardised principal components defined from RNA-seq gene expression counts. Ellipses represent 6 the 95% confidence interval of a tissue's gene expression distribution. Distances between samples in the plot are proportional to their Mahalanobis distance. * data generated from this work. Note the strong clustering of the iPSC-nociceptors with hDRG tissue and clear separation from fibroblast identity. *PCA performed by Dr Georgios Baskozos*

3.3.8 Characterising the impact of loss of functional Nav1.7 in iPSC-nociceptors

Having characterised the neurons generated by the differentiation protocol and confirmed significant Nav1.7 expression in the iPSC-nociceptors, we next sought to evaluate the impact of loss of Nav1.7 function on cellular excitability. Gain of function mutations in Nav1.7 are associated with the painful disorders primary erythromelalgia (EM) and PEPD. When transiently expressed, EM/PEPD Nav1.7 variants render cultured mDRG hyper-excitable, with a lower threshold for action potential firing and enhanced firing to suprathreshold stimuli (Wu et al., 2017; Dib-Hajj et al., 2008). In contrast, small molecule antagonists selective for Nav1.7 have been shown to have the opposite effect - significantly increasing the rheobase in small diameter mDRG neurons (Alexandrou et al., 2016). We therefore examined whether a similar reduction in excitability is evident in CIP iPSC-nociceptors relative to those derived from healthy control subjects.

When assessed by whole cell patch clamp, the CIP lines required significantly greater ($p<0.05$) current injection to fire action potentials than the healthy control lines (CIP 149 $\pm$10.01 vs HC 102 $\pm$ 4.22) (Figure.3.14 A, B & C). This finding is consistent with the results described following the use of Nav1.7 blockers (Alexandrou et al., 2016) as well

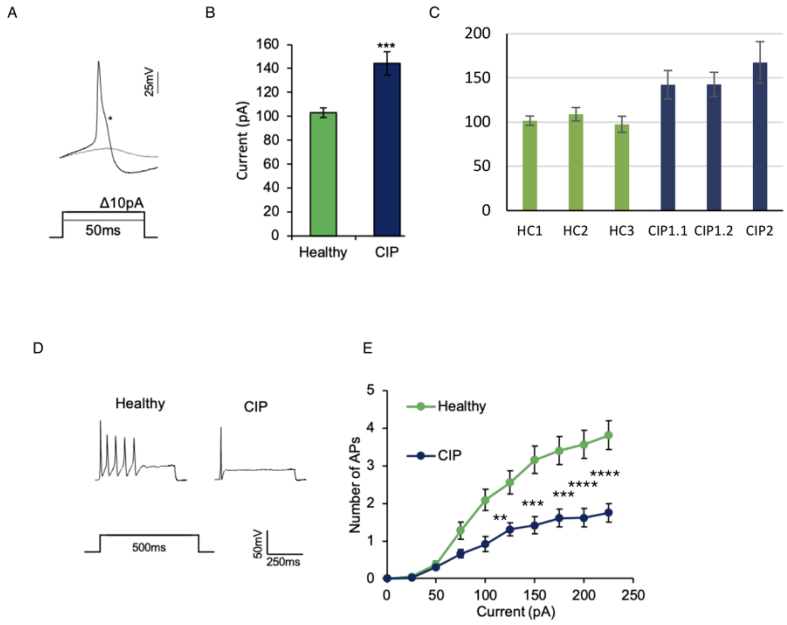


Figure 3-14 Loss of functional Nav1.7 significantly decreases cellular excitability in iPSC-nociceptors

(A) Representative trace of an iPSC-nociceptor action potential, note the shoulder in the falling phase characteristic of nociceptors (marked by *), below, current step protocol used. *). Rheobase was defined as the minimal current required to elicit an action potential from a holding potential of -60mV. Current was injected for 50ms at Δ10pA intervals. (B) Mean rheobase for HC and CIP group. The rheobase is significantly ($p<0.001$) increased in CIP neurons relative to control, Student's t-test (C) Rheobase of individual cell lines.
(D) Representative traces of action potential firing in response to prolonged (500ms) and suprathreshold depolarising current. (E) CIP neurons fire significantly fewer action potentials. Data represented as mean ± SEM, (pooled data from same group as (B). Two-way ANOVA followed by post-hoc Sidak's multiple comparison test. ** = < 0.05, ** = < 0.01, *** = < 0.001*

as recent knockout mouse studies (Shields et al., 2018). Next, we investigated the contribution of the channel to repetitive firing in the cells, on account of the increase in firing observed for EM and PEPD mutants. All patient lines demonstrated a significant reduction in their capacity to repetitively fire relative to control (Fig.3.14, D). Healthy and CIP iPSC-nociceptors did not differ in their resting state biophysical properties, including membrane potential, input resistance or capacitance (Table 3.5), suggesting this phenotype was not due to intrinsic differences between groups in non-Nav1.7 related properties. The results demonstrate a hypoexcitable phenotype for iPSC-nociceptors derived from CIP patients, in line with loss of Nav1.7 function.

Table 3.5 Biophysical properties of the iPSC-nociceptor lines

	HC1	HC3	HC2	CIP 1.1	CIP 1.2	CIP 2
RMP (mV)	-61.9 ±0.8	-60.7 ±1.2	-58.5 ±1.1	-63.1 ±1.1	-61.4 ±0.96	-62.7 ±1.5
R_{Input} (MΩ)	213.3 ±9.4	198.3 ±17.0	205.0 ±17.3	210.9 ±11.4	211.7 ±15.8	176.0 ±12.3
Cap (pF)	32.5 ±1.4	34.9 ±4.2	34.5 ±3.1	28.2 ±1.9	36.1 ±2.2	36.2 ±1.4
No. of cells	90	22	26	32	48	29

3.4 Discussion

Consistent with studies of rodent Nav1.7 KO DRGs (Raouf et al. 2012), we observed reliable hypo-excitability in CIP iPSC-nociceptors, demonstrable by an increased current threshold to activation and a reduction in action potential firing in response to prolonged supra-threshold stimulation. This is consistent with loss of channel function and is supported first by our findings in a HEK293T heterologous expression system with patient mutation cDNA constructs. The mutations located in exon 16 of SCN9A both caused a complete loss of sodium ion conductance, for R830X of CIP1 this reflects non-sense mediated decay of the transcript resulting from intra-exonal substitution of a stop codon. The mutation R896W on the other hand, is not predicted to alter the stability of the mRNA transcript. The affected arginine residue is highly conserved, both within the VGSC family and evolutionarily, lying in the S5-S6 linker pore loop, close to the selectivity filter. The results therefore demonstrate the substitution of the arginine residue with tryptophan is sufficient to cause loss of channel function, perhaps through loss of the charged sidechain. The result is also in line with a previously reported CIP mutation at the same site (R896Q) (Cox et al., 2010). The second compound mutation of CIP1 p.FS1773 occurs in the final exon of SCN9A, and thus would also be expected to give rise to a stable, albeit truncated, mRNA transcript. In the heterologous system we observed a small amount of current for this mutant, however this was 8-fold

smaller in magnitude than the wildtype channel. Other CIP mutations in the final exon have been described and show a similar substantial reduction although not complete loss of channel conduction. The residual current seen is unlikely to be physiologically relevant as the transient transfection is driven by strong constitutive promoter (in this case CMV) resulting in considerable overexpression of the protein. It is conceivable that this level of expression leads to a significant increase in ER stress, overwhelming the unfolded protein response pathway (Satpute-Krishnan et al., 2014), together this environment may erroneously allow for a small amount of mutated Nav1.7 to transit to the plasma membrane.

By using iPSC technology, we were able to differentiate patient derived cells to a relevant neuronal cell type and thus model the effect of CIP mutations in a system in which human Nav1.7 is endogenously expressed. Reassuringly, Nav1.7 was robustly expressed in mature iPSC-nociceptors as assessed by qPCR and there was a striking temporal increase in the transcript. This is consistent with findings from primary hDRG where Nav1.7 was shown to be the predominantly expressed VGSC in human DRG tissue (Chang et al. 2017). The spectrum of VGSCs expressed by the cells broadly reflects an embryonic or early postnatal stage of maturity, demonstrated by the expression of SCN3A and absence of SCN10A. The lack of human primary data at an early developmental timepoint for comparison unfortunately does not allow for a more precise resolution of the maturity of the cells. However, it should be noted that this immaturity is a broadly recognised phenomenon of cells differentiated from ESCs/iPSCs, both of neuronal and non-neuronal lineages (Arbab, Baars and Geijsen, 2014; Jiang et al., 2016; Koivumäki et al., 2018; Goversen et al., 2018). This is evidently a concern to disease modelling in which pathology manifests itself in old age, i.e. neurodegenerative disorders such as Parkinson's, Alzheimer's and Amyotrophic Lateral Sclerosis. However, it also suggests that iPSC-based models may be more useful, or rather more

representative of pain disorders of congenital onset. Given the importance of this issue, the field is actively researching means to prematurely age the progeny of iPSC (Mertens et al., 2018). Interestingly, trans-differentiation (direct conversion) of somatic cells, appears to preserve a greater degree of cellular maturity (Tang et al., 2017; Mertens et al., 2015; Victor et al., 2018). Victor et al, demonstrated in a model of Huntington's disease, that only striatal neurons transdifferentiated from patient fibroblasts recapitulated the characteristic protein aggregates of the disease *in vitro*, whereas they were absent in iPSC derived neurons. A few direct differentiation protocols for sensory neurons have been described (Blanchard et al., 2014; Wainger et al., 2014), unfortunately both suffer from a very low efficiency of conversion. If these protocols can sufficiently be improved, they may be an important complementary tool for modelling painful neuropathies associated with older age. Despite the evidence of relative immaturity, the cells themselves do acquire more mature characteristics with increasing time *in vitro* - as shown here by the increased expression of voltage gated channels, and the noted morphological changes including increasing cell size. We were also reassured to find the neurons produced clustered well with primary adult human DRG in PCA plots of RNA transcripts and were clearly separated from fibroblast and other non-neuronal lineages.

The absence of TTX-R Nav1.8 by RT-PCR analysis was surprising given expression noted by Chambers et al, but may reflect the heterogeneity in the differentiation process, or perhaps timepoint of analysis. However, several other studies using the same protocol have found a similar lack of expression (Young et al., 2014; Schwartzentruber et al., 2018). This finding also broadly reflects one of the limitations of the Chambers differentiation protocol, that is to say the method produces a limited lineage diversity, for example the cultures do not express markers of peptidergic neurons such as CGRP (data not shown). It is perhaps unrealistic to expect to replicate the full range of afferent

identities *in vitro*, however there is a clear need for the development of alternative protocols capable of generating a greater diversity of nociceptor subtypes.

Finally, the reduction in CIP cellular excitability demonstrated by an increased rheobase and reduction in capability to repetitively fire is consistent with studies of rodent Nav1.7 KO DRGs. The described work is the first study to show loss of Nav1.7 function in a human model decreases neuronal excitability. That said, our work shows that CIP cells are still able to sustain AP firing in response to a suprathreshold current. This must be interpreted in context of the recording site; all recordings were made using whole cell patch clamp of the cell soma rather than neurites which are technically very difficult to record from. As will be clear in later chapters, further work in this thesis suggests that this channel may have a more concentrated role at terminal structures.

Chapter 4

Genome engineering: targeting SCN9A using CRISPR/Cas9

4.1 Introduction

The CRISPR/Cas9 system has proven to be robust and versatile tool for gene targeting in a wide range of mammalian cells (Wang et al., 2013; Wu et al., 2014). The endogenous system has been simplified and adapted for experimental use such that precise manipulation of the genome requires only a catalytic Cas protein together with a single guide RNA. The sgRNA is a chimeric fusion of the tracRNA and crRNA, capable of assembling a hairpin structure which mimics the tracRNA:cRNA complex found in bacteria. The substitution of the 20 nucleotide sequence within the sgRNA complementary to the desired genomic loci, confers selective targeting of the Cas9 endonuclease. Sequence selectivity is limited only by the proximity of a protoadjacent motif (PAM) required immediately 3' to the genomic sgRNA sequence. The PAM site is essential for dsDNA cleavage and thought to have evolved from self/non-self discrimination (Westra et al., 2013; Mojica et al., 2009). This sequence requirement places a degree of constraint on genomic targeting, however, the commonly used SpCas9 PAM motif NGG, is thought to occur on average every 44 bp in the human genome (Kleinstiver et al., 2015).

CRISPR/Cas9 has largely superseded earlier SSN systems and has naturally attracted significant interest for disease modelling applications. The system permits the *de novo* introduction of mutations and can also be readily applied for the genetic correction of diseased alleles. Importantly, both such applications can be used to demonstrate the sufficiency and necessity of the mutation of interest for the phenotype. 'Naïve' and

edited cells can be directly compared under the assumption that they differ only at the targeted locus, creating 'isogenic' controls. This concept is particularly powerful for iPSC-disease modelling, as the heterogeneity between clones risks masking phenotypes *in vitro*. Furthermore, access to patient derived iPSC lines is generally very limited, which can make any phenotype observed difficult to attribute solely to pathogenicity of the disease. From the outset of this project only two viable iPSC CIP clones were available, and it was only in the very late stages of this work that we had access to a third clone. Mindful of the challenges associated with iPSC-based models, I chose to correct one of the compound heterozygous mutations in the CIP1.2 iPSC line, to investigate whether this was sufficient to 'rescue' the phenotype we observed in the iPSC-nociceptors, and by virtue of doing so, confirming the causal genotype: phenotype relationship.

To complement this and also establish proof of principle, I simultaneously targeted the same affected Nav1.7 protein domain (VSD II) in a healthy control iPSC line in order to generate a *de novo* Nav1.7 KO clone. Congenital insensitivity to pain is an exceptionally rare disease, therefore engineered lines such as those described herein represent a novel repository for modelling the pathogenesis of this disorder, where the patient population is extremely limited. The work described in the following chapter is the first successful targeting of SCN9A using CRISPR/Cas9 and details optimisation of the process, before evaluating the functional impact of the genomic edits.

Chapter aims:

- Optimise CRISPR Cas9 gene editing workflow in iPSCs
- Genetically correct c.2488C>T in CIP1.2
- Generate a de novo homozygous Nav1.7 KO in a healthy control line.

4.2 Methods

4.2.1 *In silico* sgRNA design

S.p.Cas9 sgRNA guide sequences specific to the target SCN9A locus were selected using the MIT CRISPR sgRNA design tool (available at http://mit.crispr.edu) and cloned into the p.SpCas9(BB)-2A-Puro (PX459) V2.0 plasmid vector (gift Feng Zhang, Addgene plasmid #62988). The Cas9 sgRNA dual cistronic expression vector included the *Streptococcus pyogenes* Cas9 CDS under the control of the CAG promoter, together with a p2A linked puromycin resistance gene and U6 RNA Polymerase III promoter.

4.2.2 Cloning of sgRNA sequences into pSpCas9(BB)-2A-Puro (PX459) V2.0

sgRNA oligonucleotides with the required BbsI ligation adaptors (bold) were ordered from IDT.

Table 4.1 Exon 16 sgRNA sequences

sgRNA	FW 5'-3'	REV 5'-3'
sgRNA_1	**CACCGG**AGCATGTTCAATGTTGGCC	**AAAC**GGCCAACATTGAACATGCT**CC**
sgRNA_2	**CACCG**GATCATTGGTAACTCAGTAG	**AAAC**CTACTGAGTTACCAATGAT**CC**
sgRNA_3	**CACCGGT**AATCAGCATGTTCAATGT	**AAAC**ACATTGAACATGCTGATTA**CC**

The oligos were heated to 95℃ for 5 minutes and passively cooled to room temperature to anneal. PX459 was digested with the restriction enzyme BbsI overnight at 37℃ and the annealed oligos were ligated into digested backbone using T4 ligase (NEB) (see Method 2.5.5). The product was then transformed into NEB stable cells. Plasmids were purified and isolated using QIAGEN miniprep. Correct insertion of the sgRNA sequence was verified by Sanger sequencing using the primer: PX459 SEQ_FW: 5'-GTTTCGCCACCTCTGACTTG-3'. Following *in vitro* sgRNA validation, the

sgRNA_2_SpCas9(BB)-2A-Puro was midi-prepped (Method 2.5.8) in preparation for iPSC transfection.

4.2.3 ssODN repair template

The ssODNs were synthesised by IDT technologies; phosphothioate linkages were applied to two most terminal bases. All ssODNs were stored lyophilised at -20℃ prior to use. The templates were rehydrated using ddH_2O on the day of the experiment. See Appendix for full sequence.

4.2.4 T7E1 assay

Each sgRNA together with the vector p.MAX_GFP were transfected into HEK293T using JetPEI. Genomic DNA was isolated using the Qiagen DNEASY kit. A 500bp fragment spanning the sgRNA sites was amplified from 50µg of gDNA using touch down PCR and HF Phusion polymerase using the primers:

SCN9A_EXON16_F 5'-AAGTCTGCTTTACCCTTTGAAC-3',

SCN9A_EXON16_R 5'-GGTTTCCAATGACCATGACCATC-3'

under the following cycling conditions.

Table 4.2 Cycling conditions for T7E1 PCR

Step	Temperature/ Time	No. of cycles
Initial denature	95℃, 3 min	1
Denaturation	98℃, 30 sec	10
hybridisation	70-60℃ (-0.8℃/cycle), 30 sec	
Elongation	72 ℃, 1 min	
Denaturation	98℃, 30 sec	20
hybridisation	60℃ , 30 sec	
Elongation	72 ℃, 1 min	
Final Elongation	72 ℃, 5 min	1

For heteroduplex formation, 10µl of the 20µl PCR reaction was added to 1.5µl of 2.1 Buffer (NEB) and 1.5µl of ddH_2O. The solution was heated to 95℃ for 5 minutes, then

allowed to slowly cool at a rate of 2 ℃ per minute. The T7E1 nuclease (NEB) was diluted in 2.1 Buffer and 1µl (0.5 units) was added to the annealed PCR products. The reaction was incubated at 37℃ for 35 minutes, 0.5µl of 0.5M EDTA was then added to each solution to immediately stop digestion of the DNA. Products were resolved on 2% Agarose ethidium bromide gels and visualised using UVP 2UV benchtop transilluminator (Fisher Scientific) per Method 2.3.2.3.

4.2.5 T7E1 cutting analysis

Gel images were analysed using Image J, FIJI. To ensure that the cleavage bands were due to NHEJ caused by Cas9-induced DSBs, and not due to genetic polymorphism, untransfected cells were used as a negative control for each assay. Percentage gene modification was estimated using band density analysis (Method 2.6.3) and application of the following formula:

$$\% \text{ cutting efficiency} = 100 \times (1 - (1 - \text{fraction cleaved})^{1/2})$$

4.2.6 Electroporation of iPSCs

The Neon electroporation system (Invitrogen) was used during optimisation of iPSC transfections. A suspension of 1-2 x10^6 iPSC was mixed with PX458 pSpCas9(BB)-2A-GFP, gift Feng Zhang, Addgene: #48138) in Buffer R and drawn into a 100µl Neon pipette. The loaded tip was the slotted into the transfection device in a tube containing Buffer E2. The number of pulses and voltage was varied according to trial conditions. Electroporated cells were immediately transferred to prewarmed mTeSR + Y-27632 (10µM) media in Matrigel coated 6 well plates.

4.2.7 Chemical reagent based Transfection

The following chemical reagents were used during optimisation of iPSC transfections:

X-treme gene (Roche), Lipofectamine 2000K, Lipofectamine 3000K (both Invitrogen), Fugene HD (Promega), LT-1 (Mirus). For forward transfections the cells were transfected at the densities recommended by the manufacturers, with a minimum of 2 different DNA:reagent ratios trialled. For reverse transfections, cells were lifted using Accutase, resuspended in mTeSR-Y27632 and complexes diluted in OPTIMEM medium (Gibco) were added immediately prior to plating.

4.2.8 Finalised transfection method

The reagent LT-1 was added to a low DNA binding Eppendorf containing 4 µg of PX459 and 2 µg of the repair template ssODN at a 3:1 ratio, with care taken not to touch the walls of the tube whilst dispensing. The solution was tapped gently to mix and incubated at room temperature for 20 minutes. During this time, 1.5 x 10^6 iPSCs were lifted using Accutase and spun at x 400 g to pellet before being resuspended in 1 ml of warmed mTeSR-Y-27632. The DNA complexes were added drip wise to the resuspended cells, and the tube was incubated for 5 minutes before further medium was added. The cells were then divided between wells of a 12-well Matrigel coated plate. Sixteen hours after plating puromycin treatment was initiated and maintained for 48 hours.

4.2.9 Puromycin resistance curve

To establish the appropriate concentration of puromycin for efficient cell selection, a dose response curve for puromycin selection (kill curve) was performed prior to the main experiment. 0.5x10^5 iPSC were seeded on 24 well Matrigel coated plates. The following day varying concentrations of puromycin (Invivogen) (1µg/ml, 0.5µg/ml, 0.3µg/ 0.25µg/ml, 0.2µg/ml, 0.1µg/ml) were added daily for 3 days to the media, cells were monitored by eye and the lowest concentration which exhibited complete cell

death was selected for subsequent experiments. An independent curve was performed for each iPSC clone as puromycin tolerance was found to vary considerably between cell clones.

4.2.10 Clonal isolation

To isolate clonal colonies, puromycin selected cells were treated with Accutase (Gibco) for 10 minutes, pelleted at 400 x g for 5 mins and resuspended in mTeSR + Y27632. Cells were then plated at 5-20,000 per 10 cm Matrigel coated dish and left undisturbed for 36 hours before the first medium change was performed. Cells were maintained in mTeSR without addition of antibiotics for 8-10 days for clonal outgrowth. Colonies were manually transacted into quarters using a sterile 27g needle, a p20 pipette tip was then used to transfer each segment into a 96 well plate containing mTeSR and Y-27632. Plates and 10 cm dishes were frequently rotated in order to maintain a viable temperature during the colony picked process.

4.2.11 Medium throughput DNA extraction for clone screening

Genomic DNA was extracted from replica plated 96 wells using Quick Extract (QE) reagent (epiCenter). Cells were lifted using TrypLE (Invitrogen) and resuspended in 30µl of QE. The cell lysis solution was incubated at 65°C for 20 minutes, vortexed then heated to 98°C to inactivate protease K. DNA extracted using this method is generally of low quality therefore 1:10 dilutions in ddH_2O were required as input for PCR reactions to ameliorate contaminant inhibition of the amplifying polymerase.

4.2.12 BciI digest of CRISPR transfected CIP1.2 iPSC colonies

Digestions were performed essentially as per Method 2.5.4, with slight modification. In all instances the enzyme was added directly into the final PCR reaction to increase

throughput. Incubation was performed for a minimum of 4 hours before being visualised on 1.5% agarose gels.

4.2.13 Sequencing of selected colonies

Sanger sequencing was performed by Source Bioscience Ltd using purified template from a 20µl PCR reaction generated using the primer set:

SCN9A_EXON16_F 5'- AAGTCTGCTTTACCCTTTGAAC-3'

SCN9A_EXON16_R 5'GGTTTCCAATGACCATGACCATC-3'

The following primer was used for sequencing:

SCN9A_SEQ_REV 5'-ACGCGGAACACAATCAGGAA-3'

4.2.14 TIDE sequence decomposition

The software TIDE (tracking of indels by decomposition) was used according to the method described in (Brinkman et al., 2014) to determine the length of Cas9 mediated indels in HC1. An untransfected sample was used as the reference control.

4.2.15 PENK mRNA transcript analysis

To investigate the impact of Nav1.7 KO on PENK expression, mRNA transcripts were assessed in 60 DIV Nav1.7 KO and isogenic control HC1. qPCR was performed as in (general methods). cDNA from healthy Mouse DRG (gift, Dr John Dawes) was included as a positive control. Primers were intron spanning, validated and designed to recognise both human and mouse transcripts.

PENK F 5'- TGCAGCTACCGCCT 3'

PENK R 5'- TCTTCTTCTGGCTCCATGGGATA- 3'

The end product of the qPCR reaction was added to a 2% agarose ethidium bromide gel and visualised as in (general methods)

4.2.16 Patch clamp of Nav1.7 KO and CIP1.2.Corrected

Assessment of Rheobase and repetitive firing capacity was performed as in Chapter 3 with cells 50-70 DIV. To model generator potentials *in vitro* depolarisation current ramps of 1 nA amplitude were given over 100-1000ms to assess firing in response to slow depolarisation. The ability of neurons to fire at high frequency was assessed by seventeen current stimuli of 1.5x rheobase (50ms) given at 20Hz.

4.2.17 Long-term outgrowth analysis

For neurite outgrowth assays assessing long-term axonal outgrowth, 49 fields of view of a 12 mm coverslip were acquired using GE IN Cell Analyzer 6000 build 6.1 at x10 objective. Neuronal cell bodies in mature cultures cluster, making accurate determination of cell number challenging; axonal coverage was therefore normalised to somal area (μm2) following confirmation of no significant difference between cell diameter of each group. Acquired images were imported into an IN Cell Developer Toolbox analysis software build 1.9.2 and analysis was performed automatically using a custom pipeline. In brief, a soma mask and total area network mask (neuronal somas and axons) were created from binary images from Brn3A+/NF200 stained 60 DIV cultures. The soma mask was subtracted from the network to yield axonal area. Fields containing artefacts e.g. tears in axons or large debris, were manually excluded by eye. To compare fields of similar neuronal density, fields with a soma area between $1.5x10^4$ μm2 and $4.5x10^4$ μm2 (equivalent to 8.5%-25% area) were used for analysis (parameter

determined before analysis). A minimum of 9 coverslips from each group were analysed from n=3 independent differentiations.

Data Acknowledgements:

Dr Gregory Weir performed patch clamp of iPSC-nociceptors that I generated and maintained. Thank you to Val Miller of the Target Discovery Institute, Oxford for assistance and guidance with the operation of the InCell microscope and associated software.

4.3 Results

4.3.1 Targeting exon 16 of SCN9A, reversal of the pathogenic CIP1.2 c.2488C>T mutation

The patient derived line CIP1.2 harbours two compound heterozygous mutations: c.2488C>T (p.R830X) located in exon 16 of the protein coding SCN9A transcript NM_02977.3, and c.5318delA producing the frameshift p.FS1773 in exon 27 of the gene. A single allele was targeted for genetic correction on the basis that SCN9A heterozygotes are asymptomatic. The 2488C>T variant was selected as it was the only mutation predicted to cause non-sense mediated decay of the SCN9A mRNA transcript.

The wildtype *Streptococcus pyogenes* Cas9 nuclease was chosen to generate double stranded DNA breaks in the iPSC as this Cas9 species variant is highly active in mammalian cells. The Sp.Cas9 protein contains both endonuclease domains (RuvC and HNH (Anders et al., 2014)) and requires the PAM 5'-NGG-3' (where N is a degenerate base) for sgRNA mediated targeting. Of the known protein coding SCN9A transcripts the RefSeq entry NM_02977.3 was used as the reference sequence for all editing events; this transcript encodes the adult, full-length protein.

A 150bp sequence flanking the mutation c.2488C>T was submitted to the CRISPR.MIT database to generate sgRNA sequences for the target loci. The proximity of the break-site to the intended mutation site is a key determinant of repair efficiency (Paquet et al., 2016), however this must be balanced by the degree of sgRNA target selectivity determined *in silico* by the programme algorithm. The two guides closest to the SNP and ranked highest were excluded due to predicted off-target activity for SCN3A, the gene encoding Nav1.3, which if erroneously targeted would be a significant

experimental confound. Three sgRNAs were selected for further evaluation *in vitro* using the T7 endonuclease I (T7E1) assay in HEK293T cells (Fig. 4.1 A).

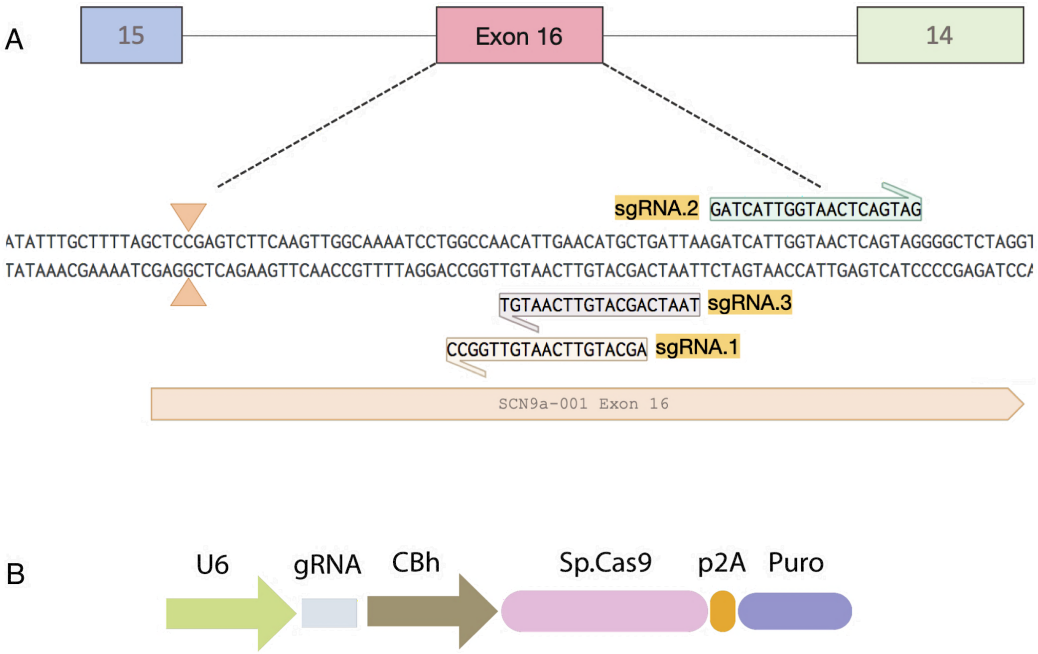


Figure 4-1 Loci of sgRNA sites relative to c.2488 in exon 16 of SCN9A

(A) Nucleotide position to be targeted (c.2488) is indicated by orange arrows. The sgRNA sequences for each guide are shown and their position relative to the edit site can be seen. (B) Linear representation of the coding sequence of the dual cistronic vector PX459. gRNA transcription is driven by the polymerase III dependent U6 promoter. SpCas9 is linked via p2A to a puromycin resistance gene, conferring transient antibiotic resistance to the iPSC and allowing selective enrichment of transfected cells. Both are under the control of the strong, ubiquitous CBh promoter. The full plasmid map can be found in the appendix.

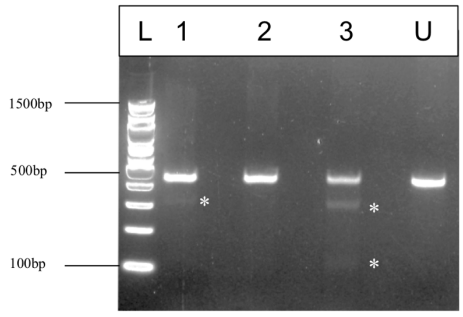
4.3.2 Investigating sgRNA efficiency *in vitro*

In silico calculations of sgRNA efficiency often do not correlate *in vitro,* therefore a T7E1 assay was used to select the guide with the highest cutting capacity. The assay exploits the selective affinity of the T7E1 endonuclease for heteroduplex DNA and can be used to semi-quantitively compare mutations produced from nuclease cleavage and

subsequent NHEJ repair of the genome thus providing an *in vitro* indicator of sgRNA efficiency.

The guides sgRNA.1-3 (Fig.4.1A) were cloned into the vector PX459 co-expressing a human codon-optimised WT-Sp.Cas9 nuclease and puromycin resistance gene (Fig.4.1B). Each vector was transfected into HEK293T together with the plasmid p.GFP-MAX. Transfection was deemed efficient at >70% as evaluated by epifluorescence microscopy. DNA was extracted from transfected cells and a sequence encompassing the target site was amplified. PCR amplicons were melted and allowed to anneal before being treated with the mismatch-sensitive T7E1 enzyme.

The frequency of Cas9 induced indels was estimated by cleavage products relative to the uncut fraction (Fig.4.2, A). The sgRNA.3 demonstrated the highest cutting efficiency (14%), whilst no visible cleavage products were observed for sgRNA.2 suggesting little to no nuclease activity *in vitro* (Fig. 4.2. B). Based on these results, sgRNA.3 was chosen for subsequent transfection into iPSC.



sgRNA	Fraction cleaved	DSB Distance from SNP
sgRNA.1	4.1%	28 bp
sgRNA.2	Not detected	67 bp
sgRNA.3	15.2%	33 bp

Figure 4-2 In vitro SCN9A sgRNA validation using a T7E1 Assay in HEK293T.

Left, Agarose gel of T7E1 cleavege products. Lane L 100bp ladder, 1; sgRNA.1, 2; sgRNA.2, 3; sgRNA.3, U; untransfected control. SgRNA.3 demonstrated the highest cutting efficiency in HEK293T cells. SgRNA.2 cutting was below detectable levels. T7E1 Cleavage products are indicated by a white asterix. *Right*, summary of cutting efficiency and the distance (bp) of the Cas9 cleavage site from c.2488 in SCN9A.

4.3.3 Optimising iPSC transfection

The transient transfection of exogenous DNA can be achieved via physical or chemical means. Unfortunately, the transfection of iPSC is known to be challenging, therefore a number of methods had to be trialled to yield optimal Sp.Cas9 expression. As electroporation is the most common means for transfecting refractory cell types, this was the first approach investigated using a Neon Electroporator (Invitrogen). No data from the manufacturer was available for iPSC transfection efficiencies, however a 30% transfection efficiency of the small GFP plasmid (p.MAX_GFP) was noted for the H9 embryonic stem cell line. Since the size of the DNA to be transfected is an important variable for transfection efficiency, the blank PX458 Sp.Cas9-EGFP vector, equivalent in size (~10kb) to PX459, was used as the control.

Following the parameters indicated for H9ESC yielded poor, highly variable transfection rates (10-12%) and was associated with significant cell death, as estimated by trypan blue exclusion. Additional trials using a two-pulse protocol significantly increased the fraction of eGFP cells, however transfections remained inconsistent. Electroporation using the Neon system requires single-use gold plated electrodes at considerable cost. It became cost prohibitive to further refine parameters therefore alternative chemical-based reagents were subsequently evaluated for efficacy in iPSC transfection.

Several commercial reagents were trialled first via standard transfection protocol wherein reagent:DNA complexes were added to adherent pre-plated cells. In the majority of cases this yielded no observable fluorescence, and at most, a maximum of 8% GFP+ cells as assessed by epifluorescence microscopy. Following the failure to transfect cells using this method an alternative means of introducing complexes via ‘reverse’ transfection was used. Here, the complexes are added whilst cells are in suspension immediately after passaging, this in theory increases the potential surface

area available for complex fusion. Although two reagents still failed to mediate any transfection of DNA, LT-1 significantly increased the fraction of iPSC transfected (67 +/- 7% n=3) (Fig 4.3). Following further refinement, a ratio of 3:1 LT1 to DNA was used for subsequent experiments.

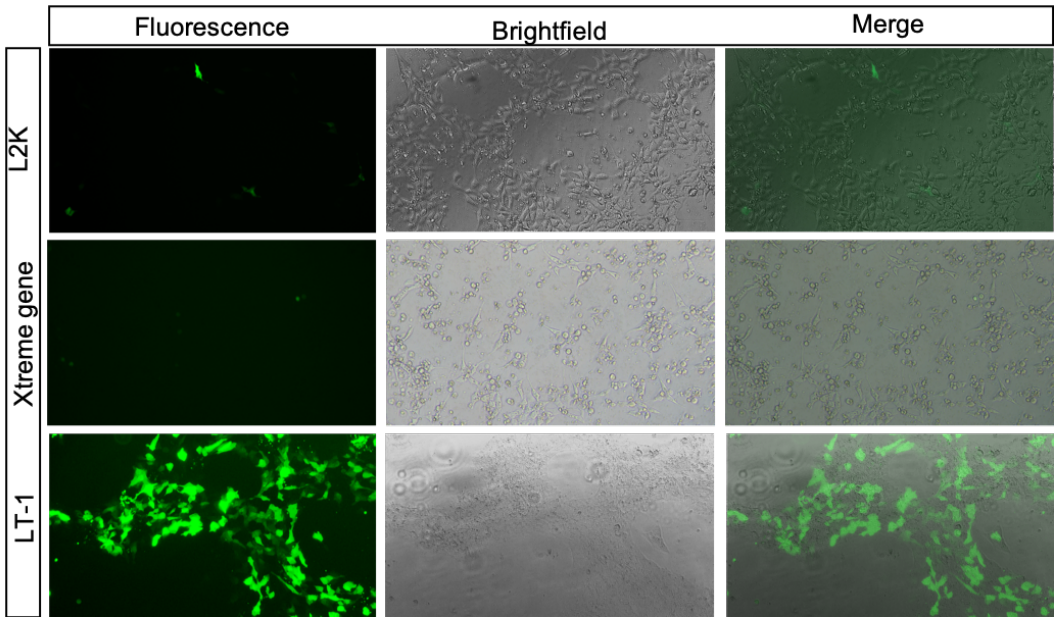


Figure 4-3 Chemical transfection of iPSC.

Representative epifluorescence images of iPSC expressing PX458 using the reagents: Lipofectamine 2000 (L2K), X-treme Gene, and Mirus LT-1. Negligible levels of fluorescence are present in populations transfected with X-treme gene and L2K, in contrast, iPSCs are efficiently transfected with LT-1. All transfections shown here were performed using the reverse protocol.

4.3.4 Strategy for gene correction

The intended modification required the substitution of cytosine with thymine to revert one allele to the control sequence. Historically, assisted HDR repair templates were constructed using linearised bacterial vectors, with large 2+ kb flanking homology arms. Such templates are an apropos substrate for large edits, however on account of the size of repair required here, I selected a single stranded oligonucleotide template (ssODN). ssODNs can be synthesised rapidly at a reasonable cost, vastly increasing throughput. Use of these templates also avoids unwanted integration of vestigial bacterial sequences derived from the plasmid vectors. ssODNs are, however, particularly vulnerable to

nucleolytic degradation by intracellular nucleases and oxidative attack. Consistent with this, the half-life of unmodified single stranded oligos *in vitro* has been shown to be c.30 minutes (de Semir and Aran, 2006). To mitigate this, phosphorothioate moieties were added to the two most terminal residues of the ssODN, replacing non-bridging oxygen atoms of the inter-nucleotide linkage with sulphur (Eckstein, 1985) (Fig 4.4, B,C). This modification significantly increases template resistance to nuclease attack, extending the ssODN half-life and availability for homology directed repair (Shaw et al., 1991).

A second element included in the repair template was a synonymous BciI restriction site within the seed region of the sgRNA complementary sequence (Fig. 4.4, A & C). This served two purposes: the *de novo* restriction site facilitates clone screening via diagnostic digest, and the silent nucleotide substitutions used in the critical seed region disrupt sgRNA binding - preventing further Cas9 endonuclease attack in the event of successful incorporation of the repair template. Ideally, the PAM motif itself should be silently mutated, however doing so at this locus would introduce a missense mutation hence the seed sequence was used in lieu.

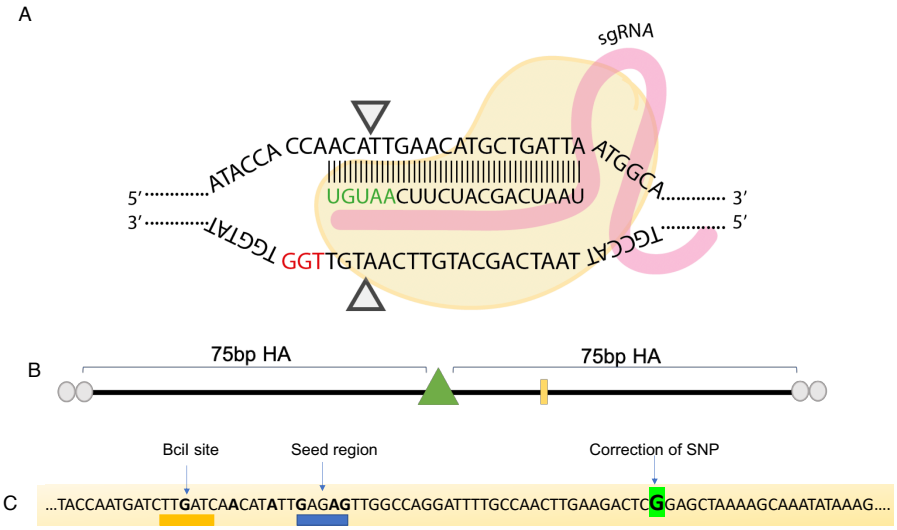


Figure 4-4 Schematic of sgRNA3 associated with Sp.Cas9 binding to target strand of SCN9A

(A) The protoadjacent motif 5'TGG'3 (red) is required for guide binding on the complementary strand. Nucleotides constituting the seed region of the sgRNA are shown in green. Inverted triangles represent the double stranded break site induced by Sp.Cas9 endonuclease domains HNH (top) and RuvC (bottom). (B) Schematic of the 150bp antisense ssODN, equal homology arms flank the desired nucleotide edit (green triangle), BciI site shown as yellow rectangle. Phosphorothioate moieties link the two most terminal residues to increase resistance to nucleolytic attack. (C) Selected nucleotide sequence of the repair template, modified residues in bold. Three silent mutations within the seed region were incorporated to block sgRNA binding in the event of successful repair. Further residues were synonymously mutated introduce a de novo BciI restriction enzyme site to facilitate the screening process. Guanine (shown in antisense here) is incorporated to genetically correct the CIP1.2 mutation, reversing to the wild type sequence c.2488C.

Following optimisation of transfection parameters and sgRNA design the CIP1.2 line was transfected with PX459 and the repair ssODN at a 3:1 ratio, cells were then transiently enriched using puromycin for 48 hours. Following recovery, cells were seeded at a limiting density for clonal isolation. Individual iPSC colonies were manually transected and transferred to 96 well plates for outgrowth. Two independent rounds of targeting were performed and in total 240 clones were picked, of these only 131 were viable following re-plating, suggesting the picking process can be a significant source of cell death.

4.3.5 Screening of CRISPR/Cas9 edited CIP.1.2 iPSC

When surviving wells reached confluency the cells were passaged into two replica plates, one of which was maintained, and the other was used for screening gene editing events. Screening proceeded immediately following genomic DNA extraction to avoid cryopreservation which, in this format, is associated with extremely low recovery rates. It was for this reason, it was critical to screen as quickly as possible as serially passaging hundreds of clones is technically challenging as synchronous growth rate per well cannot be assumed.

In order to assess editing events, a 467bp sequence flanking double strand break site and the SNP was amplified. The restriction enzyme BciI was added and digestion products were visualised on agarose gels (Fig.4.5). Successful incorporation of the ssODN repair template and thus BciI restriction site, should yield digestion products 309 bp and 158 bp in size. In total of 17 clones exhibited this pattern (table 4.3). All BciI^{+} clones were selected for further analysis using Sanger sequencing. Unfortunately, despite containing the restriction site, none of the BciI^{+} clones in fact contained the correct cytosine base, demonstrating only partial incorporation of the supplied repair template immediately 5' to the double stranded break site (DSBS).

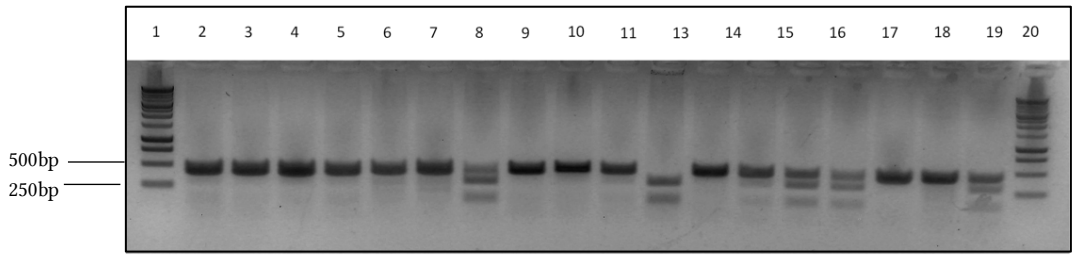


Figure 4.5. Representative screening gel of BciI digestion products.

A representative agarose screening gel from round one of gene editing. Lanes 1 and 20; 1 kB ladder, lanes 8, 13, 15, 16,19 show fragment sizes expected from a BciI digest, 158bp and 309 bp *in size*. The presence of three bands suggests either heterozygous incorporation of the repair template or a mixed clone.

Table 4.3 Summary of Screening results

Round	Clones screened (unsuccessful PCR amplification)	Evidence of repair template insertion	Successful repair
1	84 (3)	13	0
2	42 (2)	4	0
Total	**126 (5)**	**17 (13.49%)**	**0**

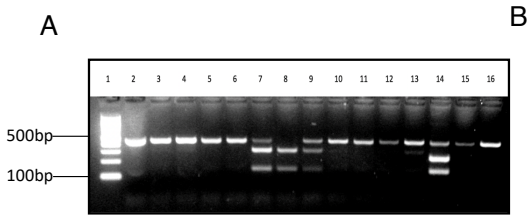
On account of this finding and following a publication by (Richardson et al., 2016), I redesigned the repair template such that the left and right homology arms were asymmetric in length; 132 bp (left) and 84 bp (right) (Fig. 4.6).



Figure 4.6 Redesigned asymmetric repair template.

Schematic of the redesigned repair template (shown in sense orientation here, but provided in anti-sense), green triangle denotes site of intended correction, yellow rectangle; BciI site.

Following this redesign, a third round of SCN9A targeting was performed (figure 4.7, A, B). Two clones were identified with successful correction of the pathogenic mutant, reverting thymine to the control cytosine base (Figure 4.7, C). The clones were expanded for further downstream experiments. A summary of the optimised CRISPR workflow to be used for further genomic edits in this thesis can be seen in Figure 4.8.



B

Clones Screened	Evidence of repair template incorporation	Successful repair
76	12 (17.8%)	2 (2.6%)

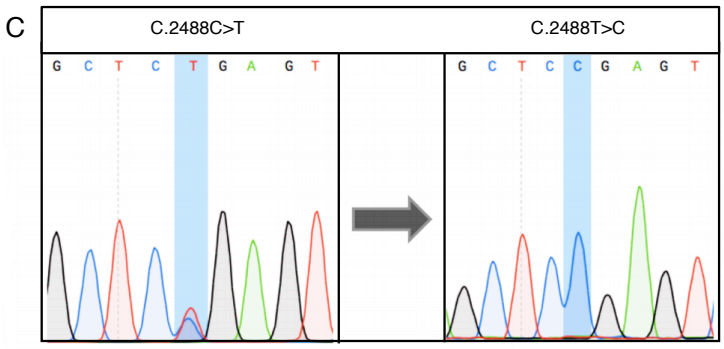


Figure 4-7 Successful correction of c.2488C>T CIP mutation in CIP1.2 iPSC

(A) Representative agarose gel from the final round of screening following repair template redesign. Lane 1; 100bp ladder, Lanes 7, 8, 9, 14 show evidence of repair template inclusion demonstrated by the presence of BciI digestion products (B) Summary of clones screened. (C) Sequencing chromatogram showing successful correction of the diseased SCN9A allele at position c.2488. reverting the thymine nucleotide to wildtype cytosine.

4.3.6 Generating a Nav1.7 knockout from the control line HC1.2

The *de novo* introduction of mutations in a healthy control line is an alternative and complementary strategy for studying the pathogenesis of SCN9A mutations. An appropriately targeted double stranded break can rapidly generate functional gene knockouts through indel formation via the error prone NHEJ repair pathway. The sgRNA previously used for c.2488T>C correction targets exon 16 of SCN9A, this region is highly conserved and encodes part of VSD II, constituting a critical functional domain for Nav1.7. The introduction of homozygous frameshift or amber mutations in this exon should truncate the protein by inducing non-sense mediated decay of the mRNA transcript, abolishing sodium ion conductance. Therefore, in order to generate a Nav1.7 KO line I transfected sgRNA.3 into the healthy control line HC1 using the workflow I optimised earlier in the chapter, see Fig. 4.8 for summary.

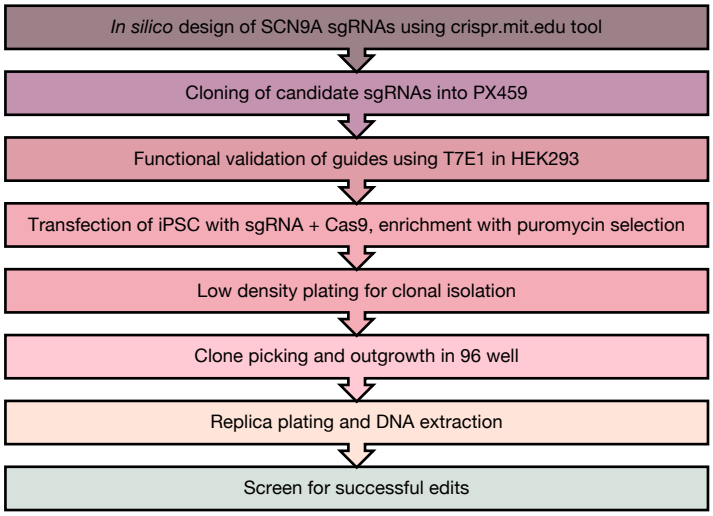


Figure 4-8 Optimised workflow for CRISPR/Cas9 gene editing in iPSCs.

4.3.7 Screening for indel formation in exon 16 of SCN9A

The iPSC line HC1 was selected for gene editing as I had previously found the line to recover well from thawing and differentiate efficiently to neurons. A total of 58 Cas9 HC1 transfected clones were picked and expanded as per Fig.4.8. In contrast to gene editing in CIP1.2, the healthy control iPSC clone demonstrated excellent survival (95%) and growth characteristics following manual picking. A selection of 10 clones were sent for sequencing analysis. The results showed highly efficient Cas9 induced indel formation with 50% showing evidence of cutting, 33% had bi-allelic targeting. Due to the limitations of Sanger sequencing for resolving multiple traces the sequence decomposition tool TIDE was used to infer the length of each indel (see Appendix) - the programme decomposes raw sequencing traces into linear combinations of indel mutations. A summary of the mutations identified can be seen in (Fig.4.9, A) and an example TIDE output is shown in Appendix.

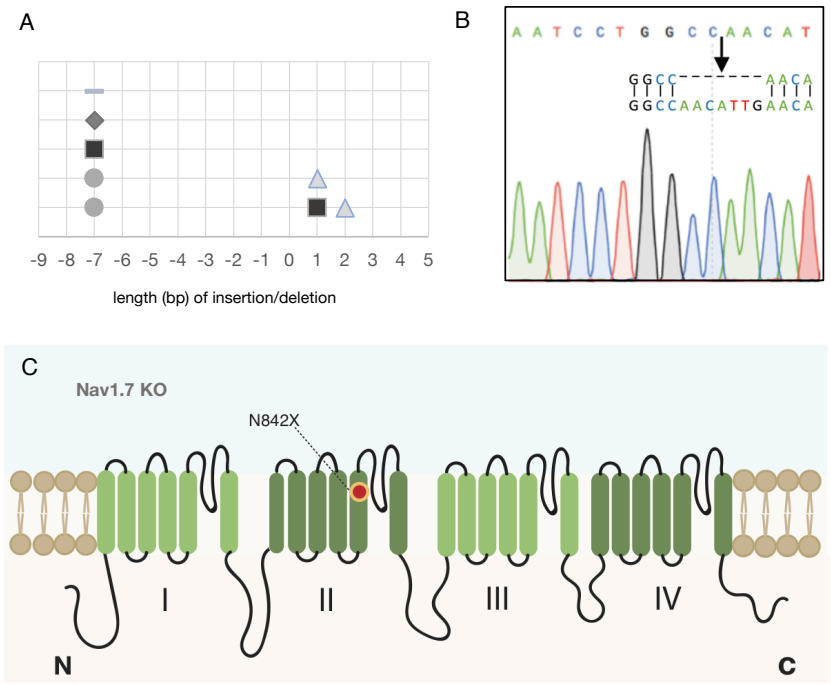


Figure 4-9 CRISPR/Cas9 generated indels in exon 16 of SCN9A HC1

Dot plot summary of allelic indel size found in selected clones, each shape represents a different sample. Sequencing chromatogram showing 7 bp homozygous deletion in exon 16 of SCN9A, (c.2517_2523delAACATTG). (B) Location of stop codon introduced by the mutation in VSDII S5 of Nav1.7. In this location the SCN9A mRNA transcript is predicted to undergo NMD.

We successfully isolated a clone containing the 7bp homozygous deletion C.2517_2523delAACATTG (Fig.4.9, B). This line was chosen for further expansion and is herein referred to as Nav1.7 KO. The 7bp nucleotide deletion causes a frameshift in the ORF of the SCN9A transcript producing a premature stop codon at position p.842X (Fig.4.9, C).

4.3.8 CRISPR edited lines retain markers of pluripotency and differentiate normally

Prior to proceeding to functional analysis, CIP1.2 Corrected and Nav1.7KO were assessed for their pluripotency using ICC. Both lines retained their pluripotency as observed by their normal morphology and ability to produce uniform immunostaining

of pluripotency marker OCT4/Nanog. The lines differentiated in a manner similar to their isogenic parent, producing highly enriched BRN3A^{+} cultures (Fig 4.10).

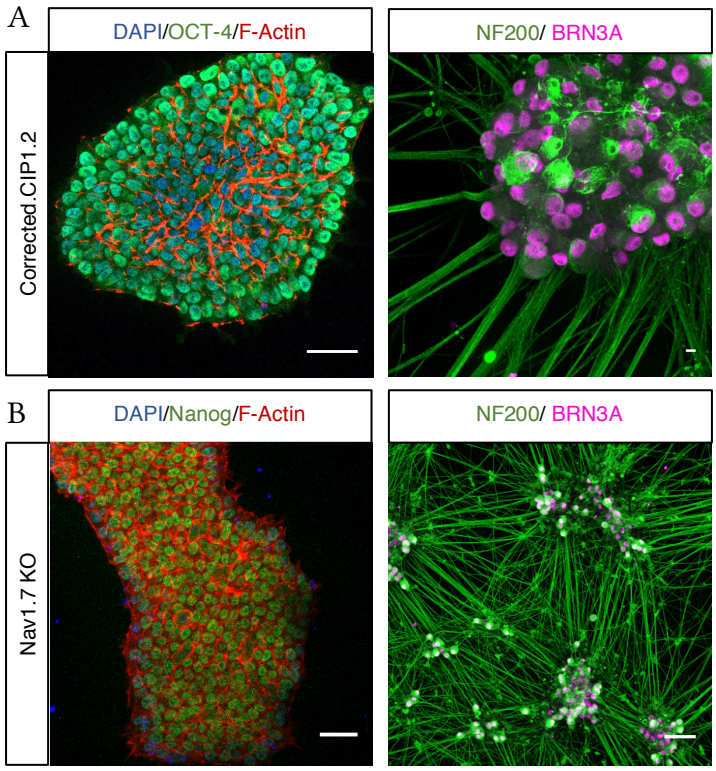


Figure 4-10 CRISPR/Cas9 edited lines differentiate similar to isogenic lines

Representative images of CRISPR/Cas9 engineered iPSC lines expressing *canonical* pluripotency marker OCT4 *(A, left)*, and Nanog *(B, left). Right*, each line differentiated to iPSC-nociceptors ~45-60 DIV. Cultures were uniformly positive for the sensory neuron marker BRN3A, and NF200, similar to parent lines *(*scale bar 50 μm).

The electrophysiological analysis performed in Chapter 3 using CIP iPSC-nociceptors suggested that loss of functional Nav1.7 may cause a significant reduction in cellular excitability. To robustly demonstrate that this is indeed the case, and by virtue prove causal genotype phenotype relationship, we evaluated the electrophysiological effect of CRISPR mediated genetic correction of the CIP mutation p.R830X in CIP1.2, and the *de novo* homozygous introduction of p.842X in HC1. The CRISPR generated lines were differentiated alongside the isogenic parent line and subjected to patch clamp at day 55-60 DIV.

4.3.9 Genetic correction of CIP1.2 variant rescues Rheobase

We first examined the effect of genetic correction on rheobase. Consistent with our expectations the corrected clone (CIP1.2.Corrected) demonstrated a significantly reduced rheobase compared to the isogenic parent CIP1.2 (CIP1.2 142.7±13.7pA *vs* Corrected 97.1±5.5pA, $p<0.05$) (Fig. 4.13, A, B) bringing the current required for AP generation in line with the healthy control cells. This was also in agreement with qPCR analysis of SCN9A mRNA expression in the corrected clones, which revealed a significant increase in SCN9A transcripts, demonstrating the substitution of thymine for the wildtype cytosine was sufficient to reverse NMD of this allele (Fig. 4.11).

Following this finding we characterised repetitive firing activity in CIP1.2.Corrected, having previously found a reduction in the capacity of CIP iPSC-nociceptors to repetitively fire. Interestingly, we found the patient phenotype of reduced firing in response to prolonged suprathreshold stimuli was not reversed by genetic correction of a single allele (Fig. 4.13 C, D).

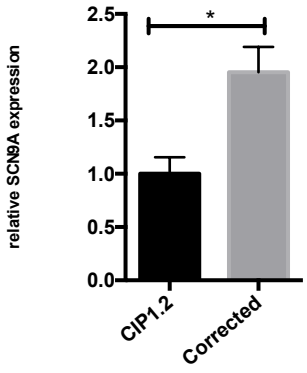


Figure 4-11 Genetic correction of 2488C>T variant increases SCN9A transcript expression relative to isogenic parent line.

Relative expression of SCN9A mRNA in CIP1.2 compared to CRISPR/Cas9 corrected clone (Corrected). SCN9A mRNA expression was rescued by allelic correction of the R830X mutation. p=0.0028 *=p<0.05, Expression was normalised to the housekeeping gene YWHAZ. Data represents mean ± s.e.m of three independent differentiations.

4.3.10 De novo introduction of the mutation N842X in Domain II of Nav1.7 causes cellular hypoexcitability in the healthy control HC1

As described in an earlier section, a Nav1.7 KO line was generated in order to study the function of Nav1.7 independent of inter-patient genetic variability. A homozygous SCN9A frameshift mutation (N842X) was introduced into the healthy control iPSC line (HC1.2), generating the Nav1.7 knockout (Nav1.7 KO). This de novo mutation produces a premature stop codon in domain II of the channel, leading to nonsense mediated decay of the SCN9A mRNA transcript. Consistent with this, I observed a greater than 80% reduction in SCN9A mRNA compared to isogenic HC1 (Fig. 4.12).

In agreement with loss of channel function, Nav1.7 KO iPSC-nociceptors recapitulated the excitability changes observed in CIP lines, including an increased rheobase (HC1 101.6±5.3pA *vs* Nav1.7 KO 145.5±9.7pA, $p<0.001$) (Fig. 4.13, A, B) and a decreased propensity to fire repetitively to suprathreshold stimulation (Fig 4.13, C, D). No significant difference in resting biophysical properties was found. These results together with the earlier study of the CIP1.2.Corrected clone suggest that to sustain repetitive firing, neurons may require two functional copies of SCN9A

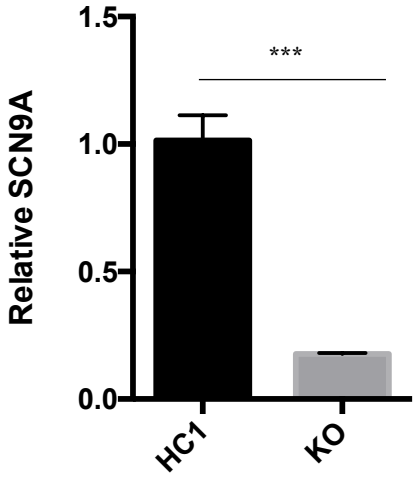


Figure 4-12 Relative SCN9A expression in CRISPR Nav1.7 KO and isogenic control

SCN9A was significantly ($p<0.0001$) reduced in Nav1.7 KO compared to HC1, consistent with NMD following a 7bp homozygous deletion in exon 16.
Data are presented as the mean ± SE of four independent differentiations (n=4). Significance was determined using an unpaired two-tailed Student's T-Test, 95 % confidence interval, *** = < 0.0001). Data are normalised to the housekeeping gene YWHAZ.

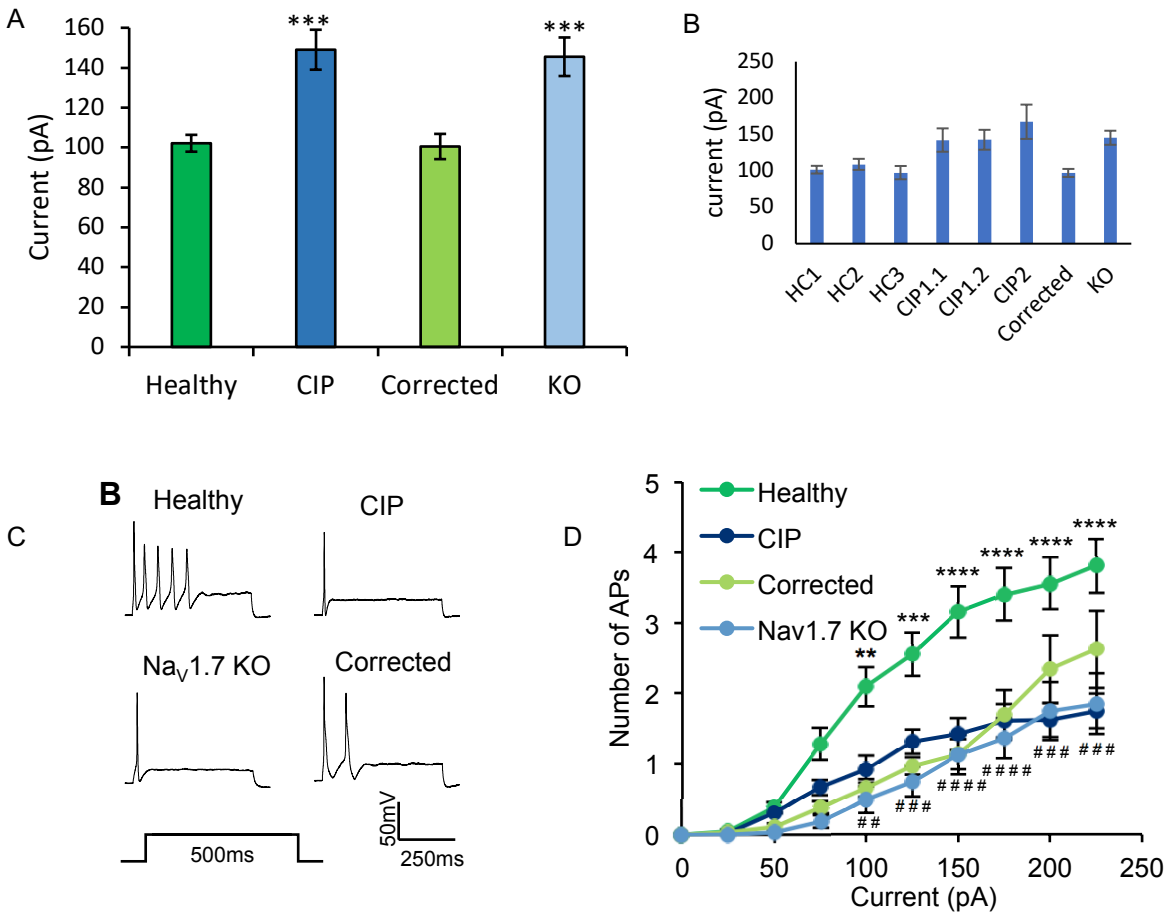


Figure 4-13 Excitability of CRISPR Cas9 SCN9A edited lines

(A) Rheobase derived from pooled data of Healthy (119 cells), CIP (85 cells), Corrected (33 cells) and Nav1.7 KO (45 cells) groups. Genetic correction of C.4888C>T CIP mutation is sufficient to rescue rheobase to healthy control levels. In contrast, the targeted disruption of SCN9A in HC1 resulted in an increase in rheobase, similar in value to lines derived from CIP patients. Significance was determined by Kruskal-Wallis followed by post-hoc Dunn's test ***p<0.001 Healthy vs CIP groups, ### p<0.001 Nav1.7 KO vs HC1 (parent clone) and + p<0.05 Corrected.CIP1.2 vs CIP1.2 (parent clone). (B) Individual rheobase values for each line. (C) Representative traces from CRISPR generated lines in response to a prolonged (500ms) depolarisation current injection. (D) Pooled data from the same cells as A. Note that whilst biallelic KO of Nav1.7 in HC1 significantly reduced repetitive firing, the correction of a single pathogenic allele in CIP1.2 was not sufficient to restore firing to control levels. Two-way ANOVA followed by post-hoc Sidak's multiple comparison test was used for all comparisons. **p<0.01, ***P<0.001, ****p<0.01 Healthy vs CIP. ## p<0.01, ### p<0.001, #### p<0.0001 NaV1.7 KO vs HC1.

4.3.11 Nav1.7 KO has an impaired response to slow, graded suprathreshold current injections

Having robustly demonstrated that bi-allelic SCN9A pathogenic mutations are sufficient to cause cellular hypoexcitability, we explored further the role of Nav1.7 in regulating excitability in response to ramped stimuli, taking advantage of the Nav1.7 KO clone and parent line HC1. The biophysical properties of Nav1.7 are thought to permit function within a voltage domain that is subthreshold for action potential generation, such that the channel can act to boost subthreshold depolarising inputs increasing the likelihood for action potential generation (Cummins, 1998). However, a recent study using cadaveric human DRG cells found a lack of low-threshold excitatory ramp currents in response slow membrane depolarization (Zhang et al., 2017), the group suggested that Nav1.7 may not therefore make a significant contribution to TTX-sensitive sodium ion current in human DRG, in contrast to its function in rodent DRG neurons. The potential role of Nav1.7 in amplifying small, subthreshold responses is important to clarify in order to decipher the pathogenesis of CIP. Stimulation of nociceptor peripheral terminals likely results in generator potentials, which slowly depolarise the membrane potential (Waxman, 2006). A loss of this activity at primary afferent terminals may significantly contribute to the phenotype of insensitivity to pain. To investigate this hypothesis, we injected ramps of suprathreshold current with increasing gradients to mimic generator potentials (Fig.4.14). While HC1 neurons were readily able to fire action potentials in response to lower gradient current, Nav1.7 KO iPSC-nociceptors were markedly less responsive to ramp depolarisation, especially to

slower stimuli, suggesting that the channel may have an enhanced role in responding to this type of stimulus.

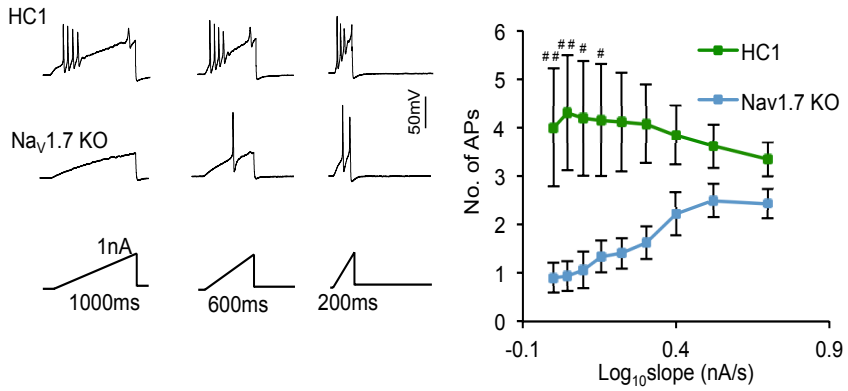


Figure 4-14 Nav1.7 KO has an impaired response to slow, graded suprathreshold current injections

Left, Representative traces from HC1 (top) and CRISPR Nav1.7 KO (bottom) following graded suprathreshold current injections. *Right,* quantification of the number of action potentials fired in response to a 1nA current injection given over 100-1000ms in 100ms increments. # P<0.05, ##P<0.01 Two-way ANOVA followed by post-hoc Sidak's multiple comparison test. (HC1- 44 cells and NaV1.7 KO- 54 cells).

4.3.12 Cellular hypoexcitability is independent of endogenous opioid expression

It has been suggested the CIP phenotype is at least partly due upregulation of endogenous opioids in the DRG following the loss of Nav1.7 activity (Minett et al., 2015). To investigate whether such an upregulation may be influencing the phenotype we found *in vitro*, I investigated the expression of enkephalin encoding transcript PENK in Nav1.7 KO vs HC1 (Fig. 4.15). No appreciable level PENK gene expression was found in either group as assessed by qPCR. These results are consistent with hDRG transcriptome data, which show a dearth of PENK expression in healthy hDRG (Ray et al 2018) and demonstrate that the observed hypoexcitability is independent of any influence of endogenous opioid expression.

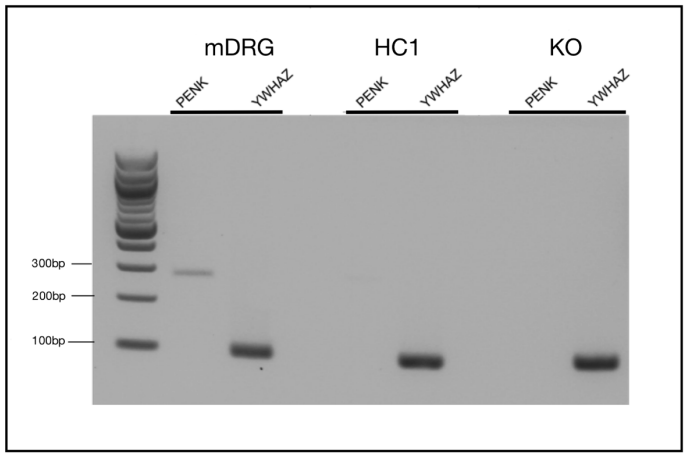


Figure 4.15 Characterising expression of PENK mRNA

PENK mRNA was undetectable by qPCR in Nav1.7 KO and HC1, surpassing the upper Ct limit of 40 cycles. Representative agarose gel loaded with the end product of the qPCR reaction (45 cycles). No bands are visible for PENK in KO and HC1, a single band of correct size can be seen for the positive control – mouse DRG whole tissue lysate. The housekeeping gene YWHAZ is shown alongside each sample as polymerase control. 100bp Ladder.

4.3.13 Investigating the contribution of Nav1.7 to axonal outgrowth using the Nav1.7 KO line

The original SCN9A CIP pedigree described a normal intraepidermal nerve fibre density and indeed this was thought to distinguish CIP due to SCN9A mutations from CIP due to mutations in the NGF signaling pathway (*NGF* or *NTRK1* mutations (Einarsdottir et al. 2004; Indo et al. 1996), which result in severe developmental degeneration of nociceptors. However, laterally, skin biopsies taken from a number of independent CIP patients have revealed a significant reduction in intraepidermal nerve density (IENFD) (Marchi et al., 2018; Bogdanova-Mihaylova et al., 2015). It is not clear whether this phenotype is caused by degeneration or an intrinsic reduction in axonal outgrowth/targeting. The majority of recorded CIP skin biopsies have been obtained from distal sites which may have been affected by early injuries to the extremities, however our group has recently obtained proximal biopsies from the CIP patients included in this work. These samples have also revealed a significant decrease, more

suggestive of a global reduction in IENFD (McDermott et al., *in press*). Interestingly, this phenotype is not replicated in global or selective Nav1.7 KO mice (Gingras et al. 2014).

In vitro studies have previously described a reduction in outgrowth in dorsal root ganglia transfected with Nav1.7 EM mutant constructs, however this phenotype is more likely to reflect a degeneration of the neurites due to calcium ion dysfunction, rather than a perturbation in axonogenesis. The effect of loss of Nav1.7 on *in vitro* neuronal outgrowth has not been previously described. Axonal generation is a complex polygenic process, therefore to minimise inherent heterogeneity between iPSC lines I took advantage of the Nav1.7 KO and parent healthy control HC1 to investigate the effect of loss of endogenous Nav1.7 expression on long-term axonal coverage.

Following my finding in Chapter 5, I chose to assess outgrowth at a time *in vitro* in which Nav1.7 protein was localised to axonal and terminal structures. Assessing axonal coverage in these cultures is, however, challenging due to the extensive and elaborate networks formed by the cells. Efforts to perform the assay in 96 well plates in order to increase the throughput and ease of imaging, were thwarted by a repeated loss of cultures due to central 'aggregation' of somal bodies over time, leading to destabilisation and loss of adhesion. This effect was common to multiple plating densities. The format was therefore scaled, and images were obtained from cultures grown on 12 mm^2 coverslips. A total of 49 fields of view were acquired per coverslip equivalent to >75% of total area.

As the iPSC-nociceptors mature, cell bodies cluster precluding accurate cell counting, therefore in lieu total axonal area was normalised to total soma area having ascertained cell diameter does not significantly differ between groups (HC1 25.13 μm ± 0.47 N=100, KO 25.54 ± 0.4198, N=125). The image analysis pipeline was refined using multiple example images to ensure appropriate segmentation. Soma masks accurately

thresholded the cell body and axonal segmentation improved with local contrast enhancement enabling even fine axonal structures to be accurately segmented. Fig 4.16, A). Following refinement of the pipeline, images were automatically analysed and tiles were manually checked. Fields with obvious artefacts including tears in axonal networks and large debris were excluding from data. Ultimately, analysis revealed no significant difference between HC1 and KO, suggesting at least *in vitro* Nav1.7 does not significantly affect axonal outgrowth (Fig 4.15, B, C & D).

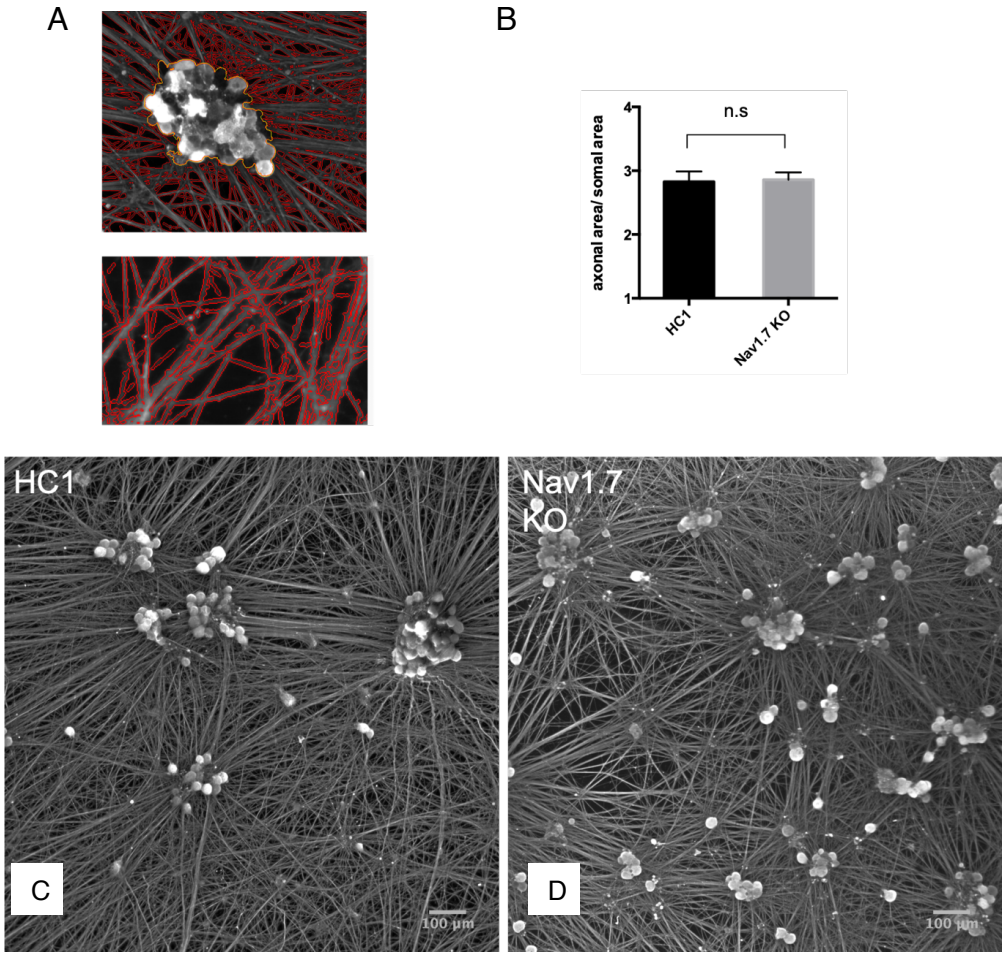


Figure 4-16 Long term axonal outgrowth does not significantly differ between Nav1.7 KO and HC1

(A) Representative image thresholding, yellow outline depicts somal area, axonal area is contained in red, below magnified image of axons, fine structures are accurately delimited from background, (B) Quantification of axon area relative to somal area. No significant difference between the two groups was found, data represents the mean ± s.e.m of 11 (HC1) and 9 (Nav1.7 KO) coverslips taken from three independent differentiations. Student's T-test for significance. Representative images from HC1 (C) and (D) Nav1.7 KO 60DIV cultures.

4.4 Discussion

The results demonstrate the flexibility of the CRISPR/Cas9 system for iPSC gene editing. The co-transfection of cells with a ssODN repair template allowed for the successful correction of the CIP variant c.2488C>T in a patient derived line, whilst the transfection of a healthy control iPSC line in the absence of an exogenously supplied repair substrate led to the rapid and highly efficient generation of multiple Nav1.7 KO iPSC clones.

The genetic correction of the patient polymorphism was challenging and required multiple targeting rounds before successful insertion of the repair template was achieved. This is most probably due to the distance of the sgRNA site from the target loci. A significant decrease in the efficiency of HDR repair occurs with increasing distance from the Cas9 DSB site. Several groups have found HDR mediated ssODN repair (Bialk et al., 2015; Yang et al., 2013) decreases to negligible levels greater than >25bp from the break site (cf, 33bp here), a phenomenon reflecting a progressive decline in the frequency of gene conversion tracts with increasing length. This reflects my findings during early attempts - a number of alleles had incorporated the synonymous CRISPR/Cas-9 blocking mutation immediately adjacent to the cleavage site but, frustratingly, did not contain the intended corrected base. Following findings by Richardson et al., I chose to redesign the repair template such that the homology arms were synthesised to asymmetrically flank the mutation. The group demonstrated Cas9 slowly dissociates from dsDNA, taking ~6 hours to do so. Prior to complete detachment however, the endonuclease first releases the 3' end of the cleaved DNA strand non-complementary to the sgRNA. This asymmetric release of the target DNA suggests the strand is available for template binding, this is consistent with earlier findings that NTSc

(non-target strand complementary) ssODNs may be more efficiently incorporated than TSc (target strand complimentary) templates (Lin et al., 2014).

Longer sequences of homology distal to the PAM site were also associated with significantly increased successful repair events, the mechanism underlying this has yet to be fully resolved, however it is thought that the short PAM proximal arm can rapidly associate with the free cleaved 3' strand, enabling subsequent strand invasion of the longer arm and displacing the homologous base-paired DNA strand at the other side of the break. The longer PAM distal arm may also be helpful to mitigate 3' exonucleolytic hydroxyl attack (in the case of NTSc), although the incorporation of the phosphorothioate bonds as described here also offers protection (Skerra, 1992).

At the time the experiments were performed ssODN synthesis was limited to ~220nt, however so called 'long' ssODNs (LssODN) are now commercially available (albeit at a significant cost) and may also be synthesised using *in vitro* transcription. They appear to demonstrate good efficacy in microinjection of mouse ES cells (Codner et al., 2018) but have yet to be described for iPSC. These LssODNs offer an alternative approach to classic plasmid-based dsDNA donors for the seamless introduction of larger edits, and they may also prove a more effective repair substrate where the DSB site is significantly distal to the desired edit. However (unpublished correspondence) longer ssODNs may be associated with an increased level of toxicity, perhaps reflecting potent activation of intracellular DNA sensors (Atianand and Fitzgerald, 2013).

A significant challenge encountered during the course of the experiments was clonal survival; a difficulty not unique to the CRISPR/Cas9 system, rather more broadly applicable to the practice of gene editing in iPSC. This appeared to be line dependent as a far greater fraction of the healthy control line HC1 survived the clone picking process compared to the patient line. The editing process and subsequence clonal isolation and outgrowth is significant source of stress. Inclusion of the rho-kinase inhibitor Y-27632

can increase cellular survival, however, it cannot prevent spontaneous differentiation frequently observed following clone detachment and outgrowth.

Following optimisation of the pipeline required to produce the corrected clone, I was able to rapidly generate several Nav1.7 KOs in a control iPSC line via the transfection of Cas9 in absence of a repair template. This method exploits the predominant DSB repair pathway, NHEJ. NHEJ and other non-homology directed repair cellular repair pathways are inherently error prone as they do not require sequence homology (Chiruvella, Liang and Wilson, 2013). In the canonical NHEJ repair the heterodimeric DNA binding proteins Ku70 and Ku86 (also known as Ku80) bind the exposed DNA ends preventing extensive re-sectioning. Following the recruitment of artemis-PKC complex the ends are directly ligated by DNA ligase IV, this results in the genomic incorporation of small insertion and deletion repair products known as indels, typically 1-4 nucleotides in length (McVey and Lee, 2008). Of the 10 clones picked, Sanger sequencing revealed 5 had Cas9 mediated indels, interestingly many of the clones had a larger deletion, 7 bp in length suggesting the MMEJ (microhomology mediated end joining) pathway is highly active following Cas9 cleavage in iPSC. The pattern of repair we observed here is intriguing and appears to fit well with a recent observation in the field (Taheri-Ghahfarokhi et al., 2018; van Overbeek et al., 2016). Repair outcome following DSB formation was thought to be random on the basis that NHEJ acts as the predominant repair pathway in absence of a repair template. However, there is now increasing recognition that at select genomic sites Cas9 induced DSBs have stereotyped repair preferences showing reproducible repair outcomes, with a preference for class (insertion or deletion) and size of indels. The frequency of the 7 bp deletion observed here appears consistent with this phenomenon.

The functional analysis of the CRISPR generated clones greatly supported our earlier results in CIP derived iPSC-nociceptors. A surprising finding was that single allelic

correction of CIP1.2 was sufficient to rescue the rheobase but did not return repetitive firing to healthy control levels. Yet, the *de novo* introduction of *bi-allelic* non-sense mutations in SCN9A of HC1 was sufficient to decrease firing to levels similar to CIP derived lines. Together these results may indicate that human nociceptors require two functional copies of SCN9A to be fully excitable. Although heterozygotes are thought to be asymptomatic, perhaps haplo-insufficiency has some effect on excitability under prolonged, high intensity stimulus conditions, it would therefore be interesting to pursue in depth clinical phenotyping of these individuals.

It has previously been shown that loss of Nav1.7 in mice causes an upregulation in the transcription of the endogenous opioid enkephalin, encoded by PENK. We investigated this in our human cellular model by comparing the transcription of the gene in the Nav1.7 KO line and the isogenic parent HC1 line. We were unable to find PENK expression in these cells when assessed by qPCR. This result demonstrates the excitability phenotype we observed here is independent of any interaction with endogenous opioid signalling system.

We extended our investigation into the role of human Nav1.7 by attempting to model generator potentials *in vitro* by applying a graded suprathreshold stimuli that slowly depolarised the membrane potential (Cheng et al., 2011). Nav1.7 KO iPSC-nociceptors were markedly less able to respond than healthy control iPSC-nociceptors, especially in response to slower depolarising stimuli suggesting a critical role for the channel in facilitating generator potentials and consistent with the described biophysical properties. This role is physiologically important if considered in the context of the spatial expression of the channel. As is to be shown in Chapter 5, Nav1.7 is concentrated in terminal structures, in pathological states, any increase in Nav1.7 activity could significantly contribute to allodynia and hyperalgesia by lowering the threshold for activation from the periphery.

Finally, following the observation that CIP patients have a significantly reduced IENFD we assessed outgrowth *in vitro* of Nav1.7 KO compared to isogenic control. Characterising axonal coverage in these cultures was technically challenging. Accurate cell counts are difficult to obtain in mature cultures due to an inherent proclivity of cell bodies to cluster and cell counts obtained during the initial plating are not reflective of mature cultures as they are inclusive of non-neuronal cells that are eliminated following anti-mitotic treatment. Technical challenges aside, it is perhaps unsurprising that significant deficits in outgrowth were not observed *in vitro*. The cultures do not reflect *in vivo* target driven axonogenesis; the epidermal targeting of endogenous nociceptive afferents undoubtedly requires complex environmental and chemical cues which we cannot fully replicate in our model system. Our results therefore do not rule out a role for Nav1.7 in target innervation. A notable theme in the developing nervous system is the requirement for electrical activity to maintain and substantiate end organ innervation and axon pathfinding (Spitzer, 2006; Ming et al., 2001). It is plausible given the contribution of the channel to ramp currents that Nav1.7 may play an active role during development perhaps functioning to amplify small subthreshold depolarisations sufficient to activate local calcium transients in developing terminals (Gomez, Snow and Letourneau, 1995). The channel could either contribute to an initial deficit in *ab initio* innervation or equally in the maintenance phase of connections (Nelson et al., 1989). Further work to investigate this function could include the development of co-cultures with target cells including for instance keratinocytes in the periphery or spinal dorsal horn neurons in the spinal cord and characterisation of axon growth and the number and function of synapses *in vitro*.

Chapter 5

Epitope tagging hNa$_v$1.7

5.1 Introduction

The localisation of a protein is often informative of its function, or, at the very least, serves as an investigative lead. Protein specific antibodies are classically used in culture to visualise protein localisation, however their function and, critically, specificity vary considerably (Rhodes and Trimmer, 2006). Commercially available VGSC antibodies, particularly those directed against hNav1.7 and hNav1.8 are generally poor, demonstrating nonspecific staining (Eberhardt et al., 2015 and unpublished correspondence). The extensive homology between family members as discussed in the introduction, may underlie the difficulty in raising human VGSC isoform-specific antibodies. An alternative approach to visualising protein location is the construction of fusion proteins, wherein a tag (a fluorescent protein or defined epitope) is placed in frame with the open reading frame of the gene such that the translation of the protein is contiguous with the tag. For fixed cell imaging, highly specific antibodies directed against the appended sequence are then used in lieu of those against the native protein. The site of tag integration must be considered carefully. Large tags such as those encoding for fluorescent proteins e.g. GFP derivatives, can interfere with protein trafficking confounding data. Furthermore, native protein-protein interactions can be inhibited following the addition of the tag via steric hindrance or through the masking of important interaction motifs (Snapp, 2005; Thielges et al., 2011).

In view of these considerations, a small peptide (HA) sequence tag was selected for knock-in into the SCN9A genomic locus. The hemagglutinin (HA) tag is a short, 8 amino

acid peptide sequence derived from the influenza hemagglutinin glycoprotein. Perhaps as a function of its genetic provenance, the epitope is highly antigenic. A number of specific antibodies are commercially available, which have been validated for use in multiple experimental applications including Western blot, ICC and immunoprecipitation (IP). The HA sequence is also uncharged, in contrast to other frequently used epitopes of similar length (e.g. FLAG, HIS-tag), this reduces the potential for any electrostatic interaction- an important consideration for ion channels. Endogenous hNav1.7 channel tagging has not previously been performed, therefore few *a priori* assumptions on suitable loci for insertion could be made. Typically, selection is informed by structural data, however at the time of initiating this project, a human sodium channel anatomic scale structure was not available (note that such information has very recently been published for human Nav1.4 (Pan et al., 2018)). In its absence, a conservative C-terminal location was chosen such that the tag resides intracellularly. Whilst this location precludes the prospect of live cell imaging, it is unlikely to affect electrophysiological function of the channel or inhibit drug binding, leaving experimental opportunities open. The cellular role of Nav1.7 is partly conferred by its cellular location, an enrichment in terminal structures would further support the hypothesis that hNav1.7 functions in part, to amplify generator potentials. The characterisation of the spatial expression of the channel is therefore of significant interest, having important downstream implications for analgesic targeting. Finally, in the latter half of this chapter we begin to explore native human Nav1.7 protein interactions. One of the inherent advantages of iPSC models is the capacity to scale cultures as required. This is particularly useful for protein-based applications where a large volume of cellular material is often needed, and this is unlikely to be achievable using primary cadaveric tissue. We exploit this aspect of the model and take advantage

of the strong specificity of the HA tag to perform the first co-immunoprecipitation of endogenous human Nav1.7, establishing an important proof of principle for future work.

Chapter aims:

- Generate an epitope tagged hNav1.7 via the genomic knock-in of a HA sequence into the SCN9A locus
- Characterise subcellular distribution of hNav1.7 protein in iPSC-nociceptors
- Perform a co-immunoprecipitation to isolate interacting hNav1.7 proteins

5.2 Methods

5.2.1 SgRNA design and validation

The design and validation of CRISPR Cas9 guides was performed as in Chapter 4, the following sgRNA sequences were cloned into the Sp.Cas9 plasmid PX459:

Table 5.1 Oligonucleotide sequences of HA_sgRNAs.

Sequence	Forward 5' – 3'	Reverse 5' – 3'
HA_sgRNA_1	CACCGAGACAAAGGGAAAGACAGCA	AAACTGCTGTCTTTCCCTTTGTCTC
HA_sgRNA_2	CACCGCACAAATAAATCACTTTCAC	AAACGTGAAAGTGATTTATTTGTGC

The following primers were used to amplify the C-terminal of SCN9A for the T7E1 assay:

C_TERMScreen_FW 5'-GTTAGTGGTGACCGGATCCAT-3',

C_TERM_Screen_RV 5'CTACAGAGTTCTCTTACGATTC-3'

5.2.2 Genetic screen for inclusion of the HA tag sequence

Genomic DNA was extracted using method described in Chapter 4, 1µl of DNA was used for the PCR screen with the following primer set:

C_TERM Screen_FW 5'-GTTAGTGGTGACCGGATCCAT-3',

C_TERM_Screen_HA_RV 5-TACCCATACGATGTTCCAGAT-3'

5.2.3 Allele specific PCR

To resolve the suggestion of upstream Cas9 cutting I used 'allele specific PCR'. This technique exploits bacterial plasmid incompatibility that is, only a single plasmid can be stably inherited during bacterial transformation. The C-terminal of SCN9A was amplified as before from HA+ clones using the primer set 5.2.1. 1µl of the crude PCR was blunt cloned into pJET1.2 linearised plasmid (ThermoFisher) at a 3:1 ratio, DHB10

E. coli (NEB) cells were thawed on ice and transformed with 1 µl of the ligation reaction. Plasmid DNA was extracted and sequenced using the follow primer:

pJET1.2_FW 5'-CGACTCACTATAGGGAGAGCGGC-3'

5.2.4 Terminal structure ICC staining

To better preserve terminal structures and growth cones, the fixation process (Method 2.4.2) was modified with the addition of 20% sucrose to the fixation buffer.

5.2.5 Schwann cell extraction

Schwann cells were harvested from the sciatic nerve and brachial plexus of postnatal day 3/4 Sprague Dawley rats. Nerves were enzymatically digested with collagenase (Sigma, 3 mg/ml) and dispase II protease (Sigma, 2.5 mg/ml) for 1 hour at 37°C. Following digestion, the nerves were gently triturated with a glass blown pipette before plating on PDL/Laminin coated flasks in DMEM/F12 + 10% FBS (Invitrogen). The following day, the cultures were transitioned to Expansion Medium (DMEM/F12, 10% FBS, 10mM NRG1-β1 EGF Domain (R&D Systems), 10ng/ml recombinant murine NGF (Peprotech), 4μM Forskolin (Sigma). Cells were treated with 5-10μm AraC (Sigma) to eliminate Fibroblasts. Following expansion, cells were frozen and stored in liquid nitrogen until required.

5.2.6 Establishing co-cultures

Myelinating co-cultures were prepared as previously described (Clark et al. 2017). In brief, 30,000 Rat Schwann cells were added to 30 DIV iPSC-derived neurons in Schwann cell basal medium [DMEM/F12 (ThermoFisher), 5 mg/ml insulin (Sigma), 100 mg/ml transferrin (Millipore), 25 ng/ml recombinant-human NGF (Peprotech), 25 ng/ml

Selenium (Sigma), 25 ng/ml thyroxine (Sigma), 30 ng/ml progesterone (Sigma), 25 ng/ml triiodothyronine (Sigma), 8 mg/ml putrescine (Sigma)].

Cells were either maintained in this medium where 'non-myelinating' conditions were required experimentally, or myelination was induced one week after Schwann cell addition by exposing the cells to myelination medium ((N2 medium, 1:300 phenol-free Matrigel (Corning), 5% charcoal-stripped FBS (ThermoFisher), 25 ng/ml recombinant-human NGF (Peprotech), 50mg/ml ascorbic acid (Sigma)).

5.2.7 ICC processing of myelinating co-cultures

In order to preserve myelin sheaths the staining process was adapted from Method 2.4.2, Cells were fixed for 10 minutes in 1%PFA, before being incubated with ice cold 100% methanol for 20 minutes. Detergent was omitted in all wash steps.

5.2.8 Western blotting

SCN9A-HA cells were grown under described iPSC/neuronal culture conditions. 50-60DIV iPSC-nociceptors and iPSC were lysed with ice cold modified RIPA (unless stated otherwise) (Sigma) supplemented with protease inhibitor cocktail (cOmplete Mini, EDTA-free, Roche) and lysates were cleared by centrifugation. Total protein (10 µg, determined as in Method 2.6.2 was incubated at 35°C for 5 min with 5X Lamelli Buffer (ThermoFisher). Proteins were separated on 4-12% BIS-TRIS mini gels (ThermoFisher) and transferred to a nitrocellulose membrane using Bio-Rad Wet Tank transfer system. Membranes were blocked for 1 hour in 8% skimmed milk, 0.1% PBS-T and incubated overnight with anti-HA (1:1000, Cell Signalling Technology) and β-actin (1:10,000, Sigma) in blocking solution. Membranes were washed 3 X in 0.1% PBS-T, then incubated at room temperature for 45 minutes with a HRP-conjugated secondary antibody

1:10,000 (Amersham, G.E healthcare). Signal was detected with ECL Prime using X-ray film (G.E. healthcare).

5.2.9 Pilot detergent screen

A small-scale detergent screen was performed as follows. 1 x 10^6 60 DIV iPSC were lifted using Versene EDTA, cells were spun at 400 x g for 3 minutes and resuspended in 1 ml of PBS. The suspension was divided into 4 aliquots and the cells were spun again at 800 x g for 4 minutes. The supernatant was removed, and each pellet was vigorously resuspended with one of the following detergents at 1% w/v in a Tris Base (50 mM Tris, 150 mM NaCl, pH 7.4): Digitonin, 3-[(3-Cholamidopropyl) dimethylammonio]-1-propanesulfonate (CHAPS), NP-40, Triton-X100 (all Sigma). Solutions were rotated end to end for 30 minutes at 4℃. An aliquot (10 μl) was removed (sample: 'before spin'), the remainder was then spun at 16,000 x g for 30 minutes to pellet insoluble material. A further 10 µl was taken from the supernatant (sample: 'after spin'). Both samples were then run on 4-12% BIS-TRIS gel and intensities compared following immunoblot with rabbit α-HA 1:1000. Band densitometry was performed using the protocol described in Method 2.6.3.

5.2.10 SCN2B co-immunoprecipitation

For the co-immunoprecipitation of SCN2B, 2 x 10^6 70 DIV iPSC-nociceptors were lysed in an ice-cold buffer comprising 0.1% NP40 in a Tris-HCl base (50 mM Tris, 150 mM NaCl, pH 7.4) supplemented with a protease inhibitor cocktail (complete Mini, EDTA-free, Roche) and PMSF (Sigma). Total protein (2mg) was incubated with 30µl of washed, pre-bound anti-HA paramagnetic beads (Pierce, ThermoFisher) in a low protein binding tube (Eppendorf). The sample was rotated end to end for 30 minutes to bind at RT. The

bound solution was then placed in a magnetic stand and the supernatant was removed. The lysis buffer was used to wash and resuspend the beads, and the process was repeated 3 times. On the final wash, ddH_2O was used in place of the lysis buffer. Proteins were eluted from beads by the addition of a non-reducing sample buffer, (pH 6.8; 0.3M Tris HCl, 5% SDS, 50% glycerol, lane marker tracking dye) at 35℃. The eluate was immediately processed for immunoblotting as before, with the exception that BOLT-Bis-TRIS Plus wedge well gels (Invitrogen) were used in order to accommodate increased sample volume. Membranes were incubated with 1:1000 SCN2B, and anti-HA (both 1:1000, CST).

5.3 Results

Precise genomic knock-in of a HA epitope tag into the SCN9A locus.

The intracellular C-terminus of Nav1.7 protein was selected as the insertion site for the HA epitope, this region is encoded by exon 27 of the SCN9A gene. The CRISPR single guide RNA sequence was designed as in Chapter 4. A 150bp sequence spanning the C-terminus of SCN9A NM_002977.3 was submitted to the MIT CRISPR database (http://mit.crispr.edu) and for further evaluation, guides were compared to the CHOP-CHOP database (http://chopchop.cbu.uib.no/). Two guides were selected based on the algorithmic score and on account of proximity to the desired loci (Figure 5.1). As before, the *in vitro* cutting efficacy was evaluated with the T7E1 assay in HEK293T. Both guides facilitated robust Cas9 cutting and evidence of double stranded break formation (Figure 5.2). Semi-quantification of the T7E1 cleavage products revealed HA.sgRNA_1 had slightly higher cutting efficiency (~26% vs 20%) than HA.sgRNA_2. Importantly, it also lay closer to the C-terminus therefore this guide was chosen for iPSC genomic editing.

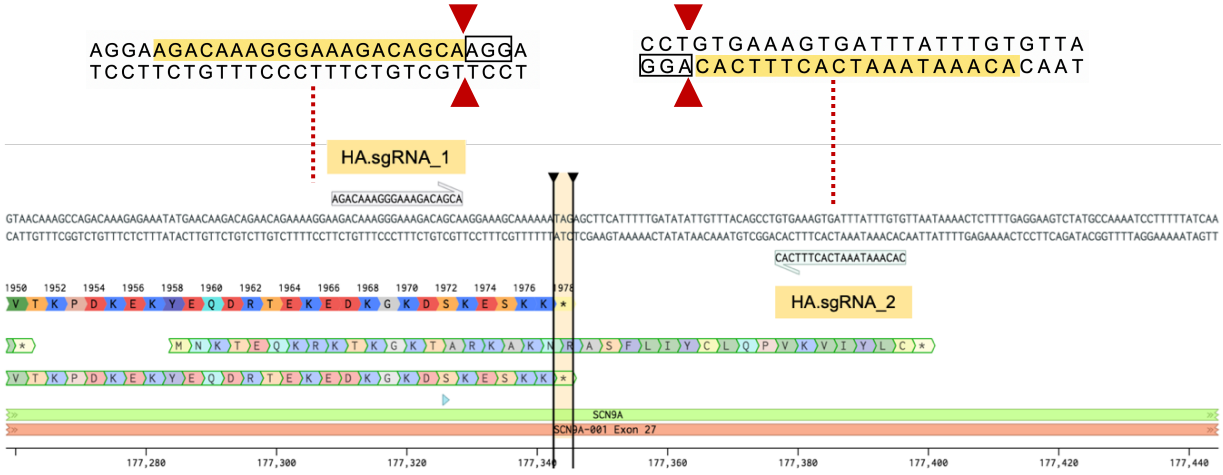
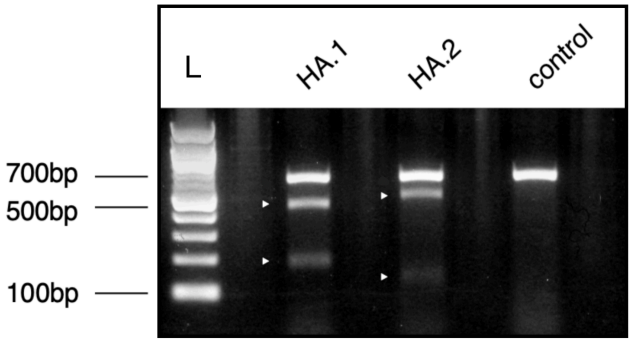


Figure 5.1. Selected genomic site for knock-in of HA tag sequence in HC1 iPSC.

Location of the sgRNA sites relative to the SCN9A stop codon p.1978* (highlighted in the peptide sequence). A magnified sequence is shown for HA.sgRNA_1 (left) and HA.sgRNA_2 (right) containing the sgRNA (yellow) and PAM site nucleotides (boxed), note that the PAM motif is not included in the final sgRNA sequence. Red arrows indicate cut site of Sp.Cas9 at a fixed distance of 3 bp upstream of the PAM site.



sgRNA	Fraction cleaved (%)	Distance from p.X1978 (bp)
HA.sgRNA_1	26.37	17
HA.sgRNA_2	20.05	37

Figure 5-2 Assessing HA sgRNA efficiency in vitro using T7E1
SCN9A Cas9 induced indel formation in HEK293T cells estimated by T7E1 Assay. Arrows indicate T7E1 cleavage products. Untransfected control population shown to confirm T7E1 activity is due to Cas9 indels and not due to the presence of a natural SNP in the amplified fragment. Both guides demonstrated good cutting efficiency as determined by densitometry ratio relative to the uncut fraction. A slightly higher efficiency was demonstrated by HA.sgRNA_1 (26.37%) vs HA.sgRNA_2 (20.05%).

5.3.1 Repair template design

Following the successful repair of the patient mutations using an asymmetric repair template the same principal was adopted for the knock in of the HA epitope tag. A 185 bp phosphorothioate capped ssODN template was synthesised incorporating a 27bp

nucleotide sequence corresponding to amino acids 98-106 (YPYDVPDYA) of the human influenza hemagglutinin glycoprotein (HA) immediately 3' to the stop codon (Fig. 5.3, Appendix).

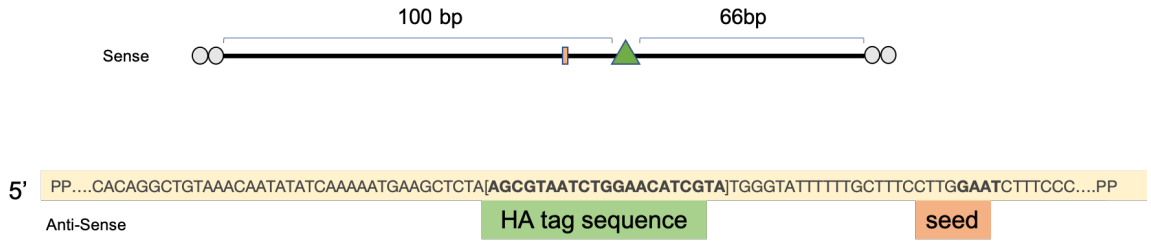
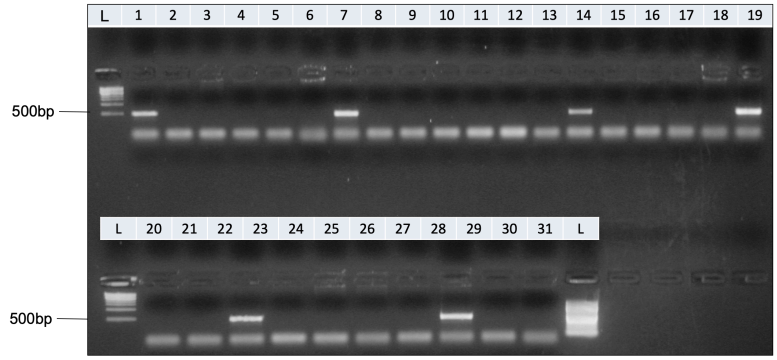


Figure 5-3 Asymmetric Repair template incorporating HA tag sequence

Top, schematic representation of the offset ssODN targeting the terminal codon of exon 27, shown here in sense orientation, 100bp and 66bp flank the HA tag nucleotide sequence. Phosphorothioate moieties link the two most terminal residues to increase resistance to nucleolytic attack. Bottom, selected nucleotide sequence of the repair template, modified residues in bold. Four silent mutations within the seed region were incorporated to block sgRNA binding in the event of successful repair. The ssODN was provided in anti-sense to the iPSC, as depicted.

HC1 iPSC were transfected as before using the optimised method from Chapter 4 and a total of 60 clones were picked. Cell survival post clone-picking was consistent with the earlier editing experiment with the HC1 line (92%). Clonal outgrowth in 96 well format was also similar; 8 clones were excluded due to evidence of spontaneous differentiation. In order to assess repair template insertion, a PCR based screening strategy was used prior to Sanger sequencing. A HA specific reverse primer was used to selectively amplify edited loci. An example agarose screening gel can be seen in Figure 5.4.

Eleven candidates were selected for outgrowth and a second PCR amplifying a 400bp segment was run and the product was analysed using Sanger sequencing.



Total screened	HA⁺ sequence
48	8 (16.6%)

Figure 5-4 Screening for HA tag insertion

Representative agarose screening gel using a HA specific reverse primer, positive fragments are 495bp in length. Lanes L; 1kb ladder. Six HA positive samples can be seen (Lanes:1,7,14,19,23,29). Note the visible lower bands <100bp are primer-dimer artifacts. In total, 48 samples were screened with 8 demonstrating positive PCR products equating to approximately to a 16% instance of HA insertion rate.

Curiously, in all traces analysed mixed chromatograms were observed at defined intervals upstream of the Cas9 cut-site (where usually they would occur downstream of the DSB site). I used 'allele specific' PCR to resolve this anomaly. I found, in contrast to earlier sequencing, no evidence of upstream cutting in any of the sequenced plasmids, where the HA tag was present the sequence was in frame with no evidence of indel insertion, implying perfect homology directed repair (Fig.5.5). The proportion of WT vs HA sequences however suggested a mixed clone was present, therefore the population was later re-clonally isolated, revealing heterozygous insertion of the HA-sequence in the selected clone. The C-terminal of Nav1.7 has extended regions of polynucleotide tracts therefore it is possible these gave rise to polymerase slippage during sequencing attempts, producing the misleading traces.

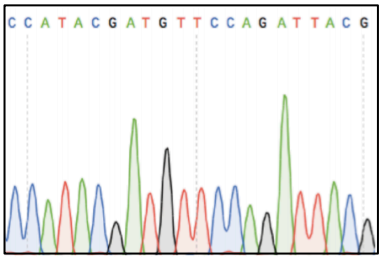


Figure 5-5 HA tag chromatogram

Resolved sequencing Chromatogram showing successful incorporation of the ssODN repair template and in-frame knock in of the HA sequence

5.3.2 Characterising Nav1.7 protein expression and localisation in iPSC-nociceptors

The utility of this cellular model depends upon the appropriate localisation of the Nav1.7 to the cell surface and insertion into the membrane; only there may the channel contribute to sodium ion conductance. A patching time point of 50 DIV was initially chosen based on published data demonstrating electrophysiological 'maturity' and laterally by qPCR analysis (see Chapter 3). However, mRNA levels are not always a direct correlate of protein, and they do not inform localisation. I therefore sought to characterise the temporal expression of the protein in Nav1.7-HA iPSC-nociceptors.

To confirm the channel was only expressed following cellular differentiation I first performed a Western blot of SCN9A-HA iPSCs and as anticipated, no expression of the channel was found (Fig. 5.6). I next explored the subcellular distribution of the channel

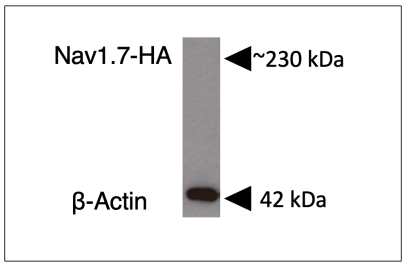


Figure 5-6 Western blot of SCN9A-HA iPSC

No expression of Nav1.7 protein can be seen in the SCN9A-HA undifferentiated iPSC. Beta actin shown as loading control. Arrows indicate predicted molecular weight (kDa)

in iPSC-nociceptors. Marked changes in intracellular location and intensity were observed during neuronal maturation. Early (25DIV) cells showed weak staining and prominent clustering of the channel was observed at the ER (Fig. 5.7 A). This result is in stark contrast to the localisation at 50 DIV, where Nav1.7 is clearly localised and enriched at the cell surface membrane and expressed at a higher level in the axons (Fig. 5.7. B, C & D). No staining was observed in cultures of the unedited parent line (HC1) (Fig. 5.8), demonstrating stringent antibody specificity.

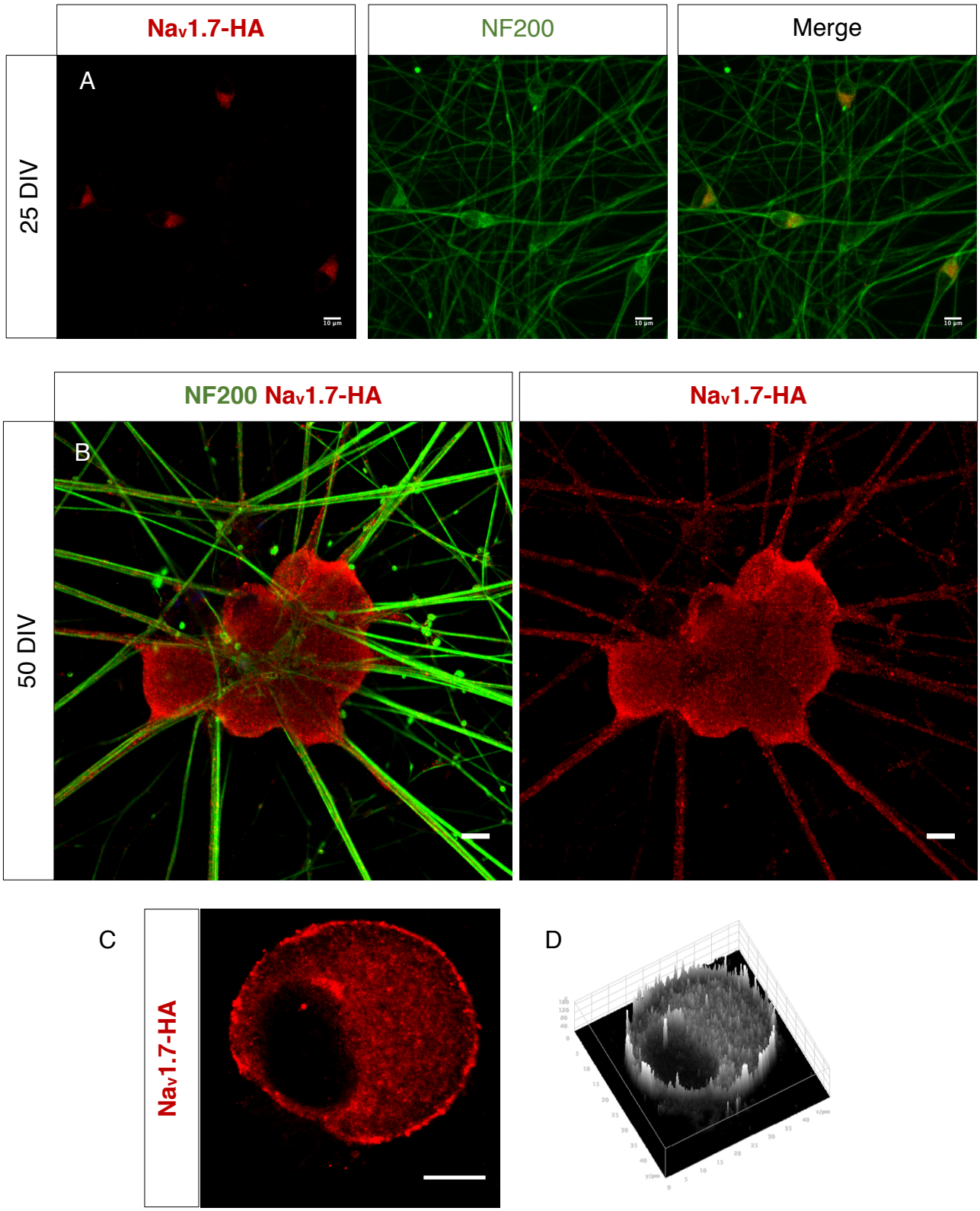


Figure 5.7 Nav1.7-HA localisation in iPSC-nociceptors

(A) Representative split and merged image of 25DIV HA-Nav1.7 iPSC-nociceptors, Nav1.7 (red) appeared to be lowly expressed and clustered in a hemi-nuclear ring, consistent with ER retention. The channel did not appear to be expressed in axonal structures. In contrast, at 50DIV (B) there was striking increase and clear change in spatial expression of Nav1.7, shown as flattened Z-stack. The channel was visibly expressed in axons and pronounced punctate staining was visible at the plasma membrane of the soma (C). (D) 3D surface plot of (C). Scale bars: all 10µm.

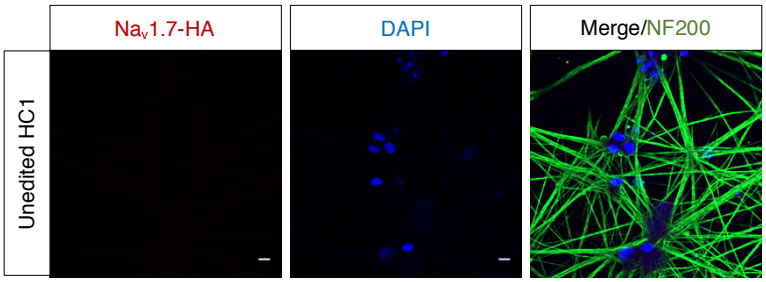


Figure 5-8 Verification of HA antibody specificity using the isogenic control HC1

Two species of anti-HA antibody raised in mouse and rabbit respectively were validated using the unedited parent control line HC1, no HA signal above secondary background was seen in the unedited control. Representative image of rabbit α-HA stained HC1 iPSC-nociceptors, scale bar: 10 μm.

5.3.3 Characterising hNav1.7 expression at axon terminals *in vitro*

The biophysical properties of Nav1.7, as demonstrated in Chapter 4, suggest it may be important for producing generator potentials, to fulfil this role the channel should be expressed in terminal endings. We therefore sought to characterise expression in axonal terminal structures present *in vitro*. Staining revealed a striking enrichment of the channel in growth cones, including in filipodia and lamellipodia structures, demonstrated by colocalization of the channel with the microfilament protein f-actin (Fig.5.9 A & B).

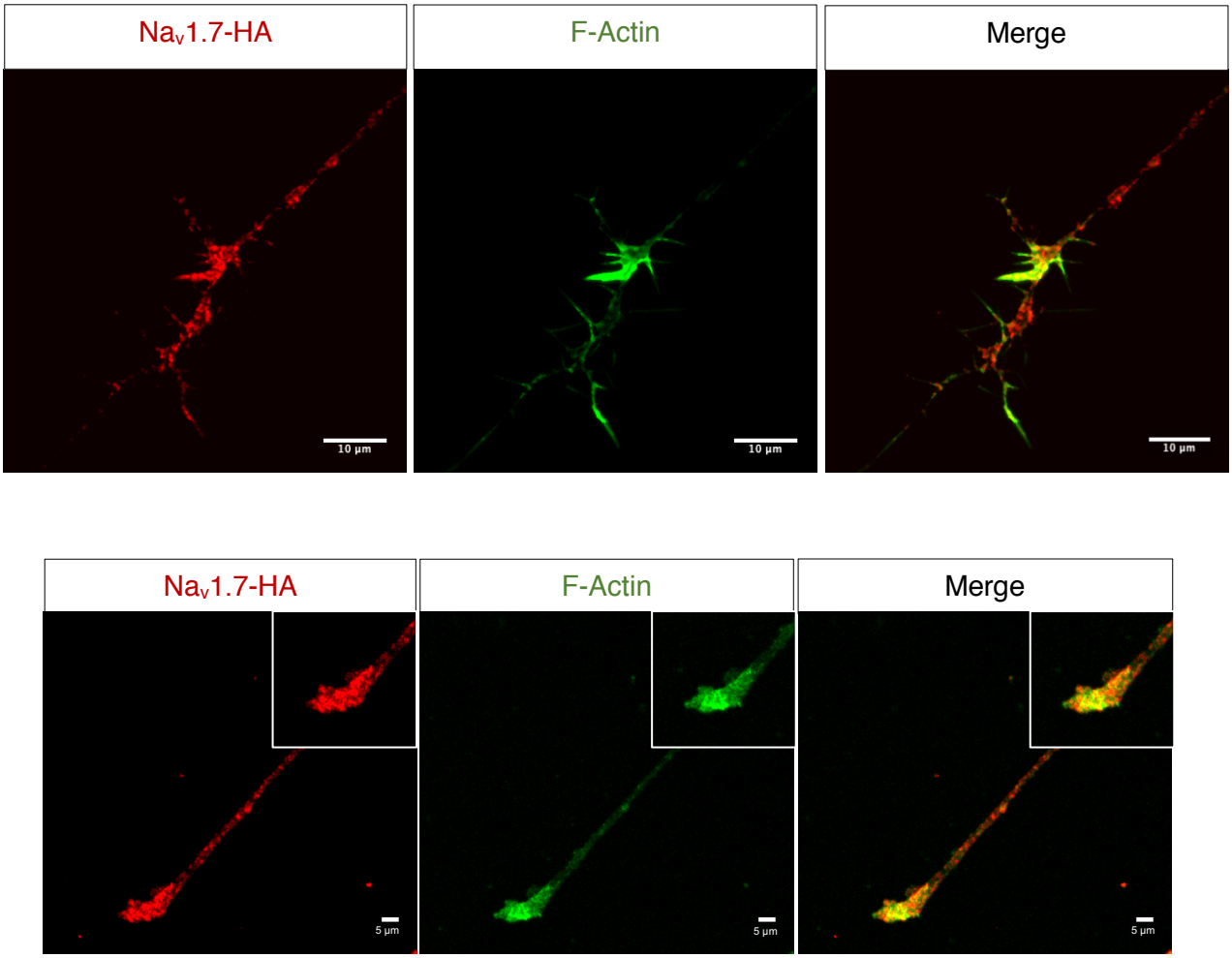


Figure 5-9. hNav1.7 localised to growth cones in vitro

Representative images of terminal structures *in vitro*, Nav1.7 (red) is enriched in growth-cone filopodia (A) and lamellipodia (B) co-stained with f-actin (green) a filament enriched in cellular growth cones. Inset images in (B) are magnified.

5.3.4 Nav1.7 is trafficked to the nodes of Ranvier in myelinating co-cultures.

The heterogenous distribution of sodium channels is particularly pronounced in myelinating fibres. Ion channels are sequestered in dense clusters between gaps in the myelin sheaths, known as nodes of Ranvier. Sodium channel subtypes show distinct stereotypical patterns of expression in myelinating neurons, for instance Nav1.6 is predominantly found at the nodes in both the CNS and PNS, whereas Nav1.2 expression is restricted to the axon initial domain and cell soma (Caldwell et al., 2000; Boiko et al., 2001). Previously, Nav1.7 has been shown to be expressed in a subset of nodes of Ranvier

in Aδ-fibres within the sciatic nerve and dorsal root using an antibody that only recognises the rat isoform (Black et al., 2012), therefore we sought to determine if this pattern of expression is replicated *in vitro*.

To assess if the channel is trafficked to the nodes in iPSC-nociceptors we established Schwann cell co-cultures (Fig. 5.10). Unfortunately, at present no protocols have been described for the production of human myelinating Schwann cells, therefore rat Schwann cells were used in lieu. These cells have previously been shown to robustly myelinate the iPSC-nociceptors *in vitro* (Clark et al., 2017). Establishing the co-culture provided an opportunity to directly observe defined stages of myelination and characterise concomitant changes in Nav1.7 trafficking.

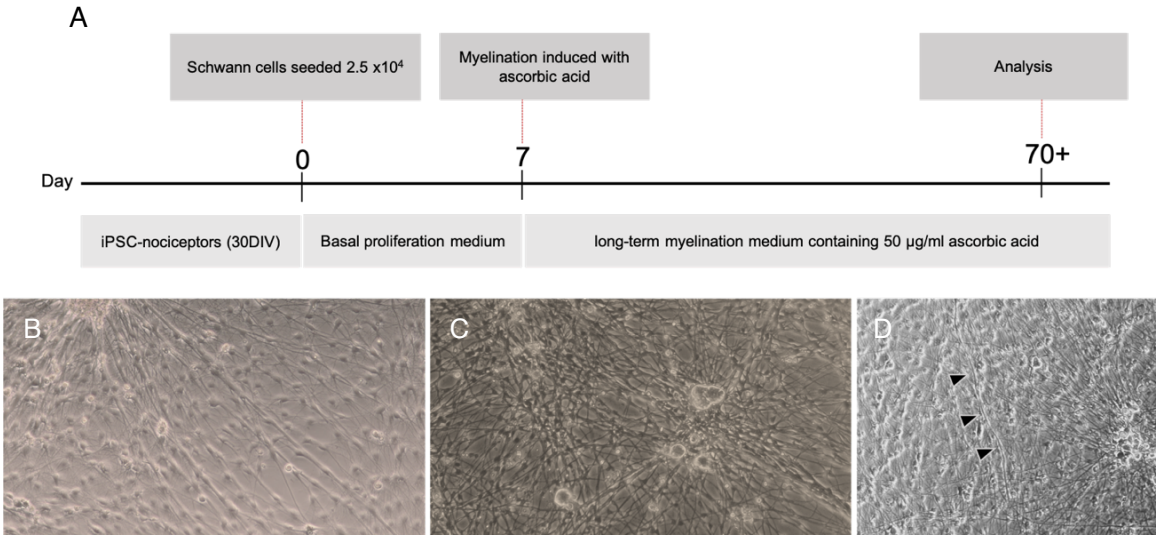


Figure 5-10 Nav1.7-HA iPSC-nociceptor co-cultures with rat Schwann cells

(A) Timeline of culture protocol. Rat Schwann cells efficiently myelinate iPSC-nociceptors *in vitro*. Representative phase-contrast images taken during day 3 (B), day 14 (C) and day 40 (D) in culture. Schwann cells rapidly proliferate following seeding (B) and align with axons shortly thereafter (C). Maintenance in ascorbic acid containing medium induces myelination of axons visible as phase-bright structures enveloping axons (D).

Harvested Schwann cells from P10 Sprague Dawley rats were added to SCN9A-HA iPSC-nociceptor DIV30 cultures. Schwann cells rapidly proliferated and migrated to

axons within 3 days in culture (Fig. 5.10, B), shortly thereafter many formed close alignment with axonal processes (Fig. 5.10, C). *In vivo* C-fibres are associated with non-myelinating Schwann cells which envelope the unmyelinated axons forming Remak Bundles. To first examine the influence of Schwann cell alignment on Nav1.7 expression I maintained co-cultures in non-myelinating conditions for 21 days. Staining with *α*-S100, a Schwann cell cytoplasmic marker, revealed the cells formed a close alignment with the axons, with no overt differences in Nav1.7 localisation when compared to a-Schwann cell conditions (Fig. 5.11, A). Interestingly, however, the neurons adopted pseudo-unipolar morphology, typically not presented in standard *in vitro* culture conditions - suggested the non-myelinating Schwann cells are capable of significantly influencing neuronal structures and consistent with early description observing the

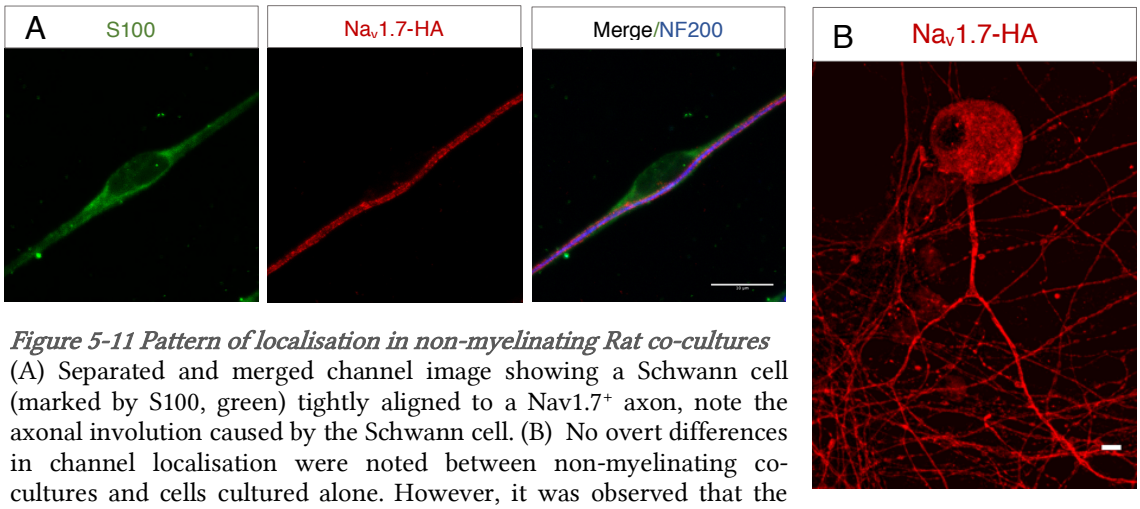


Figure 5-11 Pattern of localisation in non-myelinating Rat co-cultures
(A) Separated and merged channel image showing a Schwann cell (marked by S100, green) tightly aligned to a Nav1.7$^+$ axon, note the axonal involution caused by the Schwann cell. (B) No overt differences in channel localisation were noted between non-myelinating co-cultures and cells cultured alone. However, it was observed that the majority of neurons in co-cultures adopted a pseudo-unipolar structure, characteristic of DRG morphology *in vivo.*

same effect in murine-rat co-cultures (Mudge, 1984) (Fig 5.11, B).

Next, in order to establish whether hNav1.7 localises to the nodes of Ranvier, myelination of the co-cultures was induced through the addition of ascorbic acid to the medium. Ascorbic acid has previously been shown to regulate basal lamina assembly and myelin formation *in vitro* (Eldridge et al., 1987). Myelin sheaths began to form within 10-14 days as assessed by brightfield microscopy (Fig. 5.10 D), to enrich the

number of nodes present, the cultures were allowed to mature for a further 40 days before analysis. Myelin was stained with the α-myelin basic protein (MBP), a major constituent of the myelin sheath in the PNS. hNav1.7 was clearly localised to the nodes of Ranvier, demarcated and flanked by MBP expression (Fig. 5.12, A). The percentage of Nav1.7^{+} nodes was >93% (41/44), determined by the presence of CASPR and MBP

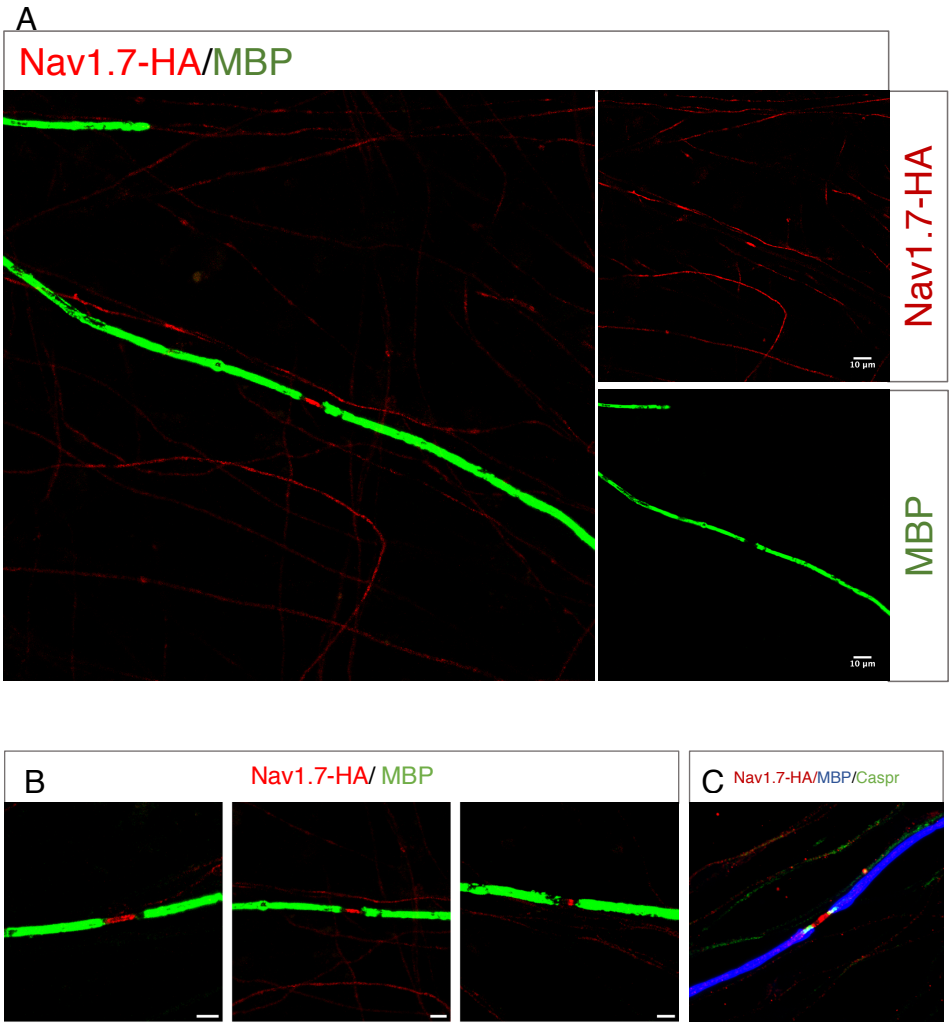


Figure 5.12 Nav1.7 is trafficked to the nodes of Ranvier in iPSC Nociceptors.

(A) Representative split and merged channel image showing hNav1.7 (red) is localised to the nodes of Ranvier (arrow) in Schwann cell co-cultures. MBP (green) marks the myelin sheath. (B) Maturation of nodes *in vitro*, left to right, gradual compaction of Nav1.7 localisation consistent with inter-distance reduction in glial contacts and assembly of paranodal proteins including CASPR (c)

staining (Fig. 5.12, C) In immature nodes present within the culture, Nav1.7 expression was concentrated, but notably elongated (Fig. 5.12, B). This is consistent with lateral

compaction following an inter-distance reduction between glial contacts and subsequent maturation of the node. Together, the results demonstrate Nav1.7 is clearly localised to nodal structures in myelinated iPSC-nociceptors.

5.3.5 Optimising co-immunoprecipitation using the HA tag

The addition of the HA-tag to Nav1.7 provides a significant experimental opportunity. The practical difficulties of working with the channel have hindered many basic characterisations of its function. Indeed, the dearth of known interacting proteins is reflective of such. Voltage gated sodium channels exist in large multi-molecular complexes and the restriction to precise intracellular locations are a result of a multitude of interactions with components of the secretory pathway. There appears to be VGSC subtype specific interactions, suggesting alternate trafficking pathways for different family members (Su et al., 2013). The potential discovery of interactors serves as an attractive source of novel therapeutic targets and would significantly add to the fundamental biological study of the channel. With this in mind, we sought to develop a co-immunoprecipitation protocol for Nav1.7 using the HA tag, ultimately in view to performing affinity purified LC/MS/MS.

Earlier in the chapter Nav1.7 had been solubilised using RIPA buffer; a reasonably stringent lysis solution due to a high percentage of the ionic detergent SDS in combination with NP40. In order to maintain protein interactions a fine balance must be sought between solubilisation and stringency. Ionic detergents may produce a low background, but low affinity interactions are also lost, therefore, co-immunoprecipitation is typically performed under conditions of low stringency using zwitterionic or non-ionic detergents to preserve weak or non-covalent interactions.

Ideally, a comprehensive screen of non-ionic detergents should be performed to assess protein solubility (le Maire, Champeil and Møller, 2000), due to the time and cost

associated with generating a large amount of nociceptor derived total protein, a small initial screen was performed using 4 detergents.

Three non-ionic detergents; Tritonx-100, Nonidet-p40 (NP-40) and digitonin, and one zwitterionic; CHAPS, were selected and their ability to solubilise hNav1.7 before and after centrifugation was evaluated (Fig. 5.13, A). Digitonin poorly solubilised the channel and during buffer preparation the detergent continually precipitated, even with prolonged heating. CHAPS solubilised the protein satisfactorily, however it demonstrated the same tendency as digitonin, therefore it was also excluded. The two non-ionic detergents NP-40 and Triton-X100 performed well, and little difference was found between the two - perhaps owing to a similar molecular structure. A further evaluation suggested NP40 was slightly more effective in solubilising, therefore this detergent was chosen for the first co-immuno-precipitation experiment of endogenous hNav1.7. During the course of these experiments it was noted the channel had a strong tendency to aggregate when denatured prior to loading and a significant fraction remained in the wells of the Tris-gel unable to migrate, likely due to the strong hydrophobicity of the transmembrane domains. Lowering and omitting the heat step prior to loading both significantly increased protein migration, therefore heat steps in subsequent protocols were omitted.

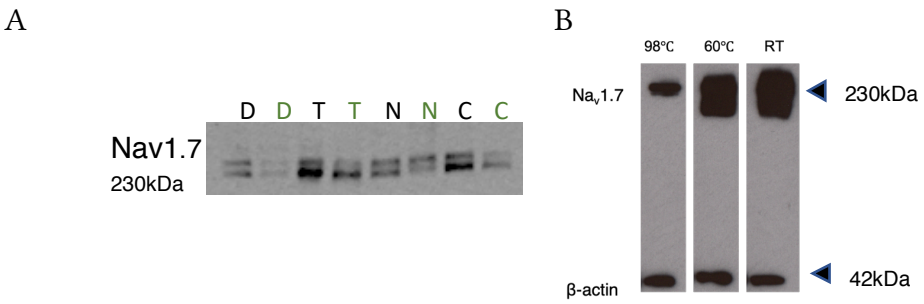


Figure 5-13 Nav1.7-HA Western blot conditions

Immunoblot from detergent pilot, from left to right: D; Digitonin, T; Triton-X100, N;NP40, C; CHAPS, before (black) and after (green) spinning to remove insoluble material, A significant fraction of Nav1.7 remained soluble following pelleting when cells were lysed with NP40 and TX-100, suggesting these detergents were suitable for downstream co-immunoprecipitation experiment.(B) Nav1.7 aggregates with increasing heat. Equal amounts of total protein were lysed then either subject to a 2 minute heating step or loaded without heat treatment. Beta-actin shown as loading control.

5.3.6 Co-immunoprecipitation of the sodium channel beta subunit SCN2B

Following the spatial characterisation of Nav1.7 expression in the iPSC-nociceptors, I decided to investigate protein interactors of the channel. VGSCs associate with at least one of four auxiliary beta subunits encoded by the genes SCN1-4B (Isom, 2014). Beta subunits are small intrinsic type I membrane proteins with a highly conserved extracellular Immunoglobulin loop (IG). These proteins modulate the kinetics and gating of VGSC alpha subunits, however the respective effect appears to be highly cell type dependent and significant experimental discrepancies are apparent between *in vivo* and heterologous expression studies (Zhao, O'Leary and Chahine, 2011; Chen et al., 2004). In the rodent DRG, SCN1-3B are highly and differentially expressed, β1 and β2 mRNA levels are significantly correlated with medium and large diameter neurons and β2 and β3 are associated with small (<25 μm) diameter neurons. In heterologous expression systems Nav1.7 is usually co-transfected with the β1 and β2 subunits (Cox et al., 2010; Blesneac et al., 2017; Zhang et al., 2018) Although this combination has become the *de facto* standard for *in vitro* work, previous studies of Nav1.7 beta subunit regulation have produced conflicting data on the functional relevance of β1/2 co-expression. In initial studies performed in *Xenopus* oocytes β1/ β2 did not appear to accelerate the inactivation kinetics of Nav1.7 (Sangameswaran et al., 1996) whilst others have suggested only β 1 has an appreciable influence on Nav1.7 kinetics.

In vivo, studies using *Scn2b-/-* mice have shown a profound reduction in the TTX-S I_{na} suggesting the β2 may be required for membrane insertion. Later work from the same group however failed to find significant colocalization of Nav1.7 and β 2. In view of this conflicting data I sought to investigate whether Nav1.7 interacts with SCN2B in our model by using co-immunoprecipitation of the HA tag. Moreover as we found SCN2B to be highly expressed in the iPSC-nociceptors at mRNA level (not shown), this work established a proof of principle for isolating and investigating native Nav1.7 protein interactions.

Following the detergent screen an NP40 based buffer was used to lyse 65 DIV SCN9A-HA iPSC-nociceptor cultures, commercial paramagnetic anti-HA beads (Fig. 5.12, A) were used to precipitate Nav1.7 and immunoblotting was performed using an anti-SCN2B antibody (previously validated). Immunoblotting revealed a robust signal corresponding to the correct mW of the beta subunit, no signal was observed in the negative control (HC1 unedited). Interestingly, a strong band was observed at the same weight as Nav1.7 c.250kDA, which could represent a fraction of SCN2B still covalently linked to the alpha-subunit as non-denaturing conditions were used throughout the IP and high temperature steps were omitted in order to avoid aggregation.

As the total protein was not fractionated prior to input, using this data alone it is not possible to comment on the localisation of the interaction. However, subsequent ICC experiments showed significant co-localisation with Nav1.7 in the axons and striking enrichment in the proximal region of the axon (Fig. 5-14, C).

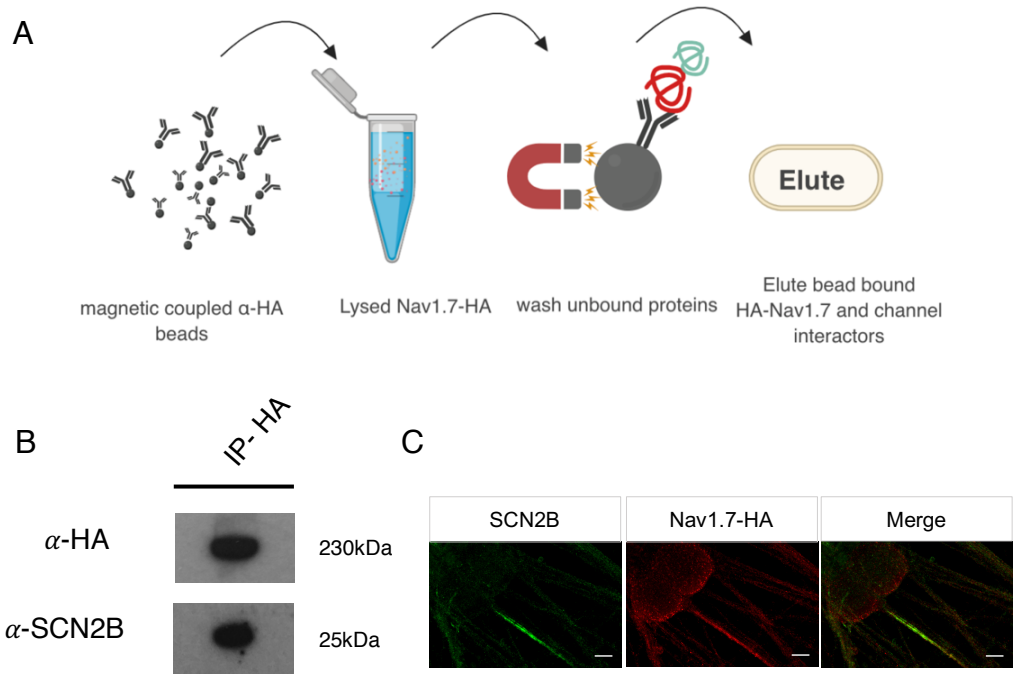


Figure 5-14 co-immunoprecipitation of SCN2B

(A) Outline of the co-immunoprecipitation using α-HA paramagnetic beads. (B) immunoblot of α-HA and α-SCN2B using input from the immunoprecipitation. (C) Co-localisation of Nav1.7 and SCN2B interaction in iPSC-nociceptors. Negligible levels were seen in the soma, the strongest signal was observed in an axonal region immediately proximal to the cell body.

5.4 Discussion

The results describe the first endogenous tagging of human Nav1.7 protein. We efficiently achieved a knock in of the HA epitope tag to the C-terminus of SCN9A using CRISPR/Cas9 in conjunction with an asymmetric ssODN repair template.

The endogenous tagging of genomic loci is preferable to expression achieved via the transfection of exogenous cDNA constructs or via viral means. Overexpression by heterologous promoters can often result in protein mis-localisation and aggregation, confounding studies of protein trafficking (Costantini et al., 2012; Zhao et al., 2010) . In contrast, the targeting of native genomic loci ensures the tagged proteins are subject to regulation by endogenous regulatory elements and importantly, native protein expression is preserved at a physiologically relevant level. In this respect, the approach

used here is also arguably superior to the targeting of safe-harbor sites (a commonly used strategy for iPSC gene knock-in) (Lombardo et al., 2011).

A strong temporal increase in protein expression was observed, in line with the results from SCN9A mRNA transcript analysis performed in Chapter 3. The protein was localised to a number of neuronal compartments in mature nociceptors including the soma, axons, growth cones and nodes of Ranvier. The pattern of Nav1.7 localisation revealed is consistent with early descriptions of the channel in rat DRG which also showed an enrichment in growth cones in culture (Toledo-Aral et al., 1997). The enrichment of the human channel in this location is an important finding when placed in context of our earlier results from the KO line, demonstrating a reduction in firing probability in response to slow depolarisation. This pattern of localisation suitably positions Nav1.7 to amplify local generator potentials within the terminal facilitating action potential generation.

Aside from a local electrophysiological function a non-canonical role for the channel in terminal structures has also previously been suggested. In rodents, Nav1.7 has recently been shown to regulate semaphorin 3A signalling in conjunction with CRMP1 thereby modulating axon path-finding (Yamane et al., 2017). hNav1.7 could act as a local signal transducer in extending neurites, perhaps mediating appropriate target innervation peripherally and/or centrally. The reduction in intra-epidermal nerve count described in CIP patients may be suggestive of such, however further research into the role the channel may play in axonal pathfinding is required. I did not observe a deficit in axon density in the CRISPR generated Nav1.7 knockout line versus control (see Chapter 4) although this result should be placed in context of the previously discussed limitations of a model system.

A high percentage of nodes of Ranvier were immuno-positive for Nav1.7 (>93%), in rat the channel was shown to be present in only a subset of nodes in small

diameter neurons (36%) in the dorsal root and sciatic nerve. This discrepancy may either be a species difference or reflect the degree of homogeneity in the type of nociceptive neurons generated by the differentiation protocol. The biophysical properties of the channel appear, *prima facie*, ill-fitting for nodal occupation in isolation, however co-expression with Nav1.6 may offer the neuron a high 'safety factor' for faithful conduction of the action potential.

In the latter half of this chapter, I performed the first co-immunoprecipitation of endogenous human Nav1.7, demonstrating Nav1.7 associates with the β2 subunit. This finding is in contrast to those recently made by (Kanellopoulos et al., 2018). *Scn2b* was not featured in a list of interacting proteins identified using mass-spectrometry analysis of a Nav1.7 affinity tagged (TAP) mouse model, curiously the authors only found *Scn3b*. Ho et al also failed to find significant co-localisation with Nav1.7 at the plasma membrane in mDRG (Ho et al., 2012). This finding is, however, in agreement with our ICC data - no co-localisation was observed at the soma membrane, rather, the co-localisation was concentrated in the initial/proximal segment of select processes which Ho et al did not specifically examine. The enrichment here is interesting, as I had previously noted strong staining of Nav1.7 at select axonal regions close to the soma. It has been suggested that the stem structure of DRG neurons contains a region with a composition similar to the AIS, but this remains poorly characterised (Nascimento, Mar and Sousa, 2018). However, the high density of Nav1.7 and evidence for SCN2B colocalization limited only to this region suggest perhaps that this proximal segment has unique function to the neuron (I also found asymmetric localisation of other markers in this region e.g. MAP2, data not shown). Changes in the density of sodium channels and length of the AIS in CNS neurons has been shown to compensate for perturbations in neuronal activity (Grubb and Burrone, 2010), one could speculate that this proximal segment may serve a similar purpose, for instance modulating AP

propagation into the central branch. This would require further work to determine, however in any case, the clear evidence of a neuronal domain specific interaction show here further challenges the relevancy of co-expressing SCN2B with Nav1.7 in HEK293.

Finally, to date, very few proteins that interact with Nav1.7 have been identified and even fewer for the human channel. In fact, the results in this chapter describe, to our knowledge, the first co-immunoprecipitation of hNav1.7 performed in a neuronal model. An important area for future research therefore is the identification of trafficking partners, these may present a significant pool of new therapeutic targets, particularly if specific to Nav1.7 - there is already good evidence to suggest that several of the VGSC α isoforms differentially associate with trafficking partners (Dash et al., 2018).

The co-immunoprecipitation performed here is an important proof of concept and ideally could be used to achieve this aim in conjunction with mass-spectrometry analysis. iPSC-nociceptors are highly enriched in Nav1.7 protein as reflected in the low total protein input required for the co-IP and minimal amount required for Nav1.7 western blot. The cultures can also be scaled as desired, a significant advantage to iPSC technology.

In addition to categorical identification, the localisation of the interactions could be spatially resolved using ICC as performed here for SCN2B, or through the use of other methods such as proximity ligation assays. A further development to the model would be the generation of a fluorescent tag knock-in for the purposes of live cell imaging. This would require a careful selection of insertion site owing to the increased size of the appended protein. It would be prudent to preliminary screen sites in a heterologous expression system prior to genomic knock-in. If the C-terminal site proves accommodating for larger modifications, the sgRNA validated here could be used to

facilitate genomic insertion. The use of canonical fluorescent proteins would require modification to the repair strategy since even the smallest described surpasses the ssODN production limit of 250bp. Therefore, long ssODNs or a classic plasmid based template would be required, which may decrease the efficiency of repair. Alternatively, split fluorescent protein variants have been described (Leonetti et al., 2016), however this approach would require two steps of genomic targeting, or exogenous transfection of the second larger fragment.

Chapter 6 Discussion and future perspectives

The work in this thesis was performed to gain a greater understanding of the contribution of Nav1.7 to the pathogenesis of congenital insensitivity to pain and more broadly, for insight into the form and function of Nav1.7 in human nociceptor physiology. It describes to our knowledge the first reported instance of CRISPR Cas9 targeting of human SCN9A.

The CRISPR Cas system is a more facile tool than its predecessors, however, the idiosyncrasies of iPSCs and the genomic sequence of Nav1.7 itself, nevertheless presented a significant experimental challenge. Following optimisation, I was able to successfully generate 3 novel engineered lines with which we have derived several important insights. From both Chapters 3 and 4 it is evident that the channel is a key regulator of human nociceptor excitability, contributing a significant fraction of current in the cells. The channel is highly expressed in iPSC-nociceptors, both at the transcriptional and protein level and this is in keeping with findings from primary cadaveric human neurons and similar to those from mice – suggesting, together, that this is not a feature peculiar to the differentiation process. Our findings are in contrast to the conclusions made by Zhang et al, who suggested a limited role for the channel in the excitability of cadaveric-derived human nociceptors. This was notably based on the result that Protoxin-II failed to inhibit TTX-S currents (and the assumption that this compound selectively targets Nav1.7), curiously they simultaneously demonstrated the compound PF-05089771, also putatively selective for Nav1.7, to completely inhibit the same currents. The authors favoured the hypothesis of loss of PF-05089771 selectivity, rather than loss of Protoxin-II potency, when expressed neuronally rather than in a

heterologous system. In our laboratory, we have found PF-05089771 to impact the function of only iPSC-nociceptors expressing Nav1.7, strongly suggestive of good specificity (McDermott et al., in press).

Although we robustly demonstrated a reduction in excitability in CIP/KO lines, it is quite apparent that following stimulation of the cell soma, neurons retained the capacity to fire action potentials in absence of Nav1.7. This finding is consistent with computer simulation models and dynamic clamp recordings, which describe a linear relationship between Nav1.7 conductance and the threshold for firing a single action potential, as well as firing in response to suprathreshold depolarising stimuli (Choi, J.-S.; Waxman 2011; Vasylyev et al. 2014). It is plausible that a greater electrophysiological effect may have been revealed if recording of the cell soma were performed following selective stimulation of terminal structures. In support of this Jurcakova et al. (2018) demonstrated using an *ex vivo* skin-nerve preparation that application of the Nav1.7 blocker PF-05089771 to terminal compartments, blocked action potentials conduction in 65% of C-fibre nociceptors they assessed. Similarly, a role for the channel in the conduction in vagal sensory neurons has also been shown (Muroi et al., 2011). Direct patch clamp recording of neurite structures *in vitro* is technically challenging. Future work may therefore entail the culture of the iPSC-nociceptors in microfluidic devices, such that the axon terminals are fluidically isolated from somal bodies, permitting restricted axonal stimulation and evaluation of hNav1.7's role in electrogenesis at the terminal and action potential conduction.

The striking enrichment of the channel in growth cones and terminal structures *in vitro* visualised with Nav1.7-HA line, supports the importance of this locale to Nav1.7 activity. We did not find a significant difference in the long-term axonal outgrowth between CRISPR Nav1.7 KO and isogenic control; a parameter investigated following the finding that intraepidermal nerve fibre density was significantly reduced in CIP patients,

including patients from whom the iPSCs were derived. Target driven innervation requires the orchestration of multiple developmental and environmental cues, absent in this model system. Therefore, our result certainly does not preclude a role for Nav1.7 in axonal genesis, nor is it contradictory to our *in vivo* findings. It remains to be clarified whether innervation *ab initio* is reduced in CIP patients or the reduction is a reflection of axonal degeneration. Of the two, the former could be more suitably modelled in this system given the embryonic/early postnatal profile of the iPSC-nociceptors, culture conditions could therefore be extended to include target cell types e.g. keratinocytes or dorsal horn neurons, and synaptic connections could be quantified.

A notable theme for the development of appropriate target innervation throughout the developing nervous system is the requirement for activity. Could Nav1.7 be fulfilling this role in human nociceptors? By facilitating generator potentials in the axonal growth cone, Nav1.7 activation may be sufficient to locally amplify electrotonic signals leading to calcium influx via the activation of VGCCs and in doing so, promoting local calcium transients and influencing downstream axonal targeting events. Intriguingly, the TTX-R α-isoform Nav1.9 has been suggested to function in this manner in motor neurons (Subramanian et al., 2012). Whilst they mediate distinct currents, both Nav1.7 and Nav1.9 are capable of amplifying low threshold stimuli (Lolignier et al., 2015) that might reasonably be expected to arise during the course of development. Unfortunately, we do not yet have any structural data on the central terminals from individuals with CIP, therefore we do not know whether central innervation is equally affected by loss of Nav1.7 activity.

It is apparent that the combination of reduced excitability and loss of epidermal innervation in CIP likely underlies the lack of peripheral pain sensation, yet it poses a quandary between mice and humans. The former of which have normal IENFD yet

recapitulate much of the human phenotype. This strongly suggests additional contributing roles for Nav1.7. Specifically, we did not examine the role of the channel in neurotransmitter release, where in mice it has been suggested to regulate central terminal transmission. This would certainly be an interesting area to pursue in the future given our localisation data. The probability of multiple causal roles for Nav1.7 in CIP is likely of reassurance to those in industry developing Nav1.7 targeting therapeutics in an effort to recapitulate aspects of the disorder. If the phenotype was purely due to developmental structural perturbations, synthesis of Nav1.7 blockers would perhaps, in effect, constitute a fool's errand. Nav1.7 therefore remains an important therapeutic target and the CRISPR KO Nav1.7 line generated will be a useful tool for drug development. By electrophysiological comparison of isogenic controls, off-target VGSC activity of putatively selective compounds could be determined.

The homology of the family is a significant hurdle to therapeutic development and reflects the relatively slow rate of development of Nav1.7 blockers since the original CIP paper was described. As is evident from several studies the cellular milieu in which the channel is expressed also has a significant impact on channel function, therefore the use of a neuronal model in which Nav1.7 is endogenously expressed and as my work shows - capable of associating with native interacting partners, is a significant improvement to heterologous studies.

Perspective on iPSC based modelling of pain variants

Pain research is beset by inter-individual variation, a manifestation of the layering of psychological, physiological and cultural factors of pain perception. Mendelian pain disorders are undoubtedly the low hanging fruit of pain genetics; they are highly penetrant disorders which, for the purposes of *in vitro* modelling, is important. Whether

the model can be extended to investigate common variants in painful disorders is unclear. Only a few high-quality pain GWAS have been performed from select cohorts including acute postsurgical pain and chronic widespread pain (Sexton et al., 2018). The heterogeneity in these conditions can make the identification of common variants extremely challenging and arguably the functional analysis even more so - particularly, as according to the common gene common variant hypothesis, the effect size of each variant is likely to be small. Interestingly, an increasing number of fields are actively pursuing expression quantitive trait loci (eQTL) analysis using iPSCs, and are now tentatively exploring cell-type-specific eQTL following directed differentiation to a relevant cell identity (Pashos et al., 2017). Whilst possible, these efforts require hundreds of iPSC lines and are technically challenging and extremely costly, inefficiencies in cellular differentiation also have the potential to significantly skew results (Schwartzentruber et al., 2018). The model described herein is arguably more suitable to the study of rare highly penetrant variants. For instance, it could quite feasibly be used to investigate rare gain of function SCN9A variants recently identified in patients with diabetic neuropathy (Blesneac et al., 2017). The model has been previously applied to EM associated SCN9A mutations in the same manner (Cao et al., 2016).

Further work should aim to generate a greater diversity of nociceptor subtypes, although the protocol used herein is robust, it is limited by the relative homogeneity in lineage generated i.e. broadly neurons of a non-peptidergic identity. Whilst it is clear the cells generated express Nav1.7 very highly, and thus are appropriate vectors with which to study the function of the channel, the repertoire of VGSCs they express is not complete i.e. a notable absence of Nav1.8, this may be a reflection of the maturity as discussed in earlier chapters. Cadaveric human DRG are considered 'gold standard' comparators, however due to the scarcity of viable primary tissue, *in vitro* culture conditions have not been optimised. Instead, conditions have been extrapolated from

murine, which may not be physiologically appropriate. It is unclear whether the phenotypic diversity is correctly retained in culture, nor has the influence of time *in vitro* on the molecular profile of the neurons been characterised. In this respect it is challenging to conclude what in fact represents the 'ground truth'.

A few recent studies have begun to assess the transcriptional profile of fresh DRG tissue which is a significant step forward for the field (Ray et al., 2018; Flegel et al., 2015). Increasing these datasets will serve as essential source of comparative data for *in vitro* studies such as this one. Indeed, we were able to make use of published data for PCA of our iPSC-nociceptors. Even if hDRG *in vitro* protocols are sufficiently optimised, primary tissue is inherently not as amenable as iPSC, particularly for protein based work and genetic manipulation. The study of rare genetic variants is also effectively not possible with cadaveric DRG, as is implicit from their scarcity. The pain field should therefore seek to invest in the development of new methods of differentiation.

Alternative differentiation protocols have been described including the trans-differentiation of human fibroblasts by (Blanchard et al., 2014) and (Wainger et al., 2014). requiring the ectopic induction of transcription factors including NGN1. However, the reported differentiation efficiency was low. The method described by Blanchard et al. generated only 4% BRN3A positive cells from the starting population, of these only 20-21% were responsive to capsaicin. While this may still suffice for electrophysiological studies, applications in which significant channel protein is required (such as IP), would not be possible. A recent protocol has described the iPSC derived nociceptors capable of releasing CGRP (Guimaraes et al., 2018), however the neurons did not release a statistically significant amount of substance P in response to capsaicin stimulation, despite the population being 90% for TRPV1+, thus the efficient derivation of responsive peptidergic TRPV1+ population remains elusive.

CRISPR/Cas9 and pain therapeutics

We have shown here that functional knockout of Nav1.7 using CRISPR/cas9 significantly reduces neuronal excitability. To what extent could this be developed therapeutically? Genomic targeting would certainly circumvent the promiscuous selectivity of small molecule blockers; however, the permanence of this approach restricts its use. The therapeutic goal should be to dampen rather than rescind pain entirely, to pursue a binary outcome may be inappropriate. Pain, after all, serves a useful protective purpose, provided it manifests itself in a timely and appropriate manner. This is an important point that the pharmaceutical industry must reflect on in its pursuit of Nav1.7, particularly for chronic pain conditions in which extended therapeutic use is naturally implied.

A more suitable application of CRISPR/cas9 targeting could be transcriptional regulation of the channel. This could be achieved using a nuclease inactivated Cas protein. Targeting the SCN9A promoter, or enhancer elements using dCas9 fused repressive elements (Moreno et al., 2018; Gao et al., 2016) in a transient manner. Equally, the direct targeting of SCN9A mRNA transcripts could be realised with type III or IV RNA-targeting CRISPR systems if, following further development, the risk of collateral RNAse activity is reduced (Abudayyeh et al., 2017).

What remains unclear, however, is the titration of block required – could significant analgesia be expected with only a partial reduction in Nav1.7 protein? Lack of a pain phenotype in heterozygote SCN9A LOF carriers implies that pain perception per se only requires 50% of normal expression levels. However, it was interesting to note with our findings that reversal of one allele was insufficient to rescue repetitive firing, without in-depth phenotypic analysis of SCN9A LOF heterozygotes we cannot yet say if this

indeed has physiological relevance. However, dosage may become more relevant in conditions of excess Nav1.7 activity. In chronic pain states such as paclitaxel induced neuropathy, Nav1.7 has been shown to be upregulated (Li et al., 2017) so reversion to norm may show some efficacy. Studies will have to be performed to ascertain the extent to which this upregulation contributes to the pain phenotype.

Potential concerns for the therapeutic application of CRISPR *in vivo* include off-target effects of the endonuclease (Cradick et al., 2013; Pattanayak et al., 2013), Although, arguably, the threat of these has lessened; this follows the rapid development of Cas proteins with enhanced specificity and, critically, the development of assays to accurately detect off-target activity in an unbiased manner, which was difficult in the early stages. There is also now a greater appreciation of disparities between *in vitro* and *in vivo* off-target mutagenesis suggesting they do not always correlate (Tsai et al., 2017; Akcakaya et al., 2018). A final consideration to the application of CRISPR to therapeutic treatment of pain is perhaps more general to the gene therapy field and concerns the route of delivery. To achieve activity requires the transit of the system to the nucleus (at least with canonical type II system). Targeting the dorsal root ganglia from the periphery would likely require the use of viral vectors and retrograde trafficking, Herpes Simplex Virus (HSV) or AAV have both been used to achieve DRG targeting in mice (Mason et al., 2010; Glatzel et al., 2000; Chattopadhyay et al., 2005) and HSV has been trialled clinically in humans (Fink et al., 2011). However, in neuropathic conditions endocytosis and retrograde trafficking may be damaged so the efficacy of transduction may prove low. The canonical Cas9 is too large to be contained with the ITRs of AAV surpassing the ~4.7kb packaging limit. However, smaller Cas proteins from alternative bacterial species have been successfully trialled, although targeting efficacy appear to be lower (Ran et al., 2015). The rapid refinement and discovery of new variants may soon address this problem.

The rate limiting step for the application of CRISPR therapeutically appears to be the delivery of the tool. In the meantime, the application of CRISPR to disease modelling and experimental manipulation of neurons *in vitro* is certain and the pain field should be encouraged to apply the technology with haste.

Bibliography

Abdulla, F.A. and Smith, P.A. 2002. Changes in Na+ Channel Currents of Rat Dorsal Root Ganglion Neurons Following Axotomy and Axotomy-Induced Autotomy. *Journal of Neurophysiology*, 88(5), pp.2518–2529.

Abudayyeh, O.O., Gootenberg, J.S., Essletzbichler, P., Han, S., Joung, J., Belanto, J.J., Verdine, V., Cox, D.B.T., Kellner, M.J., Regev, A., Lander, E.S., Voytas, D.F., Ting, A.Y. and Zhang, F., 2017. RNA targeting with CRISPR–Cas13. *Nature*, 550(7675), pp.280–284.

Ahuja, S., Mukund, S., Deng, L., Khakh, K., Chang, E., Ho, H., Shriver, S., Young, C., Lin, S., Johnson, J.P., Wu, P., Li, J., Coons, M., Tam, C., Brillantes, B., Sampang, H., Mortara, K., Bowman, K.K., Clark, K.R., Estevez, A., Xie, Z., Verschoof, H., Grimwood, M., Dehnhardt, C., Andrez, J.-C., Focken, T., Sutherlin, D.P., Safina, B.S., Starovasnik, M.A., Ortwine, D.F., Franke, Y., Cohen, C.J., Hackos, D.H., Koth, C.M. and Payandeh, J. 2015. Structural basis of Nav1.7 inhibition by an isoform-selective small-molecule antagonist. *Science*, 350(6267), pp.aac5464–aac5464.

Ahuja, S., Mukund, S., Deng, L., Khakh, K., Chang, E., Ho, H., Shriver, S., Young, C., Lin, S., Johnson, J.P., Wu, P., Li, J., Coons, M., Tam, C., Brillantes, B., Sampang, H., Mortara, K., Bowman, K.K., Clark, K.R., Estevez, A., Xie, Z., Verschoof, H., Grimwood, M., Dehnhardt, C., Andrez, J.-C., Focken, T., Sutherlin, D.P., Safina, B.S., Starovasnik, M.A., Ortwine, D.F., Franke, Y., Cohen, C.J., Hackos, D.H., Koth, C.M. and Payandeh, J. 2015. Structural basis of Nav1.7 inhibition by an isoform-selective small-molecule antagonist. *Science*, 350(6267), pp.aac5464–aac5464.

Akcakaya, P., Bobbin, M.L., Guo, J.A., Malagon-Lopez, J., Clement, K., Garcia, S.P., Fellows, M.D., Porritt, M.J., Firth, M.A., Carreras, A., Baccega, T., Seeliger, F., Bjursell, M., Tsai, S.Q., Nguyen, N.T., Nitsch, R., Mayr, L.M., Pinello, L., Bohlooly-Y, M., Aryee, M.J., Maresca, M. and Joung, J.K., 2018. In vivo CRISPR editing with no detectable genome-wide off-target mutations. *Nature*, 561(7723), pp.416–419.

Akopian, A.N., Souslova, V., England, S., Okuse, K., Ogata, N., Ure, J., Smith, A., Kerr, B.J., McMahon, S.B., Boyce, S., Hill, R., Stanfa, L.C., Dickenson, A.H. and Wood, J.N. 1999. The tetrodotoxin-resistant sodium channel SNS has a specialized function in pain pathways. *Nature neuroscience*, 2(6), pp.541–548.

Aman, T.K., Grieco-Calub, T.M., Chen, C., Rusconi, R., Slat, E.A., Isom, L.L. and Raman, I.M. 2009. Regulation of persistent Na current by interactions between beta subunits of voltage-gated Na channels. *The Journal of Neuroscience*, 29(7), pp.2027–2042.

Amaya, F., Wang, H., Costigan, M., Allchorne, A.J., Hatcher, J.P., Egerton, J., Stean, T., Morisset, V., Grose, D., Gunthorpe, M.J., Chessell, I.P., Tate, S., Green, P.J. and Woolf, C.J., 2006. The voltage-gated sodium channel Na(v)1.9 is an effector of peripheral inflammatory pain hypersensitivity. *The Journal of Neuroscience*, 26(50), pp.12852–12860.

Amitai, G. and Sorek, R. 2016. CRISPR-Cas adaptation: insights into the mechanism of action. *Nature reviews. Microbiology*, 14(2), pp.67–76.

Anders, C., Niewoehner, O., Duerst, A. and Jinek, M., 2014. Structural basis of PAM-dependent target DNA recognition by the Cas9 endonuclease. *Nature*, 513(7519), pp.569–573.

Anders, S., Pyl, P.T. and Huber, W., 2015. HTSeq--a Python framework to work with high-throughput sequencing data. *Bioinformatics*, 31(2), pp.166–169.

Baer, M., Best, P.M. and Reuter, H. 1976. Voltage-dependent action of tetrodotoxin in mammalian cardiac muscle. *Nature*, 263(5575), pp.344–345.

Bang, S., Yoo, J., Gong, X., Liu, D., Han, Q., Luo, X., Chang, W., Chen, G., Im, S.-T., Kim, Y.H., Strong, J.A., Zhang, M.-Z., Zhang, J.-M., Lee, S.-Y. and Ji, R.-R. 2018. Differential Inhibition of Nav1.7 and Neuropathic Pain by Hybridoma-Produced and Recombinant Monoclonal Antibodies that Target Nav1.7 : Differential activities of Nav1.7-targeting monoclonal antibodies. *Neurosci. Bull*, 34(1), pp.22–41.

Bant, J.S. and Raman, I.M. 2010. Control of transient, resurgent, and persistent current by open-channel block by Na channel beta4 in cultured cerebellar granule neurons. *Proceedings of the National Academy of Sciences*, 107(27), pp.12357–12362.

Bautista, D.M., Siemens, J., Glazer, J.M., Tsuruda, P.R., Basbaum, A.I., Stucky, C.L., Jordt, S.-E. and Julius, D. 2007. The menthol receptor TRPM8 is the principal detector of environmental cold. *Nature*, 448(7150), pp.204–208.

Belinsky, G.S., Rich, M.T., Sirois, C.L., Short, S.M., Pedrosa, E., Lachman, H.M. and Antic, S.D. 2014. Patch-clamp recordings and calcium imaging followed by single-cell PCR reveal the developmental profile of 13 genes in iPSC-derived human neurons. *Stem Cell Research*, 12(1), pp.101–118.

Bennett, D.L.H. and Woods, C.G. 2014. Painful and painless channelopathies. *Lancet Neurol*, 13(6), pp.587–599.

Bhaya, D., Davison, M. and Barrangou, R. 2011. CRISPR-Cas Systems in Bacteria and Archaea: Versatile Small RNAs for Adaptive Defense and Regulation. *Annu. Rev. Genet*, 45(1), pp.273–297.

Black, J.A., Frézel, N., Dib-Hajj, S.D. and Waxman, S.G., 2012. Expression of Nav1.7 in DRG neurons extends from peripheral terminals in the skin to central preterminal branches and terminals in the dorsal horn. *Mol. Pain*, 8(46), p.82.
Black, J.A., Liu, S., Tanaka, M., Cummins, T.R. and Waxman, S.G. 2004. Changes in the expression of tetrodotoxin-sensitive sodium channels within dorsal root ganglia neurons in inflammatory pain. *Pain*, 108(3), pp.237–247.

Black, J.A., Nikolajsen, L., Kroner, K., Jensen, T.S. and Waxman, S.G. 2008. Multiple sodium channel isoforms and mitogen-activated protein kinases are present in painful human neuromas. *Annals of neurology*, 64(6), pp.644–653.

Blesneac, I., Themistocleous, A.C., Fratter, C., Conrad, L.J., Ramirez, J.D., Cox, J.J., Tesfaye, S., Shillo, P.R., Rice, A.S.C., Tucker, S.J. and Bennett, D.L.H., 2017. Rare Nav1.7 variants associated with painful diabetic peripheral neuropathy. *Pain*, p.1.

Bogdanova-Mihaylova, P., Alexander, M.D., Murphy, R.P.J. and Murphy, S.M., 2015. *SCN9A-associated congenital insensitivity to pain and anosmia in an Irish patient. Journal of the Peripheral Nervous System*.

Boiko, T., Rasband, M.N., Levinson, S.R., Caldwell, J.H., Mandel, G., Trimmer, J.S. and Matthews, G., 2001. Compact Myelin Dictates the Differential Targeting of Two Sodium Channel Isoforms in the Same Axon. *Neuron*, 30(1), pp.91–104

Boyer, J.C., Umar, A., Risinger, J.I., Lipford, J.R., Kane, M., Yin, S., Barrett, J.C., Kolodner, R.D. and Kunkel, T.A. 1995. Microsatellite instability, mismatch repair deficiency, and genetic defects in human cancer cell lines. *Cancer research*, 55(24), pp.6063–6070.

Breivik, H., Collett, B., Ventafridda, V., Cohen, R. and Gallacher, D., 2006. Survey of chronic pain in Europe: prevalence, impact on daily life, and treatment. *European journal of pain*, *10*(4), pp.287-287.

Breivik, H., Eisenberg, E., O'Brien, T.OPENMinds 2013. The individual and societal burden of chronic pain in Europe: the case for strategic prioritisation and action to improve knowledge and availability of appropriate care. *BMC public health*, 13(1), p.1229.

Brinkman, E.K., Chen, T., Amendola, M. and van Steensel, B., 2014. Easy quantitative assessment of genome editing by sequence trace decomposition. *Nucleic acids research*, 42(22), pp.e168–e168.

Cao, L., McDonnell, A., Nitzsche, A., Alexandrou, A., Saintot, P.-P., Loucif, A.J.C., Brown, A.R., Young, G., Mis, M., Randall, A., Waxman, S.G., Stanley, P., Kirby, S., Tarabar, S., Gutteridge, A., Butt, R., McKernan, R.M., Whiting, P., Ali, Z., Bilsland, J. and Stevens, E.B., 2016. Pharmacological reversal of a pain phenotype in iPSC-derived sensory neurons and patients with inherited erythromelalgia. *Science Translational Medicine*, 8(335), p.335ra56-335ra56.

Caldwell, J.H., Schaller, K.L., Lasher, R.S., Peles, E. and Levinson, S.R., 2000. Sodium channel Na(v)1.6 is localized at nodes of ranvier, dendrites, and synapses. *Proceedings of the National Academy of Sciences of the United States of America*, 97(10), pp.5616–5620.

Carcamo-Orive, I., Hoffman, G.E., Cundiff, P., Beckmann, N.D., D'Souza, S.L., Knowles, J.W., Patel, A., Papatsenko, D., Abbasi, F., Reaven, G.M., Whalen, S., Lee, P., Shahbazi, M., Henrion, M.Y.R., Zhu, K., Wang, S., Roussos, P., Schadt, E.E., Pandey, G., Chang, R., Quertermous, T. and Lemischka, I. 2017. Analysis of Transcriptional Variability in a Large Human iPSC Library Reveals Genetic and Non-genetic Determinants of Heterogeneity. *Cell Stem Cell*, 20(4), pp.518–532.e9.

Caterina, M.J. 2000. Impaired Nociception and Pain Sensation in Mice Lacking the Capsaicin Receptor. *Science*, 288(5464), pp.306–313.

Catterall, W.A. 1986. Molecular properties of voltage-sensitive sodium channels. *Annu. Rev. Biochem*, 55(1), pp.953–985.

Catterall, W.A. 2000. From ionic currents to molecular mechanisms: the structure and function of voltage-gated sodium channels. *Neuron*, 26(1), pp.13–25.

Catterall, W.A. 2012. Voltage-gated sodium channels at 60: structure, function and pathophysiology. *The Journal of physiology*, 590(11), pp.2577–2589.

Chambers, S.M., Qi, Y., Mica, Y., Lee, G., Zhang, X.-J., Niu, L., Bilsland, J., Cao, L., Stevens, E., Whiting, P., Shi, S.-H. and Studer, L. 2012. Combined small-molecule inhibition accelerates developmental timing and converts human pluripotent stem cells into nociceptors. *Nature biotechnology*, 30(7), pp.715–720.

Chang, H.H.Y., Pannunzio, N.R., Adachi, N. and Lieber, M.R. 2017. Non-homologous DNA end joining and alternative pathways to double-strand break repair. *Nature reviews. Molecular cell biology*, 18(8), pp.495–506.

Chang, W., Berta, T., Kim, Y.H., Lee, S., Lee, S.-Y. and Ji, R.-R. 2018. Expression and Role of Voltage-Gated Sodium Channels in Human Dorsal Root Ganglion Neurons with Special Focus on Nav1.7, Species Differences, and Regulation by Paclitaxel. *Neurosci. Bull*, 34(1), pp.4–12.

Chattopadhyay, M., Krisky, D., Wolfe, D., Glorioso, J.C., Mata, M. and Fink, D.J., 2005. HSV-mediated gene transfer of vascular endothelial growth factor to dorsal root ganglia prevents diabetic neuropathy. *Gene Therapy*, 12(18), pp.1377–1384.

Chen, C.-L., Broom, D.C., Liu, Y., de Nooij, J.C., Li, Z., Cen, C., Samad, O.A., Jessell, T.M., Woolf, C.J. and Ma, Q. 2006. Runx1 determines nociceptive sensory neuron phenotype and is required for thermal and neuropathic pain. *Neuron*, 49(3), pp.365–377.

Chen, C., Bharucha, V., Chen, Y., Westenbroek, R.E., Brown, A., Malhotra, J.D., Jones, D., Avery, C., Gillespie, P.J., Kazen-Gillespie, K.A., Kazarinova-Noyes, K., Shrager, P., Saunders, T.L., Macdonald, R.L., Ransom, B.R., Scheuer, T., Catterall, W.A. and Isom, L.L. 2002. Reduced sodium channel density, altered voltage dependence of inactivation, and increased susceptibility to seizures in mice lacking sodium channel beta 2-subunits. *Proceedings of the National Academy of Sciences of the United States of America*, 99(26), pp.17072–17077.

Chen, C., Westenbroek, R.E., Xu, X., Edwards, C.A., Sorenson, D.R., Chen, Y., McEwen, D.P., O'Malley, H.A., Bharucha, V., Meadows, L.S., Knudsen, G.A., Vilaythong, A., Noebels, J.L., Saunders, T.L., Scheuer, T., Shrager, P., Catterall, W.A. and Isom, L.L., 2004. Mice lacking sodium channel beta1 subunits display defects in neuronal excitability, sodium channel expression, and nodal architecture. *The Journal of Neuroscience*, 24(16), pp.4030–4042.

Chen, J.S., Dagdas, Y.S., Kleinstiver, B.P., Welch, M.M., Sousa, A.A., Harrington, L.B., Sternberg, S.H., Joung, J.K., Yildiz, A. and Doudna, J.A. 2017. Enhanced proofreading governs CRISPR-Cas9 targeting accuracy. *Nature*, 550(7676), pp.407–410.

Chen, W., Liu, J., Zhang, L., Xu, H., Guo, X., Deng, S., Liu, L., Yu, D., Chen, Y. and Li, Z. 2014. Generation of the SCN1A epilepsy mutation in hiPS cells using the TALEN technique. *Sci. Rep*, 4(1), p.5404.

Chen, Y.-C., Auer-Grumbach, M., Matsukawa, S., Zitzelsberger, M., Themistocleous, A.C., Strom, T.M., Samara, C., Moore, A.W., Cho, L.T.-Y., Young, G.T., Weiss, C., Schabhüttl, M., Stucka, R., Schmid, A.B., Parman, Y., Graul-Neumann, L., Heinritz, W., Passarge, E., Watson, R.M., Hertz, J.M., Moog, U., Baumgartner, M., Valente, E.M., Pereira, D., Restrepo, C.M., Katona, I., Dusl, M., Stendel, C., Wieland, T., Stafford, F., Reimann, F., Au, von, K., Finke, C., Willems, P.J., Nahorski, M.S., Shaikh, S.S., Carvalho, O.P., Nicholas, A.K., Karbani, G., McAleer, M.A., Cilio, M.R., McHugh, J.C., Murphy, S.M., Irvine, A.D., Jensen, U.B., Windhager, R., Weis, J., Bergmann, C., Rautenstrauss, B., Baets, J., De Jonghe, P., Reilly, M.M., Kropatsch, R., Kurth, I., Chrast, R., Michiue, T., Bennett, D.L.H., Woods, C.G. and Senderek, J. 2015. Transcriptional regulator PRDM12 is essential for human pain perception. *Nature genetics*, 47(7), pp.803–808.

Cho, S.W., Kim, S., Kim, Y., Kweon, J., Kim, H.S., Bae, S. and Kim, J.S. 2014. Analysis of off-target effects of CRISPR/Cas-derived RNA-guided endonucleases and nickases. *Genome Research*, 24(1), pp.132–141.

Choi, J.S., Boralevi, F., Brissaud, O., Sánchez-Martín, J., Morsche, Te, R.H.M., Dib-Hajj, S.D., Drenth, J.P.H. and Waxman, S.G. 2011. Paroxysmal extreme pain disorder: a molecular lesion of peripheral neurons. *Nature reviews. Neurology*, 7(1), pp.51–55.

Choulika, A., Perrin, A., Dujon, B. and Nicolas, J.F. 1995. Induction of homologous recombination in mammalian chromosomes by using the I-SceI system of Saccharomyces cerevisiae. *Mol. Cell. Biol*, 15(4), pp.1968–1973.

Cohen-Tannoudji, M., Robine, S., Choulika, A., Pinto, D., Marjou, El, F., Babinet, C., Louvard, D. and Jaisser, F. 1998. I-SceI-induced gene replacement at a natural locus in embryonic stem cells. *Mol. Cell. Biol*, 18(3), pp.1444–1448.

Colburn, R.W., Lubin, M.L., Stone, D.J., Jr., Wang, Y., Lawrence, D., D'Andrea, M.R., Brandt, M.R., Liu, Y., Flores, C.M. and Qin, N. 2007. Attenuated Cold Sensitivity in TRPM8 Null Mice. *Neuron*, 54(3), pp.379–386.

Cong, L., Ran, F.A., Cox, D., Lin, S., Barretto, R., Habib, N., Hsu, P.D., Wu, X., Jiang, W., Marraffini, L.A. and Zhang, F. 2013. Multiplex Genome Engineering Using CRISPR/Cas Systems. *Science*, 339(6121), pp.819–823.

Costantini, L.M., Fossati, M., Francolini, M. and Snapp, E.L., 2012. Assessing the Tendency of Fluorescent Proteins to Oligomerize Under Physiologic Conditions. *Traffic*.

Cox, J.J., Reimann, F., Nicholas, A.K., Thornton, G., Roberts, E., Springell, K., Karbani, G., Jafri, H., Mannan, J., Raashid, Y., Al-Gazali, L., Hamamy, H., Valente, E.M., Gorman, S., Williams, R., McHale, D.P., Wood, J.N., Gribble, F.M. and Woods, C.G. 2006. An SCN9A channelopathy causes congenital inability to experience pain. *Nature*, 444(7121), pp.894–898.

Cox, J.J., Sheynin, J., Shorer, Z., Reimann, F., Nicholas, A.K., Zubovic, L., Baralle, M., Wraige, E., Manor, E., Levy, J., Woods, C.G. and Parvari, R., 2010. Congenital insensitivity to pain: novel SCN9A missense and in-frame deletion mutations. *Human Mutation*, 31(9), pp.E1670–E1686.

Cradick, T.J., Fine, E.J., Antico, C.J. and Bao, G., 2013. CRISPR/Cas9 systems targeting β-globin and CCR5 genes have substantial off-target activity. *Nucleic acids research*, 41(20), pp.9584–9592.

Cummins, T.R. and Waxman, S.G. 1997. Downregulation of tetrodotoxin-resistant sodium currents and upregulation of a rapidly repriming tetrodotoxin-sensitive sodium current in small spinal sensory neurons after nerve injury. *Journal of Neuroscience*, 17(10), pp.3503–3514.

Cummins, T.R., Howe, J.R. and Waxman, S.G. 1998. Slow closed-state inactivation: a novel mechanism underlying ramp currents in cells expressing the hNE/PN1 sodium channel. *The Journal of Neuroscience*, 18(23), pp.9607–9619.

Dhaka, A., Murray, A.N., Mathur, J., Earley, T.J., Petrus, M.J. and Patapoutian, A., 2007. TRPM8 Is Required for Cold Sensation in Mice. *Neuron*, 54(3), pp.371–378.

Dash, B., Han, C., Waxman, S.G. and Dib-Hajj, S.D., 2018. Nonmuscle myosin II isoforms interact with sodium channel alpha subunits. *Mol. Pain*, 14, p.174480691878863.

DeCaen, P.G., Yarov-Yarovoy, V., Scheuer, T. and Catterall, W.A. 2011. Gating charge interactions with the S1 segment during activation of a Na+ channel voltage sensor. *Proceedings of the National Academy of Sciences*, 108(46), pp.18825–18830.

DeCaen, P.G., Yarov-Yarovoy, V., Zhao, Y., Scheuer, T. and Catterall, W.A. 2008. Disulfide locking a sodium channel voltage sensor reveals ion pair formation during activation. *Proceedings of the National Academy of Sciences*, 105(39), pp.15142–15147.

Deltcheva, E., Chylinski, K., Sharma, C.M., Gonzales, K., Chao, Y., Pirzada, Z.A., Eckert, M.R., Vogel, J. and Charpentier, E. 2011. CRISPR RNA maturation by trans-encoded small RNA and host factor RNase III. *Nature*, 471(7340), pp.602–607.

Devor, M. 2006. Sodium Channels and Mechanisms of Neuropathic Pain. *The Journal of Pain*, 7(1), pp.S3–S12.

Dib-Hajj, S., Black, J.A., Felts, P. and Waxman, S.G. 1996. Down-regulation of transcripts for Na channel alpha-SNS in spinal sensory neurons following axotomy. *Proceedings of the National Academy of Sciences of the United States of America*, 93(25), pp.14950–14954.

Dib-Hajj, S.D., Rush, A.M., Cummins, T.R., Hisama, F.M., Novella, S., Tyrrell, L., Marshall, L. and Waxman, S.G. 2005. Gain-of-function mutation in Nav1.7 in familial erythromelalgia induces bursting of sensory neurons. *Brain : a journal of neurology*, 128(Pt 8), pp.1847–1854.

Dib-Hajj, S.D., Tyrrell, L., Black, J.A. and Waxman, S.G. 1998. NaN, a novel voltage-gated Na channel, is expressed preferentially in peripheral sensory neurons and down-regulated after axotomy. *Proceedings of the National Academy of Sciences of the United States of America*, 95(15), pp.8963–8968.

Dobin, A., Davis, C.A., Schlesinger, F., Drenkow, J., Zaleski, C., Jha, S., Batut, P., Chaisson, M. and Gingeras, T.R., 2013. STAR: ultrafast universal RNA-seq aligner. *Bioinformatics*, 29(1), pp.15–21.

Dubin, A.E. and Patapoutian, A. 2010. Nociceptors: the sensors of the pain pathway. *The Journal of clinical investigation*, 120(11), pp.3760–3772.

Durai, S. 2005. Zinc finger nucleases: custom-designed molecular scissors for genome engineering of plant and mammalian cells. *Nucleic acids research*, 33(18), pp.5978–5990.

Dustrude, E.T., Moutal, A., Yang, X., Wang, Y., Khanna, M. and Khanna, R. 2016. Hierarchical CRMP2 posttranslational modifications control NaV1.7 function. *Proceedings of the National Academy of Sciences of the United States of America*, 113(52), pp.E8443–E8452.

Dustrude, E.T., Wilson, S.M., Ju, W., Xiao, Y. and Khanna, R. 2013. CRMP2 protein SUMOylation modulates NaV1.7 channel trafficking. *The Journal of biological chemistry*, 288(34), pp.24316–24331.

Eberhardt, E., Havlicek, S., Schmidt, D., Link, A.S., Neacsu, C., Kohl, Z., Hampl, M., Kist, A.M., Klinger, A., Nau, C., Schüttler, J., Alzheimer, C., Winkler, J., Namer, B., Winner, B. and Lampert, A., 2015. Pattern of Functional TTX-Resistant Sodium Channels Reveals a Developmental Stage of Human iPSC- and ESC-Derived Nociceptors. *Stem Cell Reports*, 5(3), pp.305–313.

Eldridge, C.F., Bunge, M.B., Bunge, R.P. and Wood, P.M., 1987. Differentiation of axon-related Schwann cells *in vitro*. I. Ascorbic acid regulates basal lamina assembly and myelin formation. *The Journal of cell biology*, 105(2), pp.1023–1034.

Eriksson, J., Jablonski, A., Persson, A.-K., Hao, J.-X., Kouya, P.F., Wiesenfeld-Hallin, Z., Xu, X.-J. and Fried, K. 2005. Behavioral changes and trigeminal ganglion sodium channel regulation in an orofacial neuropathic pain model. *Pain*, 119(1-3), pp.82–94.

Faber, C.G., Lauria, G., Merkies, I.S.J., Cheng, X., Han, C., Ahn, H.-S., Persson, A.-K., Hoeijmakers, J.G.J., Gerrits, M.M., Pierro, T., Lombardi, R., Kapetis, D., Dib-Hajj, S.D. and Waxman, S.G. 2012. Gain-of-function Nav1.8 mutations in painful neuropathy. *Proceedings of the National Academy of Sciences*, 109(47), pp.19444–19449.

Favre, I., Moczydlowski, E. and Schild, L. 1996. On the structural basis for ionic selectivity among Na+, K+, and Ca2+ in the voltage-gated sodium channel. *Biophysical journal*, 71(6), pp.3110–3125.

Fertleman, C.R., Baker, M.D., Parker, K.A., Moffatt, S., Elmslie, F.V., Abrahamsen, B., Ostman, J., Klugbauer, N., Wood, J.N., Gardiner, R.M. and Rees, M. 2006. SCN9A mutations in paroxysmal extreme pain disorder: allelic variants underlie distinct channel defects and phenotypes. *Neuron*, 52(5), pp.767–774.

Fink, D.J., Wechuck, J., Mata, M., Glorioso, J.C., Goss, J., Krisky, D. and Wolfe, D., 2011. Gene therapy for pain: Results of a phase I clinical trial. *Annals of neurology*, 70(2), pp.207–212.
Finnerup, N.B., Sindrup, S.H. and Jensen, T.S. 2010. The evidence for pharmacological treatment of neuropathic pain. *Pain*, 150(3), pp.573–581.

Finnerup, N.B., Sindrup, S.H. and Jensen, T.S. 2010. The evidence for pharmacological treatment of neuropathic pain. *Pain*, 150(3), pp.573–581.

Flegel, C., Schöbel, N., Altmüller, J., Becker, C., Tannapfel, A., Hatt, H. and Gisselmann, G., 2015. RNA-Seq Analysis of Human Trigeminal and Dorsal Root Ganglia with a Focus on Chemoreceptors. *PloS one*, 10(6), p.e0128951.

Focken, T., Liu, S., Chahal, N., Dauphinais, M., Grimwood, M.E., Chowdhury, S., Hemeon, I., Bichler, P., Bogucki, D., Waldbrook, M., Bankar, G., Sojo, L.E., Young, C., Lin, S., Shuart, N., Kwan, R., Pang, J., Chang, J.H., Safina, B.S., Sutherlin, D.P., Johnson, J.P., Dehnhardt, C.M., Mansour, T.S., Oballa, R.M., Cohen, C.J. and Robinette, C.L. 2016. Discovery of Aryl Sulfonamides as Isoform-Selective Inhibitors of NaV1.7 with Efficacy in Rodent Pain Models. *ACS Med. Chem. Lett*, 7(3), pp.277–282.

Fukuoka, T., Kobayashi, K., Yamanaka, H., Obata, K., Dai, Y. and Noguchi, K. 2008. Comparative study of the distribution of the α-subunits of voltage-gated sodium channels in normal and axotomized rat dorsal root ganglion neurons. *The Journal of comparative neurology*, 510(2), pp.188–206.

Gao, Y., Xiong, X., Wong, S., Charles, E.J., Lim, W.A. and Qi, L.S., 2016. Complex transcriptional modulation with orthogonal and inducible dCas9 regulators. *Nature methods*, 13(12), pp.1043–1049.

Garneau, J.E., Dupuis, M.-È., Villion, M., Romero, D.A., Barrangou, R., Boyaval, P., Fremaux, C., Horvath, P., Magadán, A.H. and Moineau, S. 2010. The CRISPR/Cas bacterial immune system cleaves bacteriophage and plasmid DNA. *Nature*, 468(7320), pp.67–71.

Geiss-Friedlander, R. and Melchior, F. 2007. Concepts in sumoylation: a decade on. *Nature reviews. Molecular cell biology*, 8(12), pp.947–956.

Gingras, J., Smith, S., Matson, D.J., Johnson, D., Nye, K., Couture, L., Feric, E., Yin, R., Moyer, B.D., Peterson, M.L., Rottman, J.B., Beiler, R.J., Malmberg, A.B. and McDonough, S.I. 2014. Global Nav1.7 knockout mice recapitulate the phenotype of human congenital indifference to pain. *PloS one*, 9(9), p.e105895.

Glatzel, M., Flechsig, E., Navarro, B., Klein, M.A., Paterna, J.C., Bueler, H. and Aguzzi, A., 2000. Adenoviral and adeno-associated viral transfer of genes to the peripheral nervous system. *Proceedings of the National Academy of Sciences of the United States of America*, 97(1), pp.442–447.

Gold, M.S., Weinreich, D., Kim, C.-S., Wang, R., Treanor, J., Porreca, F. and Lai, J. 2003. Redistribution of NaV1.8 in Uninjured Axons Enables Neuropathic Pain. *Journal of Neuroscience*, 23(1), pp.158–166.

Goldberg, Y.P., MacFarlane, J., MacDonald, M.L., Thompson, J., Dube, M.-P., Mattice, M., Fraser, R., Young, C., Hossain, S., Pape, T., Payne, B., Radomski, C., Donaldson, G., Ives, E., Cox, J., Younghusband, H.B., Green, R., Duff, A., Boltshauser, E., Grinspan, G.A., Dimon, J.H., Sibley, B.G., Andria, G., Toscano, E., Kerdraon, J., Bowsher, D., Pimstone, S.N., Samuels, M.E., Sherrington, R. and Hayden, M.R. 2007. Loss-of-function mutations in the Nav1.7 gene underlie congenital indifference to pain in multiple human populations. *Clinical genetics*, 71(4), pp.311–319.

Goldin, A.L. 2003. Mechanisms of sodium channel inactivation. *Curr. Opin. Neurobiol*, 13(3), pp.284–290.

Goral, R.O., Leipold, E., Nematian-Ardestani, E. and Heinemann, S.H. 2015. Heterologous expression of NaV1.9 chimeras in various cell systems. *Pflügers Archiv - European Journal of Physiology*, 467(12), pp.2423–2435.

Goshima, Y., Nakamura, F., Strittmatter, P. and Strittmatter, S.M. 1995. Collapsin-induced growth cone collapse mediated by an intracellular protein related to UNC-33. *Nature*, 376(6540), pp.509–514.

Gudes, S., Barkai, O., Caspi, Y., Katz, B., Lev, S. and Binshtok, A.M. 2015. The role of slow and persistent TTX-resistant sodium currents in acute tumor necrosis factor-α-mediated increase in nociceptors excitability. *J. Neurophysiol*, 113(2), pp.601–619.

Guimaraes, M.Z.P., De Vecchi, R., Vitoria, G., Sochacki, J.K., Paulsen, B., Lima, I., da Silva, F.R., da Costa, R.F.M., Breton, L. and Rehen, S.K., 2018. Generation Of iPSC-Derived Human Peripheral Sensory Neurons Releasing Substance P Elicited By TRPV1 Agonists. *bioRxiv*, p.281675.

Hains, B.C., Klein, J.P., Saab, C.Y., Craner, M.J., Black, J.A. and Waxman, S.G. 2003. Upregulation of Sodium Channel Na v1.3 and Functional Involvement in Neuronal Hyperexcitability Associated with Central Neuropathic Pain after Spinal Cord Injury. *Journal of Neuroscience*, 23(26), pp.8881–8892.

He, B. and Soderlund, D.M. 2010. Human embryonic kidney (HEK293) cells express endogenous voltage-gated sodium currents and Na v 1.7 sodium channels. *Neuroscience letters*, 469(2), pp.268–272.

Henriques, S.T., Deplazes, E., Lawrence, N., Cheneval, O., Chaousis, S., Inserra, M., Thongyoo, P., King, G.F., Mark, A.E., Vetter, I., Craik, D.J. and Schroeder, C.I. 2016. Interaction of Tarantula Venom Peptide ProTx-II with Lipid Membranes Is a Prerequisite for Its Inhibition of Human Voltage-gated Sodium Channel NaV1.7. *The Journal of biological chemistry*, 291(33), pp.17049–17065.

Hensley, K., Venkova, K., Christov, A., Gunning, W. and Park, J. 2011. Collapsin response mediator protein-2: an emerging pathologic feature and therapeutic target for neurodisease indications. *Molecular neurobiology*, 43(3), pp.180–191.

Herzog, R.I., Cummins, T.R., Ghassemi, F., Dib-Hajj, S.D. and Waxman, S.G. 2003. Distinct repriming and closed-state inactivation kinetics of Nav1.6 and Nav1.7 sodium channels in mouse spinal sensory neurons. *J. Physiol*, 551(Pt 3), pp.741–750.

Ho, C., Zhao, J., Malinowski, S., Chahine, M. and O'Leary, M.E., 2012. Differential expression of sodium channel β subunits in dorsal root ganglion sensory neurons. *The Journal of biological chemistry*, 287(18), pp.15044–15053.

Hockemeyer, D., Wang, H., Kiani, S., Lai, C.S., Gao, Q., Cassady, J.P., Cost, G.J., Zhang, L., Santiago, Y., Miller, J.C., Zeitler, B., Cherone, J.M., Meng, X., Hinkley, S.J., Rebar, E.J., Gregory, P.D., Urnov, F.D. and Jaenisch, R. 2011. Genetic engineering of human pluripotent cells using TALE nucleases. *Nature biotechnology*, 29(8), pp.731–734.

Hockley, J.R.F., Boundouki, G., Cibert-Goton, V., McGuire, C., Yip, P.K., Chan, C., Tranter, M., Wood, J.N., Nassar, M.A., Blackshaw, L.A., Aziz, Q., Michael, G.J., Baker, M.D., Winchester, W.J., Knowles, C.H. and Bulmer, D.C. 2014. Multiple roles for NaV1.9 in the activation of visceral afferents by noxious inflammatory, mechanical, and human disease-derived stimuli. *Pain*, 155(10), pp.1962–1975.

Hu, K. 2014. All roads lead to induced pluripotent stem cells: the technologies of iPSC generation. *Stem Cells Dev*, 23(12), pp.1285–1300.

Huang, J., Vanoye, C.G., Cutts, A., Goldberg, Y.P., Dib-Hajj, S.D., Cohen, C.J., Waxman, S.G. and George, A.L. 2017. Sodium channel NaV1.9 mutations associated with insensitivity to pain dampen neuronal excitability. *The Journal of clinical investigation*, 127(7), pp.2805–2814.

Indo, Y. 2001. Molecular basis of congenital insensitivity to pain with anhidrosis (CIPA): mutations and polymorphisms in TRKA (NTRK1) gene encoding the receptor tyrosine kinase for nerve growth factor. *Hum. Mutat*, 18(6), pp.462–471.

Indo, Y., Tsuruta, M., Hayashida, Y., Karim, M.A., Ohta, K., Kawano, T., Mitsubuchi, H., Tonoki, H., Awaya, Y. and Matsuda, I. 1996. Mutations in the TRKA/NGF receptor gene in patients with congenital insensitivity to pain with anhidrosis. *Nature genetics*, 13(4), pp.485–488.

Isom, L., 2014. Sodium Channel β1 Subunits: Overachievers of the Ion Channel Family. *Biophysical journal*, 106(2), p.9a.

Isom, L.L., De Jongh, K.S., Patton, D.E., Reber, B.F., Offord, J., Charbonneau, H., Walsh, K., Goldin, A.L. and Catterall, W.A. 1992. Primary structure and functional expression of the beta 1 subunit of the rat brain sodium channel. *Science*, 256(5058), pp.839–842.

Isom, L.L., Ragsdale, D.S., De Jongh, K.S., Westenbroek, R.E., Reber, B.F., Scheuer, T. and Catterall, W.A. 1995. Structure and function of the beta 2 subunit of brain sodium channels, a transmembrane glycoprotein with a CAM motif. *Cell*, 83(3), pp.433–442.

Jansen, R., Embden, J.D.A.V., Gaastra, W. and Schouls, L.M. 2002. Identification of genes that are associated with DNA repeats in prokaryotes. *Molecular Microbiology*, 43(6), pp.1565–1575.

Jasin, M. and Rothstein, R. 2013. Repair of Strand Breaks by Homologous Recombination. *Cold Spring Harb. Perspect. Biol*, 5(11), pp.a012740–a012740.

Jiang, F., Taylor, D.W., Chen, J.S., Kornfeld, J.E., Zhou, K., Thompson, A.J., Nogales, E. and Doudna, J.A. 2016. Structures of a CRISPR-Cas9 R-loop complex primed for DNA cleavage. *Science*, 351(6275), pp.867–871.

Jurcakova, D., Ru, F., Kollarik, M., Sun, H., Krajewski, J. and Undem, B.J., 2018. Voltage-Gated Sodium Channels Regulating Action Potential Generation in Itch-, Nociceptive-, and Low-Threshold Mechanosensitive Cutaneous C-Fibers. *Molecular Pharmacology*, 94(3), pp.1047–1056.

Kanellopoulos, A.H., Koenig, J., Huang, H., Pyrski, M., Millet, Q., Lolignier, S., Morohashi, T., Gossage, S.J., Jay, M., Linley, J.E., Baskozos, G., Kessler, B.M., Cox, J.J., Dolphin, A.C., Zufall, F., Wood, J.N. and Zhao, J. 2018. Mapping protein interactions of sodium channel NaV1.7 using epitope-tagged gene-targeted mice. *The EMBO journal*, 37(3), pp.427–445.

Kaplan, M.R., Cho, M.H., Ullian, E.M., Isom, L.L., Levinson, S.R. and Barres, B.A. 2001. Differential control of clustering of the sodium channels Na(v)1.2 and Na(v)1.6 at developing CNS nodes of Ranvier. *Neuron*, 30(1), pp.105–119.

Kemp, M.I. 2010. Structural trends among second-generation voltage-gated sodium channel blockers. *Progress in medicinal chemistry*, 49, pp.81–111.

Kilpinen, H., Goncalves, A., Leha, A., Afzal, V., Alasoo, K., Ashford, S., Bala, S., Bensaddek, D., Casale, F.P., Culley, O.J., Danecek, P., Faulconbridge, A., Harrison, P.W., Kathuria, A., McCarthy, D., McCarthy, S.A., Meleckyte, R., Memari, Y., Moens, N., Soares, F., Mann, A., Streeter, I., Agu, C.A., Alderton, A., Nelson, R., Harper, S., Patel, M., White, A., Patel, S.R., Clarke, L., Halai, R., Kirton, C.M., Kolb-Kokocinski, A., Beales, P., Birney, E., Danovi, D., Lamond, A.I., Ouwehand, W.H., Vallier, L., Watt, F.M., Durbin, R., Stegle, O. and Gaffney, D.J. 2017. Common genetic variation drives molecular heterogeneity in human iPSCs. *Nature*, 546(7658), pp.370–375.

Kim, S., Kim, D., Cho, S.W., Kim, J. and Kim, J.-S. 2014. Highly efficient RNA-guided genome editing in human cells via delivery of purified Cas9 ribonucleoproteins. *Genome Res*, 24(6), pp.1012–1019.

Knowlton, W.M., Bifolck-Fisher, A., Bautista, D.M. and McKemy, D.D. 2010. TRPM8, but not TRPA1, is required for neural and behavioral responses to acute noxious cold temperatures and cold-mimetics in vivo. *Pain*, 150(2), pp.340–350.

Kovalevich, J. and Langford, D. 2013. Considerations for the use of SH-SY5Y neuroblastoma cells in neurobiology. *Methods in molecular biology (Clifton, N.J.)*, 1078(Chapter 2), pp.9–21.

Kovalevich, J. and Langford, D. 2013. Considerations for the use of SH-SY5Y neuroblastoma cells in neurobiology. *Methods in molecular biology (Clifton, N.J.)*, 1078(Chapter 2), pp.9–21.

Kruger, L.C. and Isom, L.L. 2016. Voltage-Gated Na+ Channels: Not Just for Conduction. *Cold Spring Harb. Perspect. Biol*, 8(6).

Laedermann, C.J., Abriel, H. and Decosterd, I. 2015. Post-translational modifications of voltage-gated sodium channels in chronic pain syndromes. *Front. Pharmacol*, 6, p.263.

Laedermann, C.J., Syam, N., Pertin, M., Decosterd, I. and Abriel, H. 2013. β1- and β3- voltage-gated sodium channel subunits modulate cell surface expression and glycosylation of Nav1.7 in HEK293 cells. *Front. Cell. Neurosci*, 7, p.137.

Lai, J., Gold, M.S., Kim, C.-S., Bian, D., Ossipov, M.H., Hunter, J.C. and Porreca, F. 2002. Inhibition of neuropathic pain by decreased expression of the tetrodotoxin-resistant sodium channel, NaV1.8. *Pain*, 95(1), pp.143–152.

Laird, J.M.A., Souslova, V., Wood, J.N. and Cervero, F. 2002. Deficits in visceral pain and referred hyperalgesia in Nav1.8 (SNS/PN3)-null mice. *The Journal of Neuroscience*, 22(19), pp.8352–8356.

le Maire, M., Champeil, P. and Møller, J. V, 2000. Interaction of membrane proteins and lipids with solubilizing detergents. *Biochimica et Biophysica Acta (BBA) - Biomembranes*, 1508(1–2), pp.86–111.

Lee, J.-H., Park, C.-K., Chen, G., Han, Q., Xie, R.-G., Liu, T., Ji, R.-R. and Lee, S.-Y. 2014. A monoclonal antibody that targets a NaV1.7 channel voltage sensor for pain and itch relief. *Cell*, 157(6), pp.1393–1404.

Leipold, E., Liebmann, L., Korenke, G.C., Heinrich, T., Giesselmann, S., Baets, J., Ebbinghaus, M., Goral, R.O., Stödberg, T., Hennings, J.C., Bergmann, M., Altmüller, J., Thiele, H., Wetzel, A., Nürnberg, P., Timmerman, V., De Jonghe, P., Blum, R., Schaible, H.-G., Weis, J., Heinemann, S.H., Hübner, C.A. and Kurth, I. 2013. A de novo gain-of-function mutation in SCN11A causes loss of pain perception. *Nature genetics*, 45(11), pp.1399–1404.

Leonetti, M.D., Sekine, S., Kamiyama, D., Weissman, J.S. and Huang, B., 2016. A scalable strategy for high-throughput GFP tagging of endogenous human proteins. *Proceedings of the National Academy of Sciences*, 113(25), pp.E3501-8.

Li, Y., North, R.Y., Rhines, L.D., Tatsui, C.E., Rao, G., Edwards, D.D., Cassidy, R.M., Harrison, D.S., Johansson, C.A., Zhang, H. and Dougherty, P.M., 2018. DRG Voltage-Gated Sodium Channel 1.7 Is Upregulated in Paclitaxel-Induced Neuropathy in Rats and in Humans with Neuropathic Pain. *The Journal of Neuroscience*, 38(5), pp.1124–1136.

Lin, Y., Cradick, T.J., Brown, M.T., Deshmukh, H., Ranjan, P., Sarode, N., Wile, B.M., Vertino, P.M., Stewart, F.J. and Bao, G. 2014. CRISPR/Cas9 systems have off-target activity with insertions or deletions between target DNA and guide RNA sequences. *Nucleic acids research*, 42(11), pp.7473–7485.

Lindia, J.A., Köhler, M.G., Martin, W.J. and Abbadie, C. 2005. Relationship between sodium channel NaV1.3 expression and neuropathic pain behavior in rats. *Pain*, 117(1-2), pp.145–153.

Liu, C., Li, Q., Su, Y. and Bao, L. 2010. Prostaglandin E2 promotes Na1.8 trafficking via its intracellular RRR motif through the protein kinase A pathway. *Traffic*, 11(3), pp.405–417.

Liu, D., Tseng, M., Epstein, L.F., Green, L., Chan, B., Soriano, B., Lim, D., Pan, O., Murawsky, C.M., King, C.T. and Moyer, B.D. 2016. Evaluation of recombinant monoclonal antibody SVmab1 binding to Na V1.7 target sequences and block of human Na V1.7 currents. *F1000Res*, 5, p.2764.

Livak, K.J. and Schmittgen, T.D., 2001. Analysis of Relative Gene Expression Data Using Real-Time Quantitative PCR and the 2−ΔΔCT Method. *Methods*, 25(4), pp.402–408.

Lolignier, S., Bonnet, C., Gaudioso, C., Noël, J., Ruel, J., Amsalem, M., Ferrier, J., Rodat-Despoix, L., Bouvier, V., Aissouni, Y., Prival, L., Chapuy, E., Padilla, F., Eschalier, A., Delmas, P. and Busserolles, J., 2015. The Nav1.9 Channel Is a Key Determinant of Cold Pain Sensation and Cold Allodynia. *Cell Reports*, 11(7), pp.1067–1078.

Lombardo, A., Cesana, D., Genovese, P., Di Stefano, B., Provasi, E., Colombo, D.F., Neri, M., Magnani, Z., Cantore, A., Lo Riso, P., Damo, M., Pello, O.M., Holmes, M.C., Gregory, P.D., Gritti, A., Broccoli, V., Bonini, C. and Naldini, L., 2011. Site-specific integration and tailoring of cassette design for sustainable gene transfer. *Nature methods*, 8(10), pp.861–869.

Love, M.I., Huber, W. and Anders, S., 2014. Moderated estimation of fold change and dispersion for RNA-seq data with DESeq2. *Genome Biology*, 15(12), p.550.

Lopez-Santiago, L.F., Pertin, M., Morisod, X., Chen, C., Hong, S., Wiley, J., Decosterd, I. and Isom, L.L. 2006. Sodium channel beta2 subunits regulate tetrodotoxin-sensitive sodium channels in small dorsal root ganglion neurons and modulate the response to pain. *The Journal of Neuroscience*, 26(30), pp.7984–7994.

Luo, S., Perry, G.M., Levinson, S.R. and Henry, M.A. 2008. Nav1.7 expression is increased in painful human dental pulp. *Mol. Pain*, 4(2), p.16.

Marchi, M., Provitera, V., Nolano, M., Romano, M., Maccora, S., D'Amato, I., Salvi, E., Gerrits, M., Santoro, L. and Lauria, G., 2018. A novel SCN9A splicing mutation in a compound heterozygous girl with congenital insensitivity to pain, hyposmia and hypogeusia. *Journal of the Peripheral Nervous System*, 23(3), pp.202–206.

Mason, M.R.J., Ehlert, E.M.E., Eggers, R., Pool, C.W., Hermening, S., Huseinovic, A., Timmermans, E., Blits, B. and Verhaagen, J., 2010. Comparison of AAV Serotypes for Gene Delivery to Dorsal Root Ganglion Neurons. *Molecular Therapy*, 18(4), pp.715–724.

Matsukawa, S., Miwata, K., Asashima, M. and Michiue, T. 2015. The requirement of histone modification by PRDM12 and Kdm4a for the development of pre-placodal ectoderm and neural crest in Xenopus. *Special Section: Gene Expression and Development*, 399(1), pp.164–176.

Matsukawa, S., Miwata, K., Asashima, M. and Michiue, T. 2015. The requirement of histone modification by PRDM12 and Kdm4a for the development of pre-placodal ectoderm and neural crest in Xenopus. *Special Section: Gene Expression and Development*, 399(1), pp.164–176.

McCormack, K., Santos, S., Chapman, M.L., Krafte, D.S., Marron, B.E., West, C.W., Krambis, M.J., Antonio, B.M., Zellmer, S.G., Printzenhoff, D., Padilla, K.M., Lin, Z., Wagoner, P.K., Swain, N.A., Stupple, P.A., de Groot, M., Butt, R.P. and Castle, N.A. 2013. Voltage sensor interaction site for selective small molecule inhibitors of voltage-gated sodium channels. *Proceedings of the National Academy of Sciences*, 110(29), pp.E2724–32.

McDermott, L.A., Weir, G.A. , Themistocleous, A.C., Segerdahl, A.R., Blesneac, I., Baskozos, G , Millar, V, Clark A.J., Peck L.J, Ebner, D, Tracey, I, Serra, J, Bennett, D.L. Defining the functional role of NaV1.7 in human nociception. *Neuron,* In press.

Meadows, L.S., Chen, Y.H., Powell, A.J., Clare, J.J. and Ragsdale, D.S. 2002. Functional modulation of human brain Nav1.3 sodium channels, expressed in mammalian cells, by auxiliary beta 1, beta 2 and beta 3 subunits. *Neuroscience*, 114(3), pp.745–753.

Minett, M.S., Nassar, M.A., Clark, A.K., Passmore, G., Dickenson, A.H., Wang, F., Malcangio, M. and Wood, J.N. 2012. Distinct Nav1.7-dependent pain sensations require different sets of sensory and sympathetic neurons. *Nat. Commun*, 3(1), p.85.

Moreno, A.M., Fu, X., Zhu, J., Katrekar, D., Shih, Y.-R. V, Marlett, J., Cabotaje, J., Tat, J., Naughton, J., Lisowski, L., Varghese, S., Zhang, K. and Mali, P., 2018. In Situ Gene Therapy via AAV-CRISPR-Cas9-Mediated Targeted Gene Regulation. *Molecular Therapy*, 26(7), pp.1818–1827.

Moutal, A., Dustrude, E.T., Largent-Milnes, T.M., Vanderah, T.W., Khanna, M. and Khanna, R. 2017. Blocking CRMP2 SUMOylation reverses neuropathic pain. *Mol. Psychiatry*.

Moyer, B., Yin, R., Liu, D., Chhoa, M., Li, C., Luo, Y., Zhang, M., Lehto, S. and Immke, D. 2012. Voltage-gated sodium channel expression and function in injured and uninjured sensory ganglia neurons. *The Journal of Pain*, 13(4), p.S41.

Mudge, A.W., 1984. Schwann cells induce morphological transformation of sensory neurones *in vitro*. *Nature*, 309(5966), pp.367–369.

Muroi, Y., Ru, F., Kollarik, M., Canning, B.J., Hughes, S.A., Walsh, S., Sigg, M., Carr, M.J. and Undem, B.J., 2011. Selective silencing of Na V1.7 decreases excitability and conduction in vagal sensory neurons. *The Journal of physiology*, 589(23), pp.5663–5676.

Nagy, V., Cole, T., Van Campenhout, C., Khoung, T.M., Leung, C., Vermeiren, S., Novatchkova, M., Wenzel, D., Cikes, D., Polyansky, A.A., Kozieradzki, I., Meixner, A., Bellefroid, E.J., Neely, G.G. and Penninger, J.M. 2015. The evolutionarily conserved transcription factor PRDM12 controls sensory neuron development and pain perception. *Cell cycle (Georgetown, Tex.)*, 14(12), pp.1799–1808.

Nahorski, M.S., Chen, Y.-C. and Woods, C.G., 2015. New Mendelian Disorders of Painlessness. *Trends in Neurosciences*, 38(11), pp.712–724.

Nassar, M.A., Stirling, L.C., Forlani, G., Baker, M.D., Matthews, E.A., Dickenson, A.H. and Wood, J.N. 2004. Nociceptor-specific gene deletion reveals a major role for Nav1.7 (PN1) in acute and inflammatory pain. *Proceedings of the National Academy of Sciences of the United States of America*, 101(34), pp.12706–12711.

Nuñez, J.K., Kranzusch, P.J., Noeske, J., Wright, A.V., Davies, C.W. and Doudna, J.A. 2014. Cas1-Cas2 complex formation mediates spacer acquisition during CRISPR-Cas adaptive immunity. *Nature structural & molecular biology*, 21(6), pp.528–534.

Ohlemacher, S.K., Sridhar, A., Xiao, Y., Hochstetler, A.E., Sarfarazi, M., Cummins, T.R. and Meyer, J.S. 2016. Stepwise Differentiation of Retinal Ganglion Cells from Human Pluripotent Stem Cells Enables Analysis of Glaucomatous Neurodegeneration. *Stem cells (Dayton, Ohio)*, 34(6), pp.1553–1562.

Pan, X., Li, Z., Zhou, Q., Shen, H., Wu, K., Huang, X., Chen, J., Zhang, J., Zhu, X., Lei, J., Xiong, W., Gong, H., Xiao, B. and Yan, N. 2018. Structure of the human voltage-gated sodium channel Nav1.4 in complex with β1. *Science*, 362(6412), p.eaau2486.

Paquet, D., Kwart, D., Chen, A., Sproul, A., Jacob, S., Teo, S., Olsen, K.M., Gregg, A., Noggle, S. and Tessier-Lavigne, M., 2016. Efficient introduction of specific homozygous and heterozygous mutations using CRISPR/Cas9. *Nature*, 533(7601), pp.125–129.

Pashos, E.E., Park, Y., Wang, X., Raghavan, A., Yang, W., Abbey, D., Peters, D.T., Arbelaez, J., Hernandez, M., Kuperwasser, N., Li, W., Lian, Z., Liu, Y., Lv, W., Lytle-Gabbin, S.L., Marchadier, D.H., Rogov, P., Shi, J., Slovik, K.J., Stylianou, I.M., Wang, L., Yan, R., Zhang, X., Kathiresan, S., Duncan, S.A., Mikkelsen, T.S., Morrisey, E.E., Rader, D.J., Brown, C.D. and Musunuru, K., 2017. Large, Diverse Population Cohorts of hiPSCs and Derived Hepatocyte-like Cells Reveal Functional Genetic Variation at Blood Lipid-Associated Loci. *Cell Stem Cell*, 20(4), p.558–570.e10.

Pattanayak, V., Lin, S., Guilinger, J.P., Ma, E., Doudna, J.A. and Liu, D.R., 2013. High-throughput profiling of off-target DNA cleavage reveals RNA-programmed Cas9 nuclease specificity. *Nature biotechnology*, 31(9), pp.839–843.

Pero, J.E., Rossi, M.A., Lehman, H.D.G.F., Kelly, M.J., Mulhearn, J.J., Wolkenberg, S.E., Cato, M.J., Clements, M.K., Daley, C.J., Filzen, T., Finger, E.N., Gregan, Y., Henze, D.A., Jovanovska, A., Klein, R., Kraus, R.L., Li, Y., Liang, A., Majercak, J.M., Panigel, J., Urban, M.O., Wang, J., Wang, Y.-H., Houghton, A.K. and Layton, M.E. 2017. Benzoxazolinone aryl sulfonamides as potent, selective Nav1.7 inhibitors with in vivo efficacy in a preclinical pain model. *Bioorg. Med. Chem. Lett*, 27(12), pp.2683–2688.

Polstein, L.R., Perez-Pinera, P., Kocak, D.D., Vockley, C.M., Bledsoe, P., Song, L., Safi, A., Crawford, G.E., Reddy, T.E. and Gersbach, C.A., 2015. Genome-wide specificity of DNA binding, gene regulation, and chromatin remodeling by TALE- and CRISPR/Cas9-based transcriptional activators. *Genome Research*.

Prato, V., Taberner, F.J., Hockley, J.R.F., Callejo, G., Arcourt, A., Tazir, B., Hammer, L., Schad, P., Heppenstall, P.A., Smith, E.S. and Lechner, S.G. 2017. Functional and Molecular Characterization of Mechanoinsensitive 'Silent' Nociceptors. *Cell Rep*, 21(11), pp.3102–3115.

Price, T.J. and Flores, C.M. 2007. Critical evaluation of the colocalization between calcitonin gene-related peptide, substance P, transient receptor potential vanilloid subfamily type 1 immunoreactivities, and isolectin B4 binding in primary afferent neurons of the rat and mouse. *The journal of pain : official journal of the American Pain Society*, 8(3), pp.263–272.

Ramachandra, R., McGrew, S.Y., Baxter, J.C., Howard, J.R. and Elmslie, K.S., 2013. Na V 1.8 channels are expressed in large, as well as small, diameter sensory afferent neurons. *Channels*, 7(1), pp.34–37.

Ramirez, J.D., Habib, A.M., Cox, J.J., Themistocleous, A.C., McMahon, S.B., Wood, J.N. and Bennett, D.L.H. 2014. Null mutation in SCN9A in which noxious stimuli can be detected in the absence of pain. *Neurology*, 83(17), pp.1577–1580.

Ran, F.A., Cong, L., Yan, W.X., Scott, D.A., Gootenberg, J.S., Kriz, A.J., Zetsche, B., Shalem, O., Wu, X., Makarova, K.S., Koonin, E. V., Sharp, P.A. and Zhang, F., 2015. In vivo genome editing using Staphylococcus aureus Cas9. *Nature*, 520(7546), pp.186–191.

Ray, P., Torck, A., Quigley, L., Wangzhou, A., Neiman, M., Rao, C., Lam, T., Kim, J.-Y., Kim, T.H., Zhang, M.Q., Dussor, G. and Price, T.J., 2018. Comparative transcriptome profiling of the human and mouse dorsal root ganglia: an RNA-seq-based resource for pain and sensory neuroscience research. *Pain*, 159(7), pp.1325–1345.
Renganathan, M., Cummins, T.R. and Waxman, S.G. 2001. Contribution of Nav1.8 Sodium Channels to Action Potential Electrogenesis in DRG Neurons. *Journal of Neurophysiology*, 86(2), pp.629–640.

Rhodes, K.J. and Trimmer, J.S., 2006. Antibodies as valuable neuroscience research tools versus reagents of mass distraction. *The Journal of Neuroscience*, 26(31), pp.8017–8020.
Ritchie, J.M. and Rogart, R.B. 1977. The binding of saxitoxin and tetrodotoxin to excitable tissue. *Reviews of physiology, biochemistry and pharmacology*, 79, pp.1–50.

Ritchie, J.M. and Rogart, R.B. 1977. The binding of saxitoxin and tetrodotoxin to excitable tissue. *Reviews of physiology, biochemistry and pharmacology*, 79, pp.1–50.

Rostock, C., Schrenk-Siemens, K., Pohle, J. and Siemens, J. 2017. Human vs. Mouse Nociceptors - Similarities and Differences. *Neuroscience*.

Ryan, S.D., Dolatabadi, N., Chan, S.F., Zhang, X., Akhtar, M.W., Parker, J., Soldner, F., Sunico, C.R., Nagar, S., Talantova, M., Lee, B., Lopez, K., Nutter, A., Shan, B., Molokanova, E., Zhang, Y., Han, X., Nakamura, T., Masliah, E., Yates, J.R., Nakanishi, N., Andreyev, A.Y., Okamoto, S.-I., Jaenisch, R., Ambasudhan, R. and Lipton, S.A. 2013. Isogenic human iPSC Parkinson's model shows nitrosative stress-induced dysfunction in MEF2-PGC1α transcription. *Cell*, 155(6), pp.1351–1364.

Sakuma, T., Nakade, S., Sakane, Y., Suzuki, K.-I.T. and Yamamoto, T. 2016. MMEJ-assisted gene knock-in using TALENs and CRISPR-Cas9 with the PITCh systems. *Nature protocols*, 11(1), pp.118–133.

Samad, O.A., Tan, A.M., Cheng, X., Foster, E., Dib-Hajj, S.D. and Waxman, S.G. 2013. Virus-mediated shRNA knockdown of Na(v)1.3 in rat dorsal root ganglion attenuates nerve injury-induced neuropathic pain. *Molecular therapy : the journal of the American Society of Gene Therapy*, 21(1), pp.49–56.

Sances, S., Bruijn, L.I., Chandran, S., Eggan, K., Ho, R., Klim, J.R., Livesey, M.R., Lowry, E., Macklis, J.D., Rushton, D., Sadegh, C., Sareen, D., Wichterle, H., Zhang, S.-C. and Svendsen, C.N. 2016. Modeling ALS with motor neurons derived from human induced pluripotent stem cells. *Nature neuroscience*, 19(4), pp.542–553.

Sander, J.D., Dahlborg, E.J., Goodwin, M.J., Cade, L., Zhang, F., Cifuentes, D., Curtin, S.J., Blackburn, J.S., Thibodeau-Beganny, S., Qi, Y., Pierick, C.J., Hoffman, E., Maeder, M.L., Khayter, C., Reyon, D., Dobbs, D., Langenau, D.M., Stupar, R.M., Giraldez, A.J., Voytas, D.F., Peterson, R.T., Yeh, J.-R.J. and Joung, J.K. 2011. Selection-free zinc-finger-nuclease engineering by context-dependent assembly (CoDA). *Nature methods*, 8(1), pp.67–69.

Sangameswaran, L., Fish, L.M., Koch, B.D., Rabert, D.K., Delgado, S.G., Ilnicka, M., Jakeman, L.B., Novakovic, S., Wong, K., Sze, P., Tzoumaka, E., Stewart, G.R., Herman, R.C., Chan, H., Eglen, R.M. and Hunter, J.C. 1997. A novel tetrodotoxin-sensitive, voltage-gated sodium channel expressed in rat and human dorsal root ganglia. *The Journal of biological chemistry*, 272(23), pp.14805–14809.

Sanjana, N.E., Cong, L., Zhou, Y., Cunniff, M.M., Feng, G. and Zhang, F. 2012. A transcription activator-like effector toolbox for genome engineering. *Nature protocols*, 7(1), pp.171–192.

Schmelz, M., Schmidt, R., Ringkamp, M., Handwerker, H.O. and Torebjörk, H.E. 1994. Sensitization of insensitive branches of C nociceptors in human skin. *J. Physiol*, 480 (Pt 2)(Pt 2), pp.389–394.

Schmidt, J., Rossie, S. and Catterall, W.A. 1985. A large intracellular pool of inactive Na channel alpha subunits in developing rat brain. *Proceedings of the National Academy of Sciences of the United States of America*, 82(14), pp.4847–4851.

Schmidt, R., Schmelz, M., Forster, C., Ringkamp, M., Torebjörk, E. and Handwerker, H. 1995. Novel classes of responsive and unresponsive C nociceptors in human skin. *The Journal of Neuroscience*, 15(1 Pt 1), pp.333–341.

Schwab, A.J. and Ebert, A.D. 2015. Neurite Aggregation and Calcium Dysfunction in iPSC-Derived Sensory Neurons with Parkinson's Disease-Related LRRK2 G2019S Mutation. *Stem Cell Reports*, 5(6), pp.1039–1052.

Sexton, J.E., Cox, J.J., Zhao, J. and Wood, J.N., 2018. The Genetics of Pain: Implications for Therapeutics. *Annu. Rev. Pharmacol. Toxicol.*, 58(1), pp.123–142.
Sherrington, C.S. 1906. Observations on the scratch-reflex in the spinal dog. *J. Physiol*, 34(1-2), pp.1–50.

Sherrington, C.S. 1906. Observations on the scratch-reflex in the spinal dog. *J. Physiol*, 34(1-2), pp.1–50.

Shi, Y., Kirwan, P. and Livesey, F.J. 2012. Directed differentiation of human pluripotent stem cells to cerebral cortex neurons and neural networks. *Nature protocols*, 7(10), pp.1836–1846.

Shields, S.D., Deng, L., Reese, R.M., Dourado, M., Tao, J., Foreman, O., Chang, J.H. and Hackos, D.H. 2018. Insensitivity to Pain upon Adult-Onset Deletion of Nav1.7 or Its Blockade with Selective Inhibitors. *Journal of Neuroscience*, 38(47), pp.10180–10201.

Silverman, J.D. and Kruger, L. 1990. Selective neuronal glycoconjugate expression in sensory and autonomic ganglia: relation of lectin reactivity to peptide and enzyme markers. *Journal of neurocytology*, 19(5), pp.789–801.

Slaymaker, I.M., Gao, L., Zetsche, B., Scott, D.A., Yan, W.X. and Zhang, F. 2016. Rationally engineered Cas9 nucleases with improved specificity. *Science*, 351(6268), pp.84–88.

Snapp, E., 2005. Design and Use of Fluorescent Fusion Proteins in Cell Biology. *Current Protocols in Cell Biology*, 27(1), p.21.4.1-21.4.13.

Stamboulian, S., Choi, J.S., Ahn, H.-S., Chang, Y.-W., Tyrrell, L., Black, J.A., Waxman, S.G. and Dib-Hajj, S.D. 2010. ERK1/2 mitogen-activated protein kinase phosphorylates sodium channel Na(v)1.7 and alters its gating properties. *The Journal of Neuroscience*, 30(5), pp.1637–1647.

Storer, R.I., Pike, A., Swain, N.A., Alexandrou, A.J., Bechle, B.M., Blakemore, D.C., Brown, A.D., Castle, N.A., Corbett, M.S., Flanagan, N.J., Fengas, D., Johnson, M.S., Jones, L.H., Marron, B.E., Payne, C.E., Printzenhoff, D., Rawson, D.J., Rose, C.R., Ryckmans, T., Sun, J., Theile, J.W., Torella, R., Tseng, E. and Warmus, J.S. 2017. Highly potent and selective NaV1.7 inhibitors for use as intravenous agents and chemical probes. *Bioorg. Med. Chem. Lett*, 27(21), pp.4805–4811.

Strickland, I.T., Martindale, J.C., Woodhams, P.L., Reeve, A.J., Chessell, I.P. and McQueen, D.S., 2012. Changes in the expression of NaV1.7, NaV1.8 and NaV1.9 in a distinct population of dorsal root ganglia innervating the rat knee joint in a model of chronic inflammatory joint pain. *European Journal of Pain*, 12(5), pp.564–572.

Su, Y.-Y., Ye, M., Li, L., Liu, C., Pan, J., Liu, W.-W., Jiang, Y., Jiang, X.-Y., Zhang, X., Shu, Y. and Bao, L., 2013. KIF5B promotes the forward transport and axonal function of the voltage-gated sodium channel Nav1.8. *The Journal of Neuroscience*, 33(45), pp.17884–17896.

Subramanian, N., Wetzel, A., Dombert, B., Yadav, P., Havlicek, S., Jablonka, S., Nassar, M.A., Blum, R. and Sendtner, M., 2012. Role of Na(v)1.9 in activity-dependent axon growth in motoneurons. *Hum. Mol. Genet.*, 21(16), pp.3655–3667.

Sugiura, Y., Lee, C.L. and Perl, E.R. 1986. Central projections of identified, unmyelinated (C) afferent fibers innervating mammalian skin. *Science*, 234(4774), pp.358–361.

Sun, Y.M., Favre, I., Schild, L. and Moczydlowski, E. 1997. On the structural basis for size-selective permeation of organic cations through the voltage-gated sodium channel. Effect of alanine mutations at the DEKA locus on selectivity, inhibition by Ca2+ and H+, and molecular sieving. *The Journal of general physiology*, 110(6), pp.693–715.

Szostak, J.W., Orr-Weaver, T.L., Rothstein, R.J. and Stahl, F.W. 1983. The double-strand-break repair model for recombination. *Cell*, 33(1), pp.25–35.

Takahashi, K. and Yamanaka, S. 2006. Induction of pluripotent stem cells from mouse embryonic and adult fibroblast cultures by defined factors. *Cell*, 126(4), pp.663–676.

Tan, Z.-Y., Priest, B.T., Krajewski, J.L., Knopp, K.L., Nisenbaum, E.S. and Cummins, T.R. 2014. Protein kinase C enhances human sodium channel hNav1.7 resurgent currents via a serine residue in the domain III-IV linker. *FEBS Lett*, 588(21), pp.3964–3969.

Theile, J.W., Jarecki, B.W., Piekarz, A.D. and Cummins, T.R. 2011. Nav1.7 mutations associated with paroxysmal extreme pain disorder, but not erythromelalgia, enhance Navbeta4 peptide-mediated resurgent sodium currents. *The Journal of physiology*, 589(Pt 3), pp.597–608.

Thielges, M.C., Chung, J.K., Axup, J.Y. and Fayer, M.D., 2011. Influence of Histidine Tag Attachment on Picosecond Protein Dynamics. *Biochemistry*, 50(25), pp.5799–5805.

Toledo-Aral, J.J., Moss, B.L., He, Z.J., Koszowski, A.G., Whisenand, T., Levinson, S.R., Wolf, J.J., Silos-Santiago, I., Halegoua, S. and Mandel, G., 1997. Identification of PN1, a predominant voltage-dependent sodium channel expressed principally in peripheral neurons. *Proceedings of the National Academy of Sciences of the United States of America*, 94(4), pp.1527–1532.

Usoskin, D., Furlan, A., Islam, S., Abdo, H., Lönnerberg, P., Lou, D., Hjerling-Leffler, J., Haeggström, J., Kharchenko, O., Kharchenko, P.V., Linnarsson, S. and Ernfors, P. 2015. Unbiased classification of sensory neuron types by large-scale single-cell RNA sequencing. *Nature neuroscience*, 18(1), pp.145–153.

Vandewauw, I., De Clercq, K., Mulier, M., Held, K., Pinto, S., Van Ranst, N., Segal, A., Voet, T., Vennekens, R., Zimmermann, K., Vriens, J. and Voets, T. 2018. A TRP channel trio mediates acute noxious heat sensing. *Nature*, 555(7698), pp.662–666.

Vijayaragavan, K., Boutjdir, M. and Chahine, M. 2004. Modulation of Nav1.7 and Nav1.8 peripheral nerve sodium channels by protein kinase A and protein kinase C. *J. Neurophysiol*, 91(4), pp.1556–1569.

Wainger, B.J., Buttermore, E.D., Oliveira, J.T., Mellin, C., Lee, S., Saber, W.A., Wang, A.J., Ichida, J.K., Chiu, I.M., Barrett, L., Huebner, E.A., Bilgin, C., Tsujimoto, N., Brenneis, C., Kapur, K., Rubin, L.L., Eggan, K. and Woolf, C.J., 2014. Modeling pain *in vitro* using nociceptor neurons reprogrammed from fibroblasts. *Nature neuroscience*, 18(1), pp.17–24.

Watanabe, K., Ueno, M., Kamiya, D., Nishiyama, A., Matsumura, M., Wataya, T., Takahashi, J.B., Nishikawa, S., Nishikawa, S., Muguruma, K. and Sasai, Y., 2007. A ROCK inhibitor permits survival of dissociated human embryonic stem cells. *Nature Biotechnology*.

Weiss, J., Pyrski, M., Jacobi, E., Bufe, B., Willnecker, V., Schick, B., Zizzari, P., Gossage, S.J., Greer, C.A., Leinders-Zufall, T., Woods, C.G., Wood, J.N. and Zufall, F. 2011. Loss-of-function mutations in sodium channel Nav1.7 cause anosmia. *Nature*, 472(7342), pp.186–190.

Wilson, L.O.W., O'Brien, A.R. and Bauer, D.C. 2018. The Current State and Future of CRISPR-Cas9 gRNA Design Tools. *Front. Pharmacol*, 9, p.705.

Wilson, S.M. and Khanna, R. 2015. Specific binding of lacosamide to collapsin response mediator protein 2 (CRMP2) and direct impairment of its canonical function: implications for the therapeutic potential of lacosamide. *Molecular neurobiology*, 51(2), pp.599–609.

Wu, X., Scott, D.A., Kriz, A.J., Chiu, A.C., Hsu, P.D., Dadon, D.B., Cheng, A.W., Trevino, A.E., Konermann, S., Chen, S., Jaenisch, R., Zhang, F. and Sharp, P.A. 2014. Genome-wide binding of the CRISPR endonuclease Cas9 in mammalian cells. *Nature biotechnology*, 32(7), pp.670–676.

Xiao, Y., Xia, Z., Wu, Y. and Zhao, B. 2016. Sodium channel Nav1.7 expression is upregulated in the dorsal root ganglia in a rat model of paclitaxel-induced peripheral neuropathy. *SpringerPlus*, 5(1), p.1738.

Yamane, M., Yamashita, N., Hida, T., Kamiya, Y., Nakamura, F., Kolattukudy, P. and Goshima, Y., 2017. A functional coupling between CRMP1 and Nav1.7 for retrograde propagation of Semaphorin3A signaling. *J. Cell Sci.*, 130(8), pp.1393–1403.

Yang, F., Sun, W., Yang, Y., Wang, Y., Li, C.-L., Fu, H., Wang, X.-L., Yang, F., He, T. and Chen, J. 2015. SDF1–CXCR4 signaling contributes to persistent pain and hypersensitivity via regulating excitability of primary nociceptive neurons: involvement of ERK-dependent Nav1.8 up-regulation. *Journal of Neuroinflammation*, 12(1), p.307.

Yarov-Yarovoy, V., DeCaen, P.G., Westenbroek, R.E., Pan, C.-Y., Scheuer, T., Baker, D. and Catterall, W.A. 2012. Structural basis for gating charge movement in the voltage sensor of a sodium channel. *Proceedings of the National Academy of Sciences*, 109(2), pp.E93–102.

Ye, L., Wang, J., Beyer, A.I., Teque, F., Cradick, T.J., Qi, Z., Chang, J.C., Bao, G., Muench, M.O., Yu, J., Levy, J.A. and Kan, Y.W. 2014. Seamless modification of wild-type induced pluripotent stem cells to the natural CCR5Δ32 mutation confers resistance to HIV infection. *Proceedings of the National Academy of Sciences*, 111(26), pp.9591–9596.

Young, G.T., Gutteridge, A., Fox, H.D.E., Wilbrey, A.L., Cao, L., Cho, L.T., Brown, A.R., Benn, C.L., Kammonen, L.R., Friedman, J.H., Bictash, M., Whiting, P., Bilsland, J.G. and Stevens, E.B., 2014. Characterizing Human Stem Cell–derived Sensory Neurons at the Single-cell Level Reveals Their Ion Channel Expression and Utility in Pain Research. *Molecular Therapy*, 22(8), pp.1530–1543.

Zannino, D.A. and Sagerström, C.G. 2015. An emerging role for prdm family genes in dorsoventral patterning of the vertebrate nervous system. *Neural development*, 10(1), p.24.

Zeisel, A., Hochgerner, H., Lönnerberg, P., Johnsson, A., Memic, F., van der Zwan, J., Häring, M., Braun, E., Borm, L.E., La Manno, G., Codeluppi, S., Furlan, A., Lee, K., Skene, N., Harris, K.D., Hjerling-Leffler, J., Arenas, E., Ernfors, P., Marklund, U. and Linnarsson, S. 2018. Molecular Architecture of the Mouse Nervous System. *Cell*, 174(4), pp.999–1014.e22.

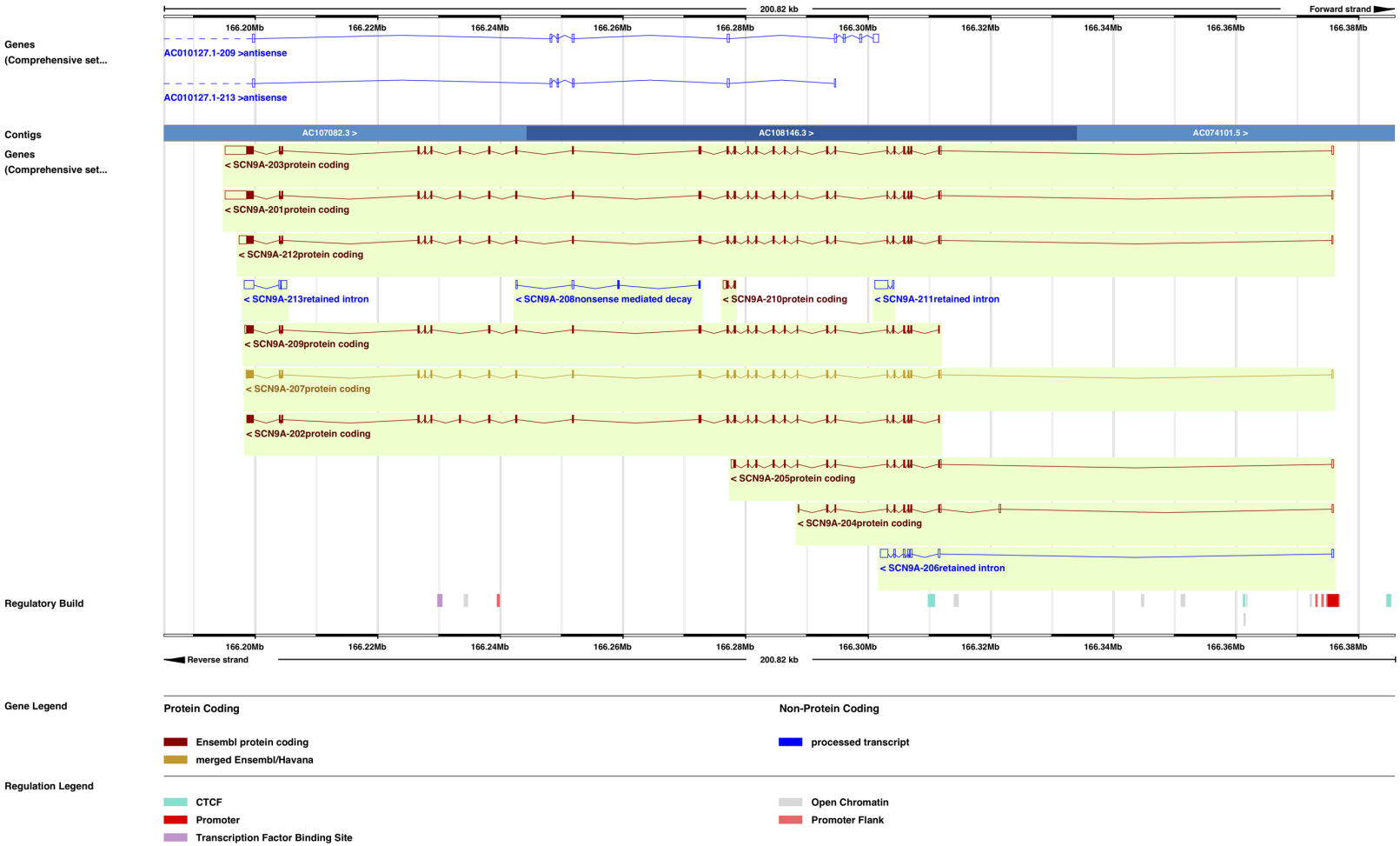
Zhang, X.-Y., Bi, R.-Y., Zhang, P. and Gan, Y.-H., 2018. Veratridine modifies the gating of human voltage-gated sodium channel Nav1.7. *Acta pharmacologica Sinica*, 39(11), pp.1716–1724.

Zhao, J., O'Leary, M.E. and Chahine, M., 2011. Regulation of Na v1.6 and Na v1.8 peripheral nerve Na +channels by auxiliary β-subunits. *J. Neurophysiol.*, 106(2), pp.608–619.

Zhao, Y.O., Könen-Waisman, S., Taylor, G.A., Martens, S. and Howard, J.C., 2010. Localisation and Mislocalisation of the Interferon-Inducible Immunity-Related GTPase, Irgm1 (LRG-47) in Mouse Cells. *PloS one*, 5(1), p.e8648.

Zhou, X., Xiao, Z., Xu, Y., Zhang, Y., Tang, D., Wu, X., Tang, C., Chen, M., Shi, X., Chen, P., Liang, S. and Liu, Z. 2017. Electrophysiological and Pharmacological Analyses of Nav1.9 Voltage-Gated Sodium Channel by Establishing a Heterologous Expression System. *Front. Pharmacol*, 8, p.555.

Zhou, X., Xiao, Z., Xu, Y., Zhang, Y., Tang, D., Wu, X., Tang, C., Chen, M., Shi, X., Chen, P., Liang, S. and Liu, Z. 2017. Electrophysiological and Pharmacological Analyses of Nav1.9 Voltage-Gated Sodium Channel by Establishing a Heterologous Expression System. *Front. Pharmacol*, 8, p.555.



SCN9A transcripts

Human SCN9A transcripts found in the Ensembl Genome database (available at http://ensembl.org)

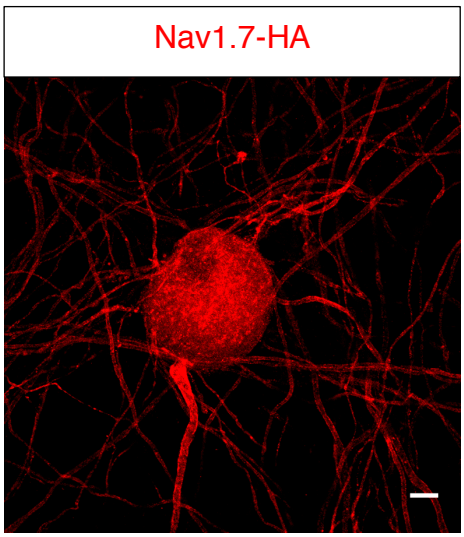
Clinical phenotyping of patients CIP1 and CIP2, performed by Prof Bennett and Dr Thermistocleous.

Table A.1 Clinical phenotyping of CIP patients included in this work

	CIP1	**CIP2**
Age	31	34
Gender	Male	Male
History		
Painless injuries e.g. fractures, burns	Y	Y
Congenital onset	Y	Y
Normal cognitive development	Y	Y
Self-mutilation	Y	N
Absent visceral pain	Y	Y
Joint replacement	Y	N
Charcot joints	Y	Y
Affected siblings	Y	Y
Examination		
Anosmia	Y	Y
Normal autonomic function (sweating, bowel function, blood pressure)	Y	Y
Corneal reflex intact	Y	Y
Normal motor examination	Y	Y
Normal deep tendon reflexes	Y	Y
Vibration, mechanical detection, proprioception normal	Y	Y
Pin prick not felt as painful nor sharp	Y	Y
Bedside temperature normal	N	Y
Investigations		

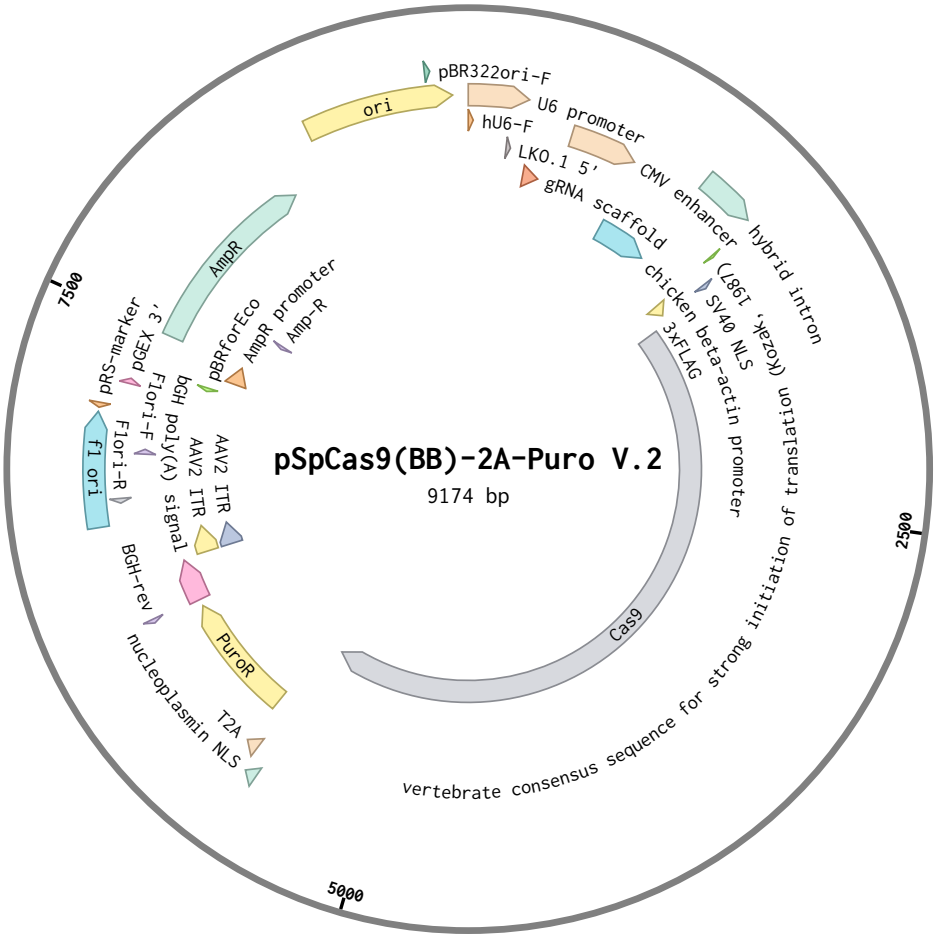
Histamine flare	Y	Y
Mustard oil flare	Y	Y
Nerve conduction studies normal	N*	Y
Threshold tracking normal	Y	Y
fMRI	N	Y
Microneurography	Y	Y
IENFD		
Proximal thigh (fibres/mm)	0.2	0.00
Distal leg (fibres/mm) (0.05 Quantile; Median)	3.98 (5.3 ;10.2)	0.00 (5.3 ;10.2)

* Sural amplitudes are reduced. N- No; Y- Yes; ND- Not done; IENFD – intra-epidermal nerve fibre density

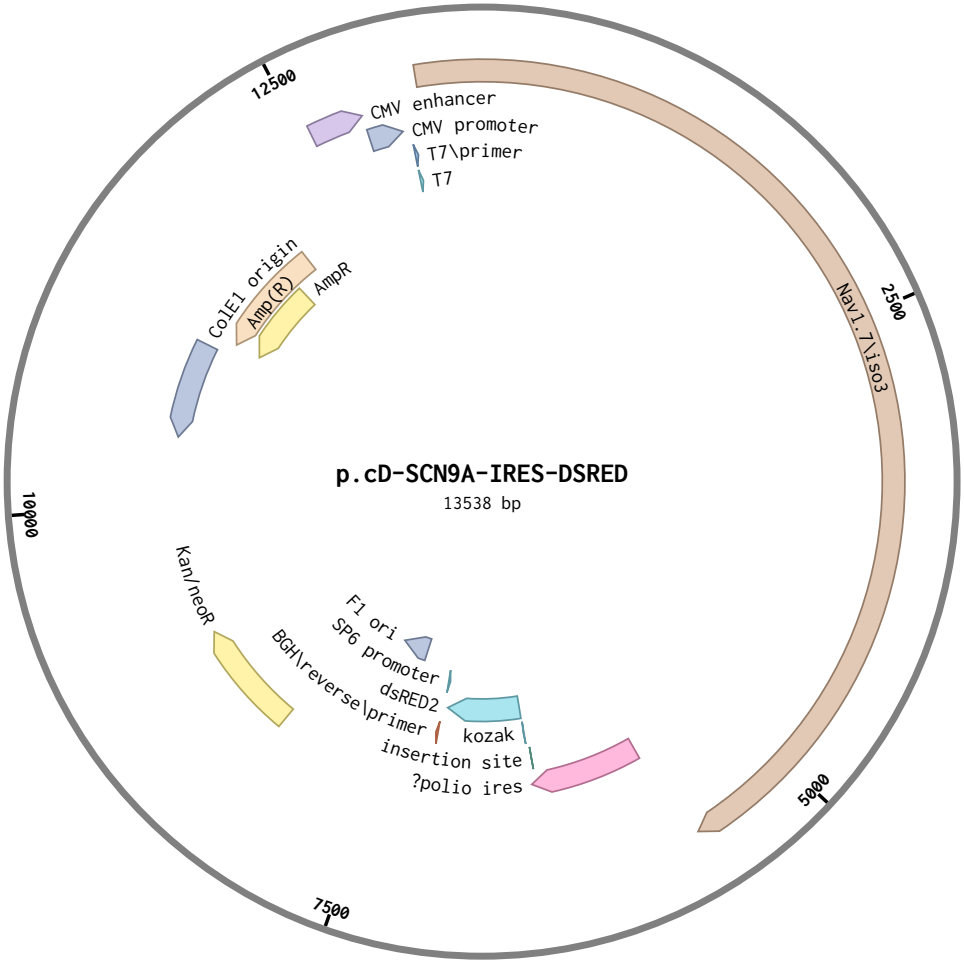


Representative image of neurons found in 100+DIV cultures. The cell body significantly increases in size with extended time in culture. Also note the enrichment of Nav1.7-HA staining at one of the processes proximal to soma (discussed in Chapter 5). Scale bar 10µm.

Annotated plasmid map of the Sp.Cas9 vector PX459. Available at Addgene (Plasmid #62988)



Annotated plasmid map of SCN9A cDNA plasmid used for site directed mutagenesis



Screenshots of TIDE output (https://tide.deskgen.com/). Example shown is HC1 targeted heterozygous +1bp mutant

